

**THE PREPARATION AND PROPERTIES OF
METAL-SCHIFF BASE COMPLEXES AS MODEL
INTERMEDIATES IN THE REACTIONS OF
VITAMIN B₆ AND RELATED COMPOUNDS**

A Thesis submitted for the degree of

DOCTOR OF PHILOSOPHY

in the faculty of science of the

University of London

by

ABDOLREZA RAFATI

Department of Chemistry

Bedford College

University of London

February 1983



ProQuest Number: 10098470

All rights reserved

INFORMATION TO ALL USERS

The quality of this reproduction is dependent upon the quality of the copy submitted.

In the unlikely event that the author did not send a complete manuscript and there are missing pages, these will be noted. Also, if material had to be removed, a note will indicate the deletion.



ProQuest 10098470

Published by ProQuest LLC(2016). Copyright of the Dissertation is held by the Author.

All rights reserved.

This work is protected against unauthorized copying under Title 17, United States Code.
Microform Edition © ProQuest LLC.

ProQuest LLC
789 East Eisenhower Parkway
P.O. Box 1346
Ann Arbor, MI 48106-1346

**TO MY WIFE
FARIBA**

ACKNOWLEDGEMENTS

I would like to thank my supervisor, Dr. M.E. Farago for all her help and enthusiasm, for her valued guidance, experienced comment and forbearance throughout the period of this research.

I would also like to thank Dr. K.E. Howlett for his constant help and invaluable discussion.

My thanks are also due to Dr. R. Bolton for his helpful discussion and Professor G.H. Williams for the provision of research facilities.

I am also grateful to Dr. A.D. Oduwole of the Chemistry Department, Queen Mary College, for his helpful assistance with E.S.R. spectrometry, and Mr. D. Carter of the School of Pharmacy, University of London, for assistance with Mass Spectrometry, and to the entire technical staff of the Chemistry Department, Bedford College, for help and technical assistance.

I am indebted to my brother, Mr. Alireza Rafati for the constant financial support during this research.

Thanks are also due to Mrs. V. Brown for the typing of this thesis.

ABSTRACT

The aim of this research was to isolate metal-Schiff base complexes which occur as intermediates in the metal catalysis of the transamination reaction of Vitamin B₆ (and its analogues) and amino acids (glycine and ethylenediamine). Metal ions used were: Fe^{III}, Co^{II}, Ni^{II}, Cu^{II}, Zn^{II}, Cd^{II} and Ag^I.

The spectral absorption maxima of the complexes have been measured at various pH values using ultraviolet techniques. The infrared and ultraviolet-visible spectra of the complexes have been discussed and assignments of bands are made. Mass spectra were obtained for all of the complexes, and fragmentation patterns have been evaluated. The electron spin resonance technique was applied to copper complexes only, and in each case the "g" and "A" parameters were calculated satisfactorily.

In most of the complexes, the ratio of metal ion to Schiff base was found to be 1:1, but in a few the ratio was found to be 2:1 (e.g. Cu₂(PLGly)₂·3H₂O) and 1:2 (e.g. Cu(PNen)₂(SO₄)₂·Cl₂·5H₂O). The remaining positions around the metal ion are occupied by either water or an amino acid molecule, or anions (such as OH⁻ or SO₄⁻).

The kinetics of the transamination reaction of pyridoxamine phosphate with α-ketoglutaric acid and copper^{II} ion have been investigated spectrophotometrically. The reaction products were analysed by paper chromatography. The reaction was found to be preceded by an induction period and to be first order in α-ketoglutaric acid. It exhibits a maximum rate at a copper concentration of twice that of pyridoxamine phosphate. This maximum is justified mathematically by assuming that the concentration of a complex of copper^{II} and the Schiff's base from pyridoxamine phosphate

and α -ketoglutarate is very low, and that the complex accepts a further copper^{II} ion at high concentrations of copper^{II}. This makes the ratio 1:1:2 (1PMP:1 α -KG:2Cu⁺²).

The rates of formation of metal-Schiff base complexes of pyridoxal phosphate-glycine with Cu^{II}, Co^{II}, Cd^{II}, Mn^{II} and Al^{III} were measured at various pH values spectrophotometrically. The rates are dependent on the concentration of pyridoxal phosphate and of amino acid. The metal concentration has no effect on the rate, which would be consistent with the metal ion trapping the Schiff base as soon as it is formed.

The rate of formation of metal-Schiff base complexes of pyridoxal phosphate-glycine-Aluminium^{III} is dependent, however, on the concentration of aluminium when its concentration is in excess over the other species.

CONTENTS

	Page
CHAPTER 1: GENERAL INTRODUCTION	1
1-1: Discovery and Structural Elucidation of Vitamin B ₆ and Related Compounds	2
1-2: Chemical and Physical Properties of Vitamin B ₆	8
1-2-1: Chemical Properties	8
1-2-2: Physical Properties	10
1-3: Relationship between Chemical Structures of Vitamin B ₆ -type Compounds and their Catalytic Activities	14
1-3-1: Equilibrium Forms of Vitamin B ₆ in Aqueous Solution	14
1-3-2: Schiff-Base Formation between Pyridoxal or Pyridoxal Phosphate and Amino Acids	19
1-3-3: Physical Properties of Schiff-Bases	25
1-3-4: Formation of Schiff Base-Metal Chelates	27
1-3-5: Structural Features of Vitamin B ₆ and Related Compounds required for Catalysis of Non-Enzymatic Transamination	30
1-4: Relationship of Metal Ions to the Non-Enzymatic Transamination Reaction	42
1-5: Mechanism of Non-Enzymatic Transamination Reactions	47
1-6: Effect of Structure of Amino Acids on the Rate of Transamination Reactions	51
1-7: Relationship between Non-Enzymatic and Enzymatic Transamination Reactions	53
References	55

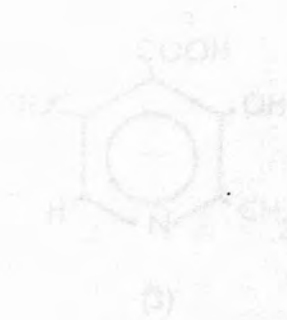
	Page
CHAPTER 2: PREPARATION OF METAL-SCHIFF BASE COMPLEXES OF VITAMIN B ₆ AND RELATED COMPOUNDS	59
2-1: Introduction	60
2-2: Proposed Structures of Metal-Schiff Base Complexes	63
2-3: Preparation of Metal-Schiff Base Complexes, Analytical Results and Proposed Structures of Complexes	70
2-4: Discussion	85
References	88
CHAPTER 3: ULTRA-VIOLET STUDY OF METAL-SCHIFF BASE COMPLEXES IN AQUEOUS SOLUTION	90
3-1: Introduction	91
3-1-2: Ultra-Violet Spectra of Schiff-Bases of Pyridoxal and its Analogues	99
3-1-3: Assignment of the Various U.V. Bands of Vitamin B ₆ Species	103
3-2: Experimental	106
3-3: Results	107
3-3-1: Measurements of Absorption Maxima of Metal-Schiff Base Complexes	107
3-4: Discussion	132
References	134
CHAPTER 4: ULTRAVIOLET-VISIBLE SOLID STATE STUDY OF METAL-SCHIFF BASE COMPLEXES	135
4-1: Experimental	136
4-2: Results	137
4-3: Discussion	152
(a) Assignment of the U.V. Bands	152
(b) Assignment of the d-d Bands	154
References	160

	Page
CHAPTER 5: INFRARED STUDY OF METAL-SCHIFF BASE COMPLEXES	162
5-1: Introduction	163
5-2: Experimental	165
5-3: Results and Discussion	166
References	194
CHAPTER 6: MASS SPECTROMETRIC STUDY OF METAL-SCHIFF BASE COMPLEXES	196
6-1: Introduction	197
6-2: Mass Spectrometric Study of Pyridoxine (Vitamin B ₆) and its Analogues	200
6-3: Experimental	204
6-4: Schemes for the Dissociation and Fragmentation of PL, PLP, PMP, PN and their Metal-Schiff Base Complexes by Mass Spectrometry	205
6-5: Results and Discussion	214
References	223
CHAPTER 7: ELECTRON SPIN RESONANCE STUDY OF COPPER ^{II} - SCHIFF BASE COMPLEXES	224
7-1: Introduction	225
7-2: The E.S.R. Spectra of Cu ^{II} -Schiff Base Complexes	228
7-3: Experimental	229
7-4: Results and Discussion	230
7-4-1: Powder Spectra	230
7-4-2: Solution Spectra	242
References	264

	Page
CHAPTER 8: KINETICS OF TRANSAMINATION REACTIONS	265
8-1: Reaction between Pyridoxamine Phosphate (PMP) and α -Ketoglutaric Acid (α -KG) in the Presence of Copper ^{II} Ion.	266
8-2: Experimental	271
8-2-1: The Effect of Variation of pH on the Initial Reaction Rate	272
8-2-2: The Effect of Variation of the Concentration of α -KG on the Initial Reaction Rate	275
8-2-3: The Effect of Variation of the Concentration of Copper ^{II} Ion on the Initial Reaction Rate	277
8-3: Kinetics Associated with the Isosbestic Point	279
8-4: Discussion	283
References	295
APPENDIXES:	296
Appendix 1: Rate Measurements for Formation of Metal-Schiff Base Complexes at various pH values	297
Appendix 2: Buffers used in the Present Work	301
Appendix 3: Abbreviations	302

CHAPTER 1

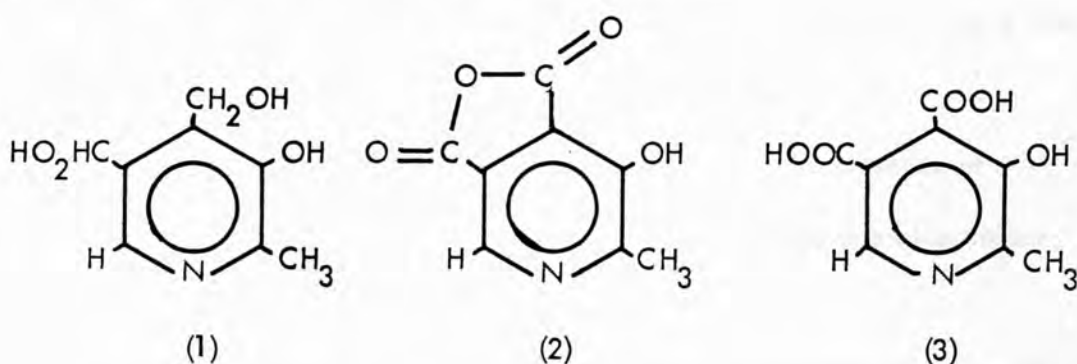
General Introduction



- (a) The following reactions were the following:
- (b) The methyl group could be acetylated by diazomethane, and the hydroxyl group was phenolic.
- (c) The methyl group was unaffected by lead tetra-acetate, so the hydroxyl group was not an adjacent carbon atom.
- (d) Monomethyl pyridoxine was oxidized by cold permanganate to a monocarboxylic acid which could readily form a lactone.
- (e) Pyridoxine and 3-hydroxy pyridine had very similar ultra-violet spectra.
- (f) Monomethyl pyridoxine was oxidized with hot permanganate to a tricarboxylic acid which had the properties of a pyridine-1-carboxylic acid. When this tricarboxylic acid was heated, the molecule lost a molecule of water and a molecule of carbon dioxide. 1 The resulting anhydride could then be

1.1 Discovery and Structural Elucidation of Vitamin B₆ and Related Compounds

Vitamin B₆ was first differentiated satisfactorily from other members of the Vitamin B complex during the period 1934-1937 by György et al¹, who found it to be a nitrogen-containing base which could form a hydrochloride. The structure of Vitamin B₆, or pyridoxine (1), was elucidated by Kuhn^{2,3} and his co-workers a few years later:



The main steps in the structural proof of pyridoxine were the following:

- (a) Only one of the hydroxyl groups could be methylated by diazomethane, thus two of the hydroxyls were alcoholic and one was phenolic.
- (b) Monomethyl pyridoxine was unaffected by lead tetra-acetate, so the two alcoholic hydroxyls were not on adjacent carbon atoms.
- (c) Monomethyl pyridoxine was oxidized by cold permanganate to a monocarboxylic acid which could readily form a lactone.
- (d) Pyridoxine and 3-hydroxy pyridine had very similar ultra-violet spectra.
- (e) Monomethyl pyridoxine was oxidized with hot permanganate to a tricarboxylic acid which had the properties of a pyridine-1 carboxylic acid. When the tricarboxylic acid was heated, the molecule lost a molecule of water and a molecule of carbon dioxide. The resulting anhydride could then be

hydrolysed to a dibasic acid which did not have the properties of pyridine-1 carboxylic acid.

From the evidence quoted above, Kuhn^{2,3} put forward the structure (2) for the anhydride, and subsequent synthetic work proved this structure to be correct. Careful oxidation of monomethyl pyridoxine gave a dibasic acid (3) with an intact methyl group. This dibasic acid did not have the properties of pyridine-1 carboxylic acid. Kuhn^{2,3} then elucidated the structure (1) for pyridoxine and this was later confirmed independently by Stiller et al⁴ and then "pyridoxine" and "Vitamin B₆" became synonymous terms.

Stiller et al⁴ provided the additional evidence of the presence of a phenol with an unsubstituted para position, as the Vitamin gave a blue colour with 2,6-dichloro quinonechlorimide.

Kuhn's synthesis⁵ of pyridoxine started from the synthetic dibasic acid (3) and his route is outlined below:

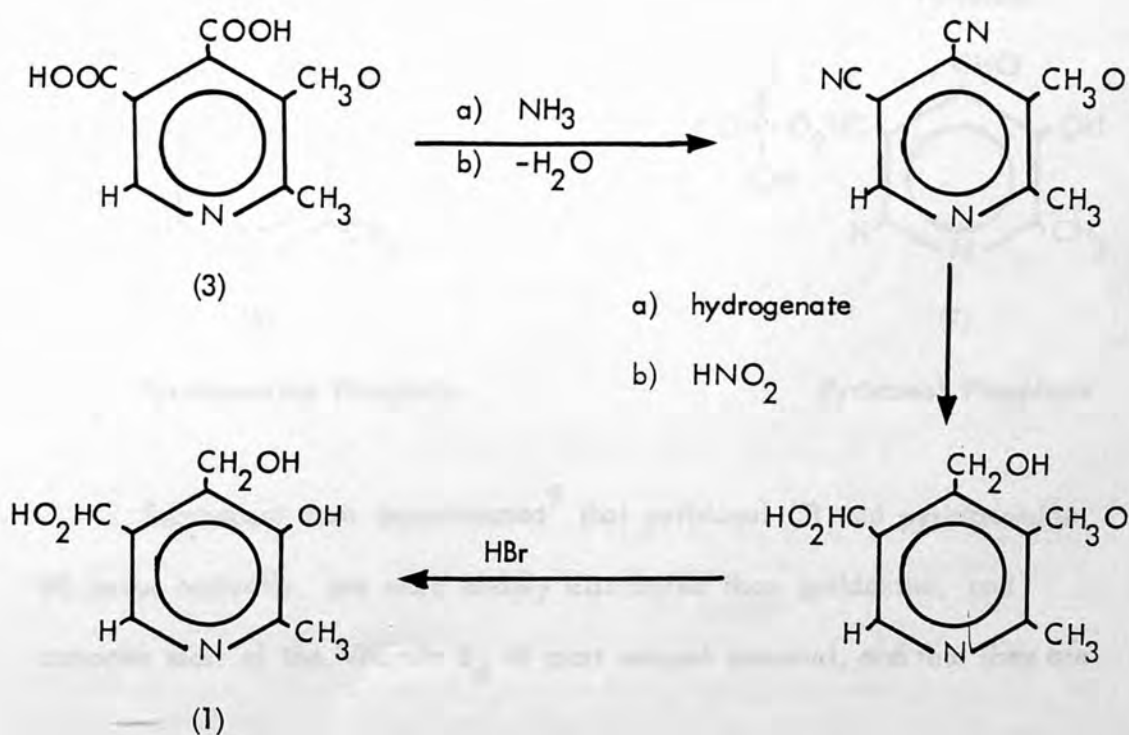
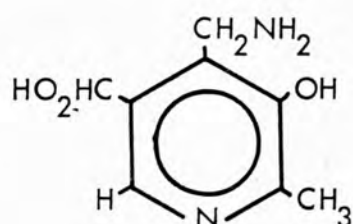


Fig. 1-1: Synthesis of Pyridoxine from Dibasic Acid

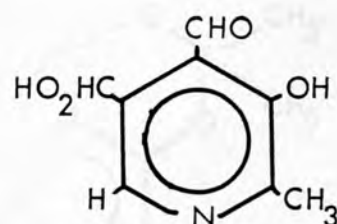
After the discovery of pyridoxine, Snell and Conn et al^{6,7} demonstrated that natural materials contained additional substances, derivable from pyridoxine, but with much higher growth-promoting activity than pyridoxine.

Further work demonstrated⁸ that oxidation of pyridoxine yielded an aldehyde, and amination yielded an amine, both of which were highly active for microorganisms and for which there were only six possible structures. In a collaborative study, four of these possible structures were synthesised.



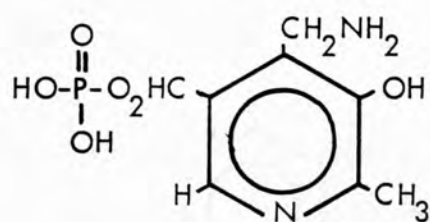
(4)

Pyridoxamine



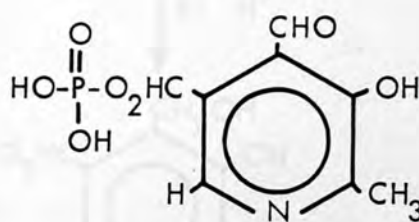
(5)

Pyridoxal



(6)

Pyridoxamine Phosphate



(7)

Pyridoxal Phosphate

Subsequent tests demonstrated⁹ that pyridoxal (5) and pyridoxamine (4) occur naturally, are more widely distributed than pyridoxine, and comprise most of the Vitamin B₆ of most natural material, and that they are

the coenzyme forms* of the vitamin.

While these studies were in progress, related findings pointed to certain functions of Vitamin B₆ in vivo. In 1944 Gale and Epps had discovered¹⁰ an unidentified coenzyme required for transamination and decarboxylation of various amino acids. Gunsalus et al¹¹, in 1944 identified this coenzyme as a phosphorylated pyridoxal. This was eventually proved¹² to be pyridoxal-5-phosphate (7). The location of the phosphoryl residue on the pyridoxal moiety remained in doubt for some years and was shown to be attached to the hydroxymethyl group of pyridoxal (5) by Baddiley and Mathias¹³. Their unambiguous synthesis from the alcohol pyridoxol** is outlined below:

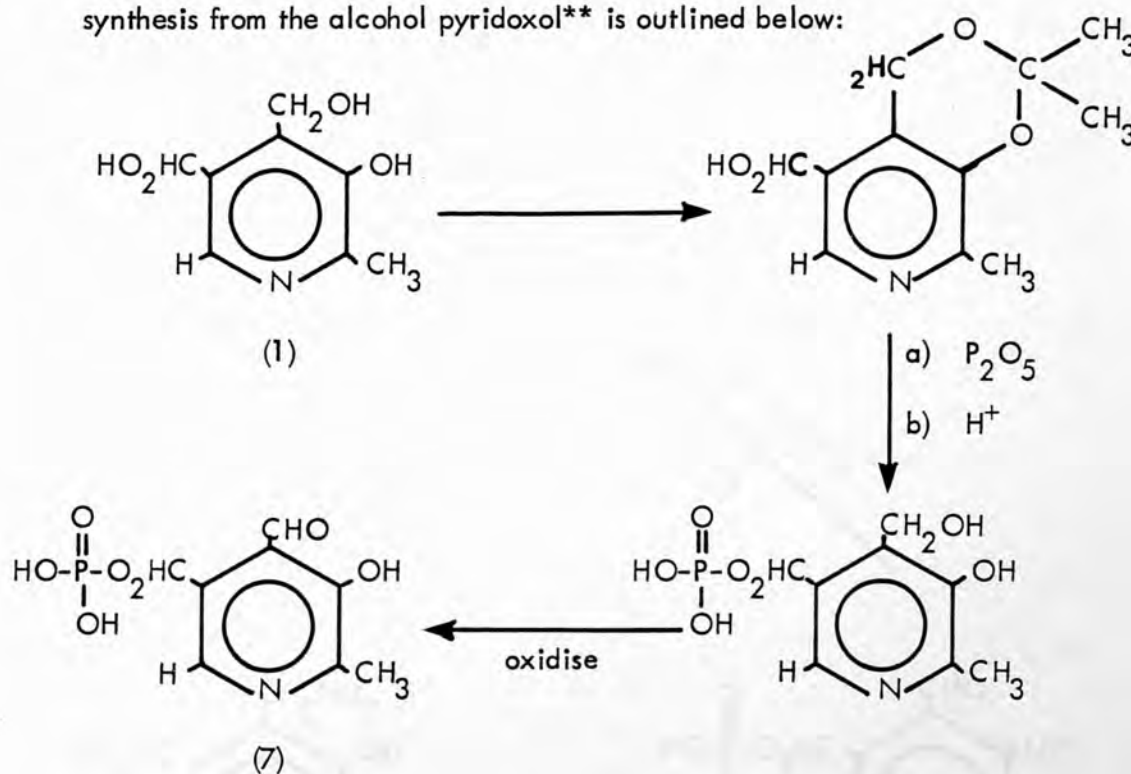


Fig. 1-2: Synthesis of Pyridoxal Phosphate from Pyridoxol

* A coenzyme is an additional substance required, by some enzyme substrate systems, in order that the reaction may proceed. The coenzyme is found to be unchanged at the end of the reaction. An enzyme is a protein with catalytic properties due to its power of specific activation.

** The alcohol of the Vitamin B₆ group is called pyridoxol; the aldehyde, pyridoxal; and the amine, pyridoxamine. The name pyridoxine will apply to the whole group of Vitamins B₆ when the exact constitution is not stated.

A fifth naturally occurring form of Vitamin B₆, pyridoxamine phosphate (6) was discovered¹⁴ by Rabinowitz and Snell by virtue of its differential activity in promoting growth of various microorganisms. Initially it was synthesised¹⁵ by nonenzymatic transamination of pyridoxal phosphate with glutamic acid. Pyridoxamine phosphate can be prepared either by direct phosphorylation of pyridoxamine or by catalytic hydrogenation of the oxime of pyridoxal phosphate¹⁶.

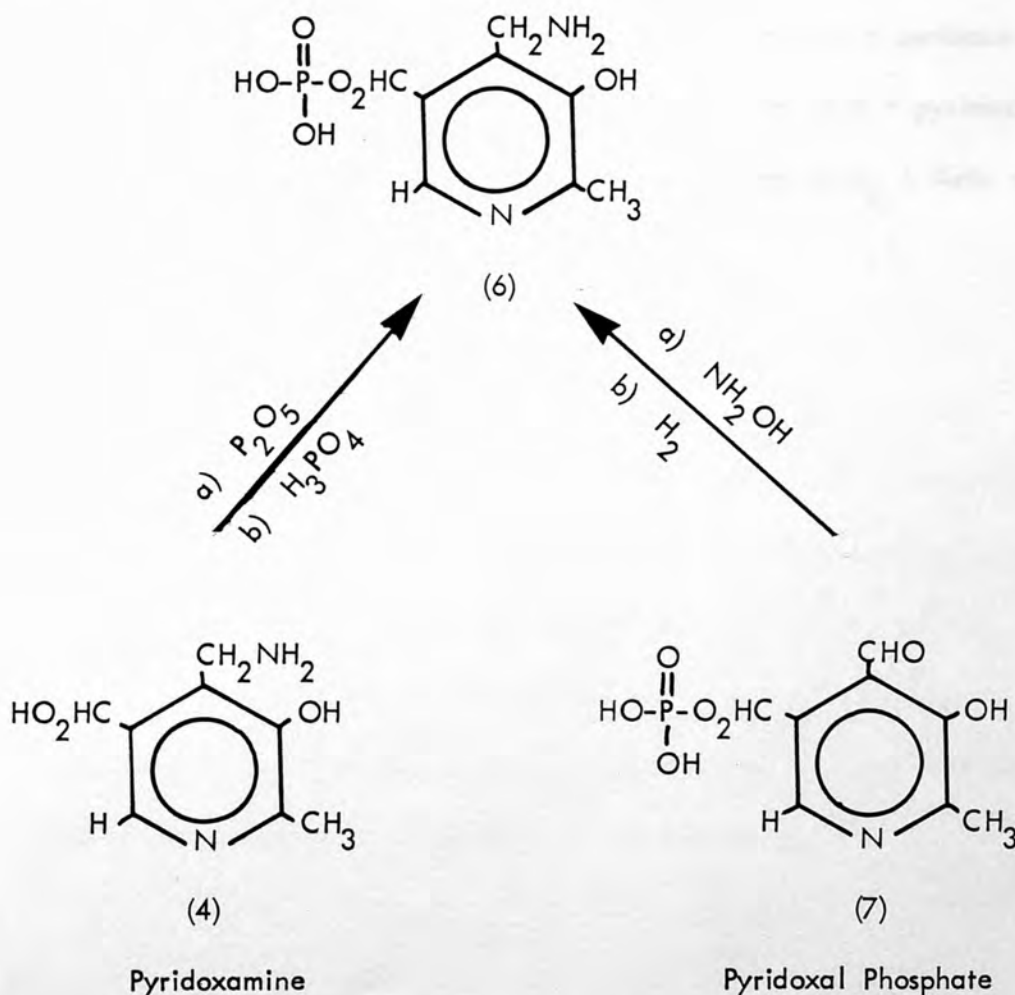
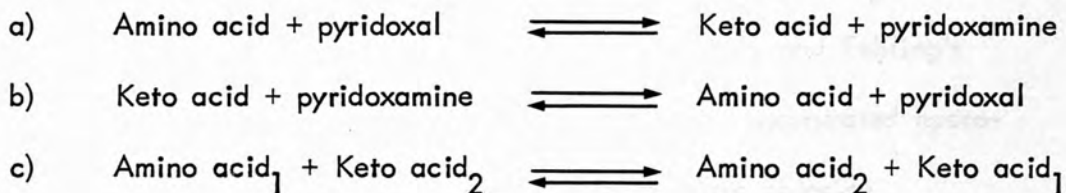


Fig. 1-3: Synthesis of Pyridoxamine Phosphate

A main functional role for Vitamin B₆ was suggested by the chemical behaviour of pyridoxal. In assessing the growth-promoting activity of this substance for various organisms, Snell and Rannefeld observed¹⁷ that autoclaving with amino acids changed its activity in a manner best explained by assuming the conversion to pyridoxamine. Further study by Metzler et al¹⁸ confirmed this and revealed that the transformation occurred via a fully reversible nonenzymatic transamination with any of a variety of amino acids. It was recognised that catalysis of transamination in vivo might result from two such coupled reactions:



1.2 Chemical and Physical Properties of Vitamin B₆

1.2.1 Chemical Properties:

Pyridoxine exhibits the properties of a stable hydroxylated weak nitrogen base. Birch and György found²⁰ that it was not precipitated from solution by salts of heavy metals such as those of lead, mercury, silver or platinum and not by picric acid, but was precipitated by phosphotungstic acid. It was not inactivated by nitrous acid. Hydrolytic agents such as mineral acids or aqueous alkali, hot or cold, do not affect the pyridoxine (Vitamin B₆). It is stable to the action of agents such as ethyl nitrite and Fehling's solution²¹. The pure substance is also stable to concentrated hydrochloric acid at elevated temperatures. With ferric chloride, pyridoxine reacts as a phenolic substance giving a reddish brown coloration, indicating the presence of a phenolic hydroxyl group. Colour reactions of Vitamin B₆ fall into two groups, namely, those which depend upon the phenolic nature of the vitamin and those which depend upon other functions of the molecule. In 1939 it was reported²² that Vitamin B₆ at high concentration in alkaline solution reacts with 2,6-dichloroquinon chlorimide and gives an immediate blue colour fading to reddish brown. This reaction was used as the basis for the colorimetric determination²³ of Vitamin B₆.

1.2.2 Physical Properties:

Pyridoxine hydrochloride ($C_8H_{11}O_3N \cdot HCl$) occurs as white platelets, with melting point about $204-206^\circ$ with decomposition. The free base of pyridoxine ($C_8H_{11}O_3N$) has a melting point of about 160° with no decomposition. The free base is optically inactive²¹. Both the base and hydrochloride readily sublime without decomposition.

The hydrochloride is freely soluble in water, but sparingly so in alcohol and acetone²⁴. The base is soluble in methanol and is not precipitated from methanol solution by ethyl ether²².

In 1943 Atkin et al discovered²⁵ the rapid destruction of pyridoxine by light in neutral and alkaline solution. This phenomenon was investigated quantitatively by physical, chemical and microbiological methods. The results and the amount of losses of pyridoxine (μg) are given in Table 1-1. During their investigation they also observed a little loss of pyridoxine in 0.1N hydrochloric acid ($pH = 1.0$).

Table 1-1: Destruction of Pyridoxine by Light in Aqueous Solution

Irradiation ^a			Pyridoxine μg		
period hours	pH	Type	Calc. from extinction coefficient ^b	By chemical test	By micro- biological test
0	6.8	Artificial ^c	25	25	25
1	6.8	"	23	23	-
4	6.8	"	18	18	-
9	6.8	"	12	12	14
20	6.8	"	5 ^d	4	-
52	6.8	"	0.8 ^d	0.3	0.1
0	6.8	Natural ^e	25	25	25
12	6.8	"	17	17	-
24	6.8	"	13	13	13
36	6.8	"	11	11	-
9	6.8	Artificial	12	12	14
9	1.0	"	24	24	22
9	13.0	"	20 ^d	11 ^f	12

- a) The temperature for the artificial irradiation varied from 35-40° and for the natural irradiation from 15-20°. Controls in the dark at 90° for 24 hours showed no pyridoxine loss.
- b) Absorption Curves were obtained for all the solutions, adjusted to pH=6.8. The extinction coefficients were calculated from the values for maximal absorption at 30800 cm^{-1} .
- c) In the irradiation experiments with artificial light the solutions were exposed in an open beaker 8 inches below a 300 watt bulb mounted in a white reflector.
- d) Distorted absorption curves were obtained for these solutions owing to the presence of decomposition products which also absorbed in the ultraviolet region.
- e) In the irradiation experiments with natural light the solutions were exposed to bright diffuse daylight.
- f) This solution showed considerable colour development with 2,6-dichloroquinone chloroimide reagent. However, much of this colour was found to be due to compounds other than pyridoxine.

The tautomeric properties of pyridoxine are well illustrated²¹ by changes in its ultraviolet absorption produced by varying the hydrogen ion concentration. The single maximum at 2925 Å at pH=2 diminishes in intensity at pH=4.5, and concomitantly a new maximum appears at 3275 Å. This latter band maximum increases in intensity when the pH is changed to 6.75, and the maximum at 2925 Å disappears but a new band appears at 2560 Å. When the pH is further raised to 10.2, both remaining bands increase in intensity and shift to shorter wavelengths. The nature of this tautomerism is discussed further by Harris et al²⁶.

Spectra and ionization of pyridoxine, pyridoxal, pyridoxamine and their respective phosphates have been investigated by Lunn et al²⁷, Christensen²⁸, Anderson et al²⁹ and Matthews³⁰. Their results are shown in Table 1-2:

Table 1-2: Acid dissociation constants of pyridoxal and various analogues

Compound	pKa ₁	pKa ₂	pKa ₃	pK'a ₃	pKa ₄	Ref.
Pyridoxine	5.00	8.60	-	-	-	31
	5.00	8.96	-	-	-	27
Pyridoxal	4.20	8.66	-	-	-	30
	4.23	8.70	-	-	-	30
Pyridoxamine	3.31	7.90	10.4	-	-	30
	3.54	8.21	10.6	-	-	31
	-	8.08	10.3	-	-	27
Pyridoxal phosphate	2.5	4.14	-	6.20	8.69	31
	-	4.00	-	6.40	8.40	28
	1.4	3.44	-	6.01	8.45	29
	1.89	3.73	-	6.32	8.69	29
	1.6	3.58	-	5.75	8.17	29
Pyridoxamine phosphate	2.5	3.69	-	5.76	8.61	31

Williams et al³¹ assigned $pK'a_3$ to the ionization of the secondary phosphate hydrogen. The ionization of the pyridine ring occurs in the course of excitation of the cationic species of the compounds, owing to the marked decrease of the pK values in the excited state³²⁻³³.

In addition to the change in spectra caused by proton uptake, the situation in the case of pyridoxal is complicated by hemi-acetal formation, and Metzler et al³⁴ suggested that the reason for the apparent effectiveness of pyridoxal phosphate compared to pyridoxal was due mainly to the fact that the pyridoxal phosphate would not exist in such a hemiacetal formation:



Fig. 1-4. Equilibrium forms of pyridoxal in aqueous solution.

1.3 Relation Between Chemical Structures of Vitamin B₆-Type

Compounds and their Catalytic Activity

1.3.1 Equilibrium Forms of Vitamin B₆ in Aqueous Solutions:

In aqueous solutions pyridoxal and related compounds exist in a variety of forms, depending upon pH, temperature and other factors. Spectral shifts with pH revealed²⁶⁻³⁴ that pyridoxine, for example, exists as the cation, in acidic solution (8), as the neutral form (1) (10) (primarily as the dipolar ion (10)) at pH 7.0, and as an anion (9) in alkaline solution. Figure 1-4 shows the four different forms of pyridoxine:

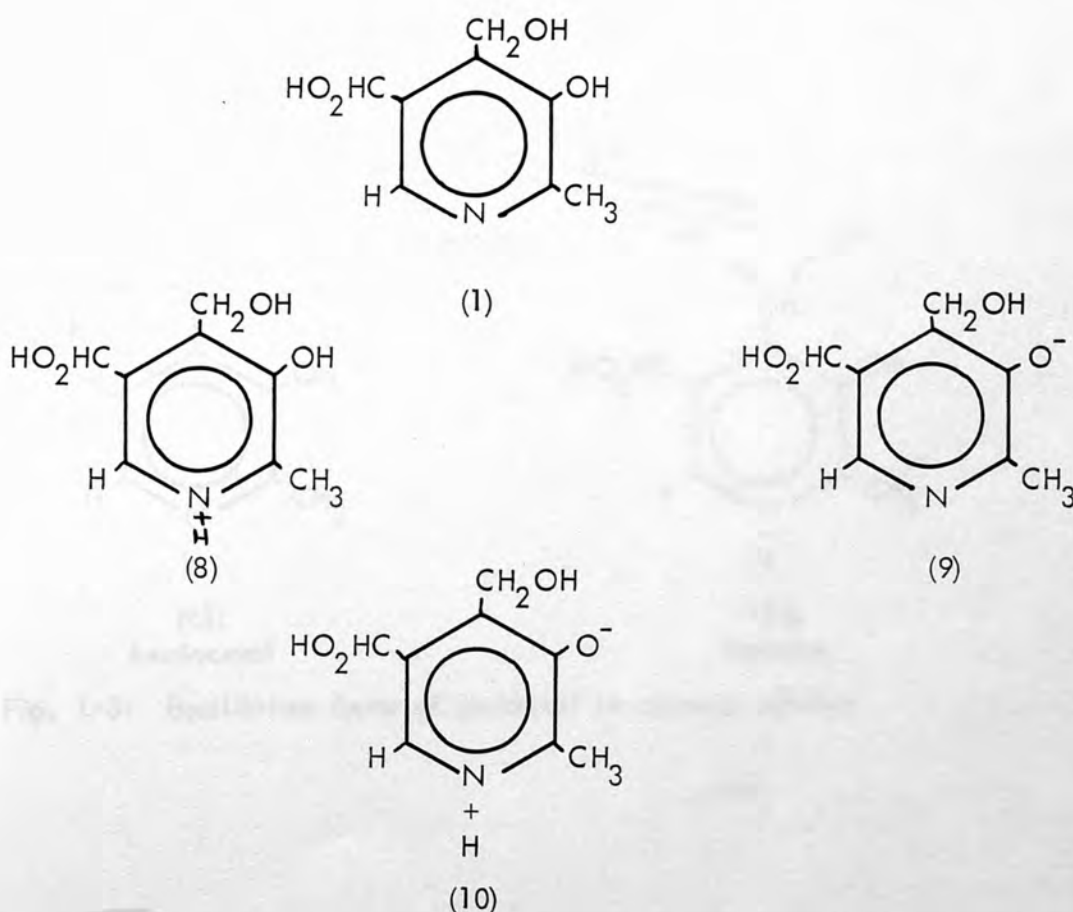


Fig. 1-4: Equilibrium forms of pyridoxine in aqueous solution

A similar situation exists with pyridoxamine, but in a physiological range of pH values. The aminomethyl group in position "4" also carries a proton and is positively charged. A more complex situation exists with pyridoxal³⁴ which may exist in any of several additional forms made possible by hemiacetal formation (11) or hydrated forms (12):

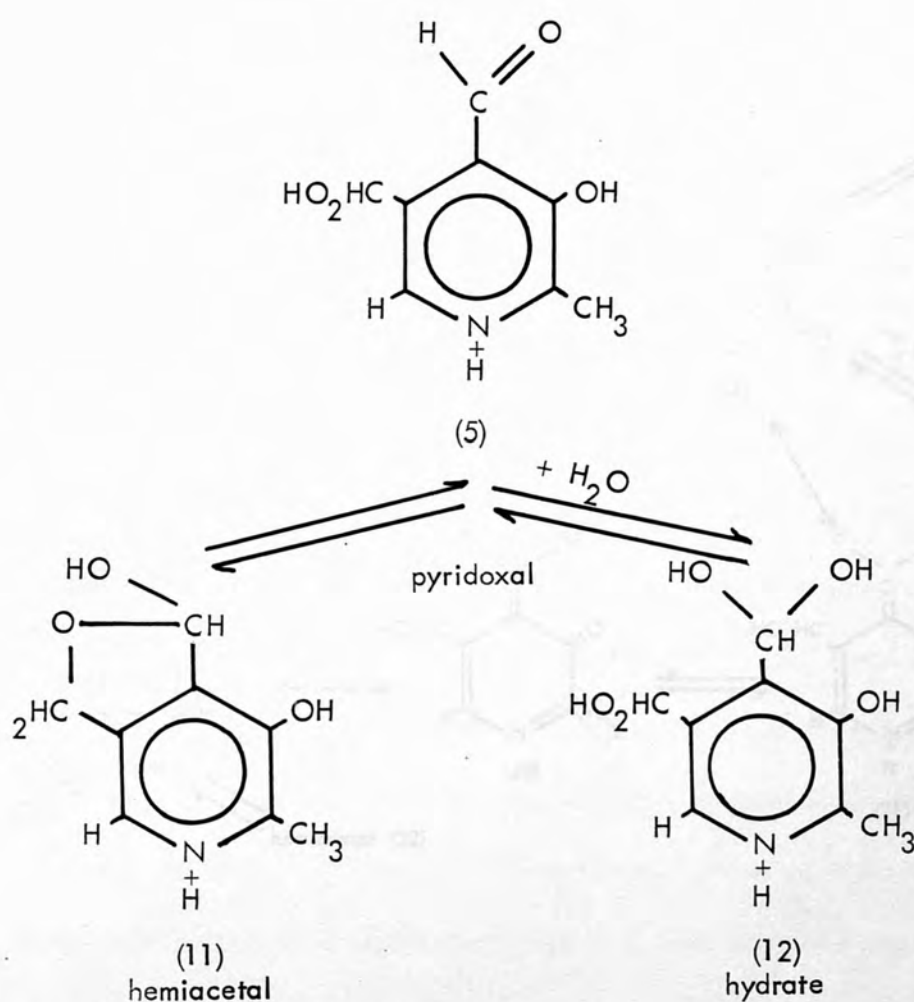


Fig. 1-5: Equilibrium forms of pyridoxal in aqueous solution

Fig. 1-5 (continued)

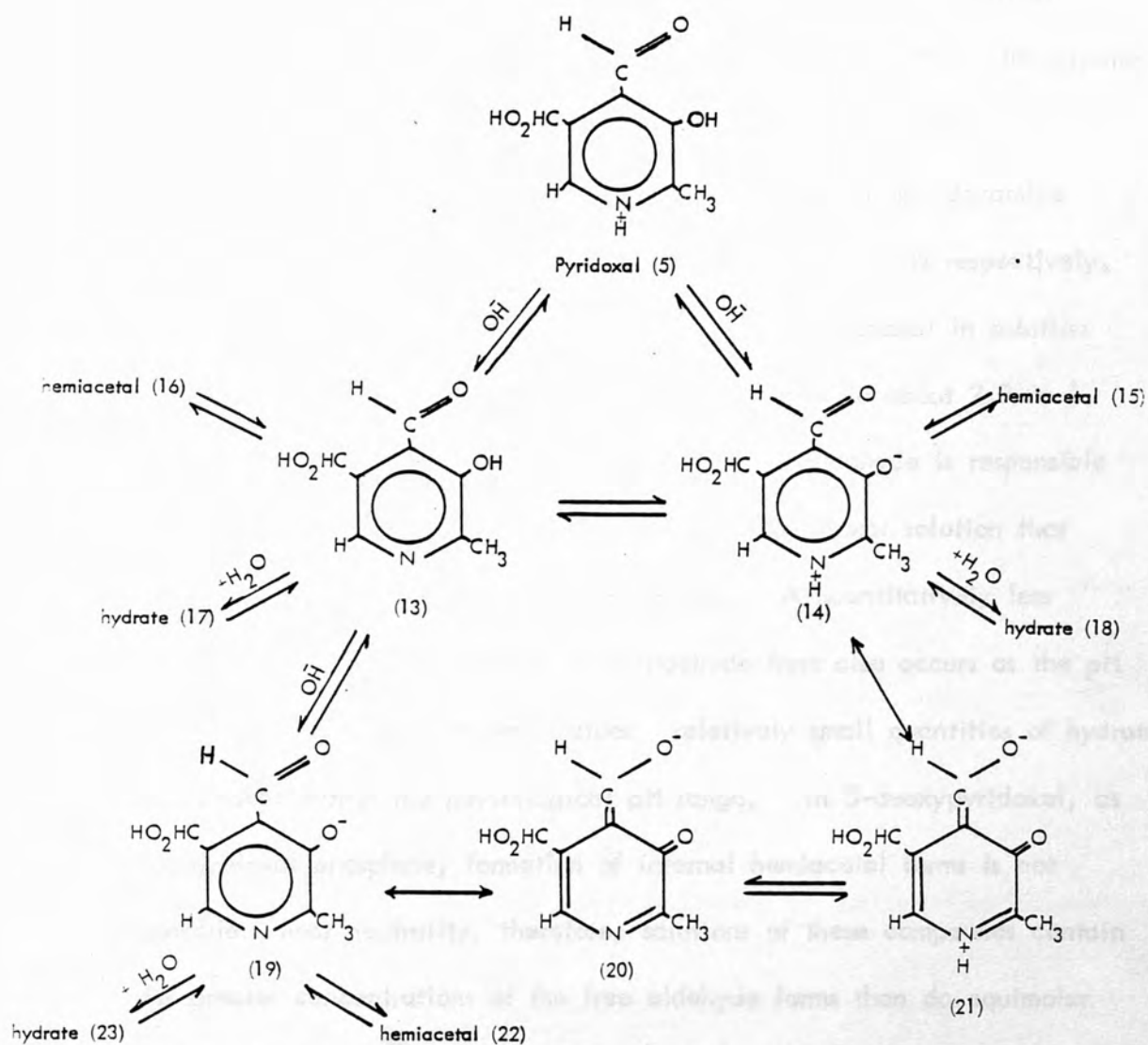


Fig. 1-5: Equilibrium forms of pyridoxal in aqueous solution

Figure 1-5 shows the various forms of pyridoxal in aqueous solution, in hemiacetal formation (11,15,16,22) or hydration (12,18,17,23). Cationic (5), neutral (14) or anionic (19) forms predominate at acidic, neutral or alkaline pH values. Spectral measurements show that at neutrality, solutions of pyridoxal contain approximately 92% of the dipolar ionic form (14) and only about 8% of nonpolar structures (13).

The corresponding percentages of pyridoxine and pyridoxamine present in dipolar ionic forms at pH 7.0 are 88% and 97% respectively. The ratio of hemiacetal to free aldehyde forms of pyridoxal in solution is approximately 80 to 1 at neutrality but decreases to about 2.8 to 1 at pH = 10. This shift from hemiacetal to free aldehyde is responsible for the progressive and reversible yellowing of pyridoxal solution that occurs as the pH is shifted to higher values. A quantitatively less important shift from hydrated to free aldehyde form also occurs as the pH is shifted from acid to neutral values; relatively small quantities of hydrate are present within the physiological pH range. In 5-deoxypyridoxal, as in pyridoxal phosphate, formation of internal hemiacetal forms is not possible: near neutrality, therefore, solutions of these compounds contain far greater concentrations of the free aldehyde forms than do equimolar pyridoxal solutions³⁴. Since the free aldehyde form of these compounds is that participating in catalysis (see page 5), one excellent chemical reason for the presence of an esterified phosphate group in pyridoxal phosphate emerges quite distinct from its necessity for effective combination between coenzyme and apoenzyme. Except for this difference, ionic forms of pyridoxal phosphate and pyridoxamine phosphate in solution appear to resemble those of pyridoxal and pyridoxamine respectively, at equivalent

pH values. At physiological pH values, both dissociable hydrogens on the phosphate residue are ionized. Available pK values for various dissociations of these compounds are summarized in Table (1-3). In most instances, these can be assigned chiefly to ionization of single groups in the molecule³¹.

Table 1-3: pK values for various forms of Vitamin B₆

Compound	pK ₁	pK ₂	pK ₃	pK ₄
Pyridoxine	5.00 ^{b,c}	8.96 ^b , 8.97 ^c	-	-
Pyridoxal	4.20 ^a , 4.23 ^b	8.66 ^a , 8.70 ^b	13.00 ^a	-
Pyridoxamine	3.31 ^a , 3.54 ^b , 3.4 ^c	7.90 ^a , 8.21 ^b	10.4 ^a , 10.63 ^b	-
Pyridoxal phosphate	2.5 ^{b,d}	4.14 ^{b,f}	6.20 ^{b,g}	8.69 ^{b,h}
Pyridoxamine phosphate	2.5 ^{b,d}	3.25 ^{a,e} , 3.69 ^{b,e}	5.76 ^{b,g}	8.61 ^{b,h}

- a) Metzler and Snell JACS, (1955), 77, 2431.
- b) Williams and Neilands, Arch. Biochem. Biophys., (1954), 53, 56.
- c) Lunn and Morton, Analyst, (1952), 77, 718.
- d) Due to ionization of phosphate group.
- e) Corresponds to pK₁ of pyridoxamine.
- f) Corresponds to pK₁ (primarily ionization of the phenolic hydroxyl) of pyridoxal.
- g) Due to ionization of secondary hydrogen of the phosphate group.
- h) Corresponds to pK₂ (primarily ionization of pyridinium nitrogen) of pyridoxal and pyridoxamine.

1.3.2 Schiff Base Formation Between Pyridoxal or Pyridoxal Phosphate and Amino Acids:

When solutions of pyridoxal and amines are mixed, an immediate yellowish colour occurs indicative of a chemical reaction, which, by analogy with the long recognized reactions between amines and other aldehydes, was recognized to represent Schiff's base (imine) formation, which appears to be hydrogen-chelated. An accompanying product with maximum absorption at 35970 to 35000 cm^{-1} probably has the same structure, but lacking the double bond in conjugation with the ring, possibly because of hydration to the carbinolamine. In addition the yellow Schiff base passes gradually over to a variable extent to a third type of Schiff base in which the H-bonding is believed to be lost so that the 3-hydroxypyridine structure is in the zwitterionic form. In this product the bathochromic effect of aldimine double bond is small or absent, perhaps also because of conversion to the carbinolamine. Upon protonation spectrophotometric evidence for the reversion to the hydrogen-bonded form is obtained. The conversion to the non-hydrogen bonded form is attributed to the electron-attracting action of vicinal groups, especially the carbonyl group of amino acid esters.

Pyridoxal phosphate behaves in a manner entirely similar to pyridoxal³⁵. Imine formation between pyridoxal phosphate and amino acids occurs even more extensively than with pyridoxal. The limited comparative data available indicate that this more ready reaction is due exclusively to the higher concentration of free aldehyde present in a solution of pyridoxal phosphate³⁴. Imine formation can be promoted by use of nonpolar solvents and crystalline imines of pyridoxal are

isolated readily from these solvents³⁶.

Study of the reactions of pyridoxal, analogous to enzymic reactions, led Snell³⁷ and Braunstein³⁸ to postulate the following mechanism for the Schiff base formation in Figure 1-6:

The interaction of pyridoxal and its analogues with α -amino acids gives Schiff bases which may exist in two tautomeric forms (24)(25). The Schiff bases can then yield pyridoxamine and α -keto acid, on hydrolysis:

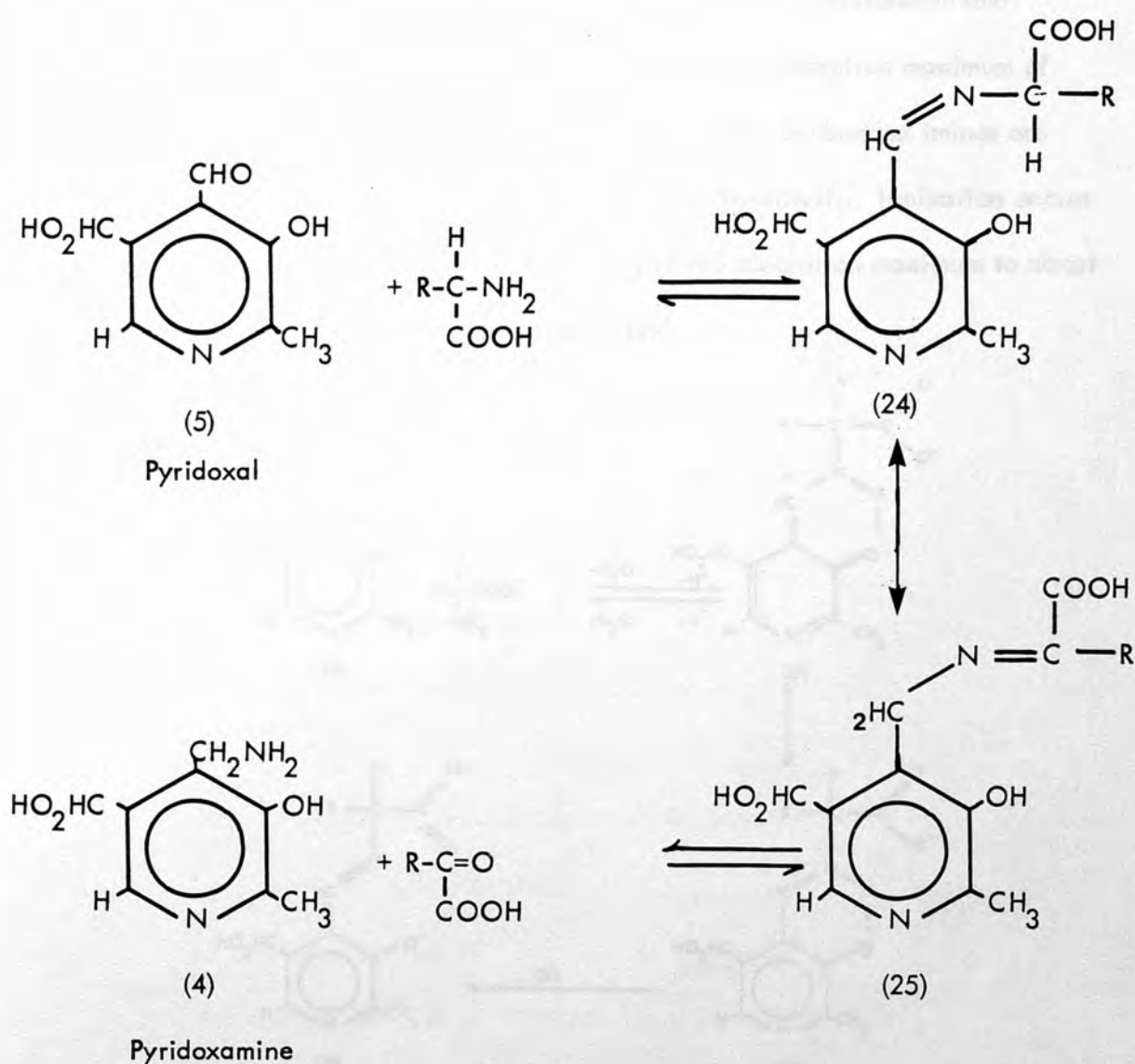


Fig. 1-6: Interaction of pyridoxal and amino acid and formation of Schiff-base.

There are about twenty specific reactions of amino acids involving pyridoxal and pyridoxal phosphate. Although each of these reactions is catalyzed by a different, specific enzyme, pyridoxal and pyridoxal phosphate (coenzymes) are necessary in all of them, they weakly bond to the enzymes forming Schiff bases which have such orientation so as to facilitate the displacement of the amino group of the enzymes by an amino acid³⁹.

The equilibrium position of this reaction in aqueous solution has been investigated by Metzler⁴⁰ for pyridoxal. In the neutral range of pH the imines appear to be hydrogen-bonded structures that can exist in tautomeric (and resonance) forms (27)(28) and have the characteristic absorption maximum of about 24150 cm^{-1} . Detectable amounts of the hydrogen-bonded imines are present even at $\text{pH} = 2.0$; acid conditions favour hydrolysis. Ionization occurs ($\text{pK} 10.5$) on addition of alkali with a shift in the absorption maximum to about 27400 cm^{-1} corresponding to formation of (29):

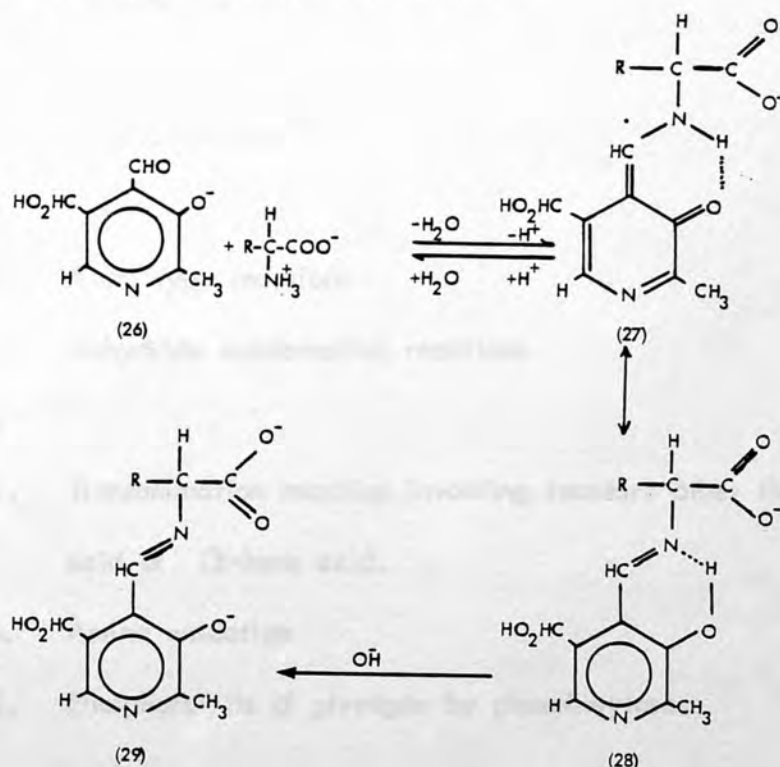


Fig. 1-7: Equilibrium forms of Schiff-base in neutral solution

Representative values of the equilibrium constant, $K = \frac{[\text{imine}^-]}{[\text{pyridoxal}^-][\text{amino acid}^-]}$ for various amino acids vary from a low of 1.6 for α -aminoisobutyric acid to 44 for valine.

These findings demonstrate conclusively that significant concentrations of pyridoxal imines are formed under physiological conditions in dilute aqueous solutions, as was postulated for both nonenzymatic⁴¹ and enzymatic⁴² reactions in which pyridoxal participates.

Schiff base (imine) can undergo four types of reaction:

TYPE I:

- A. Transamination³⁷
- B. Racemization⁴³
- C. α, β Elimination and addition reactions⁴⁴
- D. γ Elimination⁴⁴
- E. Cleavage reactions⁴⁴

TYPE II:

- A. Decarboxylation⁴⁵

TYPE III:

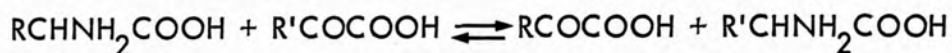
- A. Aldol type reactions
- B. Anhydride condensation reactions

TYPE IV:

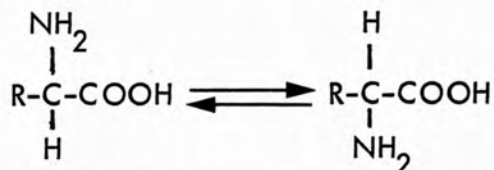
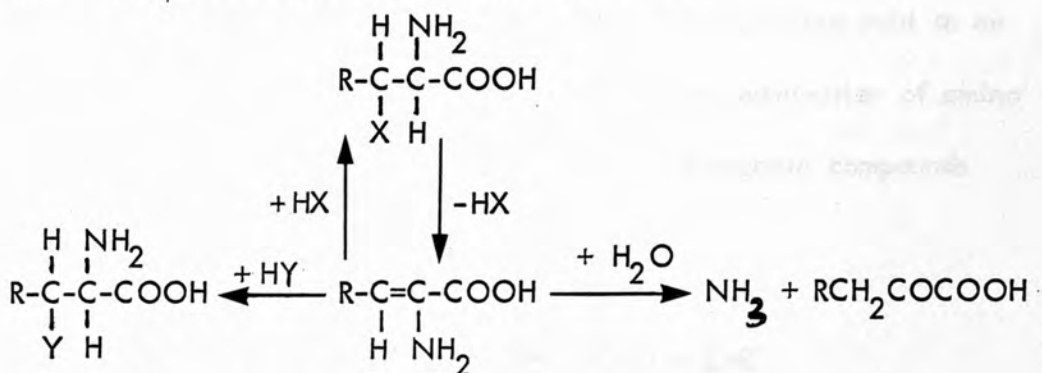
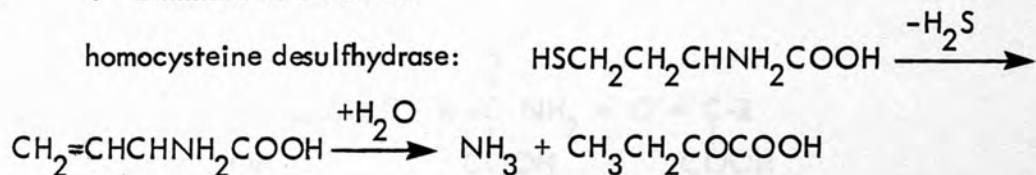
- A. Transamination reaction involving reactant other than α -amino acid or α -keto acid.
- B. Amine oxidation
- C. Phosphorolysis of glycogen by phosphorylase.

TYPE I e.g.

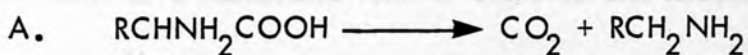
A. Transaminases:



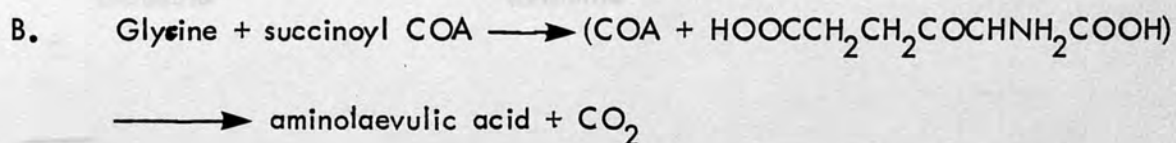
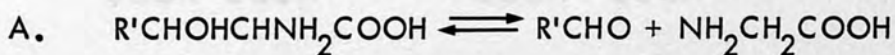
B. Racemases:

C. α, β Elimination and addition reaction:D. γ -Elimination reaction:E. Aspartate \longrightarrow CO_2 + alanine

TYPE II e.g.



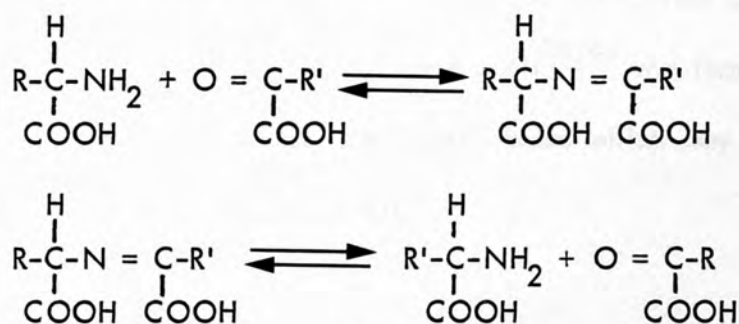
TYPE III e.g.



TYPE IV:

- A. Imidazole acetal phosphate + glutamate \rightleftharpoons
 Histidinol phosphate + α -ketoglutarate
- B. Amino oxidation: $RCH_2NH_2 + [O] \longrightarrow RCHO + NH_3$
- C. Phosphorolysis of glycogen by phosphorylase

The transamination reaction is a most prominent reaction of Schiff base reactions. In 1945 transamination reaction was defined³⁷ as "the intermolecular transfer of an amino group from an α -amino acid to an α -keto acid". This is referred to as oxidative deamination of amino acids which may be brought about by a variety of organic compounds containing the carbonyl grouping:



This intermediate molecule $\begin{array}{c} \text{H} \\ | \\ \text{R}-\text{C}-\text{N}=\text{C}-\text{R}' \\ | \quad | \\ \text{COOH} \quad \text{COOH} \end{array}$ which is the Schiff base,

can exist as a tautomeric form of aldimine and ketimine.



"aldimine"

"ketimine"

1.3.3 Physical Properties of the Schiff Bases derived from Pyridoxal and Related Compounds:

Each yellow Schiff base formed when pyridoxal reacts with amino acids has its H^+ -dissociation oddly displaced from its position in pyridoxal. A pK of 10.5 is ascribed by Metzler⁴⁰ to the phenolic group (4.2 in pyridoxal), H-bonding to the imine-N serving to explain both the firmness with which this H^+ is held and the presence of an absorption band about 24000 cm^{-1} . An additional consequence is the dissociation of the pyridinium- H^+ at about pH 5.9 rather than at 8.6 as in pyridoxal.

The spectral changes with pH may be interpreted as follows. In terms of the studies of Metzler and Snell^{34,40} the forms of the pyridoxal or pyridoxal phosphate Schiff's bases which may affect the spectra are shown in Figure (1-8):

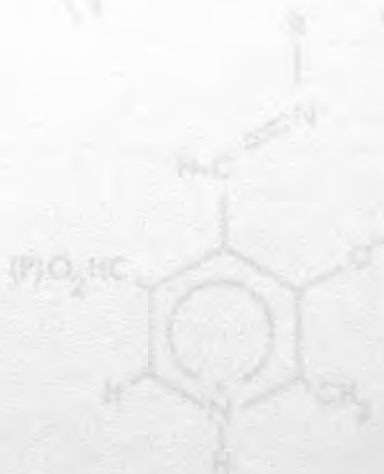


Fig. 1-8. The ionization of pyridoxal phosphate Schiff's base.

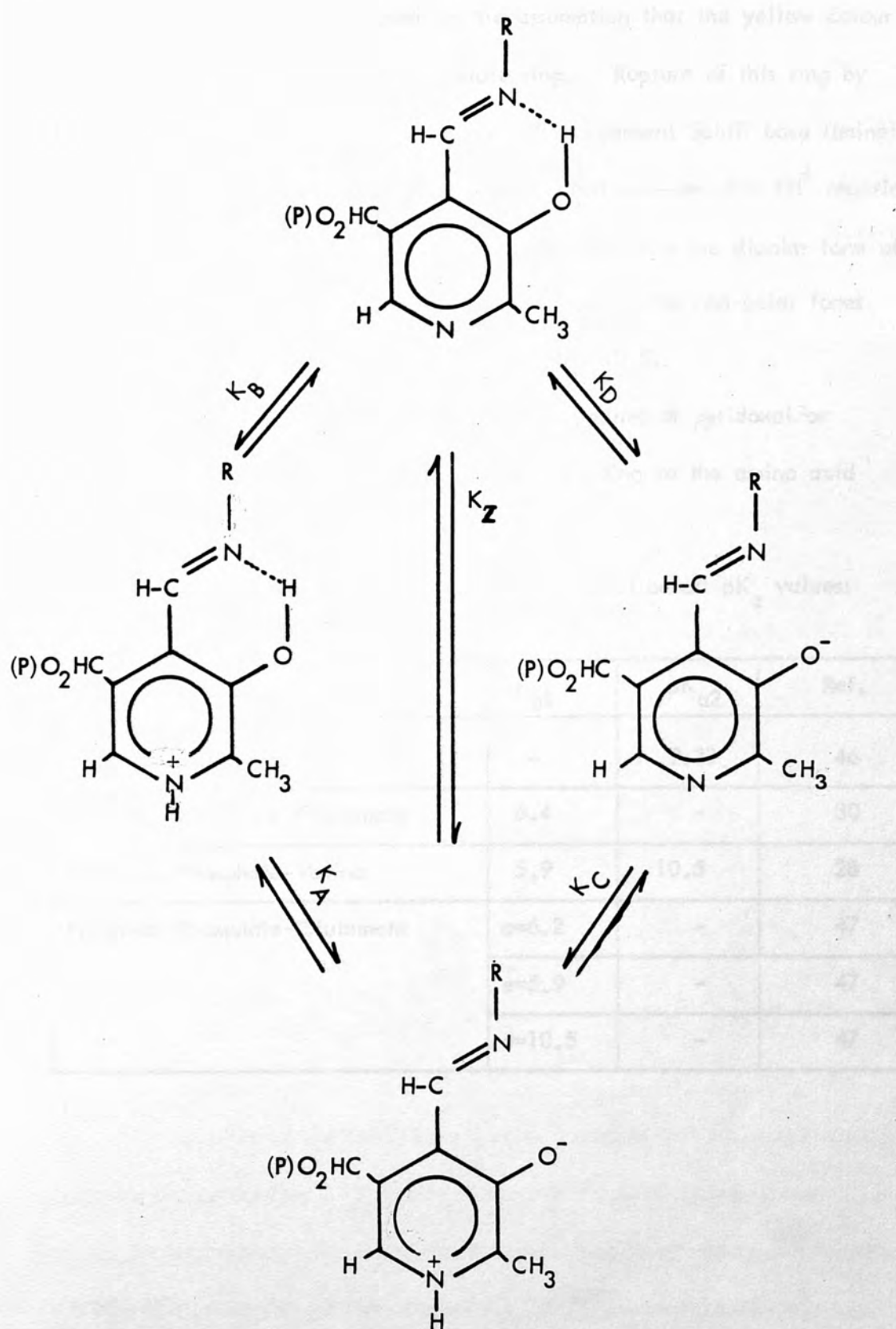


Fig. 1-8: The ionization of pyridoxal phosphate imines

These equations are based on the assumption that the yellow colour may be ascribed to the hydrogen chelate ring. Rupture of this ring by a change in pH results in loss of colour. For a general Schiff base (imine) the pH is quoted as being 6 for the overall $\text{=NH}^+ \longrightarrow \text{-N= +H}^+$ reaction. A pK_A of 6.2 for this colour change suggests that it is the dipolar form of the imine which occurs at neutrality, in contrast to the non-polar forms of the imines studied by Metzler⁴⁰ ($\text{K}_B=5$, $\text{pK}_D=10.5$).

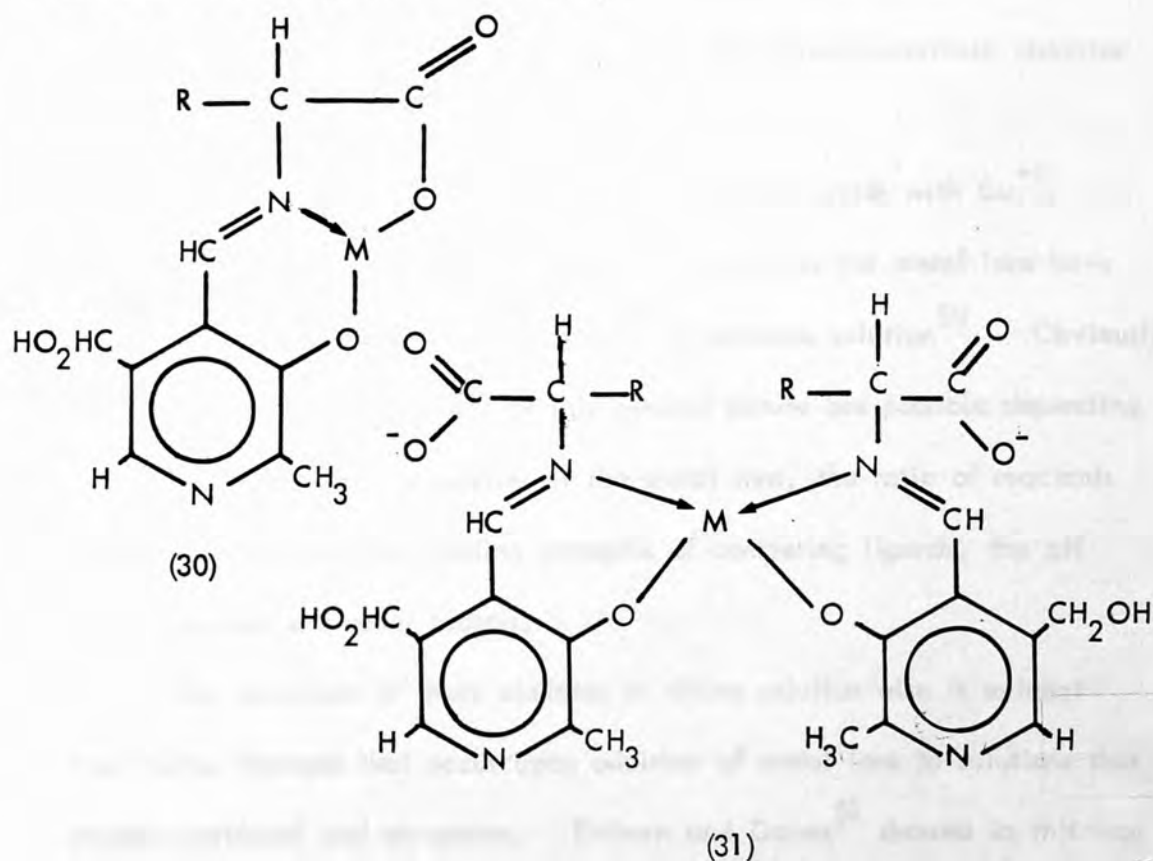
The pK_a s for the various Schiff bases (imine) of pyridoxal or pyridoxal phosphate with amino acids vary according to the amino acid used.

Table (1-4) sets out examples of some Schiff bases' pK_a values:

S.B.	pK_{a1}	pK_{a2}	Ref.
Pyridoxal-Glutamate	-	9.33	46
Pyridoxal Phosphate-Glutamate	6.4	-	30
Pyridoxal Phosphate-Valine	5.9	10.5	28
Pyridoxal Phosphate-Glutamate	a=6.2	-	47
	e=5.9	-	47
	d=10.5	-	47

1.3.4 Formation of Schiff Base-Metal Chelates:

Pyridoxal, like salicylaldehyde, is an aromatic aldehyde with an ortho phenolic group. By following the rates of nonenzymatic transamination reactions in aqueous solution, Metzler and Snell¹⁸ showed that the rate constant was greatly enhanced by the addition of certain metal ions. It was postulated that Schiff bases form at least two types of stable metal chelates, those with 1:1:1 ratio (pyridoxal, amino acid, metal ion) complexes apparently similar to (30) and 2:2:1 ratio complexes similar to (31):



The stability of the Schiff base species increases with the ring formation⁴⁸.

The more planar the ring is, the more stable the metal-Schiff base complex.

In the nonenzymatic transamination reactions catalyzed by metal ions, the essential groups for the formation of the Schiff base-metal intermediates are the aldehyde group, the hydroxy group and the heterocyclic nitrogen.

The aldehyde group is bound to the amino acids forming the Schiff-base which is stabilized by chelation with the metal ion via the phenolic oxygen, the carboxyl group of the amino acid and the nitrogen of the azomethine linkage. The chelation of the metal ion with the ring gives a planar conjugated intermediate. This intermediate assists in the displacement of the electron pair from the α -carbon atom of the amino acid to the metal which acts as an electron-attracting species. This is similar to the effect of the heterocyclic nitrogen, as Metzler⁴⁹ suggested. The metal ion catalysis involves two interconvertible chelates: an aldimine and a ketimine.

Several such chelates of pyridoxal and amino acids with Cu^{++} , Ni^{++} , Zn^{++} , Mn^{++} , Mg^{++} , Al^{+++} , Fe^{+++} ... etc. as the metal ions have now been isolated from either alcoholic³⁶ or aqueous solution⁵⁰. Obviously many closely related structures of this general nature are possible depending upon the co-ordination properties of the metal ions, the ratio of reactants present, the comparative binding strengths of competing ligands, the pH of the solution and other factors.

The formation of these chelates in dilute solution also is evident from colour changes that occur upon addition of metal ions to solutions that contain pyridoxal and an amine. Eichorn and Dawes⁵¹ showed in this way formation of a 2:2:1 alanine, pyridoxal, nickel chelate in solution. Chelate formation occurred similarly in solutions of pyruvate, pyridoxamine, and nickel ion. On standing, spectra of the two solutions became indistinguishable as transamination proceeded in each case to yield an equilibrium mixture of alanine, pyruvate, pyridoxal, pyridoxamine, and their complexes. Similarly

Fasella et al⁵² were able to separate both a 2:2:1 alanine, pyridoxal, Al⁺⁺⁺ chelate and a 2:2:1 pyruvate, pyridoxamine, Al⁺⁺⁺ chelate with paper chromatography. With Cu⁺⁺ and pyridoxal phosphate replacing pyridoxal and Al⁺⁺⁺ in this solution, a 1:1:1 amino acid, pyridoxal phosphate, Cu⁺⁺ complex and 1:1:1 keto acid, pyridoxamine phosphate, Cu⁺⁺ complexes were separated by the same technique.

Although consistent with the interpretation that metal chelates serve as intermediates in transamination, these findings do not prove such a role since formation of chelates might be incidental to, rather than prerequisite for, the appearance of pyridoxamine and pyruvate in solution. That metal chelates do serve an intermediary role was shown by Longenecker and Snell⁵³. They found that transamination between α -ketoglutarate and L-alanine produced an excess of L-glutamate. This requires that the reaction proceeds through an asymmetric intermediate that is readily provided if chelation occurs, but can not otherwise be explained. The catalytic activities of various metal ions also fall in the order of their known chelating tendencies towards ligands related to the reactants⁵⁴.

Eichorn and Dawes⁵¹ found out by various experiments and claimed that the formation of a Schiff base must occur before chelation with the metal ion, and the prior formation of metal-amino acid chelate is said to inhibit the reaction almost completely.

1.3.5 Structural Features of Vitamin B₆ and Related Compounds
Required for Catalysis of Non-enzymatic Transamination

The occurrence of rapid, metal-ion catalyzed, nonenzymatic transamination reactions between pyridoxal and amino acids¹⁸ has been referred to earlier. By providing an experimental system in which the ability of various aldehydes to undergo transamination can be compared, the nonenzymatic reaction has contributed greatly to our knowledge of mechanism of, and structure requirement for, transamination.

There are five features of the pyridoxal molecule to be considered in relating its structure to its catalytic activity. These are the presence and position of (1) the heterocyclic pyridine ring, (2) the methyl group, (3) the phenolic hydroxyl group, (4) the formyl (aldehyde) group, and (5) the hydroxymethyl group.

The study summarized in Table (1-5) permits partial assessment of the importance of each of these groupings for the overall transamination reaction⁴².

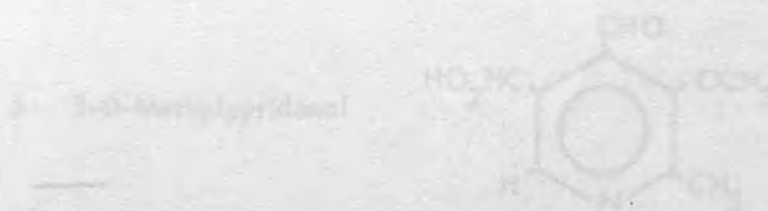
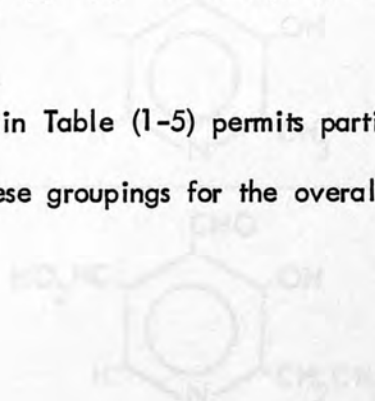


Table 1-5: Relation of Structure to Ability of Aldehydes to React with Glutamate to form α -Ketoglutarate

Aldehyde	Structure	Ketoglutarate formed*	
		+Alum	-Alum
1 Pyridoxal		+++	+
2 5-Deoxypyridoxal		+++	+
3 Pyridoxal-5'-Phosphate		+++	+
4 ω -Methylpyridoxal		+++	+
5 Isopyridoxal		-	-
6 3-O-Methylpyridoxal		-	-

Table 1-5 (continued)

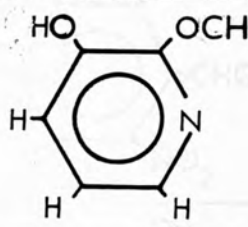
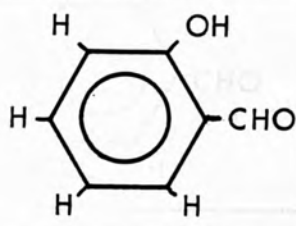
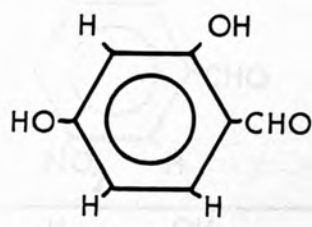
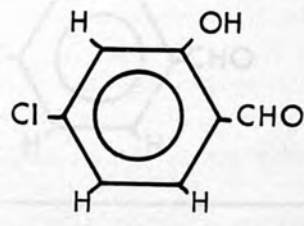
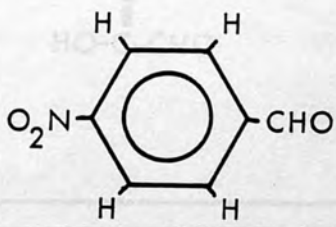
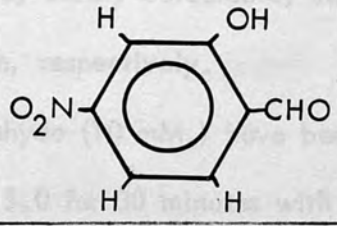
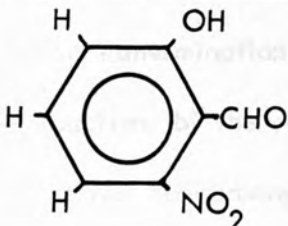
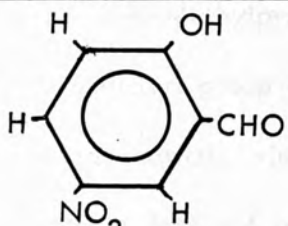
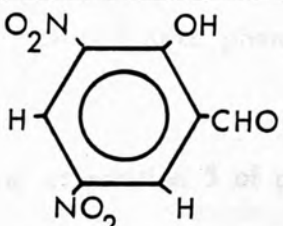
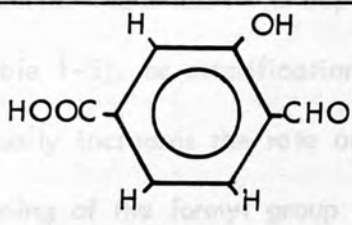
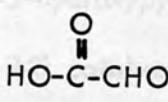
Aldehyde	Structure	Ketoglutarate formed*	
		+Alum	-Alum
7 2-Formyl-3-hydroxypyridine		+++	-
8 Salicylaldehyde		-	-
9 2,4-Dihydroxy-salicylaldehyde		-	-
10 2-Hydroxy-4-chlorosalicylaldehyde		-	-
11 p-Nitrobenzylaldehyde		±	±
12 4-Nitrosalicyl-aldehyde		+++	-

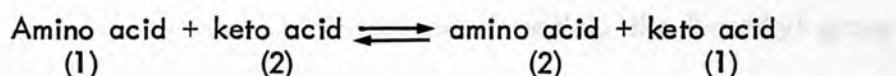
Table 1-5 (continued)

Aldehyde	Structure	Ketoglutarate formed*	
		+Alum	-Alum
13 6-Nitrosalicyl-aldehyde		+++	+
14 5-Nitrosalicyl-aldehyde		-	-
15 3,5-Dinitrosalicyl-aldehyde		-	-
16 4-Carboxysalicyl-aldehyde		-	-
17 Glyoxylic acid		+++	-

* -, $\frac{+}{-}$, +, and +++ signify no, barely detectable, slight and copious formation of α -Ketoglutarate, respectively.

Glutamate (10 mM.) and aldehyde (10 mM.) have been heated in water solution at 100°C, and pH = 5.0 for 30 minutes with or without potassium alum (1 mM.).

The primary importance of the aldehyde group of pyridoxal for the reaction of (page 7):



is evident from its conversion during transamination to the aminomethyl group of pyridoxamine; in the reverse reaction (b) the reverse transformation occurs. Neither pyridoxine nor any other known noncarbonyl compound can function in promoting the forward reaction. 3-O-Methylpyridoxal (compound 6 in Table 1-5), in which the phenolic hydroxyl group has been converted to a methyl ether, does not undergo transamination; similarly p-nitrobenzaldehyde, unlike 4- or 6-nitrosalicylaldehyde does not promote ketoglutarate formation from glutamate. An unsubstituted phenolic group is thus essential for the reaction.

The hydroxymethyl group at position 5 of pyridoxal apparently does not contribute to the chemical reaction. Its replacement by a methyl group (compound 2 in Table 1-5), or esterification with phosphate to yield pyridoxal phosphate, actually increases the rate of ketoglutarate production, it makes impossible screening of the formyl group through hemiacetal formation. Similarly, 2-formyl-3-hydroxypyridine (compound 7) and 4-nitrosalicylaldehyde (compound 12) catalyze the reaction although they lack a corresponding group. Although it is thus non-essential for chemical transamination, the hydroxymethyl group is essential for coenzymatic and vitamin activity, since it provides a site of attachment for the ester phosphate, which is required for combination of apoenzyme with coenzyme.

Compounds 7 and 12, although they catalyze transamination, lack a methyl group corresponding to that in the 2-position of pyridoxal. This

group therefore appears not to be a critical requirement for the reaction. It can be replaced by a 2-ethyl group (compound 4) without apparent effect on the reaction. Although not essential, the 2-methyl group may through its inductive effect modify the rate of the chemical reaction. A careful quantitative comparison of substituted vs. unsubstituted compounds would permit an assessment of importance of such effects. Marvel et al⁵⁵ found a decrease in the heat stability of salicylaldehyde imine chelates when a methyl group ortho to the phenolic group is present, and suggested that a similar effect of the methyl group in pyridoxal may contribute to ease of splitting of the intermediate chelate complexes in pyridoxal catalyzed reactions.

The essential function played by the heterocyclic nitrogen atom of pyridoxal is evident from the failure of salicylaldehyde to promote transamination (compounds 1,7,8). The heterocyclic nitrogen of the pyridine nucleus is a strongly electronegative group, similar in its inductive effects to a nitrogroup on a benzene nucleus⁵⁶. It is significant therefore that 4- and 6-nitrosalicylaldehyde, in which the nitro group exerts an electron-withdrawing effect similar to that of the heterocyclic nitrogen atom of pyridoxal and compound 7, also catalyze ketoglutarate formation. In each of these compounds and in glyoxylic acid, similar pronounced electronic displacements reduce greatly the electron density about the formyl group, as shown schematically in formulae (32) to (36) in Figure (1-9):

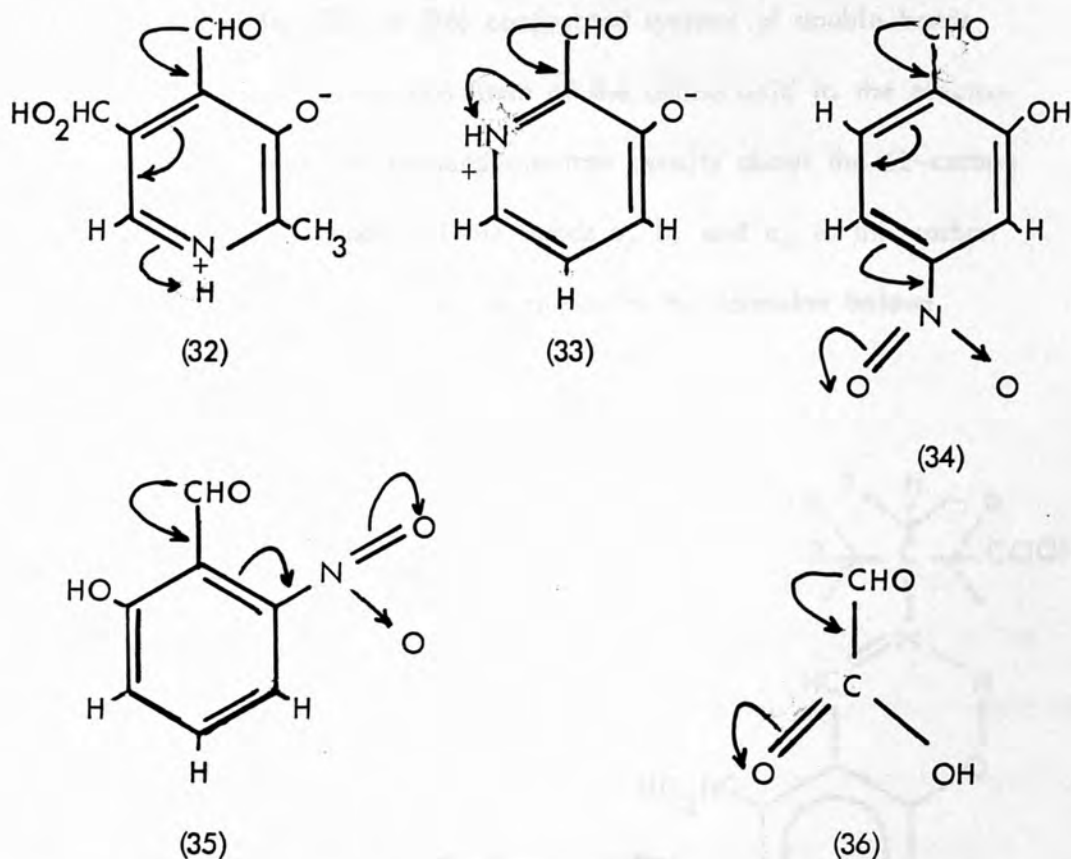
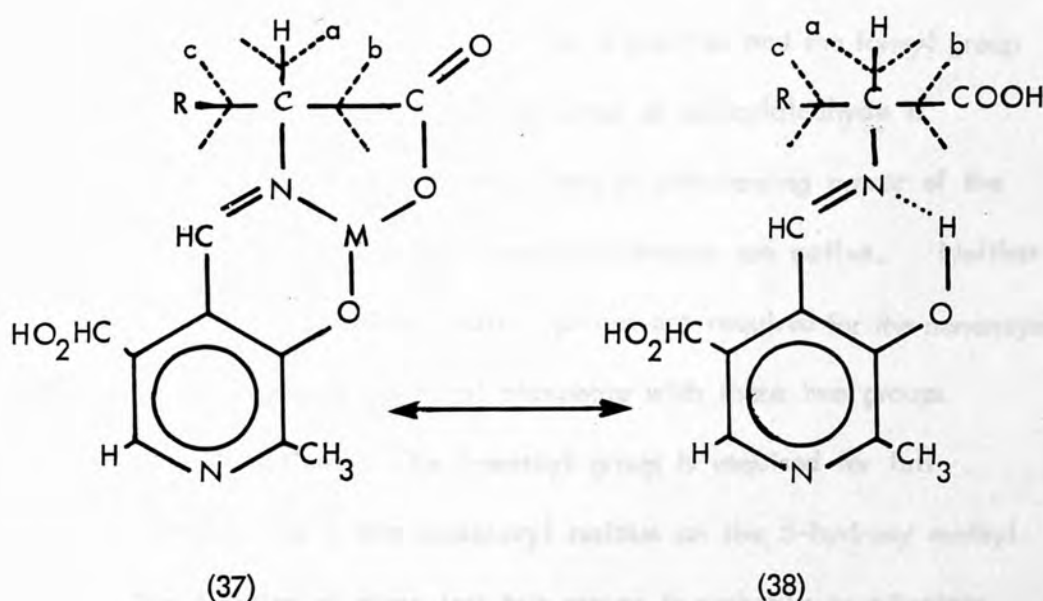


Fig. 1-9: Electron withdrawal in pyridoxal and related compounds

Similarly, substituted aldehydes such as isopyridoxal (compound 5) and 5- or 3,5-dinitrosalicylaldehyde (compound 14,15) in which the electronegative groups do not bring about this result, do not catalyze ketoglutarate formation. Groups properly placed on the benzene ring but less electronegative than the nitro group (e.g. -OH, -COOH, compounds 9, 10 and 16) do not yield effective catalysts under the same conditions. Thus the minimum structural features of the pyridoxal molecule essential for catalysis of nonenzymatic transamination and the other related reactions are those provided by 2-formyl-3-hydroxypyridine or its electronically equivalent isomer, 3-hydroxy-4-formylpyridine.

In the imine (37) (38) formed from each of the catalytically

effective aldehydes (32) to (36) conjugated systems of double bonds extending from the α -carbon atom of the amino acid to the electro-negative group results in reduced electron density about the α -carbon atom, thus weakening each of the bonds a, b, and c, to the carbon atom carrying the amino group, as shown in the formulae below:



In each of these imines, too, the essential free phenolic (or acidic) group is so placed as to stabilize the imine through hydrogen bonding (38) or in the presence of appropriate metal ions, through formation of five or six-membered chelate rings (37). Formation of the imines is thus favoured, but more importantly, the system of conjugated double bonds is maintained in the planar configuration essential for maximum withdrawal of electrons from the α -carbon atom towards the heterocyclic nitrogen atom of pyridoxal. In the chelate structures, the metal ion may also provide an additional electron-attracting group that operates in the same direction as the heterocyclic N and thus intensifies the electron displacement

from the α -carbon atom. It is this electron displacement, with its consequent weakening of bonds a, b and c (37) and (38) that constitutes "activation" of the amino acid by the pyridoxal-metal ion systems, and makes possible not only the transamination reaction, but also each of the other reactions catalyzed by these systems⁴⁸.

Structural features which must be present in the pyridoxine (V.B₆) molecule for activity in the non enzymatic transamination reaction are (I) both the free phenolic hydroxyl in the 3-position and the formyl group in the 4-position, (II) the ring nitrogen atom, as salicylaldehyde is inactive. This must be due to the electron withdrawing power of the nitrogen atom as both 4- and 6-nitrosalicylaldehyde are active. Neither the 2-methyl nor the 5-hydroxy methyl groups are required for the nonenzymatic reaction, as analogues of pyridoxal phosphate with these two groups replaced are still active. The 2-methyl group is required for full enzymatic activity, as is the phosphoryl residue on the 5-hydroxy methyl group. The function of these last two groups is probably to orientate the pyridoxal molecule on the surface of the apoenzyme.

A scheme for the non enzymatic transamination and racemization reaction involving metal chelates of pyridoxal has been put forward by Snell and his co-workers⁴⁸.

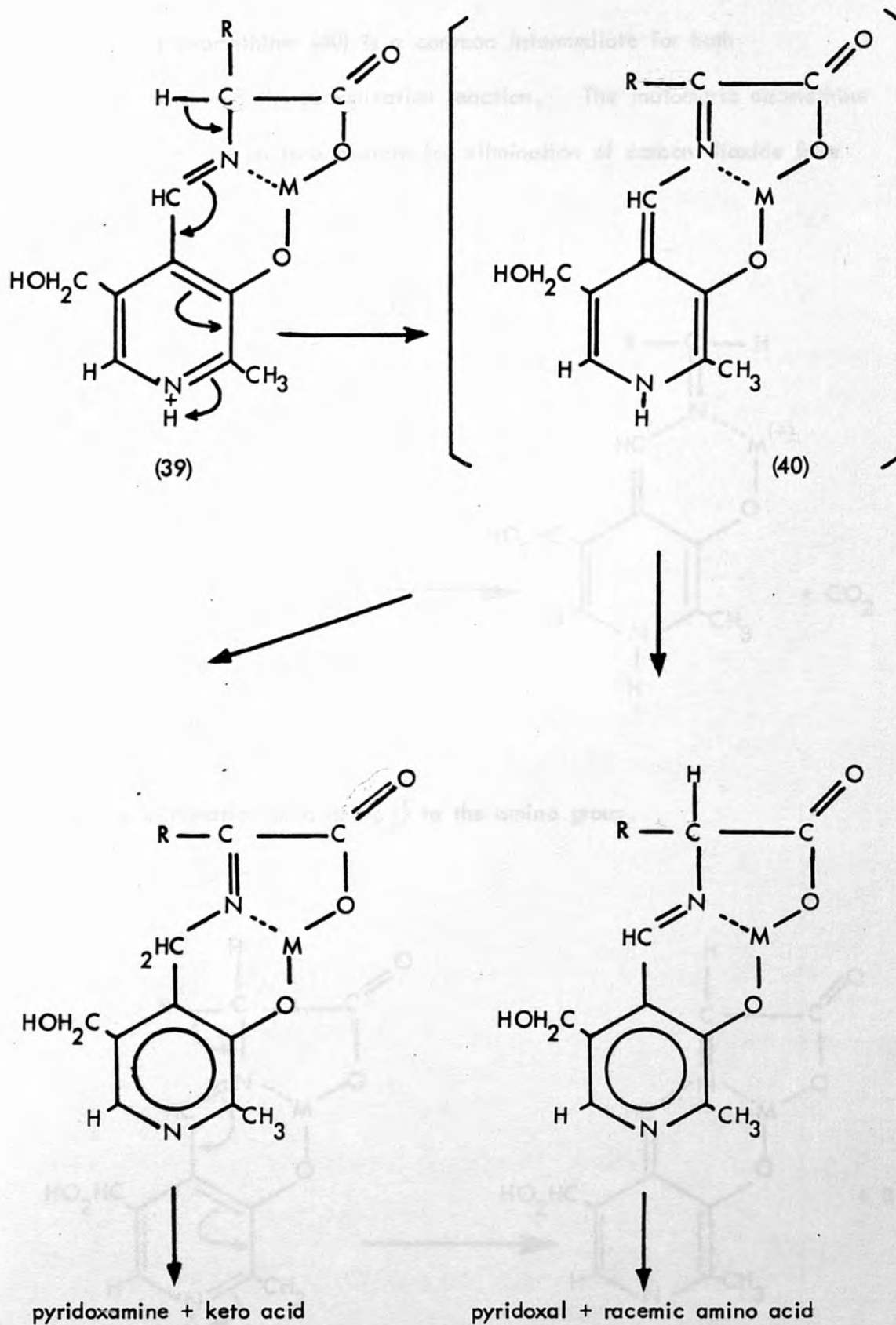
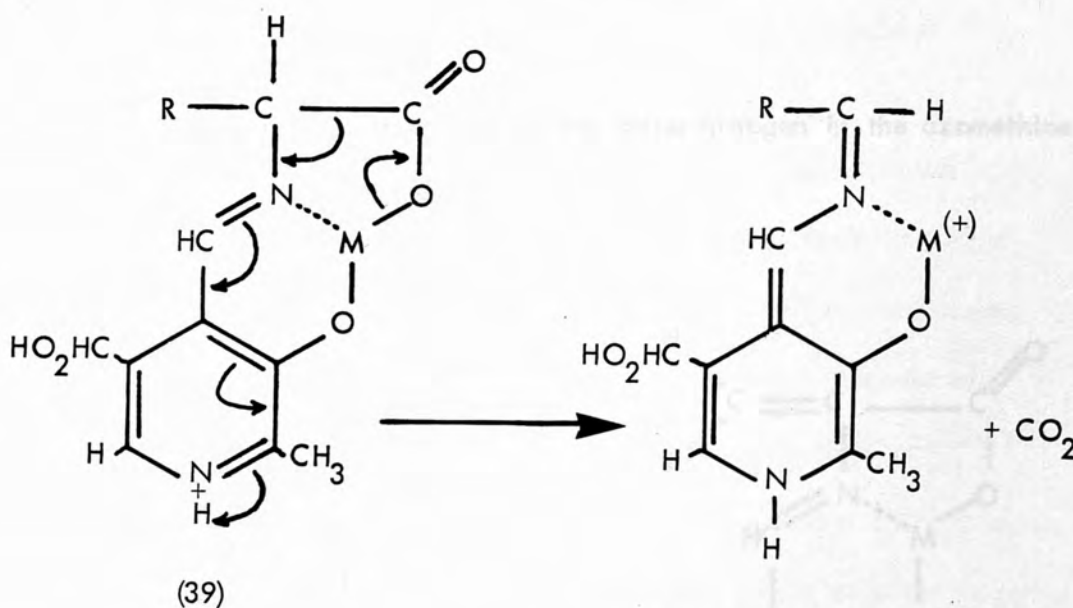
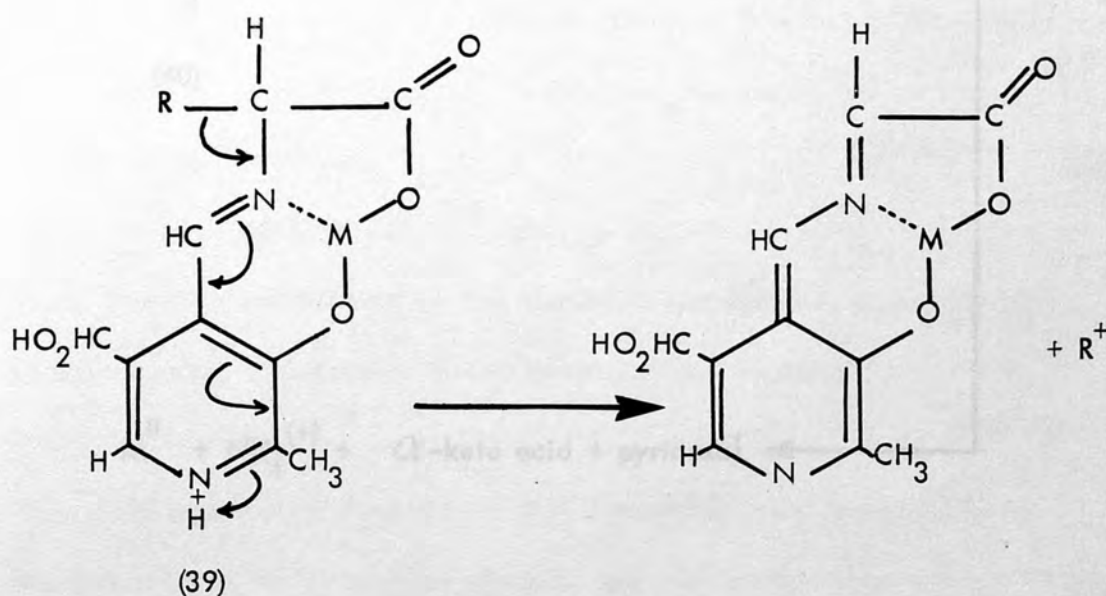


Fig. 1-10 Non-enzymatic Transamination and Racemization Reaction of Metal Chelate

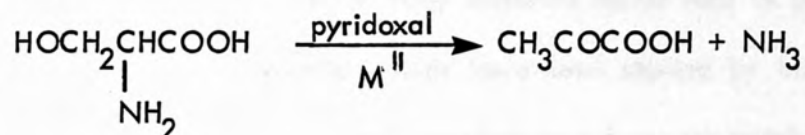
The azomethine (40) is a common intermediate for both transamination and the racemization reaction. The tautomeric azomethine (39) can also be an intermediate for elimination of carbon dioxide from the amino acid,



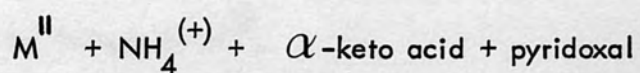
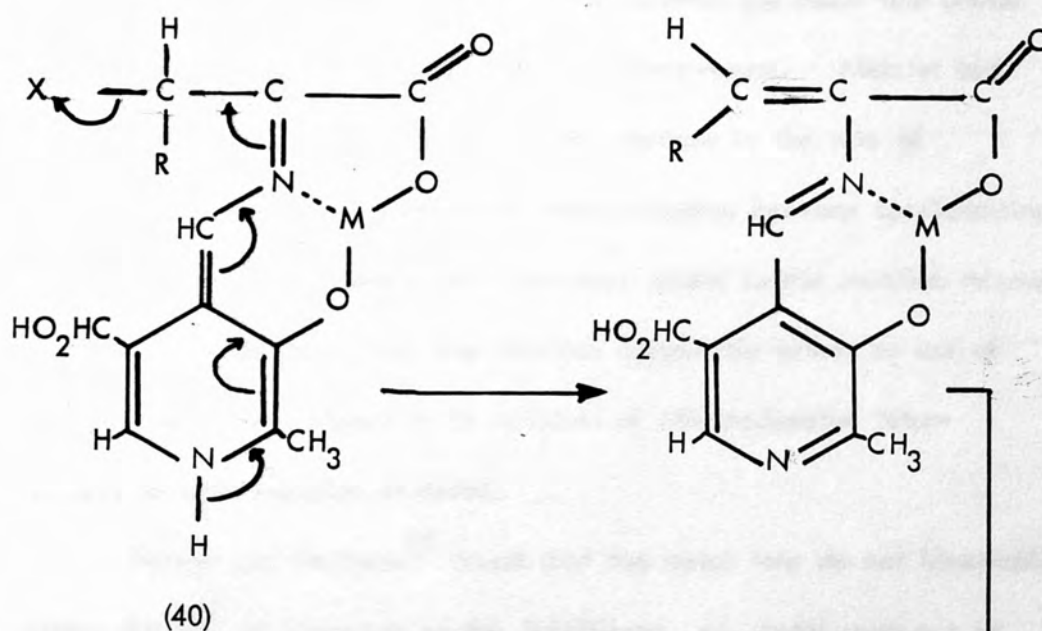
and the elimination of a group β to the amino group.



α, β -elimination reaction of amino acids, for example, the reaction of pyridoxal with serine⁵⁷ can also be explained by a similar mechanism.



Elimination of a group β to the imine nitrogen in the azomethine (40) can take place as follows:



1.4 Relationship of Metal Ions to the Nonenzymatic and Enzymatic

Transamination Reaction:

The catalytic activities of many different metal ions in promoting reactions of pyridoxal with amino acids have been studied by Longenecker and Snell⁵⁴. Nonenzymatic transamination reactions are catalyzed by a variety of metal ions including Ga^{III}, Cu^{II}, Al^{III}, Fe^{II}, Fe^{III}, Zn^{II}, In^{III}, Ni^{II}, Co^{III}, in increasing order of effectiveness with only slight activity in the case of Mn^{II}, Cd^{II}. In general, the same metal ions catalyze other model reactions between pyridoxal and amino acids in approximately the same order of effectiveness. Metzler and Snell¹⁸ demonstrated a ten to twentyfold increase in the rate of pyridoxal formation by nonenzymatic transamination between pyridoxamine and α -ketoglutarate when cupric ions were added to the reaction mixture. They were unable to prevent the reaction completely either by use of purified metal-low reagent or by addition of ethylenediamine tetraacetate to their reaction mixtures.

Farago and Mathews⁵⁸ found that the metal ions do not kinetically affect the rate of formation of the Schiff-base, so, metal must act as Metzler et al⁴⁸ suggested.

In 1963 Nakamoto et al⁵⁹, also by using spectroscopic techniques, found that the concentration of the aluminium ion does not affect the rate of the reaction. Subsequently this behaviour was found in the case of copper by Farago et al⁵⁸.

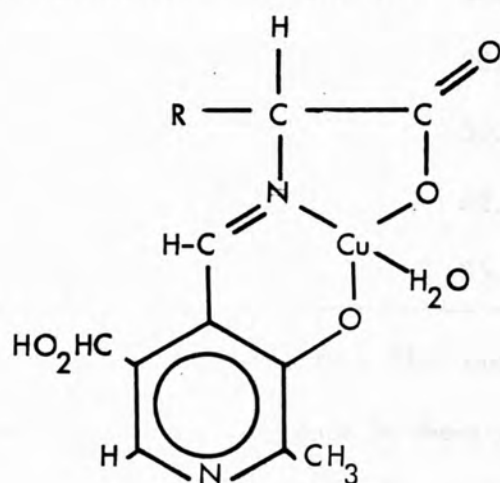
The reaction of formation of Schiff base may thus occur slowly in aqueous solution in the absence of metal ions via the hydrogen-bonded imine (38) detected by Blanks et al⁶⁰ and Metzler⁴⁰. This is consistent

with the Matsuo³⁵ report that transamination between pyridoxal and amino acids occurs readily in ethanol in the absence of added metal ions. Azomethine formation occurs to a much greater extent in ethanol than in water, both because of the reduced tendency towards hydrolysis and the greater concentration of nonpolar forms of the amino acids. The requirement for metal ions also is either absent or less critical when the reaction is carried out on paper chromatography, where relatively high local concentrations of amine and aldehyde interact⁶¹. These observations support the postulation of Metzler et al⁴⁸ that the most important functions of metal ions in aqueous solutions are as follows:

- a) Promoting the formation of the azomethine intermediates (Schiff base) (39).
- b) Maintenance of planarity in the conjugated double bonds in the planar configuration essential for the postulated electron shifts.
- c) Stabilization or destabilization of the Schiff base.
- d) Providing an additional electrophilic group that intensifies displacement of electrons from the bonds surrounding the α -carbon atom of the amino acid residue.

This latter effect of metal ions is secondary, however, to that of the heterocyclic nitrogen, since no transamination occurs with salicylaldehyde plus metal ions, while some reaction does occur with pyridoxal in the absence of metal ions. Whether each of these effects actually takes place in the chelation will depend upon the structure of catalytic intermediate and the extent of its formation. In particular, atoms of the

amino acid will not be held in the plane of the aromatic ring unless the chelation joins them to this ring in a planar structure. Snell and his associates have generally postulated a 1:1:1 chelate (e.g. formula (41)) which for copper probably yields three coplanar rings. On the other hand, several metals with strong catalytic activity may or may not tend to maintain coplanarity; these may not even be chelated to the aromatic ring:



(41)

Catalytic activity of metal ions was confirmed by Eichhorn and Trachtenberg⁶². They measured the rate constants at various temperatures for decomposition of the 1:1 copper and 1:1 nickel complexes of bis-(2-thiophenyl)-ethylenediamine in 50% water-ethyl alcohol:

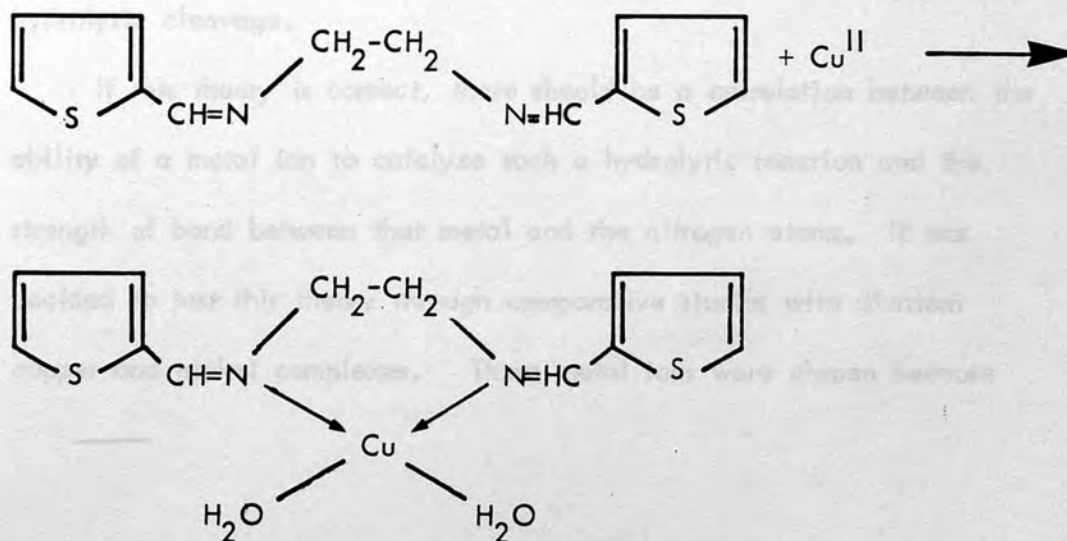


Table 1-6: Rate Constants for Decomposition of Cu^{II} , Ni^{II} Complex:

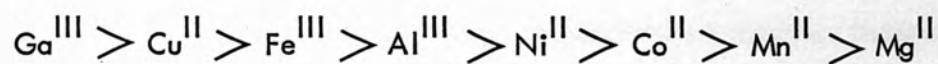
COPPER		NICKEL	
Temp. °C	$k \times 10^3, \text{sec.}^{-1}$	Temp. °C	$k \times 10^3, \text{sec.}^{-1}$
10	0.832 ± 0.008	20.0	2.34 ± 0.05
20.5	1.80 ± 0.04	25.0	3.27 ± 0.04
24.0	2.35 ± 0.06	26.8	3.61 ± 0.10
26.5	2.46 ± 0.10	28.5	4.20 ± 0.01
30.5	3.25 ± 0.07	30.0	4.72 ± 0.04
		32.5	5.21 ± 0.06
		35.0	6.22 ± 0.26

The activation energies per mole were 11.3 and 12.5Kcal. for copper and nickel respectively. The difference in these values is in accord with the theory that the ability of a metal ion to act as a catalyst in such a decomposition is related to the strength of co-ordinate covalent bonds which the metal ion can form. Bis-(2-thiophenol)-ethylendiamine forms a very unstable complex with Cu^{II} and then rapidly decomposes. It was proposed that the formation of a Cu^{II} -nitrogen bond weakens the carbon-nitrogen double-bonds, thus rendering the latter more susceptible to hydrolytic cleavage.

If this theory is correct, there should be a correlation between the ability of a metal ion to catalyze such a hydrolytic reaction and the strength of bond between that metal and the nitrogen atoms. It was decided to test this theory through comparative studies with divalent copper and nickel complexes. These metal ions were chosen because

they are relatively easy to handle experimentally. It is well known that copper forms stronger complexes than nickel. A quantitative measure of the relative catalytic effect of two metal ions is the activation energy required for the hydrolysis of the Schiff base. According to this theory, since copper forms stronger bonds than nickel with nitrogen atoms, the activation energy for decomposition of a copper complex should be lower than the activation energy in the catalysis with nickel ion.

Davies et al.⁶³ found that the relative strengths of co-ordinate bonds⁶⁴ of metal ions with pyridoxal phosphate and amino acids was in the order:



1.5 The Mechanism of Nonenzymatic Transamination Reaction:

Early studies of Herbst and Engel⁶⁵ had demonstrated exchange of the amino group (transamination) between amino acid and keto acid. When amino acid or keto acid was employed, the reaction occurred slowly at 100°C in aqueous solution but most of the newly formed keto acid was decarboxylated to yield the corresponding aldehyde and CO₂. They proposed⁶⁶ that the reaction occurred through intermediate formation of a Schiff's base between amino and keto acid with subsequent isomerization of the azomethine linkage and hydrolysis. This mechanism was extended to explain the subsequently discovered enzymatic transamination⁶⁷. With the demonstration of: (1) nonenzymatic transamination reaction between pyridoxal and amino acid, (2) the coenzymatic role of pyridoxal phosphate in the corresponding enzymatic reaction, (3) imine (azomethine) formation in dilute aqueous solution between pyridoxal or its phosphate and amino acids, and also between pyridoxamine or its phosphate and keto acids, (4) the catalytic role of metal ions for the nonenzymatic reaction, (5) chelate formation between the catalytic metal ions and pyridoxal-amino acid imines or pyridoxamine-keto acid imines, (6) the participation of such chelates in the transamination reaction, and (7) the role played by various groupings of pyridoxal in the transamination reaction, a considerable extension of this mechanism becomes possible. Such a mechanism for the nonenzymatic reaction that is compatible with all observation is illustrated in Figure (1-11). Its essential feature is an electron displacement of electrons from bond "a" of (37) with loss of a proton from the α -position of the amino acid residue, localization of the extra electron pair of the transitional form (43) at the formyl carbon atom

amino acid (optically active)

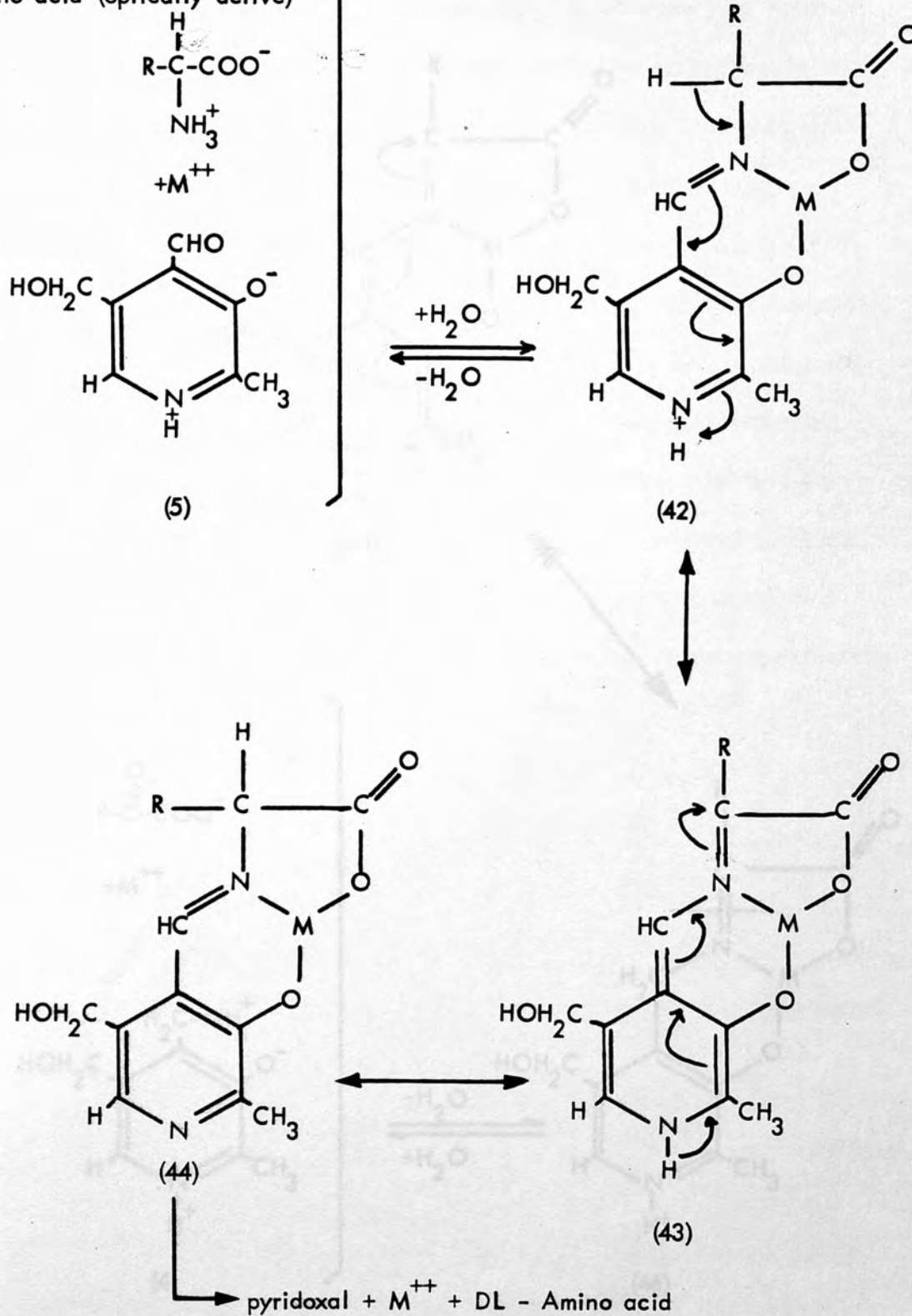
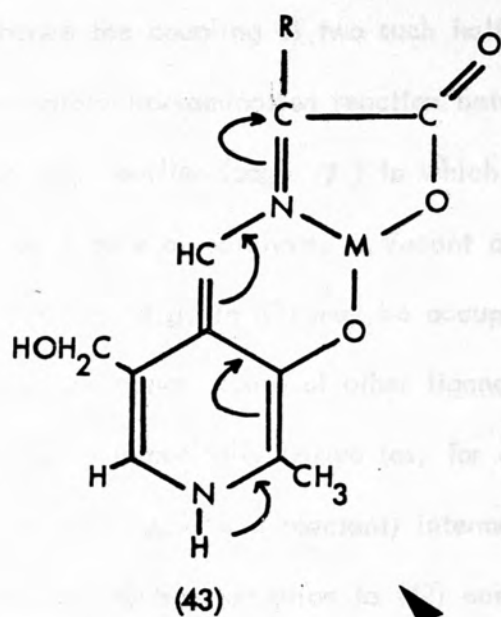
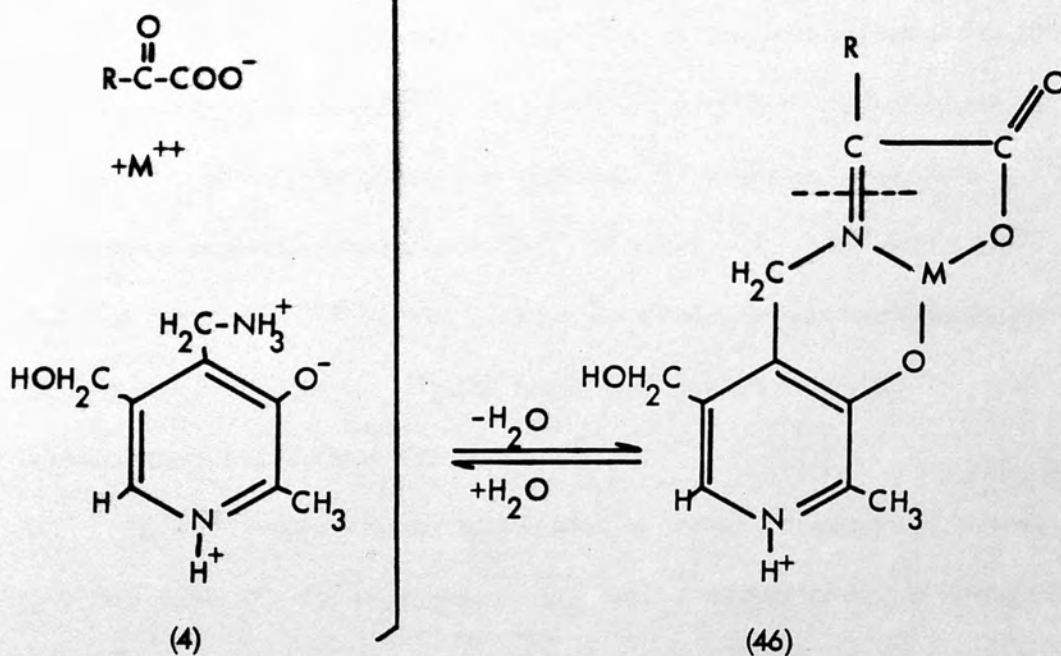


Fig. 1-11: Mechanism of nonenzymatic reaction

Fig. 1-11 (continued) a proton yields (46), the isomeric form of a keto



keto acid



and recombination with a proton yields (46), the isomeric imine of a keto acid and pyridoxamine. Both imines are in equilibrium with their components, hence the coupling of two such half-reactions results in the overall reversible transamination reaction between keto acid⁽¹⁾ and amino acid⁽²⁾ discussed earlier (page 7) in which pyridoxal and pyridoxamine serve only as catalysts. Vacant co-ordination positions in the metal chelates (e.g. in 42) may be occupied by other substances, such as water or the donor groups of other ligands. If, in the latter instance, the ligand is optically active (as, for example, where an optically active amino acid is a reactant) intermediate (46) will be asymmetric, and in the transformation to (42) one configuration of the newly formed asymmetric centre may be favoured over another, thus accounting for the partial optical specificity of the nonenzymatic reaction⁵³.

1.6 Effect of Structure of Amino Compounds on the Rate of the

Transamination Reaction

Although the metal-ion catalyzed transamination reaction between pyridoxal and amino acids is a general reaction, the rate and equilibrium position of the reaction varies greatly with the structure of the amino acid. In 1952 Metzler and Snell¹⁸ suggested that β -substitution of the amino acid reduces the rate substantially. Glycine appears to react little if at all; however, this is a consequence of the equilibrium position of the reaction, for pyridoxamine and glyoxylic acid react rapidly to yield glycine and pyridoxal almost quantitatively⁶⁸. For most other α -amino acids, the equilibrium position lies near 50% reaction. For convenience in measurement, most of these reactions should be conducted at 100°C, they also occur more slowly at room temperature⁵³. The optimum pH varies⁵⁴ in the range of 4.0 to 8.0.

With several amino acids, observation of the transamination reaction is complicated by occurrence of other, more rapid, pyridoxal-catalyzed reactions. Serine, threonine and cysteine, for example, undergo a dehydration or desulhydration reaction⁵⁷ to yield NH_3 , keto acid and H_2S (for cysteine). They also undergo an aldol-type cleavage to yield glycine and aldehydes⁵⁰. Lysine reacts with pyridoxal rapidly to yield pyridoxamine, but no keto acid appears.

Unlike α -amino acids, which readily undergo transamination with pyridoxal even at room temperature, β - and γ -amino acids and primary amines in general do not undergo nonenzymatic transamination⁶¹ to any significant extent in short times at temperatures below 90°C. The lower activation energy of the reaction with α -amino acid may be attributed

to the adjacent electrophilic carboxyl group, which enhances electron withdrawal from the α -carbon atom. Aside from this, transamination of amines other than α -amino acids would appear to occur by the same mechanism.

It is interesting to note that the findings previously thought to be inconsistent with the oxazolinone mechanism have been shown, however, either to support or to be consistent with the view that interconversion of pyridoxal phosphate occurs via oxazolinone intermediates and the mechanism depicted for the nonenzymatic reaction is a reasonable one for the enzymatic process as well. Until the mechanism of the various known enzymatic reactions involving pyridoxal phosphate is established, the apoenzyme may be visualized as substituting the various methyl skeletons. The specific nature of the apoenzyme binding remains to be established; unquestionably, the phosphate plays a role in such binding. This is the main function of the phosphate group in pyridoxal phosphate to bind the coenzyme to a specific site on the apoenzyme in order that the rest of the molecule is in position to react with a substrate. The great affinity of the formyl group of pyridoxal phosphate for amino groups suggests that interaction of these groups through oxazolinone formation also may play a role.

In 1971 Sobir suggested⁶⁹ that the hydroxyl and the aldehyde groups are the ones mainly involved in the nonenzymatic reaction. Hence for the enzymatic reaction two other groups also are important, the methyl and the phosphate groups. The methyl group is necessary for the formation of the coenzyme (i.e., phosphorylated pyridoxal), and the phosphate group is important because it prevents the formation of internal hemiacetal turns

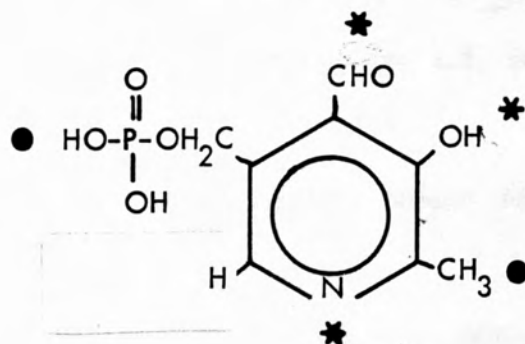
1.7 Relation of the Nonenzymatic and Enzymatic Transamination Reactions

For some time following discovery of the pyridoxal-pyridoxamine catalyzed, nonenzymatic transamination reaction, there was considerable hesitation about accepting it as a true model for the corresponding enzymatic reactions. All of the findings previously thought to be incompatible with the mechanism have been shown, however, either to be without or actually to support the view that interconversion of pyridoxal phosphate and pyridoxamine phosphate occur via azomethine intermediates on the enzyme surface. The mechanism depicted for the nonenzymatic reaction may be extended to the enzymatic process as well. Until the relationship of metal ions to various enzymatic reactions involving pyridoxal and its analogues is clarified, the apoenzyme may be visualized as substituting for the metal ion of the various metal chelates. The specific nature of coenzyme-apoenzyme binding remains to be established; unquestionably, the phosphate plays a role in such binding. This is the main function of the phosphate group in pyridoxal phosphate to bind the coenzyme to a specific site on the apoenzyme in order that the rest of the molecule is in position to react with a substrate. The great affinity of the formyl group of pyridoxal phosphate for amino groups suggests that interaction of these groups through azomethine formation also may play a role.

In 1971 Sabir suggested⁶⁹ that the hydroxyl and the aldehyde groups are the ones mainly involved in the nonenzymatic reaction. Hence for the enzymatic reaction two other groups also are important, the methyl and the phosphate groups. The methyl group is necessary for the formation of the coenzyme (i.e. phosphorylated pyridoxal), and the phosphate group is important because it prevents the formation of internal hemiacetal forms

so that a high concentration of the free aldehyde, which is the active form in catalysis, is maintained.

Braunstein⁷⁰ also suggested that the enzyme would attach to the phosphate group and the nitrogen in the ring.



- * Groups necessary for non-enzymatic reactions
- Groups necessary for enzymatic reactions only

REFERENCES

1. P. György, C.E. Edgar and H. Chick, *Biochem. J.* (1935), 29, 760.
2. R. Kuhn and G. Wendt, *Ber.* (1938), 71, 1534.
3. R. Kuhn and G. Wendt, *Ber.* (1939), 72, 305.
4. E.T. Stiller, J.C. Keresztesy and J.R. Stevens, *JACS*, (1939), 61, 1237.
5. R. Kuhn, K. Westphal and G. Wendt, *Naturwiss.* (1939), 27, 469.
6. E.E. Snell, B.M. Guirard and R.J. Williams, *J. Biol. Chem.*, (1942), 143, 519.
7. E.E. Conn and P.K. Stumpf, *Outlines of Biochemistry*, Third Edition, J. Wiley and Sons Inc. (1972).
8. E.E. Snell, *J. Biol. Chem.* (1944), 154, 313.
9. J.C. Rabinowitz and E.E. Snell, *J. Biol. Chem.* (1948), 176, 1157.
10. E.F. Gale and H.M.R. Epps, *Biochem. J.* (1944), 38, 232.
11. I.C. Gunzalus and W.D. Bellamy, *J. Biol. Chem.* (1944), 155, 357.
12. D. Heyl, E. Luz, S.A. Harris, and K. Folkers, *JACS*, (1951), 73, 3430.
13. J. Baddiley and A.P. Mathias, *J. Chem. Soc.* (1952), P.2583.
14. J.C. Rabinowitz and E.E. Snell, *J. Biol. Chem.*, (1947), 169, 643.
15. W.W. Umberit, D.J. O'Kane and I.C. Gunzalus, *J. Biol. Chem.*, (1948), 176, 629.
16. E.A. Peterson, H.A. Sober and A. Meister, *JACS*, (1952), 74, 570.

17. E.E. Snell and A.N. Rannefeld, *J. Biol. Chem.*, (1945), 157, 475.
18. D.E. Metzler and E.E. Snell, *JACS*, (1952), 74, 979.
19. E.E. Snell, *JACS*, (1944), 66, 2082.
20. T.W. Birch and P. Gyorgy, *Biochim. J.*, (1936), 30, 304.
21. J.C. Keresztesy and J.R. Stevens, *JACS*, (1938), 60, 1267.
22. E.T. Stiller, J.C. Keresztesy and J.R. Stevens, *JACS*, (1939), 61, 1237.
23. J.V. Scudi, *J. Biol. Chem.*, (1941), 139, 707.
24. J.C. Keresztesy and J.R. Stevens, *Proc. Soc. Exptl. Biol. Med.*, (1938), 38, 64.
25. L. Atkin, A.S. Schultz, W.W. Williams and C.N. Fery, *Ind. and Eng. Chem. Anal. Ed.*, (1943), 15, 141.
26. S.A. Harris, T.J. Webb and K. Folkers, *JACS*, (1940), 62, 3198.
27. A.K. Lunn and R.A. Morton, *The Analyst*, (1952), 77, 718.
28. H.N. Christensen, *JACS*, (1958), 80, 99.
29. F.J. Anderson and A.E. Martell, *JACS*, (1964), 86, 715.
30. T. Matthews, Ph.D Thesis, Bedford College, University of London (1967).
31. V.R. Williams and J.B. Neiland, *Arch. Biochem., Biophys.*, (1954), 53, 56.
32. K. Nakamoto and A.E. Martell, *JACS*, (1959), 81, 5857.
33. P. Fasella, *Ann. Revs. Biochem.* (1967), 36, 185.
34. D.E. Metzler and E.E. Snell, *JACS*, (1955), 77, 2431.
35. Y. Matsuo, *JACS*, (1957), 79, 2016.
36. H.N. Christensen and S. Collins, *J. Biol. Chem.*, (1956), 220, 279.

37. E.E. Snell, *JACS*, (1945), 67, 194.
38. A.E. Braunstein, *The Enzymes*, Ed. P.D. Boyer, H. Lardy and K. Myback, New York: Academic Press, (1960), 2, 113.
39. H.C. Dunathan, Haverford, Pennsylvania "Sterochemical Aspects of Pyridoxal Phosphate Catalysis", (1971).
40. D.E. Metzler, *JACS*, (1957), 79, 485.
41. J. Olivard, D.E. Metzler and E.E. Snell, *J. Biol. Chem.*, (1952), 199, 669.
42. D.E. Metzler and E.E. Snell, *J. Biol. Chem.*, (1952), 198, 363.
43. R.D. Gillard and P. O'Brien; *J.C.S., Dalton*, (1977), 1988.
44. J.A. Marcello, A.E. Martell and E.H. Abbott, *Chem. Comm.*, (1975), 16.
45. A. Tenenbaum, *Biochem. Biophys. Acta*, (1974), 362, 308.
46. T.C. French and T.C. Bruice, *Biochem.*, (1964), 3, 1589.
47. W.T. Jenkins and I.W. Sizer, *JACS*, (1957), 79, 2655.
48. D.E. Metzler, M. Ikawa and E.E. Snell, *JACS*, (1954), 76, 648.
49. D.E. Metzler and J. Fisher, *JACS*, (1969), 91, 138.
50. D.E. Metzler, J.B. Longenecker and E.E. Snell, *JACS*, (1954), 76, 639.
51. G.L. Eichorn and J.W. Daws, *JACS*, (1954), 76, 5663.
52. P. Fasella, H. Lis, N. Siliprandi and C. Baglioni, *Biochem. Biophys. Acta*, (1957), 23, 417.
53. J.B. Longenecker and E.E. Snell, *Proc. Nat. Acad. Sci. U.S.A.*, (1956), 42, 221.
54. J.B. Longenecker and E.E. Snell, *JACS*, (1957), 79, 142.

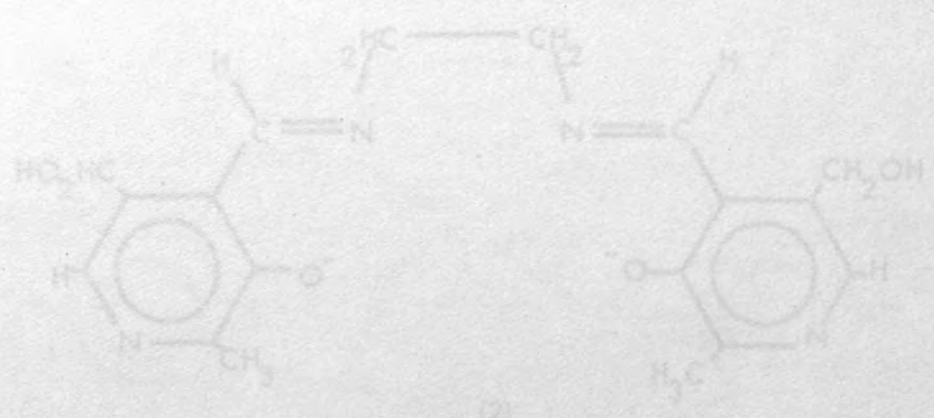
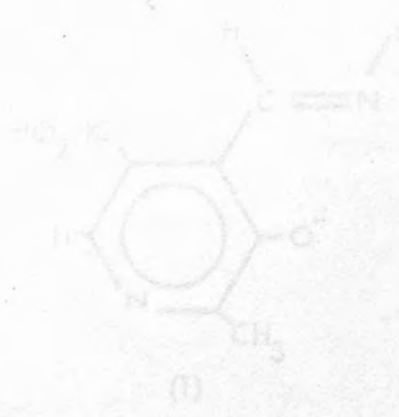
55. C.S. Marvel and N. Tarkoy, *JACS*, (1957), 79, 6000.
56. H.S. Mosher, in "Heterocyclic Compounds", Ed. R.C. Elderfield, (1950), 1, 408.
57. D.E. Metzler and E.E. Snell, *J. Biol. Chem.*, (1952), 198, 353.
58. M.E. Farago and T. Matthews, *J.C.S.*, (1969), 609.
59. K. Nakamoto and A.E. Martell, *JACS*, (1963), 85, 188.
60. E.C.B. Banks, A.A. Diamantis and C.A. Vernon, *J.C.S.*, (1961), 4235.
61. G.D. Kalyankar and E.E. Snell, *Nature*, (1957), 180, 1069.
62. G.L. Eichom and I.M. Trachtenberg, *JACS*, (1954), 76, 5183.
63. L. Davies, F. Roddy and D.E. Metzler, *JACS*, (1961), 83, 127.
64. F.A. Cotton and G. Wilkinson, 'Advanced Inorganic Chemistry', Third Edition, Interscience Publishers, J. Wiley, (1972).
65. R.M. Herbst and L.L. Engel, *J. Biol. Chem.* (1934), 107, 505.
66. R.M. Herbst, *Advances in Enzymol.*, (1944), 4, 75.
67. A.E. Braunstein, *Advances in Protein Chem.*, (1947), 3, 1.
68. D.E. Metzler, J. Olivard and E.E. Snell, *JACS*, (1954), 76, 644.
69. S.S. Sabir, Ph.D Thesis, Bedford College, University of London, (1971).
70. A.E. Braunstein, 'The Enzymes' Ed. P.D. Boyer, H. Lardy and K. Myback, (1960), 2, 140.

Introduction

Considerable research has been carried out on the metal ion complexes of pyridoxal Schiff bases ever since Metzler, Ikawa and others have shown that metal-ion catalyzed reactions of pyridoxal with amino acids are dependent on the nature of the metal ion and the nature of the Schiff base.

CHAPTER 2

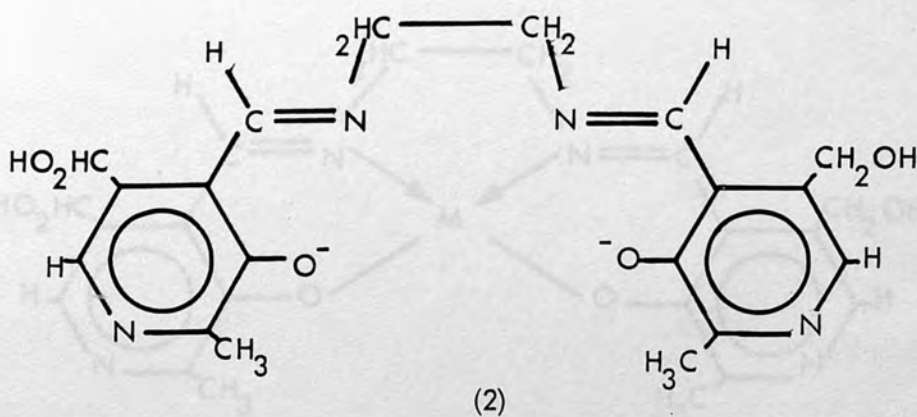
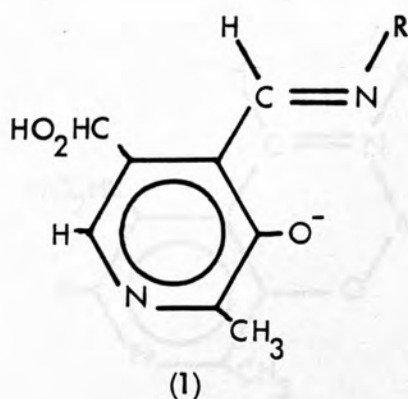
Preparation of Metal-Schiff Base
Complexes of Vitamin B₆ and Related Compounds



2.1 Introduction

Considerable research has been carried out on the metal ion interaction with pyridoxylidene Schiff bases ever since Metzler, Ikawa and Snell proposed that metal-ion catalyzed reactions of pyridoxal with amino acids involves chelation of the pyridoxal to the metal ion and Schiff base formation with the amino acid¹.

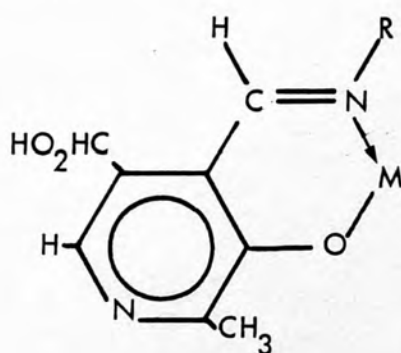
It has been suggested that Schiff bases (1,2) which are obtained from Vitamin B₆ derivatives and various amines and amino acids, can play an important role in enzymatic reactions in the presence of metal ions:



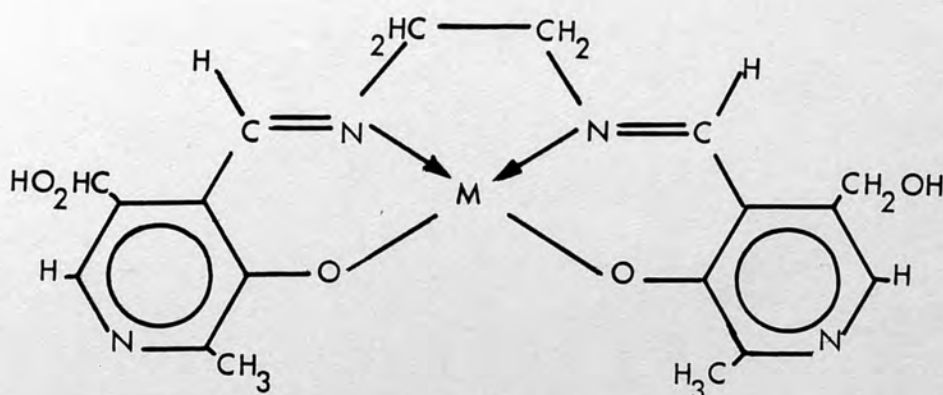
Eichorn et al² claimed that the formation of a Schiff-base must occur before chelation with the metal ions, and the prior formation of the metal-amino acid chelate is said to inhibit the reaction almost completely.

The binding sites of the chelation have been of interest, and most of the evidence obtained has supported the idea of chelation through the phenolic-oxygen and 4'-functional groups³⁻⁸. Bonding through other liganding sites has been suggested by Kelusky et al⁹.

The synthesis of these model complexes (3,4) provides information of fundamental significance in discussing the precise mechanism of reactions of Vitamin B₆ and related compounds in the presence of metal ions, as well as elucidating the interaction of metal ions with Schiff bases.

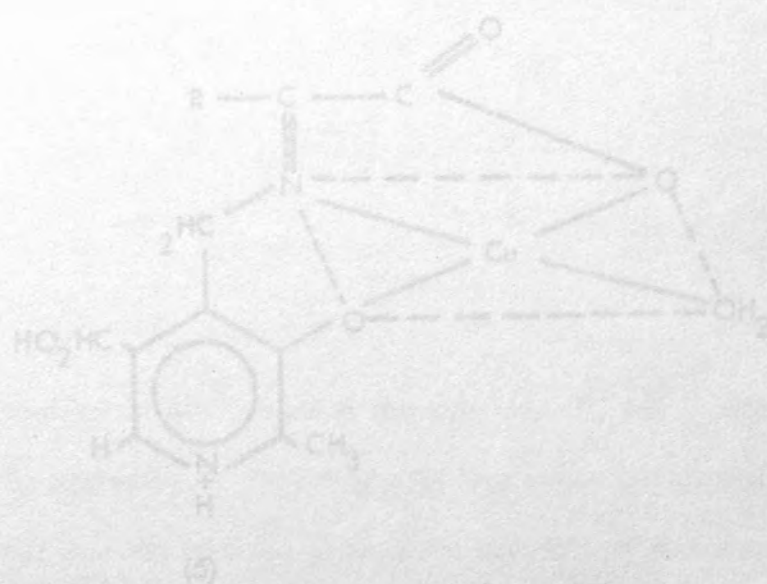


(3)



(4)

In recent years, a variety of these Schiff base complexes with first-row transition metals have been synthesised with various metal and ligand ratios by Farago et al⁴, Yamada et al¹⁰⁻¹², Wroblewski et al¹³, Kuge et al¹⁴, Thompson et al¹⁵ and Franklin et al¹⁶.

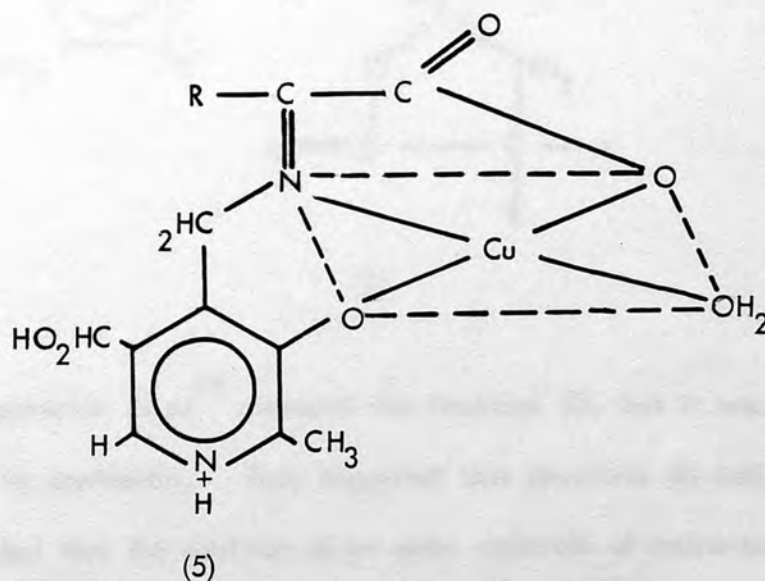


2.2 Proposed Structures of Metal-Schiff Base Complexes

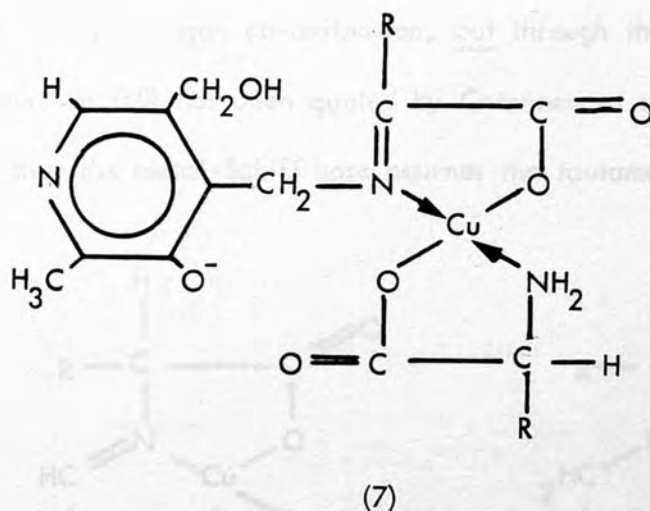
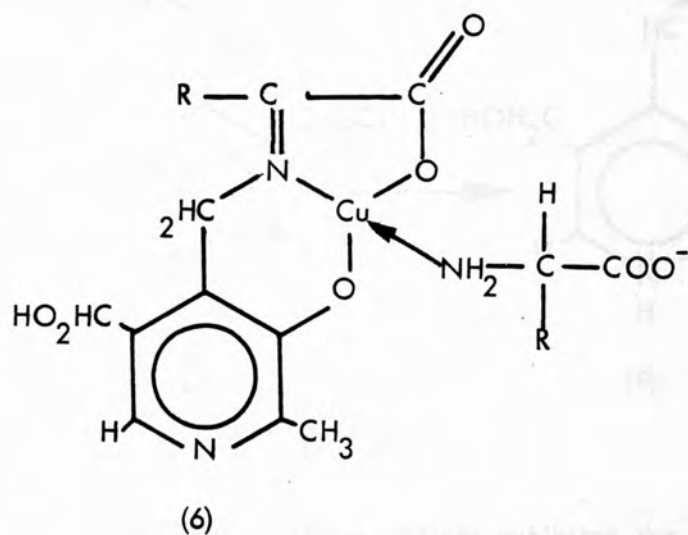
The transition-metal complexes with Schiff bases derived from Vitamin B₆ are considered to involve a number of interesting problems of fundamental importance in the field of co-ordination chemistry.

The structures of various metal-Schiff base complexes in the solid state have been suggested by a number of authors.

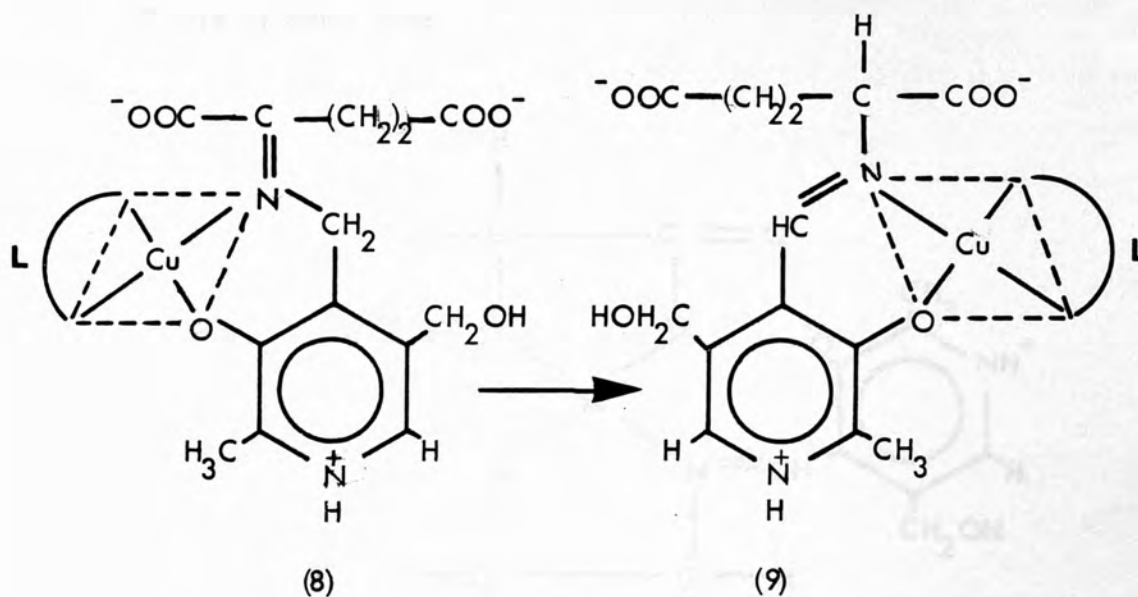
The copper-pyridoxylidene-valinate complex was discussed by Cutfield et al¹⁷ and ratio was confirmed to be 1:1:1. They elucidated the structure (5) of the complex by X-ray methods and found the structure to be a 5-co-ordinated cupric complex (with square pyramidal base) such that overlap of molecular orbitals occurred and the intermediate (Schiff base) had a polymeric structure. The overlap of molecular orbitals was said to stabilise the network, and maintain the essential planarity of the Schiff base system sterically.



The copper-pyridoxylidene-valinate structure (5) was also discussed by Christensen¹⁸. He suggested that the water molecule was displaced with another valinate molecule (6) which reacted with the complex freeing the phenolic-oxygen for metal-oxygen binding (7):

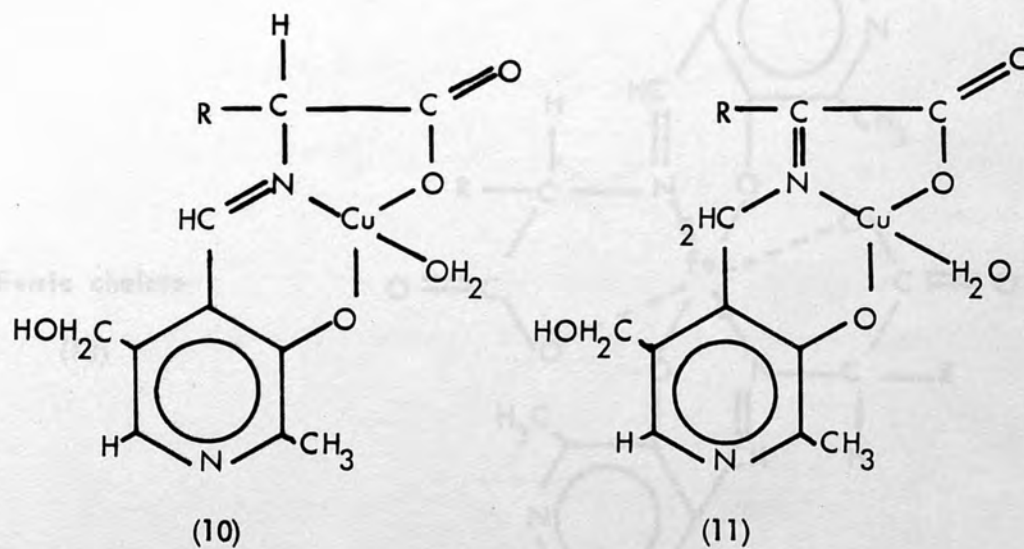


Longenecker et al¹⁹ discussed the structure (5), but it was discounted because of its asymmetry. They suggested that structures (8) and (9) were asymmetric but that the addition of an extra molecule of amino-acid attached itself to the molecule, allowing the attainment of partial symmetry.

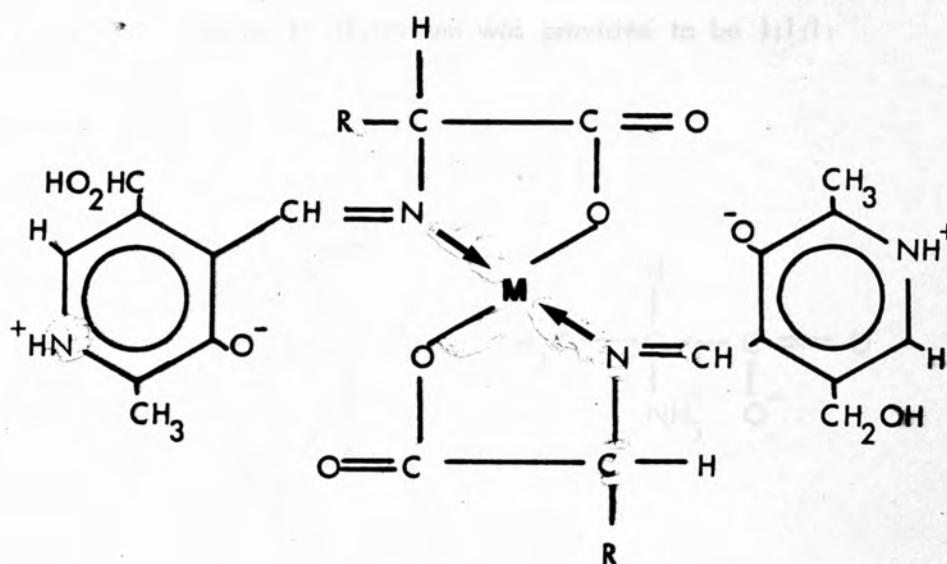


However, the Cu-PL-valinate chelate exhibited the extra stability accounted for by nitrogen co-ordination, but through the pyridine-nitrogen.

Structure (10) has been quoted by Cataneo et al²⁰, and they suggested that the metal-Schiff base assumes the tautomeric forms:



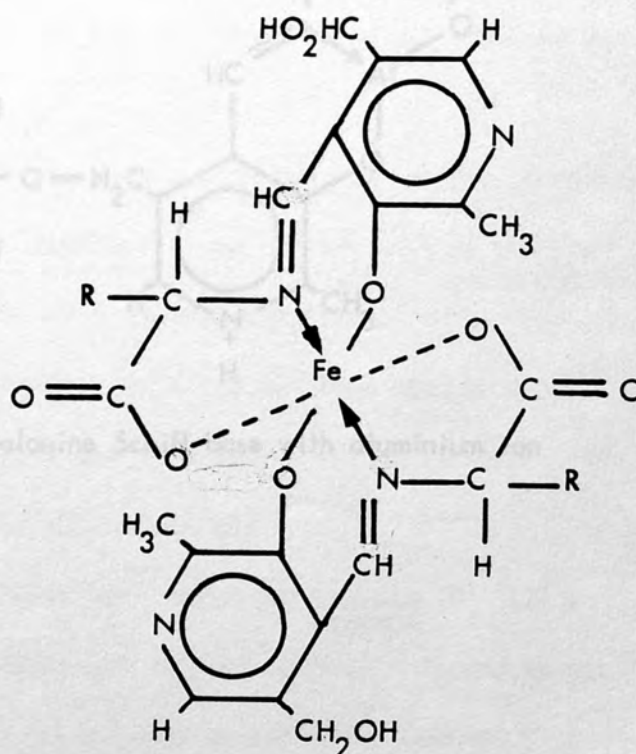
Christensen²¹ proposed metal chelate structures with 2:1 ratio of Schiff base to metal ions:



General structure (12)

Ferric chelate

(13)



Fasella et al²² studied the Al^{+3} -PLP-alanine complex. They suggested that the aluminium retained a single positive charge (Al^+) and also that the complex exhibits the same tautomeric forms as (10) and (11). The ratio of PLP, alanine to aluminium was provided to be 1:1:1:

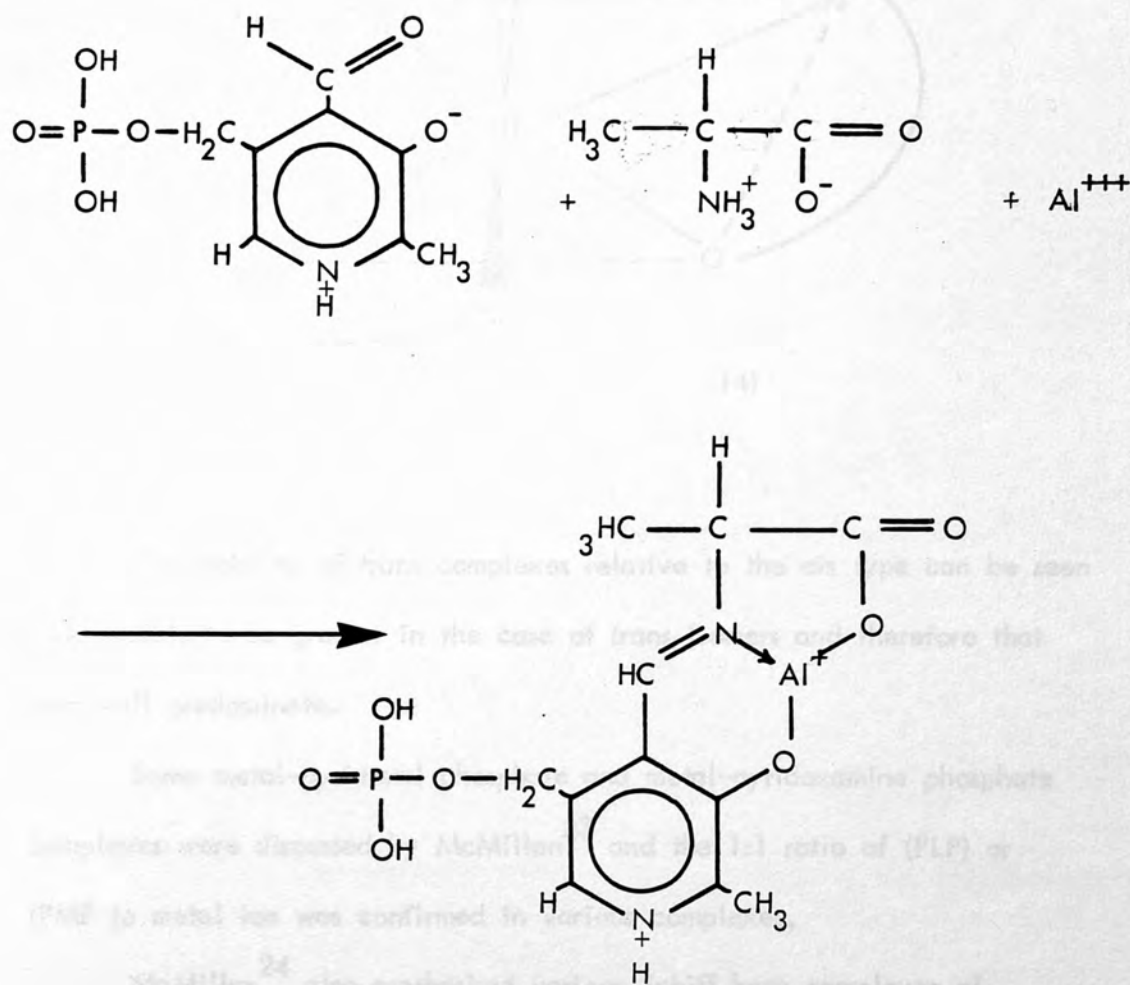
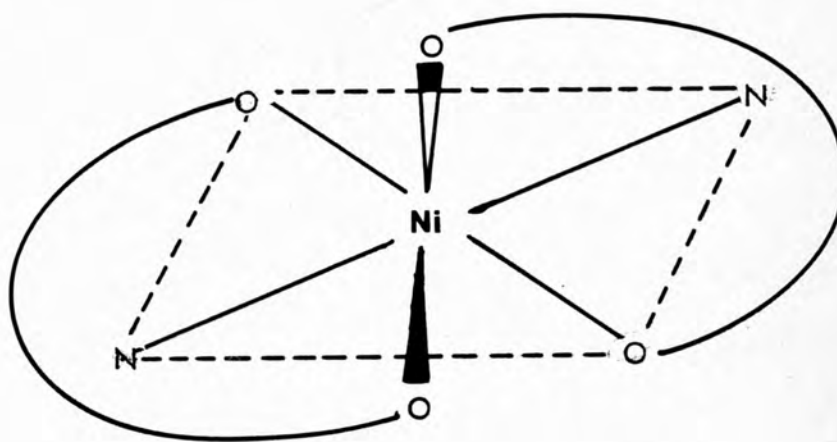


Fig. 2-1 Interaction of PLP-alanine Schiff base with aluminium ion

Nickel-pyridoxylidene-alanine complexes were studied by Eichorn et al², who postulated that a 2:1 Schiff base:metal ratio existed and further that the structures were trans:



(14)

The stability of trans complexes relative to the cis type can be seen from models to be greater in the case of trans isomers and therefore that form will predominate.

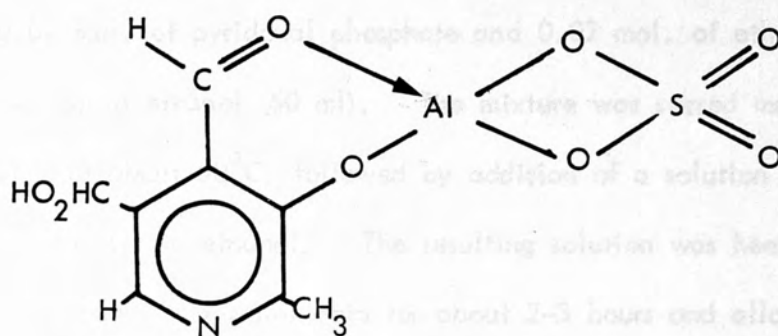
Some metal-pyridoxal phosphate and metal-pyridoxamine phosphate complexes were discussed by McMillan²³ and the 1:1 ratio of (PLP) or (PMP to metal ion was confirmed in various complexes.

McMillan²⁴ also synthesised various Schiff base complexes of pyridoxal phosphate-L-glutamate and pyridoxamine- α ketoglutaric acid with some transition metals in different ratios.

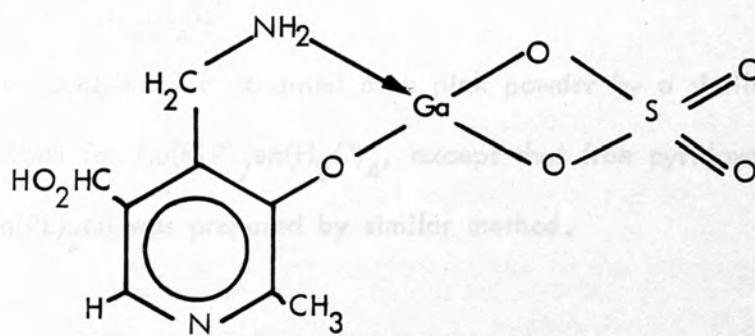
Fasella et al²⁴ and McMillan²³ suggested that the (Al-PLP) and (Ga-PMP) have similar chelation with sulphate radicals attached to the metal (Al or Ga) to achieve the required co-ordination number:

Preparation of Metal-Schiff Base Complexes

(15) $(\text{Al}(\text{NO}_3)_3 \cdot 9\text{H}_2\text{O})$



(15)



(16)

2.3 Preparation of Metal-Schiff Base Complexes:

(1) $\text{Cu(PLP)}_2\text{en}, 4\text{H}_2\text{O}$

0.02 mol. of pyridoxal phosphate and 0.02 mol. of ethylenediamine were dissolved in ethanol (50 ml). The mixture was stirred magnetically for 30 min. at about 50°C , followed by addition of a solution of $\text{CuSO}_4 \cdot 5\text{H}_2\text{O}$ (0.01 mol.) in ethanol. The resulting solution was heated at the above temperature in a water bath for about 2-3 hours and allowed to stand overnight in a refrigerator. A green precipitate was formed, filtered off, washed with methanol and dried in a desiccator over P_2O_5 .

This complex is not soluble in common organic solvents.

$\text{Zn(PLP)}_2\text{en}$ was prepared by the same procedure.

(2) $\text{Cu(PL)}_2\text{en}, (\text{H}_2\text{O})_4$

This complex was obtained as a pink powder by a similar method to that described for $\text{Cu(PLP)}_2\text{en}(\text{H}_2\text{O})_4$, except that free pyridoxal* was used.

$\text{Zn(PL)}_2\text{en}$ was prepared by similar method.

* Free pyridoxal was prepared from pyridoxal hydrochloride, as follows:

To a solution of pyridoxal hydrochloride in a small amount of water was added a 20% aqueous solution of sodium hydroxide, the pH being adjusted at about 6.5. A white crystalline precipitate was filtered off, washed with cold water, and dried in a desiccator over silica gel.

(3) $\text{Co}(\text{PL})_2\text{en}, 2\text{H}_2\text{O}$:

0.005 mol. Cobalt acetate tetrahydrate was dissolved in a small amount of water and was added to an ethanolic solution of $(\text{PL})_2\text{en}$ Schiff base, which had been prepared in advance, from pyridoxal hydrochloride* (0.02 mol.), ethylenediamine (0.01 mol.) and sodium carbonate (0.01 mol.) in ethanol-water. The resulting solution was heated for 30 min. at about 50°C with stirring. A dark-red microcrystalline precipitate was filtered off, washed with warm methanol and stored in a desiccator over P_2O_5 . The preparation ^{was} carried out under N_2 .

(4) $\text{Ni}(\text{PL})_2\text{en}, 3\text{H}_2\text{O}$

0.022 mol. pyridoxal and 0.022 mol. ethylenediamine were dissolved in ethanol (100 ml.) and heated at about 50°C with stirring, until a transparent solution was obtained containing the Schiff base of $(\text{PL})_2\text{en}$. 0.01 mol. nickel acetate tetrahydrate and an aqueous solution of sodium carbonate (0.008 mol.) were added to the resulting solution $((\text{PL})_2\text{en})$, heated at the same temperature (50°C) for 2 to 3 hours and allowed to stand overnight in a refrigerator. An orange precipitate formed was filtered off, washed with methanol, and dried in a desiccator over P_2O_5 .

* In the method described above, free pyridoxal may be used instead of the combination of pyridoxal hydrochloride and sodium carbonate.

(5) $M^{+n}(\text{PLP})_2\text{en}, x \text{H}_2\text{O}$

0.02 mol. pyridoxal phosphate and 0.02 mol. ethylenediamine were dissolved in 50 ml. ethanol (50%). The resulting solution was heated at about 50°C for about 30 min. with stirring. By addition of 0.01 mol. of metal salt* immediately the complexes appeared with good yield. They were stirred magnetically for about 30 min. then filtered off, and stored in a desiccator over silica gel.

(6) $\text{Fe}(\text{PLP}, \text{Gly}), (\text{H}_2\text{O})(\text{OAc})$:

Stoichiometric amounts of pyridoxal phosphate, glycine and $\text{Fe}(\text{NH}_4)_2(\text{SO}_4)_2 \cdot 6\text{H}_2\text{O}$ were dissolved in a neutral aqueous acetate buffer solution. The resulting solution was heated for about 15 min. at 75°C. Upon cooling a brown precipitate was filtered off, washed with cold methanol and dried at room temperature in a desiccator over P_2O_5 .

(7) $\text{Fe}(\text{PLGly}), (\text{H}_2\text{O})(\text{OAc})$:

This complex was prepared in the same manner as described above for the (PLPGly) analog except that $\text{FeSO}_4 \cdot 7\text{H}_2\text{O}$ was used. The dark red product was filtered off, washed with methanol and dried at room temperature in a desiccator over P_2O_5 .

-
- * Cu^{+2} = Copper chloride CuCl_2
 Ni^{+2} = Nickel chloride hexahydrate $\text{NiCl}_2 \cdot 6\text{H}_2\text{O}$
 Co^{+2} = Cobalt chloride hexahydrate $\text{CoCl}_2 \cdot 6\text{H}_2\text{O}$
 Fe^{+2} = Iron chloride FeCl_2

(8) $M^{+2}(\text{PLGly}), \times \text{H}_2\text{O}$:

0.02 mol. pyridoxal hydrochloride and (0.02 mol.) glycine were dissolved in 100 ml. ethanol. The mixture was heated for 15 min. with stirring at about 50°C. 0.01 mol. metal* salt and an aqueous solution of sodium carbonate (0.02 mol.) were added to the resulting solution (yellow Schiff base, PLGly), and heated at this temperature (50°C) for 2-3 hours, and allowed to stand overnight in a refrigerator. The precipitates formed were filtered off, washed with methanol, and dried in a desiccator over P_2O_5 .

(9) $M^{+2}(\text{PLPGly}), \times \text{H}_2\text{O}$:

0.02 mol. pyridoxal phosphate and 0.02 mol. glycine were dissolved in 100 ml. ethanol (50%). The resulting solution was heated for 30 min. at about 50°C with stirring followed by addition of an aqueous solution of metal** salt (0.02 mol.) which had been dissolved in a minimum volume of water. The mixture solution was heated at (50°C) for 2-3 hours with stirring, and allowed to stand overnight in a refrigerator. The precipitate was filtered off in good yield, washed and dried over silica gel.

*	Cu^{+2}	=	Copper acetate	$\text{Cu}(\text{C}_2\text{H}_3\text{O}_2)_2 \cdot \text{H}_2\text{O}$
	Ni^{+2}	=	Nickel acetate tetrahydrate	$\text{Ni}(\text{C}_2\text{H}_3\text{O}_2)_2 \cdot 4\text{H}_2\text{O}$
	Co^{+2}	=	Cobalt acetate tetrahydrate	$\text{Co}(\text{C}_2\text{H}_3\text{O}_2)_2 \cdot 4\text{H}_2\text{O}$
<hr/>				
**	Cu^{+2}	=	Copper chloride	CuCl_2
	Ni^{+2}	=	Nickel chloride hexahydrate	$\text{NiCl}_2 \cdot 6\text{H}_2\text{O}$
	Co^{+2}	=	Cobalt chloride hexahydrate	$\text{CoCl}_2 \cdot 6\text{H}_2\text{O}$

(10) $\text{Cu}(\text{PNen})_2(\text{SO}_4)_2\text{Cl}_2 \cdot 5\text{H}_2\text{O}$:

0.005 mol. of pyridoxine hydrochloride was dissolved in 50 ml. ethanol, followed by the addition of 0.005 mol. ethylenediamine. The resulting solution was heated with stirring for about 15 min. at 50°C , followed by the addition of 0.005 mol. copper sulphate ($\text{CuSO}_4 \cdot 5\text{H}_2\text{O}$). The mixture was heated for 30 min., the green precipitate was filtered off, washed with methanol and dried in a desiccator over P_2O_5 .

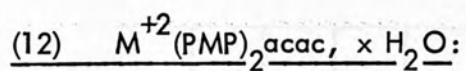
This compound was slightly soluble in the common organic solvents.

(11) $\text{Cu}(\text{PN})_2 \cdot 2\text{H}_2\text{O}$:

0.005 mol. of pyridoxine hydrochloride was dissolved in 50 ml. ethanol, followed by the addition of 0.005 mol. copper sulphate ($\text{CuSO}_4 \cdot 5\text{H}_2\text{O}$). The resulting solution was heated with stirring for about 15 min. at 50°C . The light green precipitate was filtered off, washed with methanol and dried in a desiccator over P_2O_5 .

This complex was slightly soluble in common organic solvents.

- Cu^{+2} = Copper chloride CuCl_2
 Ni^{+2} = Nickel chloride hexahydrate $\text{NiCl}_2 \cdot 6\text{H}_2\text{O}$
 Co^{+2} = Cobalt chloride hexahydrate $\text{CoCl}_2 \cdot 6\text{H}_2\text{O}$



0.02 mol. pyridoxamine phosphate hydrochloride was dissolved in the minimum volume of water, followed by the addition of 0.01 mol. acetylacetone. The mixture was heated for about 30 min. at 50°C with stirring. The resulting solution (Schiff base) was added to 0.02 mol. sodium carbonate, followed by the addition of 0.01 mol. metal salt*. After 30 min. heating at 50°C and stirring magnetically, the precipitates appeared. They were filtered off, washed with water and stored in a desiccator over P₂O₅. These compounds were not soluble in common organic solvents.

-
- * Cu^{+2} = Copper chloride $CuCl_2$
 Ni^{+2} = Nickel chloride hexahydrate $NiCl_2 \cdot 6H_2O$
 Co^{+2} = Cobalt chloride hexahydrate $CoCl_2 \cdot 6H_2O$

Table: 2-1 Analytical Data of Metal Schiff Base Complexes

No.	Complexes	Calc., %			Found, %			Colour*
		C	H	N	C	H	N	
1	Cu(PLP) ₂ en, 4H ₂ O	33.0	3.6	8.7	32.9	4.3	9.3	Green
2	Cu(PL) ₂ en, H ₂ O	49.0	4.9	12.7	49.3	4.7	12.9	Pink
3	Zn(PLP) ₂ enCl ₂ , 2H ₂ O	31.3	3.9	8.2	30.9	3.9	8.3	Orange
4	Zn(PL) ₂ en, 2H ₂ O	46.9	5.2	12.2	47.1	5.1	12.2	P. Yellow
5	Ni(PLP) ₂ en, 4H ₂ O	33.4	4.6	8.7	32.8	5.0	10.6	Red
6	Ni(PL) ₂ en, 3H ₂ O	46.0	5.1	11.9	46.1	4.7	12.3	Orange
7	Co(PLP) ₂ en, 4H ₂ O	33.4	4.6	8.7	33.8	5.3	12.5	Brown
8	Co(PL) ₂ en, 2H ₂ O	47.9	4.9	12.4	47.9	4.7	12.8	Orange
9	Cd(PLP) ₂ enCl ₃ , 6H ₂ O	25.6	4.0	6.6	25.3	3.4	6.8	Y. Brown
10	Fe(PLPGly) (OAc), H ₂ O	33.0	3.7	6.4	32.9	4.0	6.4	Brown
11	Fe(PLGly) (OAc), H ₂ O	40.5	4.2	7.9	40.6	4.3	7.7	Red. Brown
12	Co(PLPGly), H ₂ O	31.6	3.7	7.3	31.5	4.2	5.8	D. Red

* Y: yellowish, P: pale, D: dark

Table 2-1 (continued)

No.	Complexes	Calc., %			Found, %			Colour*
		C	H	N	C	H	N	
13	Co(PLGly), 2H ₂ O	37.7	4.0	8.8	37.5	3.8	8.2	L. Brown
14	(Ni) ₂ (PLPGly), 6H ₂ O	22.5	4.5	5.2	21.6	4.5	5.2	Y. Brown
15	Ni(PLGly), H ₂ O	40.1	4.4	9.4	40.3	4.7	9.8	G. Brown
16	Cu(PLPGly), 3H ₂ O	28.5	3.8	6.6	28.2	2.9	5.2	Red
17	(Cu) ₂ (PLGly), 3H ₂ O	27.5	3.8	6.4	28.0	2.9	7.3	Olive
18	Cu(PMP) ₂ acac, 5H ₂ O	35.2	5.3	7.9	35.0	4.6	8.7	Green
19	Co(PMP) ₂ , 4H ₂ O	30.5	5.1	8.9	30.0	4.8	9.0	P. Yellow
20	Ni(PMP) ₂ , 3H ₂ O	31.5	4.9	9.2	31.8	5.0	9.5	P. Green
21	Cu(PN) ₂ (SO ₄) ₂ Cl ₂ , 5H ₂ O	28.8	4.6	10.0	28.3	4.8	10.0	Green
22	Cu(PN), 2 H ₂ O	38.4	5.1	5.6	38.4	5.2	5.6	L. Green
23	Fe(PLP) ₂ en Cl, 6H ₂ O	26.2	3.9	6.8	26.2	3.5	6.3	D. Red
24	Ag(PL) ₂ en Cl ₂ , 5H ₂ O	29.5	3.8	7.7	29.8	3.2	7.9	D. Yellow

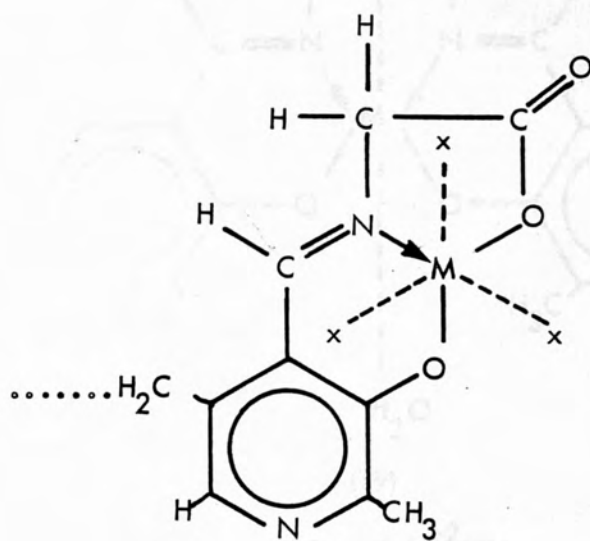
* L: Light; Y: yellowish; G: greenish; P: pale; D: dark.

Table 2-2 Empirical Formula of Metal-Schiff Base Complexes

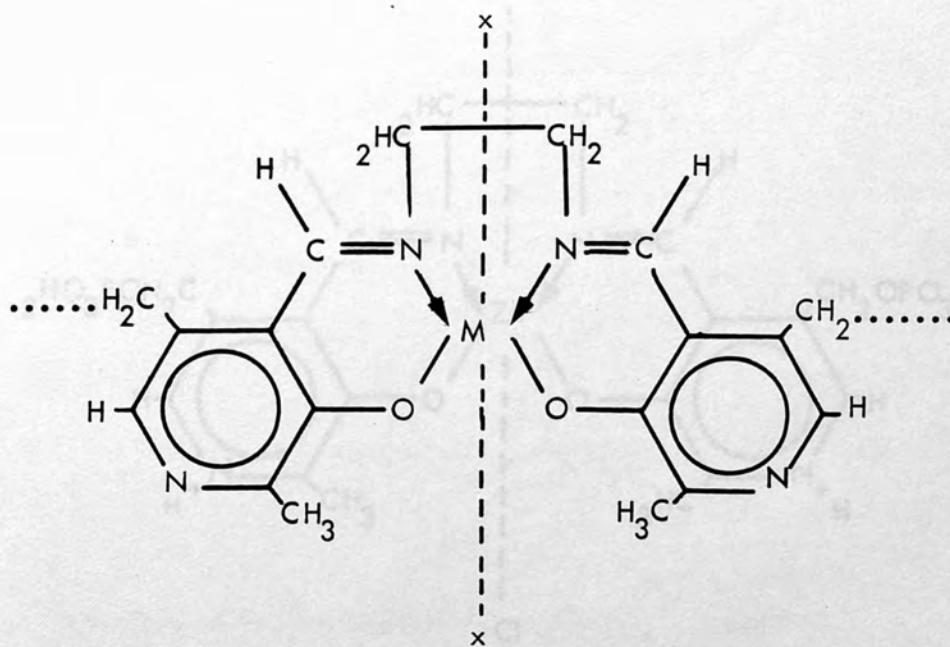
No.	Complexes	Empirical Formula
1	$\text{Cu}(\text{PLP})_2\text{en}, 4\text{H}_2\text{O}$	$\text{C}_{18}\text{H}_{28}\text{O}_{14}\text{N}_4\text{P}_2\text{Cu}$
2	$\text{Cu}(\text{PL})_2\text{en}, \text{H}_2\text{O}$	$\text{C}_{18}\text{H}_{20}\text{O}_5\text{N}_4\text{Cu}$
3	$\text{Zn}(\text{PLP})_2\text{enCl}_2, 2\text{H}_2\text{O}$	$\text{C}_{18}\text{H}_{24}\text{O}_{12}\text{N}_4\text{P}_2\text{Cl}_2\text{Zn}$
4	$\text{Zn}(\text{PL})_2\text{en}, 2\text{H}_2\text{O}$	$\text{C}_{18}\text{H}_{22}\text{O}_6\text{N}_4\text{Zn}$
5	$\text{Ni}(\text{PLP})_2\text{en}, 4\text{H}_2\text{O}$	$\text{C}_{18}\text{H}_{28}\text{O}_{14}\text{N}_4\text{P}_2\text{Ni}$
6	$\text{Ni}(\text{PL})_2\text{en}, 3\text{H}_2\text{O}$	$\text{C}_{18}\text{H}_{26}\text{O}_7\text{N}_4\text{Ni}$
7	$\text{Co}(\text{PLP})_2\text{en}, 4\text{H}_2\text{O}$	$\text{C}_{18}\text{H}_{28}\text{O}_{14}\text{N}_4\text{P}_2\text{Co}$
8	$\text{Co}(\text{PL})_2\text{en}, 2\text{H}_2\text{O}$	$\text{C}_{18}\text{H}_{22}\text{O}_6\text{N}_4\text{Co}$
9	$\text{Cd}(\text{PLP})_2\text{enCl}_3, 6\text{H}_2\text{O}$	$\text{C}_{18}\text{H}_{32}\text{O}_{16}\text{N}_4\text{P}_2\text{Cl}_3\text{Cd}$
10	$\text{Fe}(\text{PLPGly}) \text{OAc}, \text{H}_2\text{O}$	$\text{C}_{12}\text{H}_{15}\text{O}_{10}\text{N}_2\text{PFe}$
11	$\text{Fe}(\text{PLPGly}) \text{OAc}, \text{H}_2\text{O}$	$\text{C}_{12}\text{H}_{14}\text{O}_7\text{N}_2\text{Fe}$
12	$\text{Co}(\text{PLPGly}), \text{H}_2\text{O}$	$\text{C}_{10}\text{H}_{12}\text{O}_8\text{N}_2\text{PCo}$
13	$\text{Co}(\text{PLGly}), 2\text{H}_2\text{O}$	$\text{C}_{10}\text{H}_{13}\text{O}_6\text{N}_2\text{Co}$
14	$\text{Ni}_2(\text{PLPGly}), 6\text{H}_2\text{O}$	$\text{C}_{10}\text{H}_{24}\text{O}_{15}\text{N}_2\text{PNi}_2$
15	$\text{Ni}(\text{PLGly}), \text{H}_2\text{O}$	$\text{C}_{10}\text{H}_{11}\text{O}_5\text{N}_2\text{Ni}$
16	$\text{Cu}(\text{PLPGly}), 3\text{H}_2\text{O}$	$\text{C}_{10}\text{H}_{16}\text{O}_{10}\text{N}_2\text{PCu}$
17	$\text{Cu}_2(\text{PLGly}), 3\text{H}_2\text{O}$	$\text{C}_{10}\text{H}_{17}\text{O}_9\text{N}_2\text{Cu}_2$
18	$\text{Cu}(\text{PMP})_2\text{acac}, 5\text{H}_2\text{O}$	$\text{C}_{21}\text{H}_{38}\text{O}_{15}\text{N}_4\text{P}_2\text{Cu}$
19	$\text{Co}(\text{PMP})_2, 4\text{H}_2\text{O}$	$\text{C}_{16}\text{H}_{32}\text{O}_{14}\text{N}_4\text{P}_2\text{Co}$
20	$\text{Ni}(\text{PMP})_2, 3\text{H}_2\text{O}$	$\text{C}_{16}\text{H}_{30}\text{O}_{13}\text{N}_4\text{P}_2\text{Ni}$
21	$\text{Cu}(\text{PN})_2(\text{SO}_4)_2\text{Cl}_2, 5\text{H}_2\text{O}$	$\text{C}_{20}\text{H}_{38}\text{O}_{17}\text{N}_6\text{Cl}_2\text{S}_2\text{Cu}$
22	$\text{Cu}(\text{PN}), 2\text{H}_2\text{O}$	$\text{C}_8\text{H}_{13}\text{O}_4\text{NCu}$
23	$\text{Fe}(\text{PLP})_2\text{enCl}, 6\text{H}_2\text{O}$	$\text{C}_{18}\text{H}_{32}\text{O}_{16}\text{N}_4\text{P}_2\text{ClFe}$
24	$\text{Ag}(\text{PL})_2\text{enCl}_5, 5\text{H}_2\text{O}$	$\text{C}_{18}\text{H}_{28}\text{O}_9\text{N}_4\text{Cl}_5\text{Ag}$

Proposed Structures

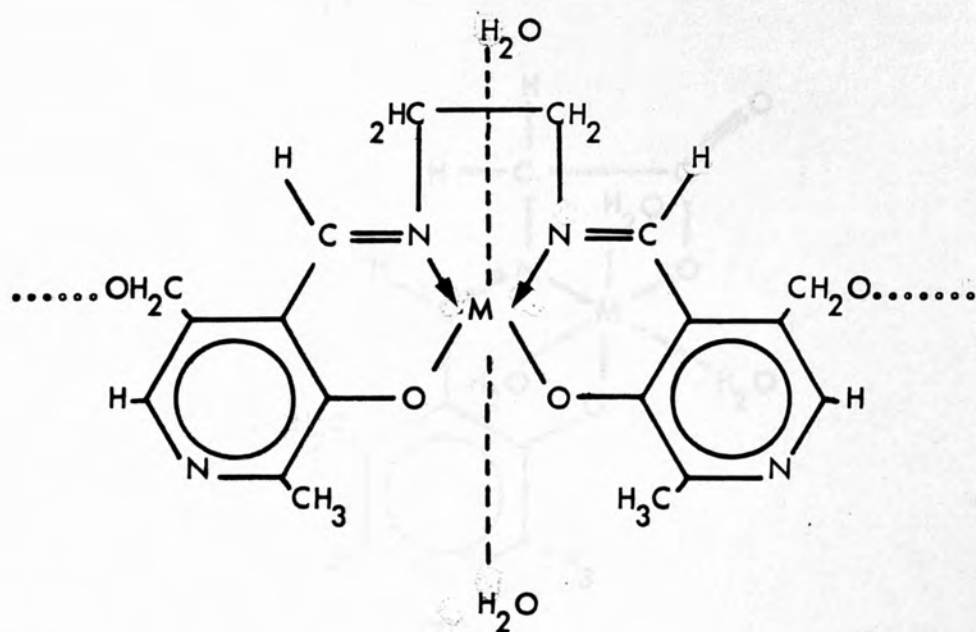
General Structures



(17)



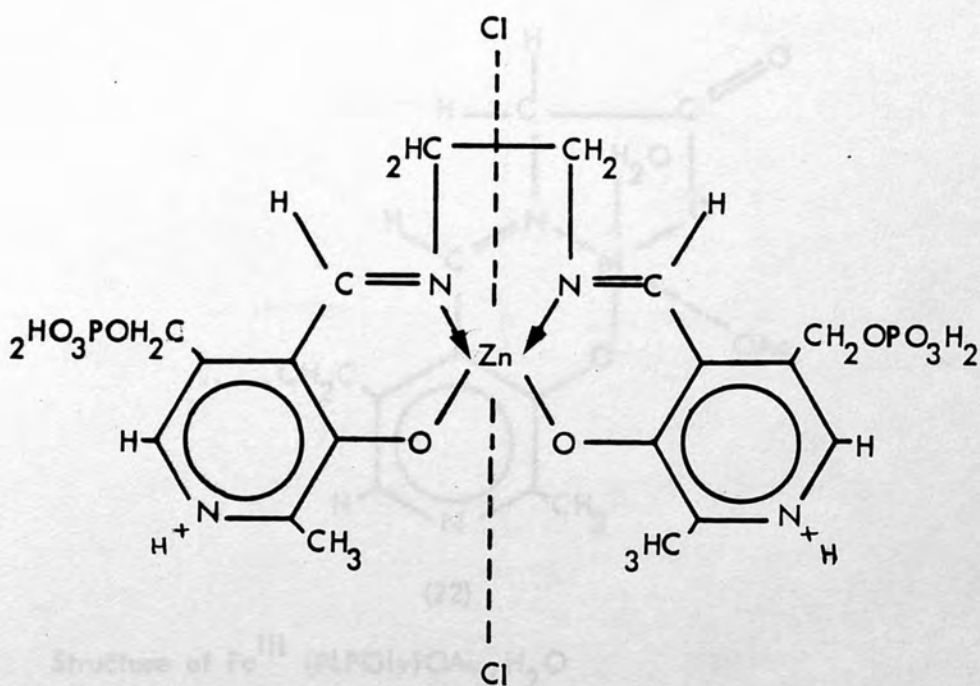
(18)



(19)

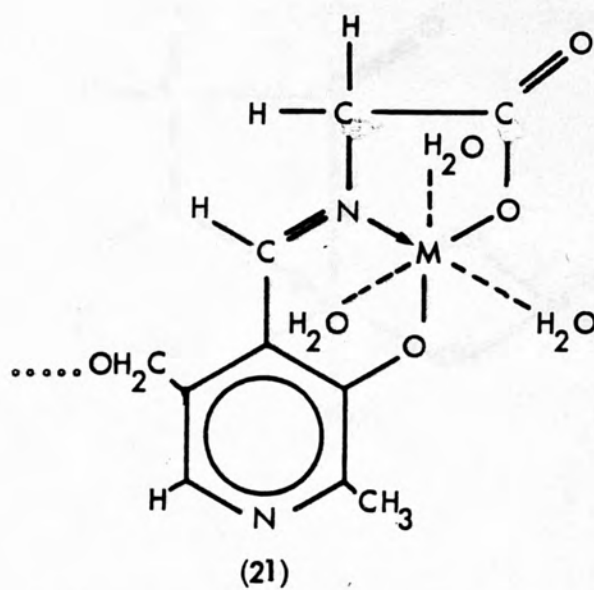
Structure of $M^{+2}(\text{PLP})_2\text{en}, x\text{H}_2\text{O}$ and $M^{+2}(\text{PL})_2\text{en}, x\text{H}_2\text{O}$

$M^{+2} = \text{Cu}^{\text{II}}, \text{Co}^{\text{II}}, \text{Ni}^{\text{II}}, \text{Zn}^{\text{II}}$

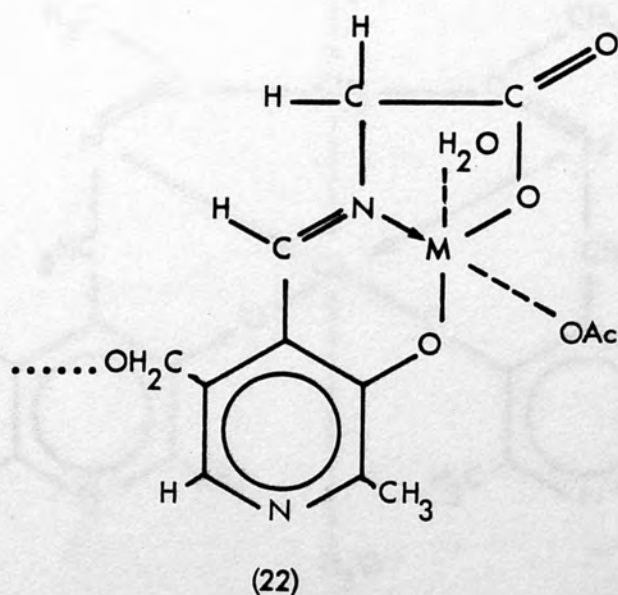
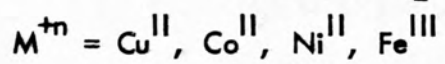


(20)

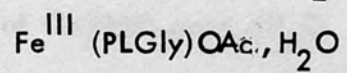
Structure of $\text{Zn}(\text{PLP})_2\text{enCl}_2, 2\text{H}_2\text{O}$

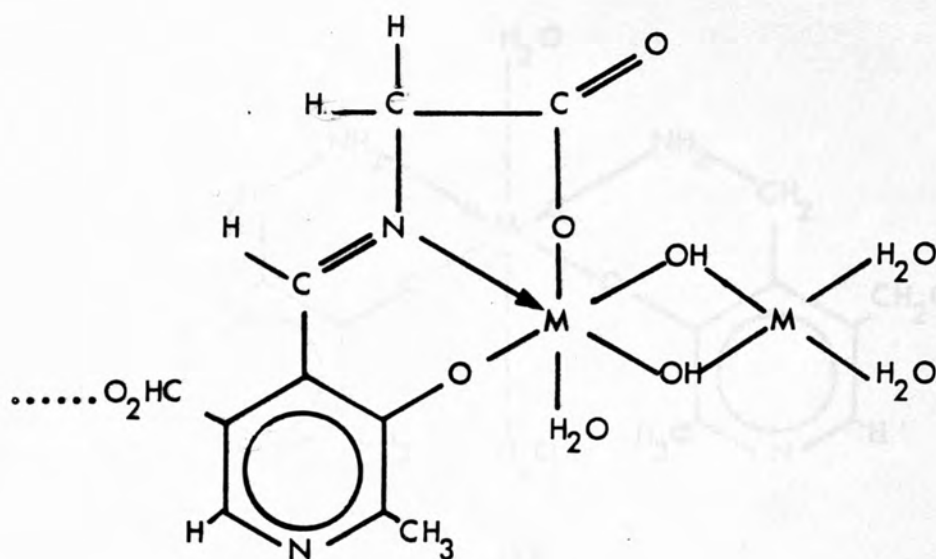


Structure of $M^{+n}(\text{PLPGly}), x\text{H}_2\text{O}$ and $M^{+n}(\text{PLGly}), x\text{H}_2\text{O}$

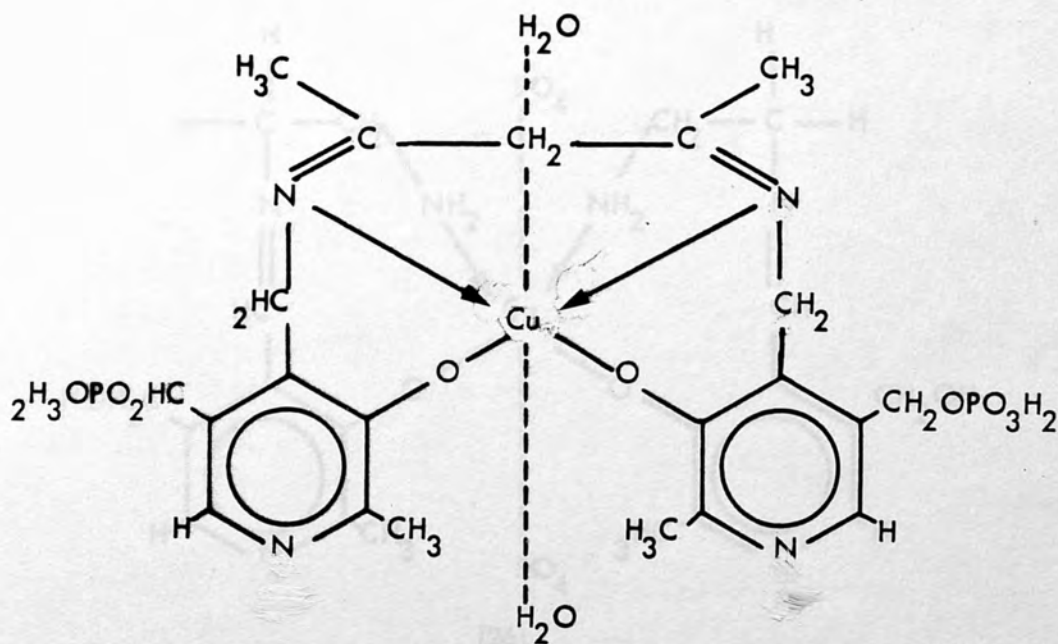


Structure of $\text{Fe}^{\text{III}}(\text{PLPGly})\text{OAc}, \text{H}_2\text{O}$





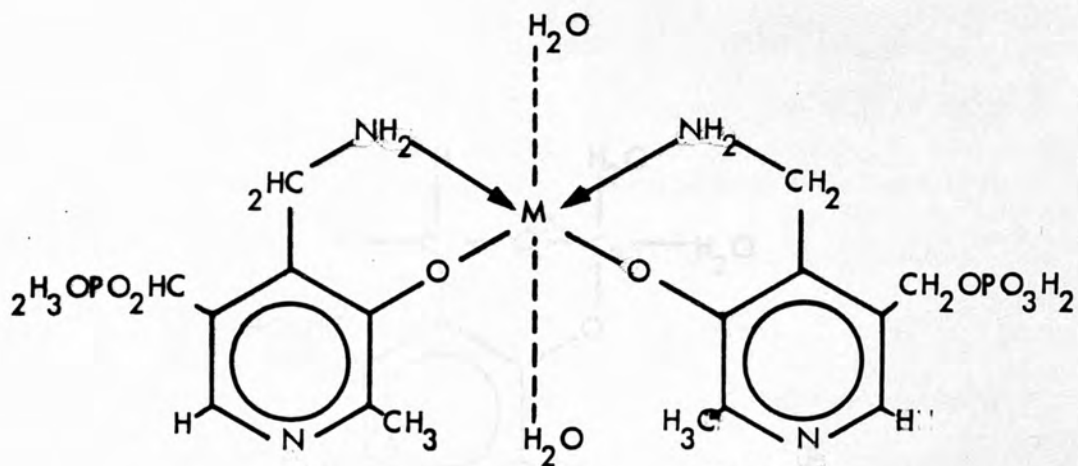
(23)

Structure of $Ni_2(PLP)Gly, 6H_2O$ $Cu_2(PLGly), 3H_2O$ 

(24)

Structure of $Cu(PMP)_2acac, 5H_2O$

P% Calc. = 8.7 Found = 9.5

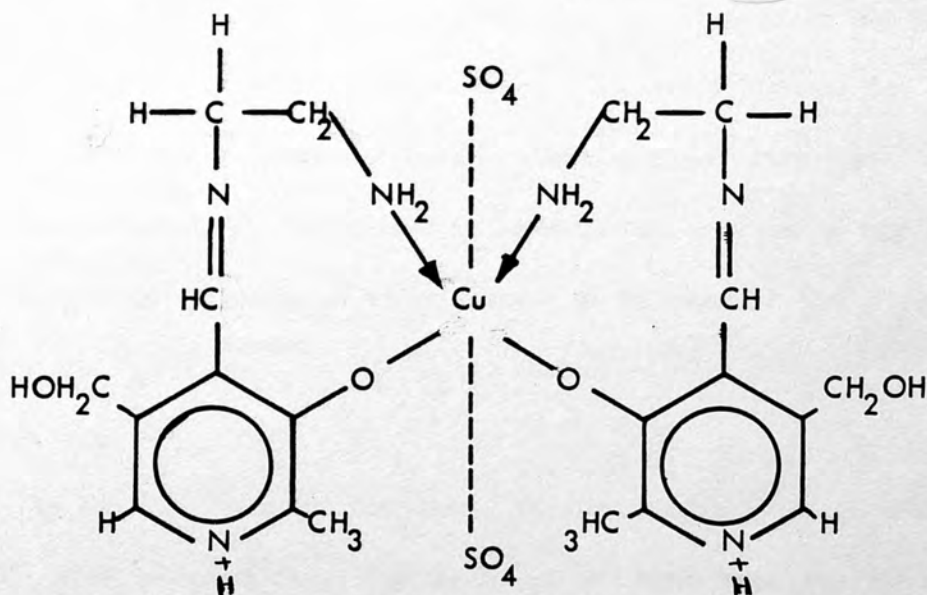


(25)

Structure of $M^{+2}(\text{PMP})_2 \cdot x\text{H}_2\text{O}$ $M^{+2} = \text{Ni}^{\text{II}}, \text{Co}^{\text{II}}$

P% Co^{II} Calc. = 9.9 Found = 8.36

P% Ni^{II} Calc. = 10.2 Found = 10.2

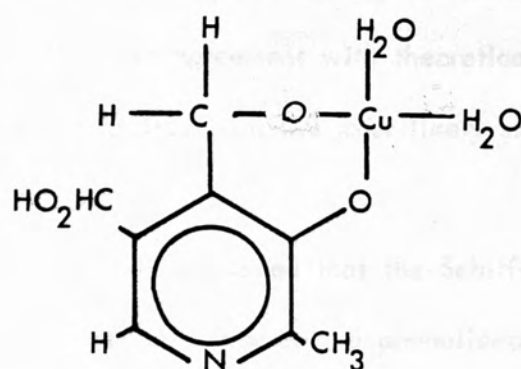


(26)

Structure of $\text{Cu}(\text{PNen})_2(\text{SO}_4)_2 \cdot \text{Cl}_2 \cdot 5\text{H}_2\text{O} \cdot 4\text{H}^+$

S% Calc. = 7.68 Found = 7.15

Cl% Calc. = 8.5 Found = 7.55



(27)

Structure of $\text{CuPN}, 2\text{H}_2\text{O}$

The structure of the Schiff base (1) consists of a pyridine ring substituted with a methyl group at the 2-position, a hydroxyl group at the 4-position, and a hydroxymethyl group at the 5-position. The nitrogen atom of the pyridine ring is coordinated to the copper ion. The oxygen atom of the hydroxyl group at the 4-position is also coordinated to the copper ion. The copper ion is also coordinated to two water molecules (H_2O).

In the Schiff base (1) complexes, the structures of (PLPGly) and (PLGly) metal complexes were considered and the ratio found was 1:1:1 (PL or $\text{PLP}:\text{Gly}:\text{M}^{2+}$), except in the case of Cu^{2+} and Mn^{2+} , which appear to be dimeric complexes with hydrogen bonds holding the two metals and changing the ratio to 1:1:2. This Schiff base (1) is a bidentate ligand and co-ordinates to metal ions through the azomethine-nitrogen and the

2.4 Discussion

General structures for all complexes are proposed (17,18).

However, distinctive analysis results are set out in table (2-1). The analysis results are in good agreement with theoretical results and it is therefore maintained that these are the most likely structures for the complexes.

In all complexes it is assumed that the Schiff-base is bonded to metal ions through the imine-nitrogen and phenolic-oxygen; bonding through the carboxylic oxygen of amino acid in some cases can take place, but this would imply that the Schiff-base is a tridentate ligand. In no case was the pyridine ring involved in co-ordination.

In the Schiff-base (2) complexes, the ratio found was 2:1:1 (2PLP or 2PL:1en:1M⁺ⁿ) and was common to this series of complexes. The Schiff-base (2) is co-ordinated to the metal ions through its two azomethine-nitrogens and two phenolic-oxygens; this would indicate that the Schiff-base (2) is a tetradentate ligand. The complexes were found to be six co-ordinated, the two remaining co-ordination positions of metal ions occupied by molecules of water, except in the cases of Zn(PLP)₂en, Cd(PLP)₂en, Fe(PLP)₂en, and Ag(PL)₂en, when they were occupied by chloride ions.

In the Schiff-base (1) complexes, the structures of (PLPGly) and (PLGly) metal complexes were considered and the ratio found was 1:1:1 (1PL or PLP:1Gly:1M⁺ⁿ), except in the case of Cu^{II} and Ni^{II}, which appear to be dimeric complexes with hydroxy radicals bridging the two metals and changing the ratio to 1:1:2. This Schiff-base (1) is a bidentate ligand and co-ordinates to metal ions through the azomethine-nitrogen and the

phenolic oxygen. The remaining co-ordination position of metal ions is occupied by a water molecule to achieve the required co-ordination number, except in $\text{Fe}^{\text{III}}\text{PLPGly}$, and $\text{Fe}^{\text{III}}\text{PLGly}$ which are five co-ordinated complexes and the fifth position is occupied by the acetate group (OAc).

In the Schiff-base complex of Cu-pyridoxamine phosphate-acetylacetone, there is one Schiff-base unit per metal ion, which shows the 2:1:1 ratio (2PMP:1acac:1Cu). The Schiff-base $((\text{PMP})_2\text{acac})$ is bonded to copper through azomethine-nitrogen and phenolic oxygen. The two remaining co-ordination positions are occupied by H_2O .

The pyridoxamine phosphate complexes of Ni^{II} and Co^{II} have a 2:1 ratio of PMP to the metal ions. The metal ions lie on the centre of symmetry and are chelated to the 4-aminomethyl and the phenolate group of PMP. Octahedral co-ordination is completed by water molecules.

The Schiff-base complex of $\text{Cu}-(\text{PNen})_2$ has a specific ratio of 2:2:1 (2PN:2en:1 Cu^{+2}). This complex is a six co-ordinated complex and the chelation of the Schiff-base to the Cu^{++} takes place through its amine groups and phenolic-oxygens. The fifth and sixth co-ordination positions of copper ion in this compound are occupied by two sulphate groups.

$\text{Cu}^{++}, \text{PN}$ was the only complex which was synthesised with a 1:1 ratio (1PN:1Cu). This complex was a four co-ordinated compound. The copper ion was chelated to pyridoxine through the phenolate-oxygen and the adjacent hydroxymethyl of the pyridoxine molecule.

In all metal complexes of pyridoxamine, and pyridoxine, the ligand exists as a Zwitterion with the ring nitrogen protonated¹⁰.

REFERENCES

1. D.E. Metzler, M. Ikawa and E.E. Snell, *JACS*, (1954), 76, 648.
2. G.L. Eichorn and J.W. Dawes, *JACS*, (1954), 76, 5663.
3. R.L. Gustafson and A.E. Martell, *Arch. Biochem. Biophys.*, (1957), 68, 485.
4. M.E. Farago, M.M. McMillan and S.S. Sabir, *Inorg. Chem. Acta.*, (1975), 14, 207.
5. M.E. Farago, and T. Matthews, *J. Chem. Soc. A.*, (1969), 609.
6. M.S. El-Ezaby and F.R. El-Eziri, *J. Inorg. Nucl. Chem.* (1976), 38, 901.
7. A. Mosset, F. Nepveu-Juras, R. Havan and Z.J. Bonnet, *J. Inorg. Nucl. Chem.*, (1978), 40, 1259.
8. K.J. Franklin and M.F. Richardson, *J. Chem. Soc. Chem. Commun.*, (1978), 97.
9. E.C. Kelusky and J.S. Hartman, *Can. J. Chem.* (1979), 57, 2118.
10. S. Yamada, Y. Kuge and T. Yamayoshi, *Inorg. Chem. Acta*, (1974), 8, 29.
11. S. Yamada, Y. Kuge, T. Yamayoshi, and H. Kuma, *Inorg. Chem. Acta.*, (1974), 11, 253.
12. S. Yamada, H. Kuma and K. Yamanouchi, *Inorg. Chem. Acta*, (1974), 10, 151.
13. J.T. Wroblewski and G. Long, *Inorg. Chem. Acta*, (1979), 36, 155.
14. Y. Kuge and S. Yamada, *Inorg. Chem. Acta*, (1977) 21, 85.
15. D.M. Thompson, W. Batenovich, and L.H.M. Hornich, *Inorg. Chem. Acta*, (1980), 46, 199.

16. T.A. Franklin and M.F. Richardson, *Inorg. Chem. Acta*, (1980), 46, 191.
17. J.F. Cutfield, D. Hall and T.N. Waters, *Chem. Comm.*, (1967), 15, 785.
18. H.N. Christensen, *JACS*, (1958), 80, 2305.
19. J.B. Longenecker and E.E. Snell, *Proc. Nat. Acad. Sci. U.S.*, (1956), 42, 221.
20. J. Cattaneo, J.C. Senez and P. Beaumont, *Biochem. Biophys. Acta*, (1960), 44, 543.
21. H.N. Christensen, *JACS*, (1957), 79, 4073.
22. P. Fasella, H. Liz, N. Siliprandi and C. Balgioni, *Biochem. Biophys. Acta*, (1956), 23, 417.
23. M.M. McMillan, M. Phil. Thesis, Bedford College, University of London, (1968).
24. P. Fasella, H. Liz, C. Balgioni and N. Siliprandi, *J. Inorg. Nucl. Chem.*, (1958), 8, 620.

CHAPTER 3

Ultra-Violet Study of Metal-Schiff Base Complexes in Aqueous Solution



Fig. 3-1: Schiff base ligand

Fig. 3-1: Various forms of Schiff base ligands in aqueous solution

Although the charges are low, the ligand is soluble in water or neutral solution, the absorption maximum increases in wavelength due to charge delocalization. This should not be surprising as probably involving some resonance with the neutral Schiff base.

Fig. 3-2:

3.1 Introduction

The ultraviolet spectrum of pyridoxal or pyridoxal phosphate is pH dependent; absorption maxima shift and bands often disappear as the pH is changed, due to protonation and deprotonation of the species which are shown in Figure 3-1:

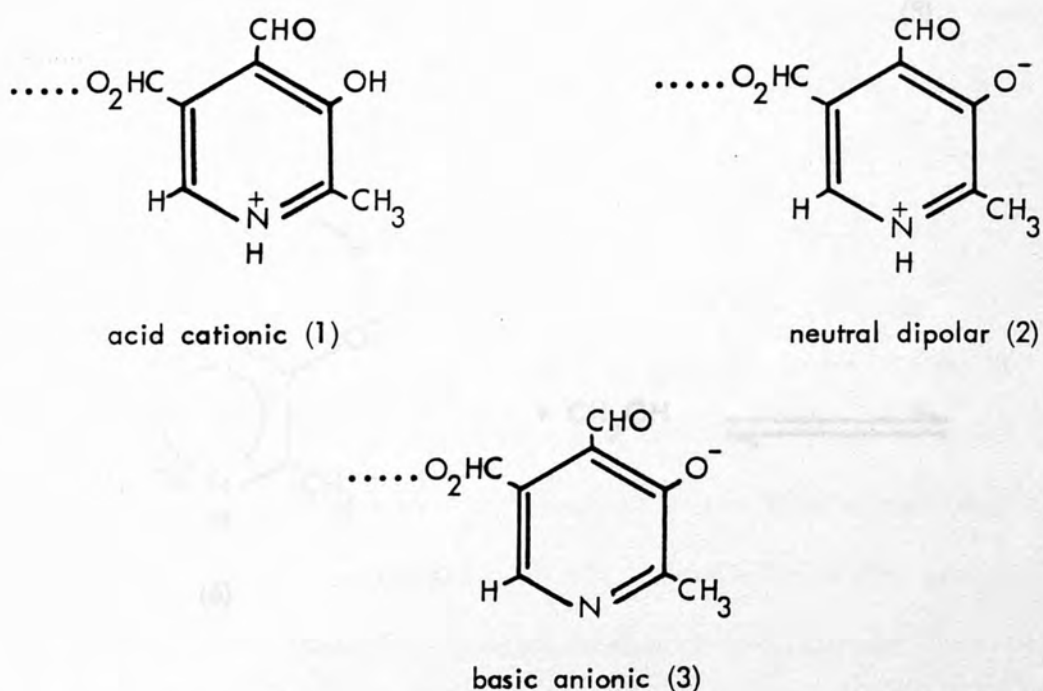


Fig. 3-1: Various forms of Pyridoxal or Pyridoxal Phosphate in Aqueous Solution

Pyridoxal exists in certain forms in aqueous solution¹. In methanol the electronic absorption spectrum of pyridoxal shows¹ gradual changes with time. Although the changes are slow, and not very noticeable in acidic or neutral solution, the absorption maximum increases in intensity but its wavelength does not change noticeably. These changes can be interpreted as probably involving acetal formation with the solvent as shown in

Fig. 3-2:

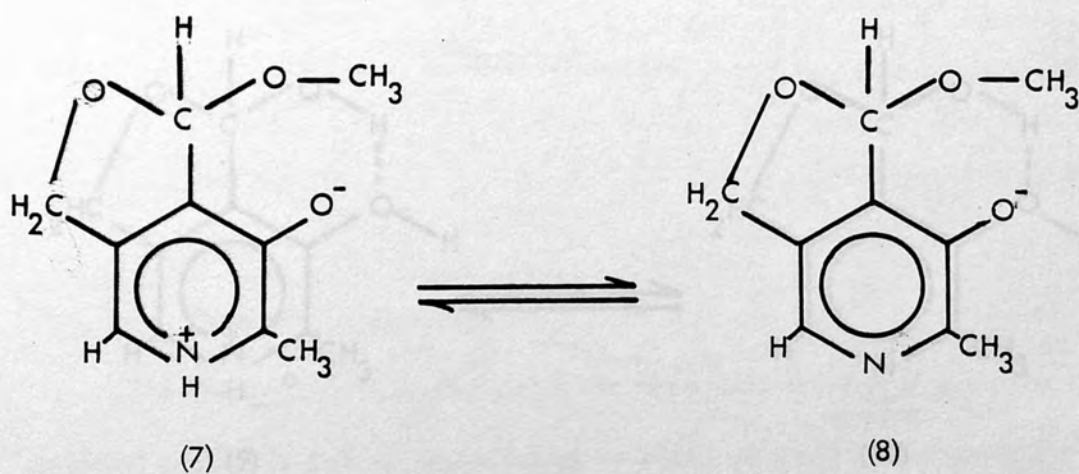
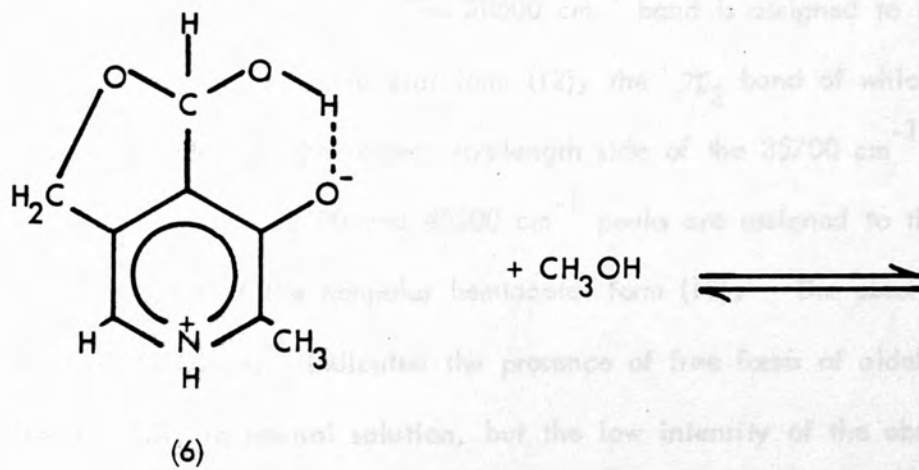
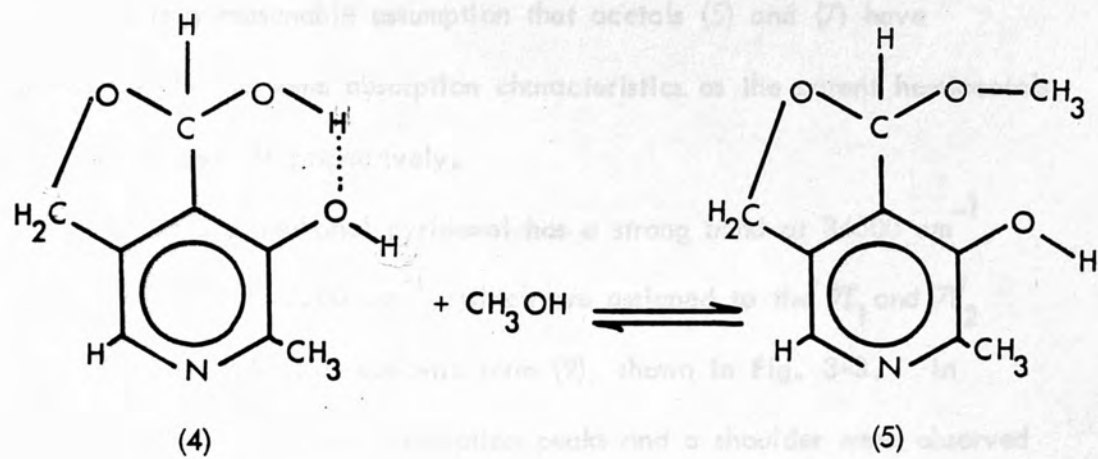


Fig. 3-2: Acetal formation of pyridoxal with methanol.

It is a reasonable assumption that acetals (5) and (7) have approximately the same absorption characteristics as the parent hemiacetals such as (4) and (6) respectively.

In acidic methanol pyridoxal has a strong band at 34500 cm^{-1} , and a shoulder at 43500 cm^{-1} , which are assigned to the π_1 and π_2 bands of the hemiacetal cationic form (9), shown in Fig. 3-3. In neutral methanol solution, absorption peaks and a shoulder were observed at 30500 , 35700 and 45500 cm^{-1} and a very weak absorption was also observed at 25000 cm^{-1} . The 30500 cm^{-1} band is assigned to the π_1 band of the dipolar hemiacetal form (12), the π_2 band of which is probably hidden by the lower wavelength side of the 35700 cm^{-1} absorption. The 35700 and 45500 cm^{-1} peaks are assigned to the π_1 and π_2 bands of the nonpolar hemiacetal form (10). The absorption band at 25000 cm^{-1} indicated the presence of free forms of aldehyde (14 and 15), in neutral solution, but the low intensity of the absorption indicated the existence of only small amounts of these species.

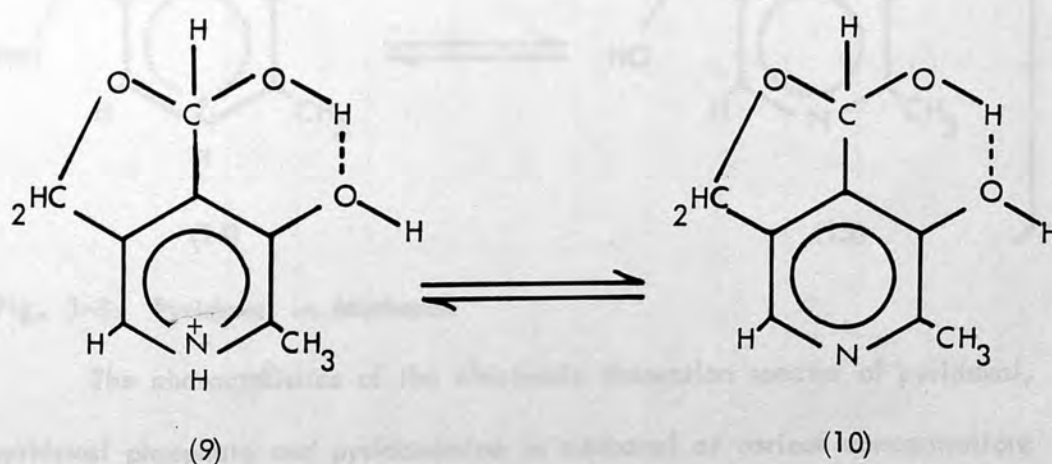


Fig. 3-3: Pyridoxal in Methanol.

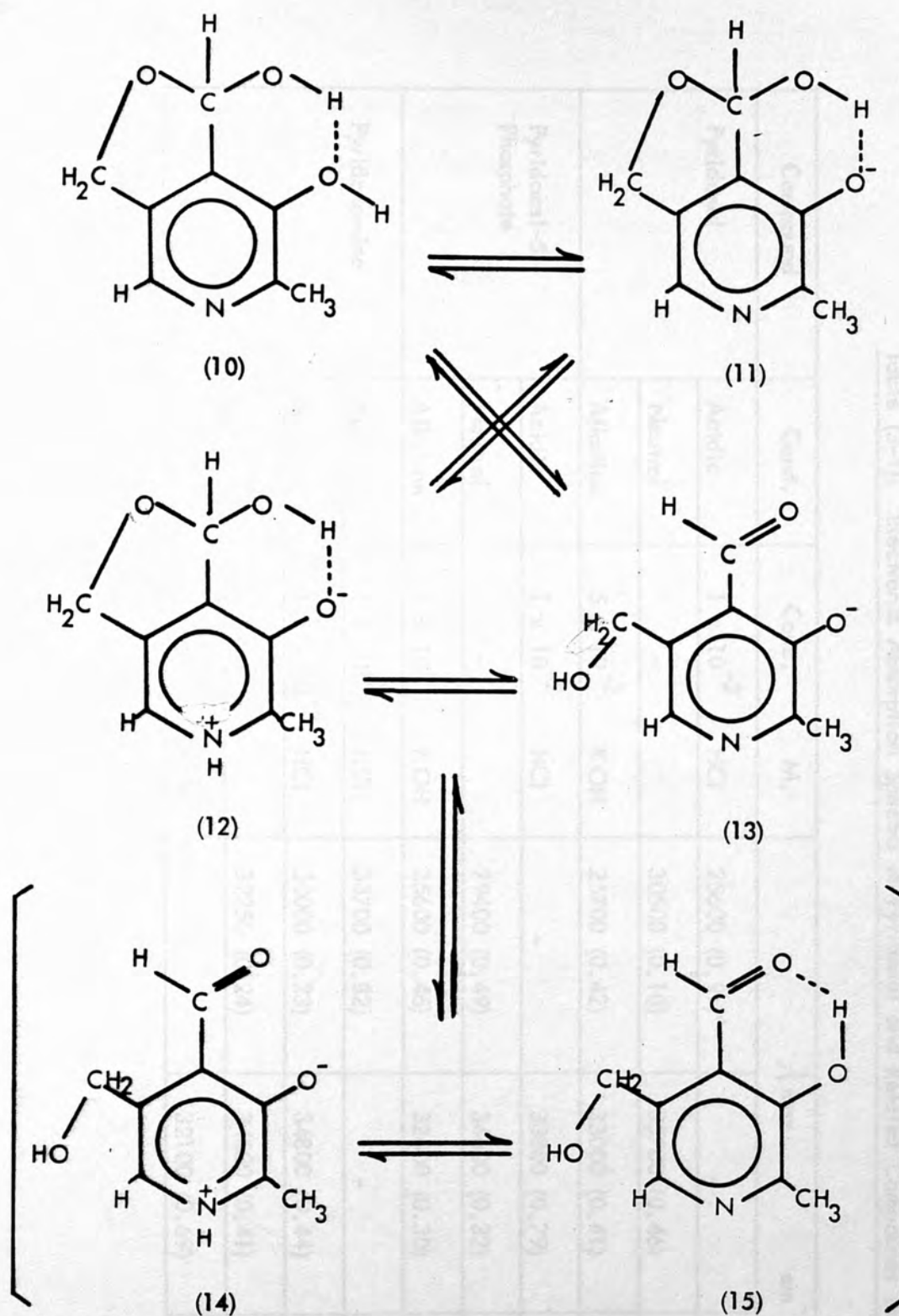


Fig. 3-3: Pyridoxal in Methanol

The characteristics of the electronic absorption spectra of pyridoxal, pyridoxal phosphate and pyridoxamine in methanol at various concentrations of acid and alkali are shown in Table (3-1):

Table (3-1): Electronic Absorption Spectra of Pyridoxal and Related Compounds in Methanol

Compound	Cond.	Conc.	M.	$\lambda_{\max.}$ cm^{-1}		
Pyridoxal	Acidic	1×10^{-2}	HCl	25600 (0.91)*	-	43500 (0.36)
	Neutral	-		30500 (0.10)	35700 (0.46)	45500 (0.67)
	Alkaline	5×10^{-2}	KOH	25700 (0.42)	33000 (0.41)	42700 (1.04)
Pyridoxal-5'- Phosphate	Acidic	1×10^{-2}	HCl	-	33800 (0.79)	43500 (0.30)
	Neutral	-		29400 (0.49)	34600 (0.32)	40000 (0.25)
	Alkaline	1×10^{-2}	KOH	25600 (0.46)	32600 (0.30)	43100 (1.05)
Pyridoxamine	Acidic	1×10^{-2}	HCl	33700 (0.82)	-	38500 (0.21)
	Acidic	1.5×10^{-4}	HCl	30000 (0.23)	34800 (0.44)	45450 (0.78)
	Neutral	-		32250 (0.24)	34600 (0.41)	40900 (0.27)
	Alkaline	1×10^{-2}	KOH	-	32100 (0.69)	40300 (0.67)

* = Numbers in parantheses give the absorbances for a 10-mm path.

Pyridoxal phosphate has a strong band at 34000 cm^{-1} and a shoulder at 43500 cm^{-1} , observed in acidic solution. These are assigned to the π_1 and π_2 bands, respectively, of the solvated cation (16) shown in Figure 3-4.

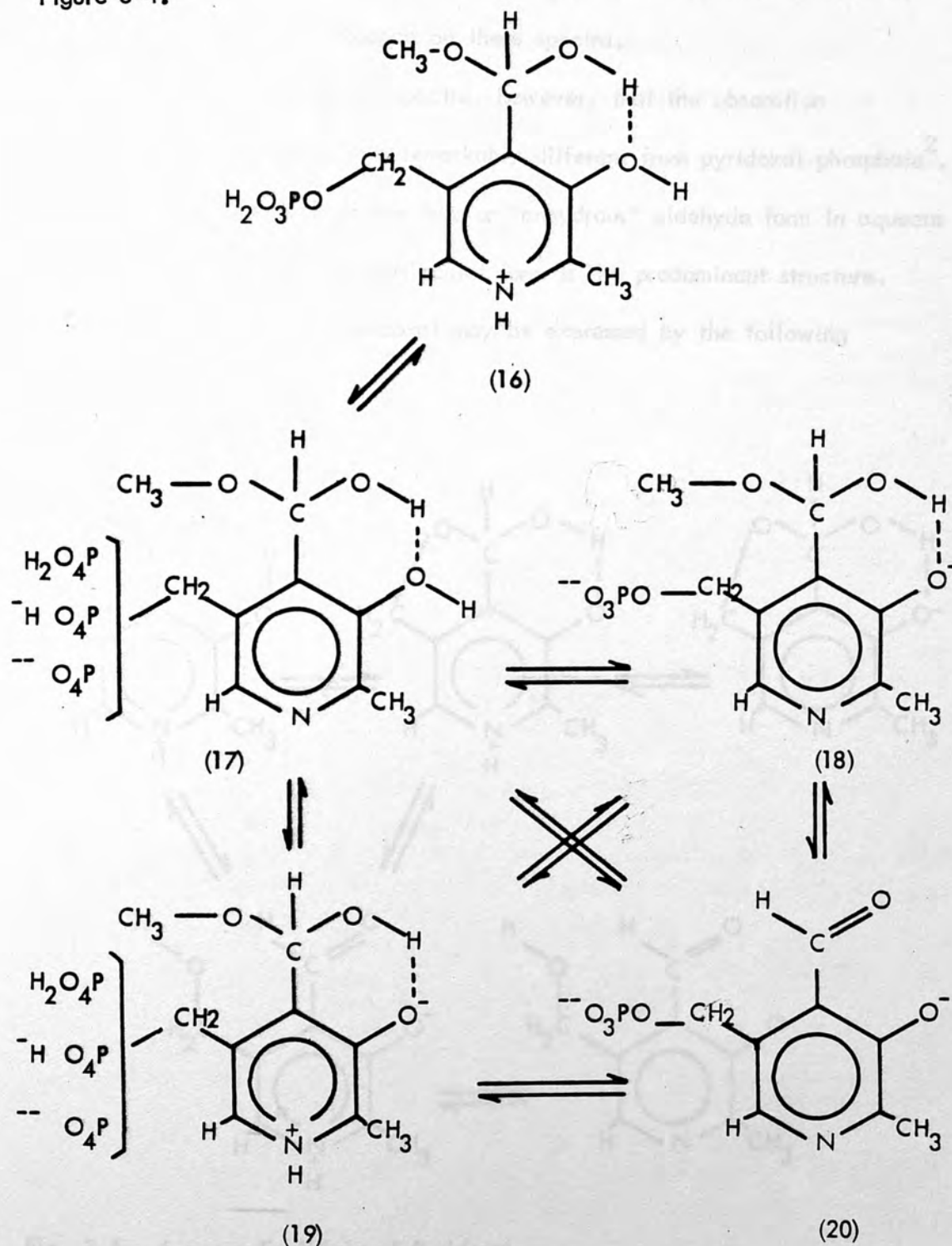


Fig. 3-4: Pyridoxal Phosphate in Acidic Solution

In neutral methanol solution three absorption peaks appear at 29400, 34600 and 40000 cm^{-1} . The 29400 and 40000 cm^{-1} bands are assigned to the π_1 and π_2 bands of the dipolar solvated form (19), in accordance with pyridoxal band assignments. Dissociation of phosphate hydrogens would be expected to have little influence on these spectra.

It is apparent from the spectra, however, that the absorption characteristics of pyridoxal are remarkably different from pyridoxal phosphate². The almost complete lack of the free or "anhydrous" aldehyde form in aqueous equilibria indicates that the hemiacetal form is the predominant structure. The aqueous equilibria of pyridoxal may be expressed by the following figure:

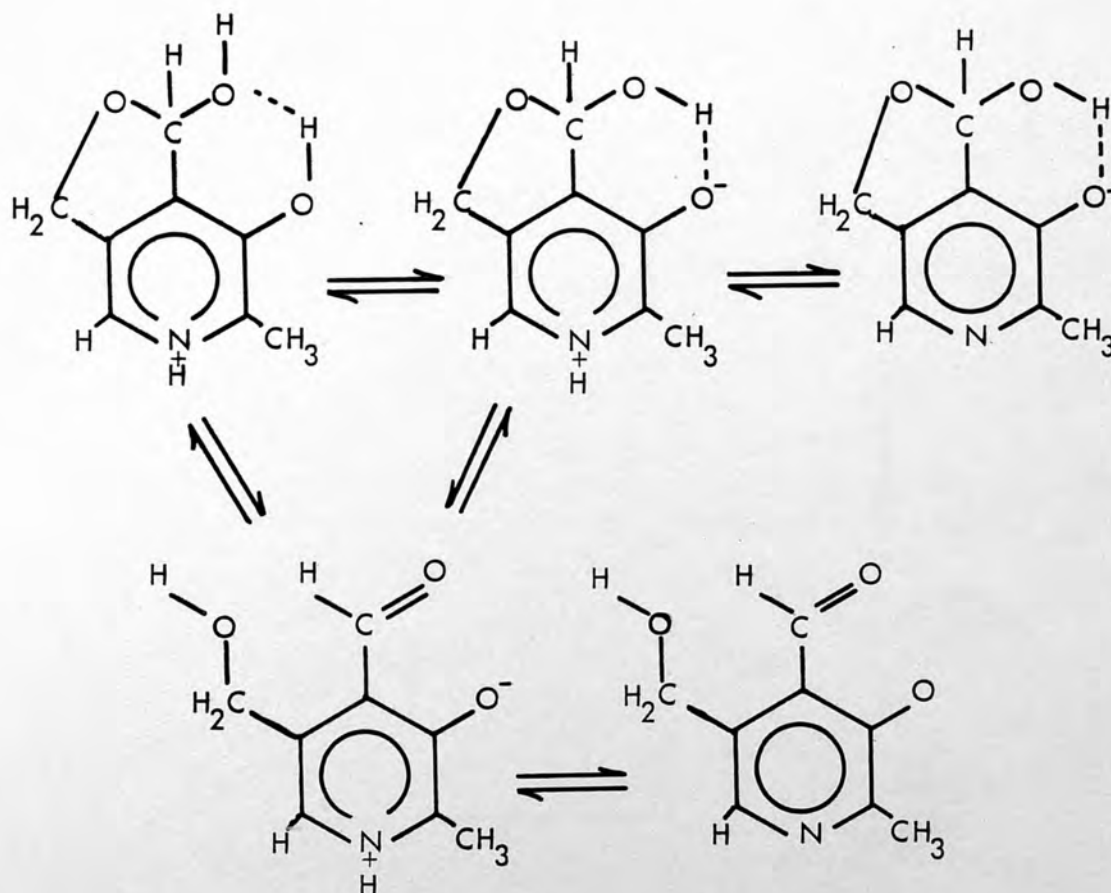
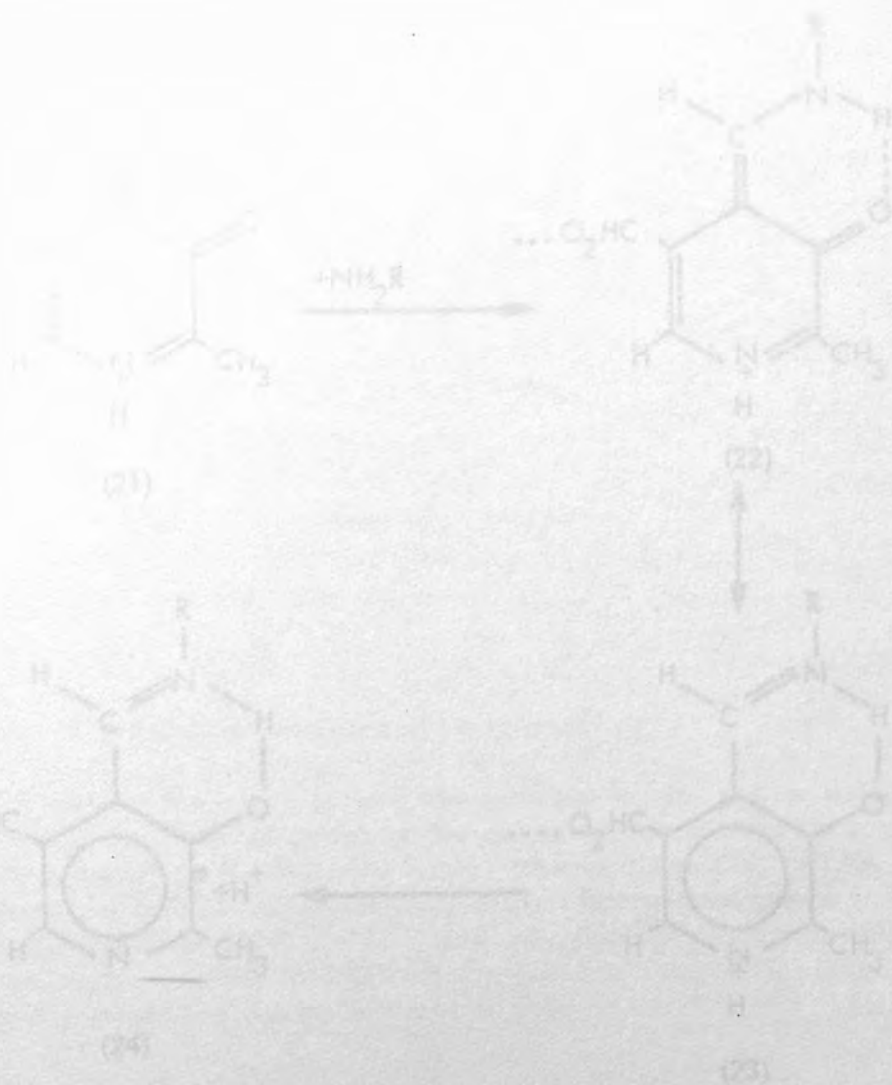


Fig. 3-5: Aqueous Equilibria of Pyridoxal

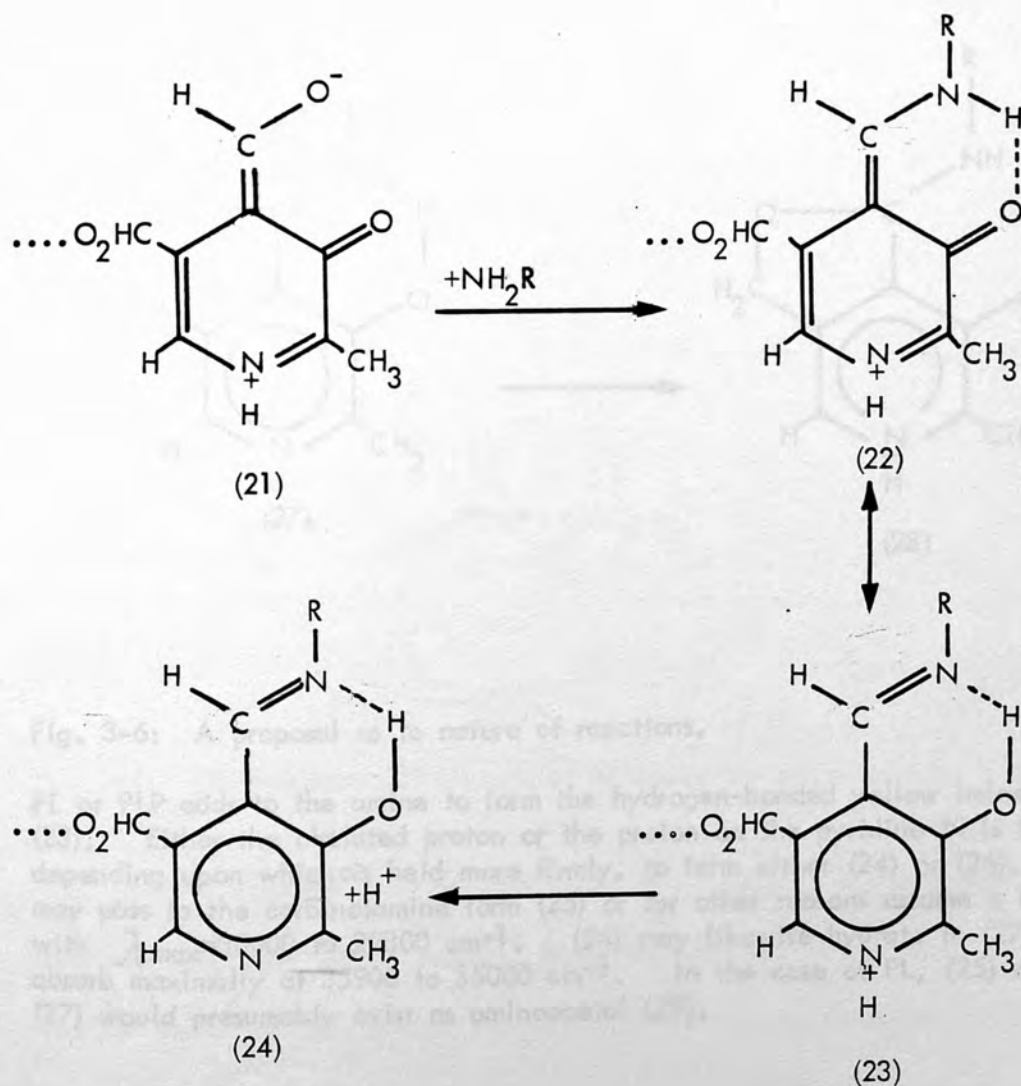
It is seen that there is no appreciable amount of the free aldehyde form in acidic solution. In neutral solution the absorption band (at 31500 cm^{-1}) assigned to the dipolar hemiacetal form is strong, while the band (at 25600 cm^{-1}) assigned to the dipolar free carbonyl form is very weak, indicating that the hemiacetal structure predominates in neutral solution. Similarly, in alkaline solution the hemiacetal form was found to predominate over the free aldehyde, although the proportion of free aldehyde increases at high pH.



3.1.2 Ultra-Violet Spectra of the Schiff Bases of Pyridoxal and its Analogues:

Formation of Schiff bases with and without metal ions has been studied by many authors. Spectrophotometric evidence has been given for the formation and subsequent reactions of various Schiff base species forms at specific wavelengths.

Christensen³ proposed that the spectrophotometric observations of Schiff bases between pyridoxal and amino acids with bands at 26547, 23852 and 25000 cm^{-1} during the reaction:



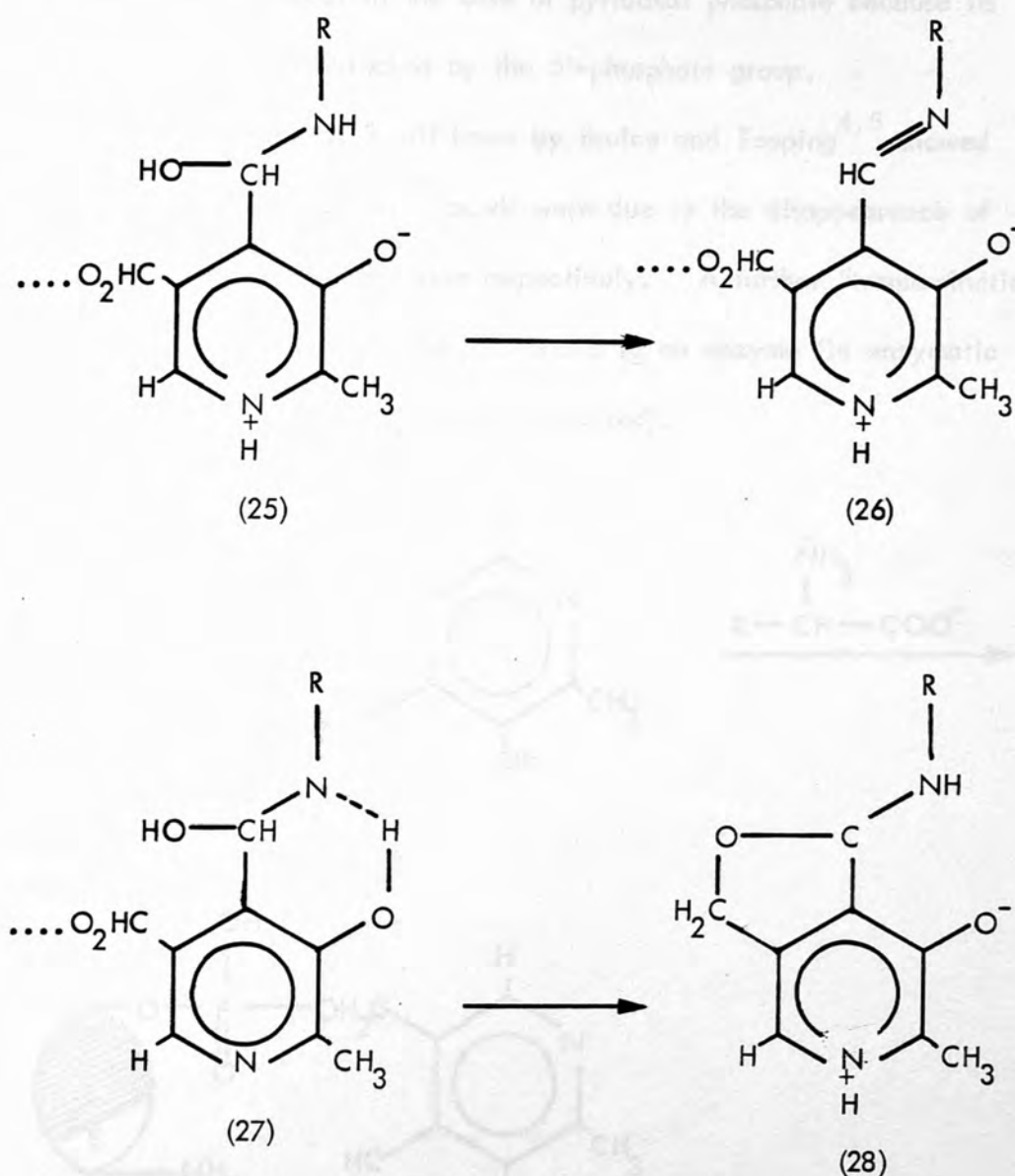


Fig. 3-6: A proposal as to nature of reactions.

PL or PLP adds to the amine to form the hydrogen-bonded yellow imine (22) (23). Either the chelated proton or the proton on the pyridine N is lost depending upon which is held more firmly, to form either (24) or (26). (26) may pass to the carbinolamine form (25) or for other reasons assume a form with $\lambda_{\max}=30000$ to 29800 cm^{-1} . (24) may likewise hydrate to (27) to absorb maximally at 35900 to 35000 cm^{-1} . In the case of PL, (25) and (27) would presumably exist as aminoacetal (28).

The amino acetal species of the cyclic hemiacetal (band $35087\text{--}35971\text{ cm}^{-1}$) cannot exist in the case of pyridoxal phosphate because its formation is effectively blocked by the 5'-phosphate group.

Kinetic studies on Schiff bases by Bruice and Topping^{4,5} showed that the 25316 and 40650 cm^{-1} bands were due to the disappearance of aldehyde and appearance of imine respectively. A further "transamination" could occur if the phosphate group is bound to an enzyme (in enzymatic catalysis metal ion may or may not be required).

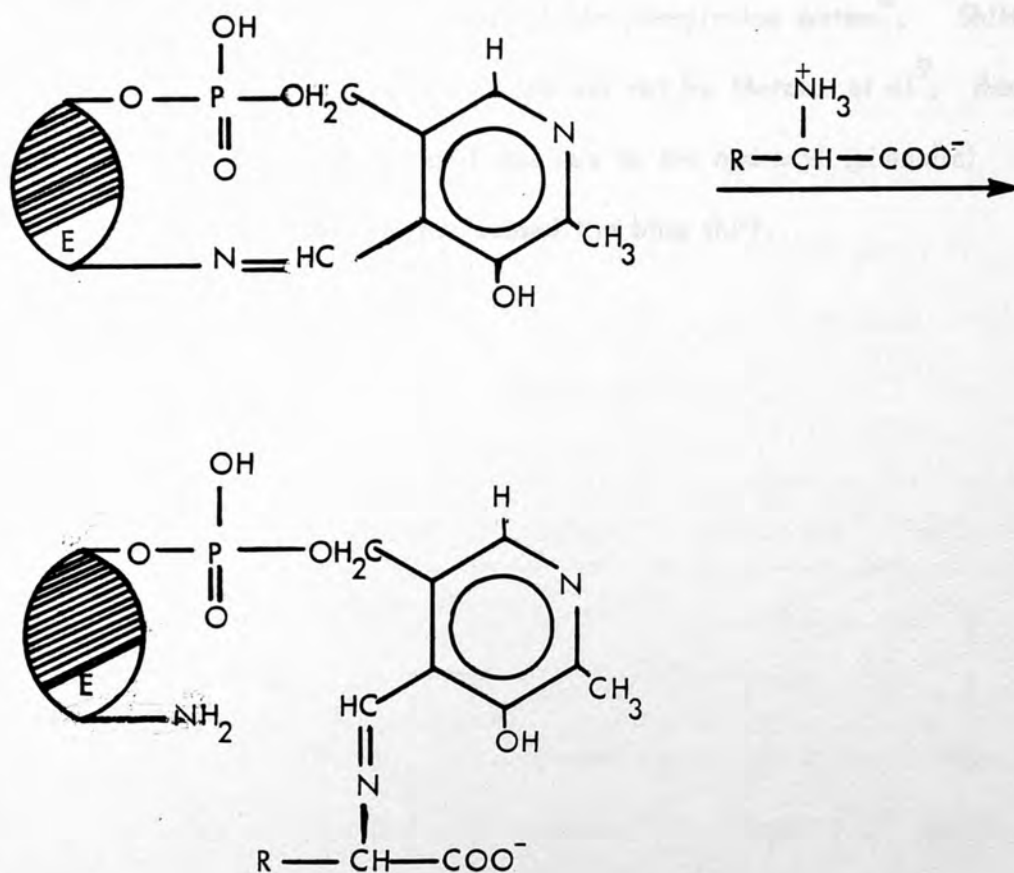


Fig. 3-7: "Transamination" interaction of phosphate group with an enzyme

It was suggested that the 3-OH did not take part in the transamination reaction, especially since Thanassi⁶ found that one of the functions of the phenolic group was to increase the concentration of the aldimine species

and to promote the intermolecular acid catalysis. The presence of the 3-OH group is thought necessary to ketimine species.

Ultraviolet spectra of Schiff bases and effects of the addition of metal ions to the system, were studied by Matsuo⁷. The action of metal ion is enhancing the rate of many organic and physiological reactions and has been frequently attributed to the formation of complex intermediates.

Metal ions were found to shift the imine absorption maxima to shorter wavelengths. One concludes that the metal ion effect occurred after Schiff base formation in the salicylaldehyde-glycine system⁸. Shifts of the bands were found to obey the rule set out by Metzler et al⁹; that the red shift (to longer wavelength) was due to the hydroxyl (phenolic) hydrogen while the pyridinium ion caused the blue shift.

Substituent	Substituents	Solvent	$\lambda_{max}/m\mu$ ¹	shift/cm ⁻¹
Pyridine	H	water	3300	0
	H	alcohol	3350	0
	3-OH	water	3310	200
	3-OH	alcohol	3370	300
	3-O ⁻	water	3300	300
	3-O ⁻	alcohol	3350	350

Table (3-3). Effect of Substituents on the Absorption Spectra of Pyridine

3.1.3 Assignment of the Various U.V. Bands of Vitamin B₆ Species

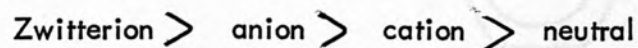
The ultraviolet spectra of Vitamin B₆ and related compounds have been studied by Nakamoto et al² at various pH values. They assigned various transitions to the molecular species. Assumptions are made that the $\pi-\pi^*$ transitions of the pyridine ring system and of the conjugated -C=N-imine will be the main contributors to absorption. $n-\pi^*$ and $\sigma-\sigma^*$ are considered weak and generally < 0.01 absorption units in 10^{-4} M solutions generally out of the spectral range considered.

It is important to point out that the assignment of the π_1^* , π_2^* transitions, considered analogous to the pyridine ring system, are bound to be those of uncharged species of this ring system. Table (3-3) will set out how the substitution of the ring system shifts the maximal absorption, and further substitution causes even larger shifts in one direction or other. Band shifts obey the rule set out by Metzler and Snell⁹.

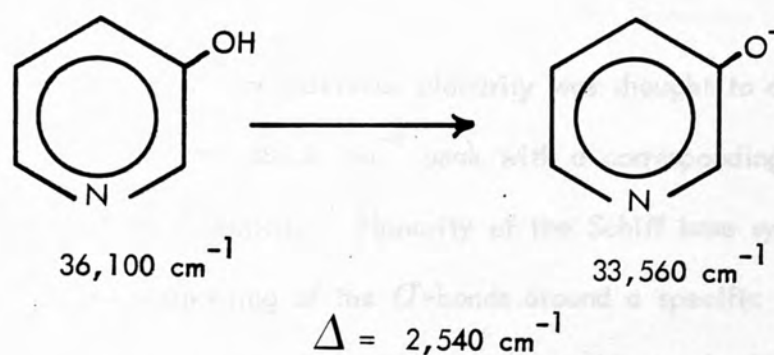
Compound	Substituent	Solvent	$\lambda_{\max}/\text{cm}^{-1}$	shift/ cm^{-1}
Pyridine	None	water	39000	0
	None	alcohol	39000	0
	3-OH	water	36100	2900
	3-OH	alcohol	35970	3030
	3-O ⁻	water	33500	5500
	3-O ⁻	alcohol	33200	5800

Table (3-3): Effect of Substituents on the Absorption Spectra of Pyridine

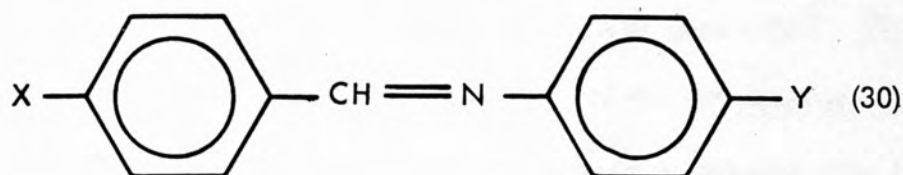
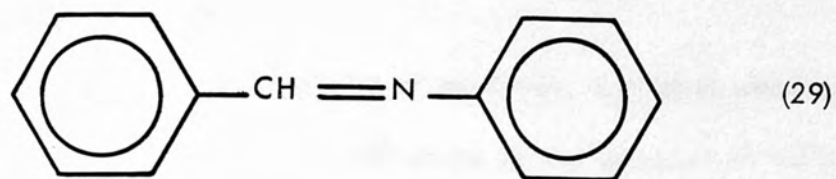
The π_1 and π_2 bands of pyridines were calculated to be in the following order, of decreasing wavelength:



Shifts of up to 2540 cm^{-1} were found on the ionization of the hydroxyl group, and the stability is accounted for by the resonance forms of the respective Schiff base:



The $\phi - \pi^*$ peak at 38168 cm^{-1} is said¹⁰ to be stabilized by an electron donating group in the p-position to the amine group, and would therefore absorb bathochromically relative to the same Schiff base with the p-position occupied by an aldehyde group (29,30).



The steric requirement for maximum planarity was thought to account for increased absorption of the 38168 cm^{-1} peak with a corresponding decrease in the 31847 cm^{-1} region. Planarity of the Schiff base system was achieved¹¹ by the weakening of the σ -bonds around a specific carbon atom (the α -carbon atom of the amino acid in this case) which was adjacent to the cofactor π -system.

3.2 Experimental

The ultra-violet spectra of pyridoxal, pyridoxal phosphate Schiff bases with glycine and ethylenediamine in the presence of various transition metals were studied on a Unicam SP8-100 recording spectrophotometer, in various acetate buffers. 10 mm silica cells were used. The wavelength range studied was $20000-50000\text{ cm}^{-1}$, and the pH range was from 1.09 to 5.25. The buffers used were acetate buffers, adjusted with hydrochloric acid (see Appendix 2) and the pH was measured on a Pye-Dynacap pH meter. The reactions were carried out at 25°C . The concentrations of the reactants were: PL, PLP = $2 \times 10^{-3}\text{ M}$, glycine, ethylenediamine = $8 \times 10^{-2}\text{ M}$, and metal ions = $4 \times 10^{-2}\text{ M}$. The metals which were used were: Fe^{+3} , Fe^{+2} , Co^{+3} , Co^{+2} , Ni^{+2} , Ca^{+2} , Zn^{+2} , Cd^{+2} and Ga^{+3} , Al^{+3} .

Spectral properties of metal chelates were described and absorption maxima were measured.

3.3 Results

3.3.1 Measurement of Absorption Maxima of Metal-Schiff Base Complexes

Initially the ultraviolet spectra of the Schiff bases were recorded (Table 3-4,5,6,7) under the same experimental conditions used for the study of metal-Schiff base complexes. Bands in the pH range 1.09-5.20 have been measured for pyridoxal-phosphate (PLP) and pyridoxal (PL) (Fig. 3-8,9). Both molecular extinction coefficients and the absorption maxima (Table 3-8,9) are in good agreement with literature values¹². Shifts from the bands of the free ligands were used as a proof for the metal-chelate formation and the products of the reactions.

Absorption maxima (cm^{-1}) of Schiff Bases at various pH Values

PLPen

Table: 3-4

pH	$\pi - \pi_1^*$ aldimine		$\pi - \pi_1^*$ ketimine		$\pi - \pi_2^*$		ν_1		ν_2	
	$\nu \text{ cm}^{-1}$	Abs.	$\nu \text{ cm}^{-1}$	Abs.	$\nu \text{ cm}^{-1}$	Abs.	$\nu \text{ cm}^{-1}$	Abs.	$\nu \text{ cm}^{-1}$	Abs.
1.09	-	-	-	-	34000	1.15	39680	0.22	43500	0.31
3.12	25400	0.13	31850	0.44	34000	0.86	39800	0.34	43500	0.58
4.19	25500	0.18	31850	0.52	34250	0.69	39700	0.45	43900	0.81
5.20	25250	0.19	31250	0.56	34250	0.59	39680	0.58	43850	1.10

Plen

Table: 3-5

pH	$\pi - \pi_1^*$ aldimine		$\pi - \pi_1^*$ ketimine		$\pi - \pi_2^*$		ν_1		ν_2	
	$\nu \text{ cm}^{-1}$	Abs.	$\nu \text{ cm}^{-1}$	Abs.	$\nu \text{ cm}^{-1}$	Abs.	$\nu \text{ cm}^{-1}$	Abs.	$\nu \text{ cm}^{-1}$	Abs.
1.09	-	-	31650	0.52	34250	1.15	-	-	43100	0.36
3.12	-	-	31450	0.75	34000	1.00	39680	0.35	43800	0.50
4.19	-	-	31750	1.06	34000	0.86	39680	0.56	43850	0.78
5.20	25250	0.15	31250	0.56	34250	0.58	39680	0.57	43850	1.08

Absorption maxima (cm^{-1}) of Schiff Bases at Various pH Values

PLPGly

Table: 3-6

pH	$\pi - \pi_1^*$ aldimine		$\pi - \pi_1^*$ ketimine		$\pi - \pi_2^*$		ν_1		ν_2	
	$\nu \text{ cm}^{-1}$	Abs.	$\nu \text{ cm}^{-1}$	Abs.	$\nu \text{ cm}^{-1}$	Abs.	$\nu \text{ cm}^{-1}$	Abs.	$\nu \text{ cm}^{-1}$	Abs.
1.09	-	-	30100	0.22	34250	1.25	39600	0.16	43400	0.24
3.12	25500	0.10	30100	0.25	34200	1.17	39600	0.21	43400	0.42
5.20	25700	0.84	30300	0.42	35500	0.27	-	-	43400	1.70

PLGly

Table: 3-7

pH	$\pi - \pi_1^*$ aldimine		$\pi - \pi_1^*$ ketimine		$\pi - \pi_2^*$		ν_1		ν_2	
	$\nu \text{ cm}^{-1}$	Abs.	$\nu \text{ cm}^{-1}$	Abs.	$\nu \text{ cm}^{-1}$	Abs.	$\nu \text{ cm}^{-1}$	Abs.	$\nu \text{ cm}^{-1}$	Abs.
1.09	-	-	-	-	34900	1.64	-	-	43800	0.36
3.12	-	-	31800	0.09	34800	1.63	-	-	43800	0.38
5.20	26800	0.02	31800	1.53	-	-	39800	1.06	44500	1.38

Table 3-8: Variation of ϵ_m of Pyridoxal Phosphate with pH

pH	maxima cm^{-1}	absorbance*	ϵ_m
1.09	29850	0.29	1450
	33800	1.58	7900
	43850	0.47	2350
3.12	25500	0.14 sh	700
	30100	0.32	1600
	33800	1.43	7150
	43450	0.82 sh	4100
4.19	25700	0.62	3100
	30300	0.43	2150
	33900	0.82	4100
	43100	1.54	7700
5.20	25750	0.98	4900
	30400	0.53	2650
	34200	0.38	1900
	43000	2.10	10500

sh = shoulder

sh = shoulder

Table 3-9: Variation of ϵ_m of Pyridoxal with pH

pH	maxima cm^{-1}	absorbance*	ϵ_m
1.09	34700	2.04	10200
	43450	0.54	2700
3.12	31450	0.17 sh	850
	34750	1.94	9700
	43850	1.02	5100
4.19	31650	0.94	4700
	34750	1.65	8250
	39350	0.57	2850
	44250	1.14	5700
5.20	31850	1.67	8350
	39700	1.13	5650
	44650	2.00	10000

sh = shoulder

Fig. 3-8: Change of Electronic Absorption Spectra of Pyridoxal Phosphate with pH.

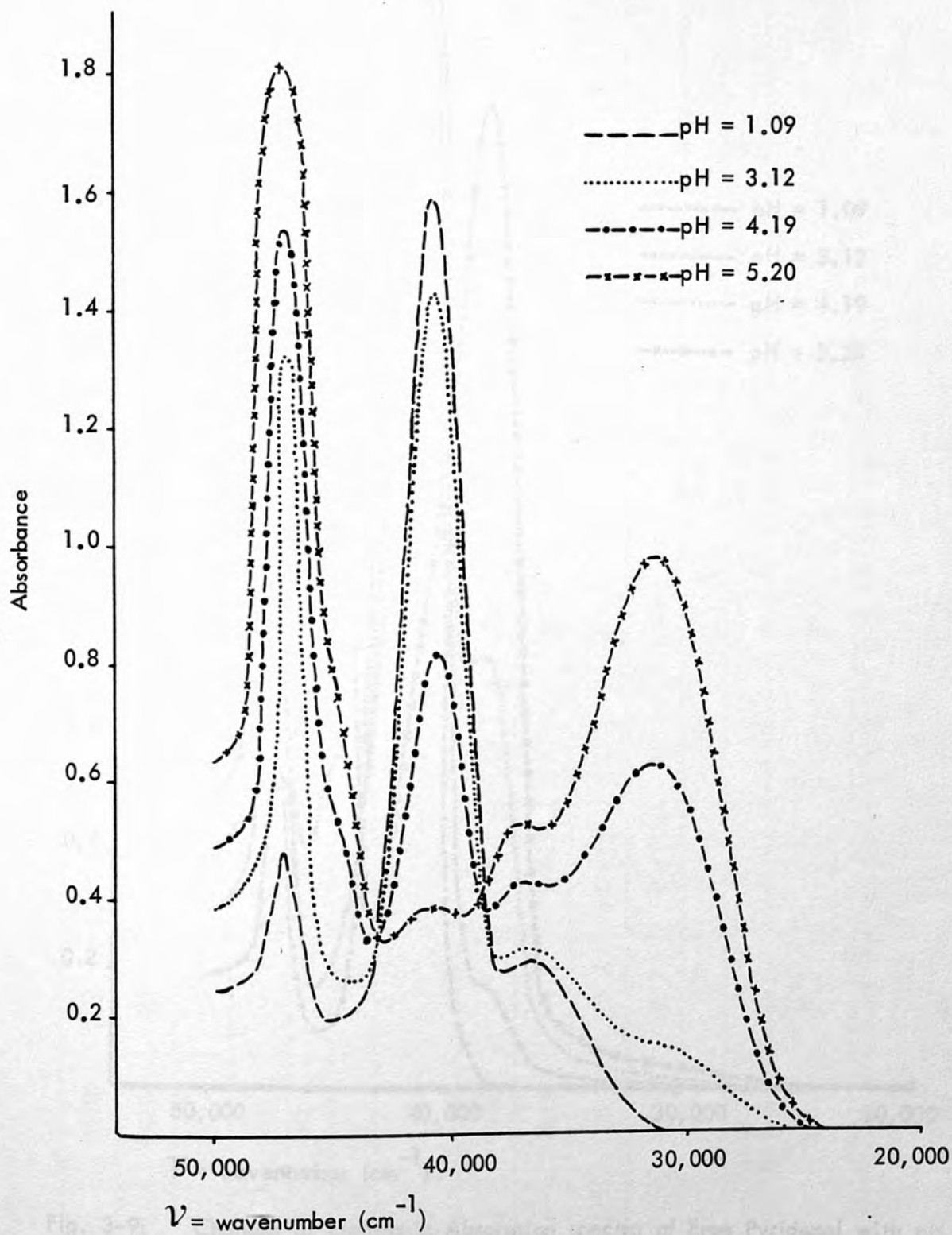


Fig. 3-8: Changes of Electronic Absorption Spectra of Pyridoxal Phosphate with pH.

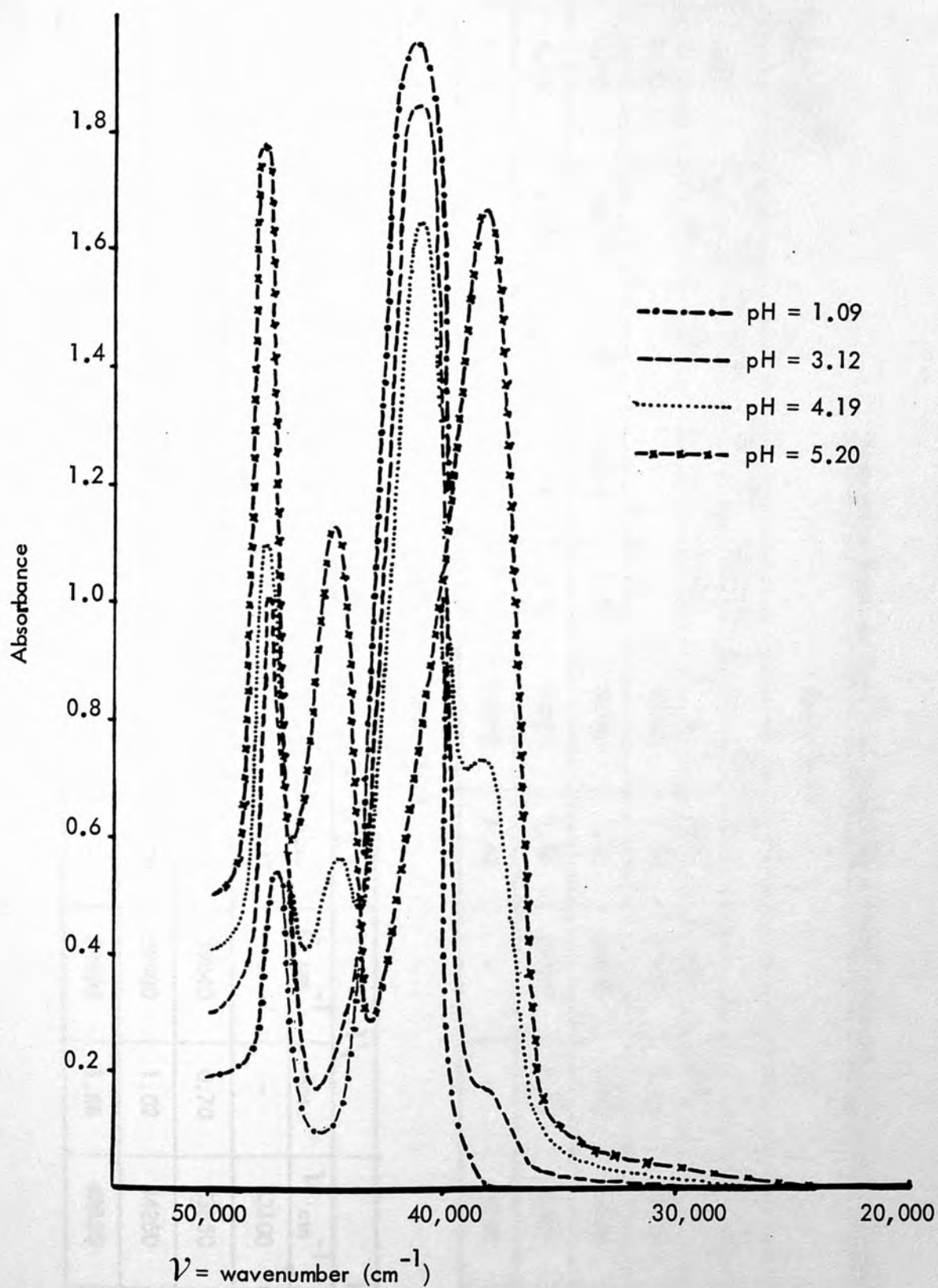


Fig. 3-9: Changes of Electronic Absorption spectra of Free Pyridoxal with pH

Absorption Maxima (cm^{-1}) of Schiff Base Metal Chelates at Various pH ValuesPLP, en, Fe⁺²

Table 3-10

pH	$\pi-\pi_1^*$ aldimine		$\pi-\pi_1^*$ ketimine		$\pi-\pi_2^*$		ν_1		ν_2	
	ν cm^{-1}	Abs.	ν cm^{-1}	Abs.	ν cm^{-1}	Abs.	ν cm^{-1}	Abs.	ν cm^{-1}	Abs.
1.09	-	-	-	-	34000	1.26	39600	0.52	43000	0.60
3.12	25000	0.42	31000	0.92	34200	1.21	39800	1.12	43100	1.28
4.19	25000	0.36	31250	0.86	34250	1.04	39900	1.10	43500	1.40
5.20	-	-	-	-	34900	1.42	-	-	43100	1.86

PL, en, Fe⁺²

Table 3-11

pH	$\pi-\pi_1^*$ aldimine		$\pi-\pi_1^*$ ketimine		$\pi-\pi_2^*$		ν_1		ν_2	
	ν cm^{-1}	Abs.	ν cm^{-1}	Abs.	ν cm^{-1}	Abs.	ν cm^{-1}	Abs.	ν cm^{-1}	Abs.
1.09	-	-	31850	0.57	34450	1.27	-	-	43100	0.68
3.12	25000	0.05	31850	0.76	34750	1.12	39840	0.70	43850	0.83
4.19	25250	0.06	31850	1.14	34750	0.98	39900	1.02	44250	1.16
5.20	-	-	31650	1.77	-	-	39600	1.65	43850	1.84

Absorption Maxima (cm^{-1}) of Schiff Base Metal Chelates at Various pH ValuesPLP, Gly, Fe⁺⁺

Table 3-12

pH	$\pi-\pi_1^*$ aldimine		$\pi-\pi_1^*$ ketimine		$\pi-\pi_2^*$		ν_1		ν_2	
	$\nu \text{ cm}^{-1}$	Abs.	$\nu \text{ cm}^{-1}$	Abs.	$\nu \text{ cm}^{-1}$	Abs.	$\nu \text{ cm}^{-1}$	Abs.	$\nu \text{ cm}^{-1}$	Abs.
1.09	-	-	30000	0.25	33700	1.26	39600	0.35	43000	0.42
3.12	25000	0.09	30000	0.28	33700	1.12	39800	0.48	43000	0.70
5.20	26500	0.61	-	-	34400	0.93	-	-	43000	1.92

PL, Gly, Fe⁺⁺

Table 3-13

pH	$\pi-\pi_1^*$ aldimine		$\pi-\pi_1^*$ ketimine		$\pi-\pi_2^*$		ν_1		ν_2	
	$\nu \text{ cm}^{-1}$	Abs.	$\nu \text{ cm}^{-1}$	Abs.	$\nu \text{ cm}^{-1}$	Abs.	$\nu \text{ cm}^{-1}$	Abs.	$\nu \text{ cm}^{-1}$	Abs.
1.09	-	-	31000	0.27	34700	1.50	-	-	43000	0.47
3.12	-	-	31000	0.34	34700	1.46	-	-	43000	0.52
5.20	-	-	31800	1.43	-	-	39800	1.19	44600	1.52

Absorption Maxima (cm^{-1}) of Schiff Base Metal Chelates at Various pH Values
 Table 3-14 PLP, en, Co^{+2}

pH	$\pi-\pi_1^*$ aldimine		$\pi-\pi_1^*$ ketimine		$\pi-\pi_2^*$		ν_1		ν_2	
	ν cm^{-1}	Abs.	ν cm^{-1}	Abs.	ν cm^{-1}	Abs.	ν cm^{-1}	Abs.	ν cm^{-1}	Abs.
1.09	-	-	-	-	33780	1.19	39600	0.22	42700	0.20
3.12	25250	0.19	31250	0.43	34000	0.80	39400	0.37	42400	0.58
4.19	25500	0.25	31450	0.50	34500	0.64	39700	0.52	43100	0.84
5.20	25600	0.29	31400	0.65	34700	0.79	-	-	43100	1.85

PL, en, Co⁺²

Table 3-15

pH	$\pi-\pi_1^*$ aldimine		$\pi-\pi_1^*$ ketimine		$\pi-\pi_2^*$		ν_1		ν_2	
	ν cm^{-1}	Abs.	ν cm^{-1}	Abs.	ν cm^{-1}	Abs.	ν cm^{-1}	Abs.	ν cm^{-1}	Abs.
1.09	-	-	31650	0.51	34450	1.20	-	-	43100	0.24
3.12	27600	0.20	31600	0.77	34250	1.00	39600	0.38	43800	0.39
4.19	27600	0.20	31850	1.08	34000	0.86	39800	0.61	44600	0.72
5.20	25000	0.25	31650	1.14	-	-	-	-	43450	1.92

Absorption Maxima (cm^{-1}) of Schiff Base Metal Chelates at Various pH ValuesPLP, Gly, Co^{+2}

Table 3-16

pH	$\pi-\pi_1^*$ aldimine		$\pi-\pi_1^*$ ketimine		$\pi-\pi_2^*$		ν_1		ν_2	
	ν cm^{-1}	Abs.	ν cm^{-1}	Abs.	ν cm^{-1}	Abs.	ν cm^{-1}	Abs.	ν cm^{-1}	Abs.
1.09	-	-	30500	0.19	33700	1.16	39900	0.17	43400	0.15
3.12	26300	0.09	30800	0.23	34000	1.90	34500	0.23	42700	0.34
5.20	26500	0.64	30400	0.40	36000	0.52	-	-	43500	1.78

PL, Gly, Co^{+2}

Table 3-17

pH	$\pi-\pi_1^*$ aldimine		$\pi-\pi_1^*$ ketimine		$\pi-\pi_2^*$		ν_1		ν_2	
	ν cm^{-1}	Abs.	ν cm^{-1}	Abs.	ν cm^{-1}	Abs.	ν cm^{-1}	Abs.	ν cm^{-1}	Abs.
1.09	-	-	31000	0.18	34900	1.58	-	-	43400	0.30
3.12	-	-	31000	0.24	34700	1.47	-	-	43500	0.30
5.20	-	-	31400	1.45	-	-	39600	0.96	44600	1.32

Absorption Maxima (cm^{-1}) of Schiff Base Metal Chelates at Various pH ValuesPLP, en, Co⁺³

Table 3-18

pH	$\pi-\pi_1^*$ aldimine		$\pi-\pi_1^*$ ketimine		$\pi-\pi_2^*$		ν_1		ν_2	
	ν cm^{-1}	Abs.	ν cm^{-1}	Abs.	ν cm^{-1}	Abs.	ν cm^{-1}	Abs.	ν cm^{-1}	Abs.
1.09	-	-	30000	0.38	33700	1.17	-	-	42300	1.96
3.12	25000	0.17	31250	0.54	33700	0.84	-	-	42300	2.00
4.19	25000	0.24	31250	0.64	34500	0.70	-	-	42500	2.05
5.20	24500	0.22	31000	0.71	34700	0.62	-	-	42800	2.10

PL, en, Co⁺³

Table 3-19

pH	$\pi-\pi_1^*$ aldimine		$\pi-\pi_1^*$ ketimine		$\pi-\pi_2^*$		ν_1		ν_2	
	ν cm^{-1}	Abs.	ν cm^{-1}	Abs.	ν cm^{-1}	Abs.	ν cm^{-1}	Abs.	ν cm^{-1}	Abs.
1.09	-	-	31000	0.62	34480	1.19	-	-	41300	1.96
3.12	-	-	31250	0.88	34250	1.04	-	-	41500	2.0
4.19	-	-	31650	1.15	34250	0.84	-	-	41800	2.07
5.20	-	-	31600	1.35	-	-	-	-	42000	2.12

Absorption Maxima (cm^{-1}) of Schiff Base Metal Chelates at Various pH ValuesPLP, Gly, Co^{+3}

Table 3-20

pH	$\pi-\pi_1^*$ aldimine		$\pi-\pi_1^*$ ketimine		$\pi-\pi_2^*$		ν_1		ν_2	
	ν cm^{-1}	Abs.	ν cm^{-1}	Abs.	ν cm^{-1}	Abs.	ν cm^{-1}	Abs.	ν cm^{-1}	Abs.
1.09	-	-	30000	0.37	34000	1.00	-	-	42000	2.0
3.12	-	-	30000	0.40	34000	0.90	-	-	42300	2.0
5.20	25500	0.47	30000	0.53	34400	0.48	-	-	42300	2.10

PL, Gly, Co^{+3}

Table 3-21

pH	$\pi-\pi_1^*$ aldimine		$\pi-\pi_1^*$ ketimine		$\pi-\pi_2^*$		ν_1		ν_2	
	ν cm^{-1}	Abs.	ν cm^{-1}	Abs.	ν cm^{-1}	Abs.	ν cm^{-1}	Abs.	ν cm^{-1}	Abs.
1.09	-	-	30000	0.44	34500	1.45	-	-	42000	2.0
3.12	-	-	30000	0.51	34500	1.45	-	-	42000	2.0
5.20	-	-	31400	1.54	-	-	-	-	42000	2.10

Absorption Maxima (cm^{-1}) of Schiff Base Metal Chelates at Various pH ValuesPLP, en, Ni⁺²

Table 3-22

pH	$\pi-\pi_1^*$ aldimine		$\pi-\pi_1^*$ ketimine		$\pi-\pi_2^*$		ν_1		ν_2	
	ν cm^{-1}	Abs.	ν cm^{-1}	Abs.	ν cm^{-1}	Abs.	ν cm^{-1}	Abs.	ν cm^{-1}	Abs.
1.09	-	-	-	-	33780	0.89	39600	0.18	42700	0.15
3.12	25600	0.19	31250	0.41	34500	0.78	39600	0.34	43500	0.52
4.19	25780	0.35	31450	0.47	34500	0.65	-	-	43480	1.04
5.20	26000	0.47	31250	0.41	34750	0.56	-	-	43480	1.55

PL, en, Ni⁺²

Table 3-23

pH	$\pi-\pi_1^*$ aldimine		$\pi-\pi_1^*$ ketimine		$\pi-\pi_2^*$		ν_1		ν_2	
	ν cm^{-1}	Abs.	ν cm^{-1}	Abs.	ν cm^{-1}	Abs.	ν cm^{-1}	Abs.	ν cm^{-1}	Abs.
1.09	25600	0.01	31800	0.48	34500	1.16	-	-	42750	0.20
3.12	25600	0.02	31650	0.72	34250	0.95	39700	0.32	43480	0.30
4.19	25600	0.03	31850	1.04	34000	0.83	39800	0.52	44600	0.63
5.20	26300	0.34	31650	0.96	-	-	40000	0.76	43850	1.54

Absorption Maxima (cm^{-1}) of Schiff Base Metal Chelates at Various pH ValuesPLP, Gly, Ni^{++}

Table 3-24

pH	$\pi-\pi_1^*$ aldimine		$\pi-\pi_1^*$ ketimine		$\pi-\pi_2^*$		ν_1		ν_2	
	ν cm^{-1}	Abs.	ν cm^{-1}	Abs.	ν cm^{-1}	Abs.	ν cm^{-1}	Abs.	ν cm^{-1}	Abs.
1.09	-	-	30000	0.19	34000	1.12	39000	0.17	43000	0.13
3.12	26300	0.12	30000	0.23	34000	1.06	-	-	43000	0.35
5.20	26000	0.68	31800	0.32	34700	0.49	-	-	43800	1.80

PL, Gly, Ni^{++}

Table 3-25

pH	$\pi-\pi_1^*$ aldimine		$\pi-\pi_1^*$ ketimine		$\pi-\pi_2^*$		ν_1		ν_2	
	ν cm^{-1}	Abs.	ν cm^{-1}	Abs.	ν cm^{-1}	Abs.	ν cm^{-1}	Abs.	ν cm^{-1}	Abs.
1.09	25000	0.01	31600	0.22	34700	1.50	-	-	43400	0.28
3.12	25000	0.01	31600	0.29	34700	1.46	-	-	43400	0.32
5.20	25000	0.05	31800	1.44	-	-	39800	0.94	44000	1.32

Absorption Maxima (cm^{-1}) of Schiff Base Metal Chelates at Various pH ValuesPLP, en, Cu^{++}

Table 3-26

pH	$\pi-\pi_1^*$		aldimine		$\pi-\pi_1^*$		ketimine		$\pi-\pi_2^*$		ν_1		ν_2	
	ν cm^{-1}	Abs.	ν cm^{-1}	Abs.	ν cm^{-1}	Abs.	ν cm^{-1}	Abs.	ν cm^{-1}	Abs.	ν cm^{-1}	Abs.	ν cm^{-1}	Abs.
1.09	-	-	-	-	34000	1.20	39500	1.23	43800	1.38				
3.12	26300	0.34	31250	0.39	34500	1.12	39600	1.04	43600	1.49				
4.19	26700	0.38	31000	0.41	34800	1.04	39800	0.80	43500	1.70				
5.20	26300	0.39	31450	0.42	34900	1.00	-	-	43450	1.92				

PL, en, Cu^{++}

Table 3-27

pH	$\pi-\pi_1^*$		aldimine		$\pi-\pi_1^*$		ketimine		$\pi-\pi_2^*$		ν_1		ν_2	
	ν cm^{-1}	Abs.	ν cm^{-1}	Abs.	ν cm^{-1}	Abs.	ν cm^{-1}	Abs.	ν cm^{-1}	Abs.	ν cm^{-1}	Abs.	ν cm^{-1}	Abs.
1.09	-	-	31850	0.50	34750	1.25	40500	1.19	43500	1.42				
3.12	25500	0.06	31650	0.70	34950	1.32	39000	1.08	43000	1.58				
4.19	25600	0.15	31650	0.88	-	-	-	-	43000	1.70				
5.20	26000	0.36	31450	0.96	-	-	-	-	-	-				

Absorption Maxima (cm^{-1}) of Schiff Base Metal Chelates at Various pH Values

PLP, Gly, Cu⁺⁺

Table 3-28

pH	$\pi-\pi_1^*$ aldimine		$\pi-\pi_1^*$ ketimine		$\pi-\pi_2^*$		ν_1		ν_2	
	ν cm^{-1}	Abs.	ν cm^{-1}	Abs.	ν cm^{-1}	Abs.	ν cm^{-1}	Abs.	ν cm^{-1}	Abs.
1.09	25600	0.06	30000	0.21	34200	1.29	40000	1.20	43800	1.54
3.12	26500	0.24	31200	0.28	34200	1.19	40800	1.98	42000	2.0
5.20	26200	0.67	31400	0.42	-	-	-	-	-	-

PL, Gly, Cu⁺⁺

Table 3-29

pH	$\pi-\pi_1^*$ aldimine		$\pi-\pi_1^*$ ketimine		$\pi-\pi_2^*$		ν_1		ν_2	
	ν cm^{-1}	Abs.	ν cm^{-1}	Abs.	ν cm^{-1}	Abs.	ν cm^{-1}	Abs.	ν cm^{-1}	Abs.
1.09	-	-	31400	0.08	34000	1.68	40800	1.06	43800	1.48
3.12	-	-	31200	0.17	34000	1.74	41000	2.0	42500	2.0
5.20	25600	0.03	31900	1.50	-	-	-	-	-	-

Absorption Maxima (cm^{-1}) of Schiff Base Metal Chelates at Various pH ValuesPLP, en, Zn^{+2}

Table 3-30

pH	$\pi-\pi_1^*$		aldimine		$\pi-\pi_1^*$		ketimine		$\pi-\pi_2^*$		ν_1		ν_2	
	$\nu \text{ cm}^{-1}$	Abs.	$\nu \text{ cm}^{-1}$	Abs.	$\nu \text{ cm}^{-1}$	Abs.	$\nu \text{ cm}^{-1}$	Abs.	$\nu \text{ cm}^{-1}$	Abs.	$\nu \text{ cm}^{-1}$	Abs.	$\nu \text{ cm}^{-1}$	Abs.
1.09	-	-	-	-	34250	1.14	39900	0.19	43480	0.16				
3.12	25380	0.17	31000	0.44	33780	0.82	39680	0.34	42380	0.52				
4.19	25250	0.23	31650	0.48	34480	0.62	39680	0.46	43100	0.72				
5.20	26300	0.24	31450	0.56	34480	0.59	39000	0.62	43850	1.16				

PL, en, Zn^{+2}

Table 3-31

pH	$\pi-\pi_1^*$		aldimine		$\pi-\pi_1^*$		ketimine		$\pi-\pi_2^*$		ν_1		ν_2	
	$\nu \text{ cm}^{-1}$	Abs.	$\nu \text{ cm}^{-1}$	Abs.	$\nu \text{ cm}^{-1}$	Abs.	$\nu \text{ cm}^{-1}$	Abs.	$\nu \text{ cm}^{-1}$	Abs.	$\nu \text{ cm}^{-1}$	Abs.	$\nu \text{ cm}^{-1}$	Abs.
1.09	-	-	31650	0.46	34250	1.12	-	-	42380	0.18				
3.12	-	-	31450	0.73	34250	0.97	39370	0.32	43500	0.30				
4.19	-	-	31850	1.08	33780	0.86	39680	0.56	44600	0.64				
5.20	-	-	31650	1.24	-	-	39680	0.70	44600	1.12				

Absorption Maxima (cm^{-1}) of Schiff Base Metal Chelates at Various pH Values

PLP, Gly, Zn⁺²

Table 3-32

pH	$\pi-\pi_1^*$ aldimine		$\pi-\pi_1^*$ ketimine		$\pi-\pi_2^*$		ν_1		ν_2	
	$\nu \text{ cm}^{-1}$	Abs.	$\nu \text{ cm}^{-1}$	Abs.	$\nu \text{ cm}^{-1}$	Abs.	$\nu \text{ cm}^{-1}$	Abs.	$\nu \text{ cm}^{-1}$	Abs.
1.09	-	-	31000	0.20	34200	1.24	39900	0.17	43400	0.15
3.12	26300	0.07	30500	0.21	34200	1.04	39500	0.20	43100	0.28
5.20	26400	0.72	30600	0.34	35900	0.46	-	-	43800	1.68

PL, Gly, Zn⁺²

Table 3-33

pH	$\pi-\pi_1^*$ aldimine		$\pi-\pi_1^*$ ketimine		$\pi-\pi_2^*$		ν_1		ν_2	
	$\nu \text{ cm}^{-1}$	Abs.	$\nu \text{ cm}^{-1}$	Abs.	$\nu \text{ cm}^{-1}$	Abs.	$\nu \text{ cm}^{-1}$	Abs.	$\nu \text{ cm}^{-1}$	Abs.
1.09	-	-	31400	0.16	34900	1.52	-	-	43800	0.27
3.12	-	-	31400	0.23	34900	1.51	-	-	43400	0.32
5.20	-	-	31400	1.47	-	-	39600	0.98	44200	1.34

Absorption Maxima (cm^{-1}) of Schiff Base Metal Chelates at Various pH Values
 PLP, en, Cd^{+2} Table 3-34

pH	$\pi-\pi_1^*$		aldimine		$\pi-\pi_1^*$		ketimine		$\pi-\pi_2^*$		ν_1		ν_2	
	$\nu \text{ cm}^{-1}$	Abs.	$\nu \text{ cm}^{-1}$	Abs.	$\nu \text{ cm}^{-1}$	Abs.	$\nu \text{ cm}^{-1}$	Abs.	$\nu \text{ cm}^{-1}$	Abs.	$\nu \text{ cm}^{-1}$	Abs.	$\nu \text{ cm}^{-1}$	Abs.
1.09	-	-	-	-	33800	1.16	39680	0.20	42300	0.16	-	-	-	-
3.12	25250	0.16	31250	0.44	33800	0.81	39400	0.34	42370	0.51	-	-	-	-
4.19	25500	0.22	31450	0.48	34500	0.63	39370	0.44	43100	0.72	-	-	-	-
5.20	25000	0.28	31000	0.56	34500	0.58	39000	0.63	43850	1.02	-	-	-	-

PL, en, Cd^{+2}

Table 3-35

pH	$\pi-\pi_1^*$		aldimine		$\pi-\pi_1^*$		ketimine		$\pi-\pi_2^*$		ν_1		ν_2	
	$\nu \text{ cm}^{-1}$	Abs.	$\nu \text{ cm}^{-1}$	Abs.	$\nu \text{ cm}^{-1}$	Abs.	$\nu \text{ cm}^{-1}$	Abs.	$\nu \text{ cm}^{-1}$	Abs.	$\nu \text{ cm}^{-1}$	Abs.	$\nu \text{ cm}^{-1}$	Abs.
1.09	-	-	31800	0.50	34500	1.16	-	-	42700	0.20	-	-	-	-
3.12	-	-	31600	0.70	34250	0.96	39600	0.34	43400	0.32	-	-	-	-
4.19	-	-	31800	1.04	34000	0.82	39800	0.53	44600	0.60	-	-	-	-
5.20	-	-	31400	1.27	-	-	39370	0.72	44200	1.11	-	-	-	-

Absorption Maxima (cm^{-1}) of Schiff Base Metal Chelates at Various pH ValuesPLP, Gly, Cd^{+2}

Table 3-36

pH	$\pi-\pi_1^*$ aldimine		$\pi-\pi_1^*$ ketimine		$\pi-\pi_2^*$		ν_1		ν_2	
	$\nu \text{ cm}^{-1}$	Abs.	$\nu \text{ cm}^{-1}$	Abs.	$\nu \text{ cm}^{-1}$	Abs.	$\nu \text{ cm}^{-1}$	Abs.	$\nu \text{ cm}^{-1}$	Abs.
1.09	-	-	30000	0.22	33700	1.18	39600	0.18	43000	0.16
3.12	25600	0.06	30400	0.23	34000	1.06	-	-	42700	0.28
5.20	25700	0.52	31000	0.38	35000	0.43	-	-	43800	1.30

PL, Gly, Cd^{++}

Table 3-37

pH	$\pi-\pi_1^*$ aldimine		$\pi-\pi_1^*$ ketimine		$\pi-\pi_2^*$		ν_1		ν_2	
	$\nu \text{ cm}^{-1}$	Abs.	$\nu \text{ cm}^{-1}$	Abs.	$\nu \text{ cm}^{-1}$	Abs.	$\nu \text{ cm}^{-1}$	Abs.	$\nu \text{ cm}^{-1}$	Abs.
1.09	-	-	31600	0.24	34700	1.46	-	-	43000	0.27
3.12	-	-	31600	0.31	34700	1.43	-	-	43000	0.32
5.20	-	-	31400	1.46	-	-	39400	0.93	44600	1.26

Absorption Maxima (cm^{-1}) of Schiff Base Metal Chelates at Various pH Values

PLP, en, Al⁺³

Table 3-38

pH	$\pi-\pi_1^*$ aldimine		$\pi-\pi_1^*$ ketimine		$\pi-\pi_2^*$		ν_1		ν_2	
	ν cm^{-1}	Abs.	ν cm^{-1}	Abs.	ν cm^{-1}	Abs.	ν cm^{-1}	Abs.	ν cm^{-1}	Abs.
1.09	-	-	30800	0.28	33780	1.19	39700	0.20	42370	0.21
3.12	25700	0.13	31650	0.51	34000	0.73	39800	0.36	43100	0.55
4.19	25500	0.19	31500	0.66	33800	0.76	39900	0.58	44250	0.70
5.20	25600	0.04	31800	0.68	33780	0.68	40000	0.61	44000	0.94

PL, en, Al⁺³

Table 3-39

pH	$\pi-\pi_1^*$ aldimine		$\pi-\pi_1^*$ ketimine		$\pi-\pi_2^*$		ν_1		ν_2	
	ν cm^{-1}	Abs.	ν cm^{-1}	Abs.	ν cm^{-1}	Abs.	ν cm^{-1}	Abs.	ν cm^{-1}	Abs.
1.09	-	-	31250	0.53	34500	1.17	-	-	42750	0.25
3.12	-	-	31000	0.81	34750	0.80	39800	0.31	44250	0.53
4.19	-	-	31250	1.05	34000	0.64	39900	0.49	44250	0.82
5.20	-	-	31250	1.34	-	-	39700	0.74	44250	1.33

PLP, Gly, Al⁺³

Absorption Maxima (cm⁻¹) of Schiff Base Metal Chelates at Various pH Values

Table 3-40

pH	$\pi-\pi_1^*$ aldimine		$\pi-\pi_1^*$ ketimine		$\pi-\pi_2^*$		ν_1		ν_2	
	ν cm ⁻¹	Abs.	ν cm ⁻¹	Abs.	ν cm ⁻¹	Abs.	ν cm ⁻¹	Abs.	ν cm ⁻¹	Abs.
1.09	-	-	30500	0.23	33780	1.16	39600	0.19	43100	0.18
3.12	25600	0.08	30300	0.31	33800	1.02	39600	0.26	43000	0.39
5.20	26800	0.17	-	-	33700	0.73	-	-	44600	1.00

PL, Gly, Al⁺³

Table 3-41

pH	$\pi-\pi_1^*$ aldimine		$\pi-\pi_1^*$ ketimine		$\pi-\pi_2^*$		ν_1		ν_2	
	ν cm ⁻¹	Abs.	ν cm ⁻¹	Abs.	ν cm ⁻¹	Abs.	ν cm ⁻¹	Abs.	ν cm ⁻¹	Abs.
1.09	-	-	31400	0.31	34700	1.42	-	-	43000	0.30
3.12	-	-	31000	0.40	34700	1.33	-	-	43800	0.39
5.20	-	-	31250	1.37	-	-	39800	0.84	44600	1.36

Absorption Maxima (cm^{-1}) of Schiff Base Metal Chelates at Various pH Values

PLP, en, Ga⁺³

Table 3-42

pH	$\pi-\pi_1^*$ aldimine		$\pi-\pi_1^*$ ketimine		$\pi-\pi_2^*$		ν_1		ν_2	
	ν cm^{-1}	Abs.	ν cm^{-1}	Abs.	ν cm^{-1}	Abs.	ν cm^{-1}	Abs.	ν cm^{-1}	Abs.
1.09	-	-	30200	0.28	33700	1.20	-	-	42400	1.90
3.12	26300	0.04	31950	0.74	33800	1.00	-	-	42500	1.96
4.19	25700	0.08	31900	0.78	34000	0.94	-	-	42750	2.04
5.20	26300	0.24	31600	0.68	33300	0.70	-	-	42800	2.09

PL, en, Ga⁺³

Table 3-43

pH	$\pi-\pi_1^*$ aldimine		$\pi-\pi_1^*$ ketimine		$\pi-\pi_2^*$		ν_1		ν_2	
	ν cm^{-1}	Abs.	ν cm^{-1}	Abs.	ν cm^{-1}	Abs.	ν cm^{-1}	Abs.	ν cm^{-1}	Abs.
1.09	-	-	31000	0.62	34200	1.14	-	-	42400	1.92
3.12	-	-	31000	0.76	34250	0.96	-	-	42500	1.97
4.19	-	-	31650	1.02	34250	0.86	39000	0.50	42750	2.0
5.20	-	-	31650	1.39	-	-	39000	1.04	42500	2.08

Absorption Maxima (cm^{-1}) of Schiff Base Metal Chelates at Various pH ValuesPLP, Gly, Ga⁺³

Table 3-44

pH	$\pi-\pi_1^*$ aldimine		$\pi-\pi_1^*$ ketimine		$\pi-\pi_2^*$		ν_1		ν_2	
	ν cm^{-1}	Abs.	ν cm^{-1}	Abs.	ν cm^{-1}	Abs.	ν cm^{-1}	Abs.	ν cm^{-1}	Abs.
1.09	-	-	30500	0.26	34000	1.30	-	-	42000	2.00
3.12	26700	0.46	-	-	34000	0.91	-	-	42000	2.02
5.20	26800	0.39	-	-	33600	1.07	-	-	42000	2.10

PL, Gly, Ga⁺³

Table 3-45

pH	$\pi-\pi_1^*$ aldimine		$\pi-\pi_1^*$ ketimine		$\pi-\pi_2^*$		ν_1		ν_2	
	ν cm^{-1}	Abs.	ν cm^{-1}	Abs.	ν cm^{-1}	Abs.	ν cm^{-1}	Abs.	ν cm^{-1}	Abs.
1.09	-	-	31250	0.42	34500	1.49	-	-	42000	1.99
3.12	-	-	31400	0.46	34500	1.45	-	-	42000	2.0
5.20	-	-	31500	1.39	-	-	39400	1.00	42000	2.05

3.4 Discussion

Assignment of Bands:

Schiff-bases of $(\text{PLP})_2\text{en}$, $(\text{PL})_2\text{en}$, PLPGly , PLGly and their chelates to various transition metals have been studied, in the pH range 1.09-5.25. Various species were noted and all bands have been assigned.

The spectra were characterized by the π_1 bands around 25000-26000 cm^{-1} , which have been assigned to the $\pi - \pi_1^*$ transition of the aldimine form of Schiff-bases. This band was considerably enhanced when compared to the band in the Schiff-base. The $\pi - \pi_1^*$ transition band of aldimine is almost absent in the free pyridoxal and appears to be rather weak, and almost absent at low pH (i.e. pH = 1.09).

In this region (25000-26000 cm^{-1}) in the pH range of 3-4 the molar extinction coefficient increases with increasing pH (Table: 3-8,9) and around pH = 6.7 ϵ_m decreases to a small extent^{13,14}. This would seem to imply that around pH 5-6 there is a change of ionic species as would have been expected, since the pK_a of this Schiff-base is expected to be around 6 (see Chapter 1, page 26).

Absorption maxima occurring in the 30000-32000 cm^{-1} region are thought to be attributable to the $\pi - \pi_1^*$ transition of the ketimine form of the Schiff-base. This band is absent in the complexes of $(\text{PLP})_2\text{en}$, with Fe^{II} , Co^{II} , Ni^{II} , Cu^{II} and Zn^{II} , at very acidic pH values.

The third band occurred at 33000-34000 cm^{-1} and is due to the $\pi - \pi_2^*$ transition of the neutral non-polar Schiff-base, which exists in acidic media. The intensity of the peak appears to decrease with increasing pH (Tables 3-8,9). This fact would tend to contradict Martell's assumption¹⁵, unless it is that this band is due partly to the free pyridoxal

phosphate or free pyridoxamine phosphate. (The Schiff-base could break down in two possible ways: (i) into the constituent pyridoxal phosphate and racemized amino acid; (ii) transamination could occur, and in this case the product would be pyridoxamine phosphate.)

The fourth and fifth transition bands (ν_1 , ν_2) occurred at 39000 cm^{-1} and 43-44000 cm^{-1} , which most likely can be assigned to the intermediate species of the pyridinium ion and pyridine aldehyde respectively.

Free pyridoxal and free pyridoxal phosphate have a band which occurs at 28000 cm^{-1} . This band was assigned by Martell¹⁵ and is due to the ionized phenolic group. In the present work this band was completely absent in all pyridoxal and pyridoxal phosphate complexes at any pH values, thus confirming co-ordination of metal ion through phenolic oxygen.

The band occurring at 35-36000 cm^{-1} may be due to the hydrolysis products¹⁴. This band appeared in the PLPGly of Zn^{II} , Cd and Co^{II} at pH = 5.2.

Christensen proposed^{16,3} that the bands occurring at 26550 and 23850 cm^{-1} are due to the intermediate species of aldimine-ketimine species.

Shifts in the absorption maxima can be correlated with increasing pH and change in ionic species. It was suggested¹³ that protonation of the heterocyclic nitrogen of the ketimine Schiff-base causes shifting of the bands to the longer wavelengths, while the protonation of the aldimine's heterocyclic nitrogen makes the bands to shorter wavelengths. Shifts to shorter wavelengths could also be the result of the chelation of the Schiff-base to the metal ion which stabilizes the complex and therefore makes the aldimine, ketimine forms interconvertible.

REFERENCES

1. Y. Matsushima and A.E. Martell, *JACS*, (1967), 89, 1322.
2. K. Nakamoto and A.E. Martell, *JACS*, (1959), 81, 5863.
3. H.N. Christensen, *JACS*, (1958), 80, 99.
4. T.C. Bruice and R.M. Topping, *JACS*, (1963), 85, 1480.
5. T.C. Bruice and R.M. Topping, *JACS*, (1962), 84, 2448.
6. J.W. Thanassi, A.R. Butler and T.C. Bruice, *Biochem*, (1965), 4, 1463.
7. Y. Matsuo, *JACS*, (1957), 79, 2011.
8. G.L. Eichorn and J.C. Bailar, *JACS*, (1953), 75, 2905.
9. D.E. Metzler and E.E. Snell, *JACS*, (1955), 77, 2431.
10. W.F. Smith, *Tetrahedron*, (1963), 19, 445.
11. A.M. Perault, B. Pullman, and C. Valdemoro, *Biochem. Biophys. Acta*. (1961), 46, 555.
12. E.A. Peterson and N.A. Sober, *JACS*, (1954), 76, 169.
13. J. Mastrantonis, Ph.D. Thesis, Bedford College, (University of London), 1982.
14. M. McMillan, M.Phil. Thesis, Bedford College (University of London), 1968.
15. D. Heinert and A.E. Martell, *JACS*, (1963), 85, 183.
16. H.N. Christensen, *JACS*, (1958), 80, 2305.

CHAPTER 4

Ultraviolet-Visible Solid State Study of Metal-Schiff Base Complexes

Complex	λ_{max} (nm)	ϵ (L mol ⁻¹ cm ⁻¹)	Assignment
Free	43000 (0.97)	29000	$\pi \rightarrow \pi^*$
Fe(III)	43000 (0.97)	30000	$\pi \rightarrow \pi^*$
Fe(III)Cl	44000 (0.14)	30000	$\pi \rightarrow \pi^*$
Fe(III)	45000 (1.06)	30000	$\pi \rightarrow \pi^*$

* Numbers in parentheses give the molar absorptivity

* The two bands overlapped

* shoulder

4.1 Experimental

The ultra-violet and visible spectra of freshly ground samples were run on the Unicam SP.700 recording spectrophotometer using the SP-735 state attachment. Freshly ground magnesium oxide (MgO) was used in the reference beam.

Table 4-1: Band Maxima (cm^{-1}) in Solid State Reflectance Spectra of Schiff-Bases

S.B.	Transition*/ cm^{-1}			
	ν_1	ν_{2a}	ν_{2b}	ν_3
(PLP) _{2en}	43500 (1.09)	38000 (1.19) sh.	31500 (1.27)	24000 (1.27)
(PL) _{2en}	42500 (1.05)	37500 (1.17) sh.	31200 (1.22)	25200 (1.29)
PLPGly	44500 (1.08)	38500 (1.09)	34000 (1.17) ■ 30500 (1.20)	23500 (0.91)
PLGly	43000 (0.99)	39000 (1.04)	34500 (0.99) ■ 29200 (1.02)	23200 (0.94)
PNen	43000 (0.97)	36500 (1.08) sh.	32200 (1.13)	28200 (1.16)
PMPHCl	44000 (1.14)	34000 (1.30)	31000 (1.25)	24000 (0.47)
PN	45000 (1.06)	39000 (1.17)	32000 (1.12)	-

* Numbers in parantheses give the absorbances

■ The two bands overlapped

sh: shoulder

Table 4-2: Band Maxima (cm^{-1}) in Solid State Reflectance Spectra of Copper Schiff-Base Complexes:

Complexes	Transitions* / cm^{-1}			
	V_1	V_{2a}	V_{2b}	V_3
$\text{Cu(PLP)}_2\text{en}, 4\text{H}_2\text{O}$	44200 (1.40)	36500 (1.60)	34000 (1.56) sh.	27500 (1.65)
$\text{Cu(PL)}_2\text{en}, \text{H}_2\text{O}$	46000 (1.20)	37000 (1.34)	31500 (1.29)	25000 (1.37) sh.
$\text{Cu(PLPGly)}, 3\text{H}_2\text{O}$	46000 (1.36)	38000 (1.54) sh.	32000 (1.66)	25500 (1.67)
$\text{Cu}_2(\text{PLGly}), 3\text{H}_2\text{O}$	44500 (1.45)	37000 (1.58)	32500 (1.63)	26000 (1.50)
$\text{Cu(PMP)}_2\text{acac}, 5\text{H}_2\text{O}$	45000 (1.29)	37500 (1.42) sh.	32000 (1.57)	23000 (0.40) sh.
$\text{Cu(PNen)}_2(\text{SO}_4)_2\text{Cl}_2, 5\text{H}_2\text{O}$	44000 (1.26)	35000 (1.47)	31200 (1.49)	26000 (1.19)
$\text{Cu(PN)}, 2\text{H}_2\text{O}$	46000 (1.26)	36000 (1.60)	32000 (1.63)	25000 (1.52)

* Numbers in parentheses give the absorbances

sh: shoulder

Table 4-3: Band Maxima (cm^{-1}) in Solid State Reflectance Spectra of Cobalt Schiff-Base Complexes:

Complexes	Transitions* / cm^{-1}			
	ν_1	ν_{2a}	ν_{2b}	ν_3
$\text{Co(PLP)}_2\text{en}, 4\text{H}_2\text{O}$	45000 (1.31)	38500 (1.34) sh.	30500 (1.44)	25500 (1.49)
$\text{Co(PL)}_2\text{en}, 2\text{H}_2\text{O}$	45000 (1.29)	37500 (1.35)	30000 (1.44)	25000 (1.52)
$\text{Co(PLPGly)}, \text{H}_2\text{O}$	45000 (1.32)	36000 (1.53)	31000 (1.55)	27000 (1.58)
$\text{Co(PLGly)}, 2\text{H}_2\text{O}$	45000 (1.44)	37500 (1.64)	32000 (1.71)	25500 (1.65)
$\text{Co(PMP)}_2, 4\text{H}_2\text{O}$	46500 (1.20)	38000 (1.26)	32000 (1.35)	23000 (0.36)

* Numbers in parentheses give the absorbances

sh: shoulder

Table 4-4: Band Maxima (cm^{-1}) in Solid State Reflectance Spectra of Nickel Schiff-Base Complexes:

Complexes	Transitions*/ cm^{-1}			
	ν_1	ν_{2a}	ν_{2b}	ν_3
Ni(PLP) ₂ en, 4H ₂ O	44500 (1.29)	37000 (1.36)	30500 (1.50)	25000 (1.52)
Ni(PL) ₂ en, 3H ₂ O	45500 (1.33)	37500 (1.28)	29000 (1.43)	23500 (1.35)
Ni ₂ (PLP)Gly, 6H ₂ O	44000 (1.22)	35000 (1.51)	30000 (1.50)	25000 (1.49)
Ni(PLGly), H ₂ O	45500 (1.40)	37500 (1.57)	31000 (1.66)	26000 (1.69)
Ni(PMP) ₂ , 3H ₂ O	44500 (1.36)	37500 (1.51)	31200 (1.67)	23000 (0.44)

* Numbers in parentheses give the absorbances

Table 4-5: Band Maxima (cm^{-1}) in Solid State Reflectance Spectra of Metal-Schiff-Base Complexes:

Complexes	Transitions* / cm^{-1}			
	ν_1	ν_{2a}	ν_{2b}	ν_3
Fe(PLPGly) OAc, H_2O	45000 (1.42)	38000 (1.60)	32500 (1.63)	26500 (1.51) sh. 24000 (1.41)
Fe(PLGly) OAc, H_2O	45000 (1.44)	37200 (1.62) sh.	32500 (1.69)	26500 (1.62) 23000 (1.56)
Fe(PLP) $_2$ enCl, $6\text{H}_2\text{O}$	44500 (1.31)	36500 (1.47)	31000 (1.50)	24000 (1.49)
Cd(PLP) $_2$ enCl $_3$, $6\text{H}_2\text{O}$	45500 (1.26)	38000 (1.33)	-	29000 (1.32)
Ag(PL) $_2$ enCl $_5$, $5\text{H}_2\text{O}$	45000 (1.45)	37500 (1.56)	30000 (1.49)	23500 (1.38)
Zn(PLP) $_2$ enCl $_2$, $2\text{H}_2\text{O}$	45500 (1.20)	37000 (1.24)	-	28000 (1.27)
Zn(PL) $_2$ en, $2\text{H}_2\text{O}$	46000 (0.94)	37000 (1.02)	-	27500 (1.07)

* Numbers in parantheses give the absorbances

sh: shoulder

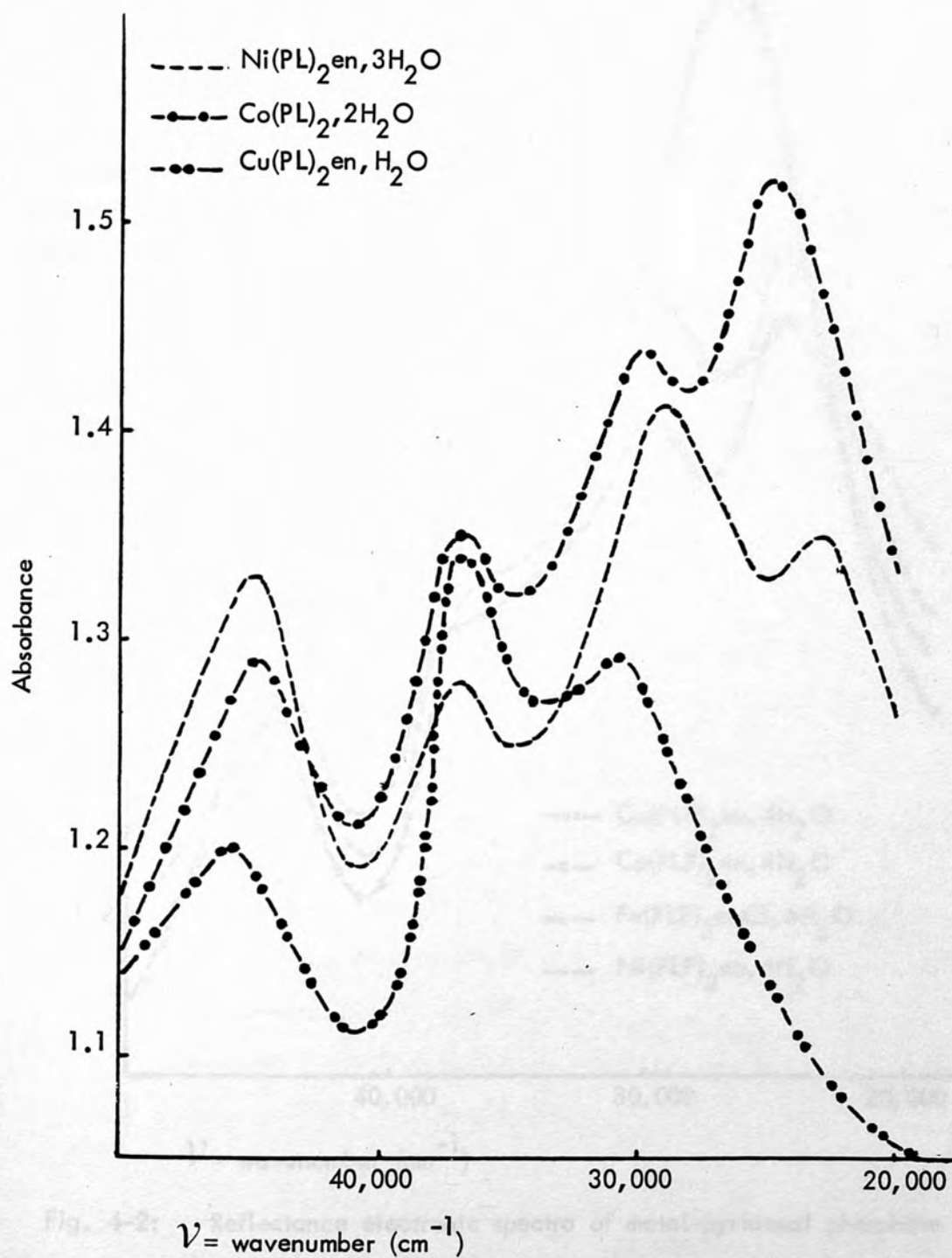


Fig. 4-1: Reflectance electronic spectra of metal-pyridoxal Schiff base complexes

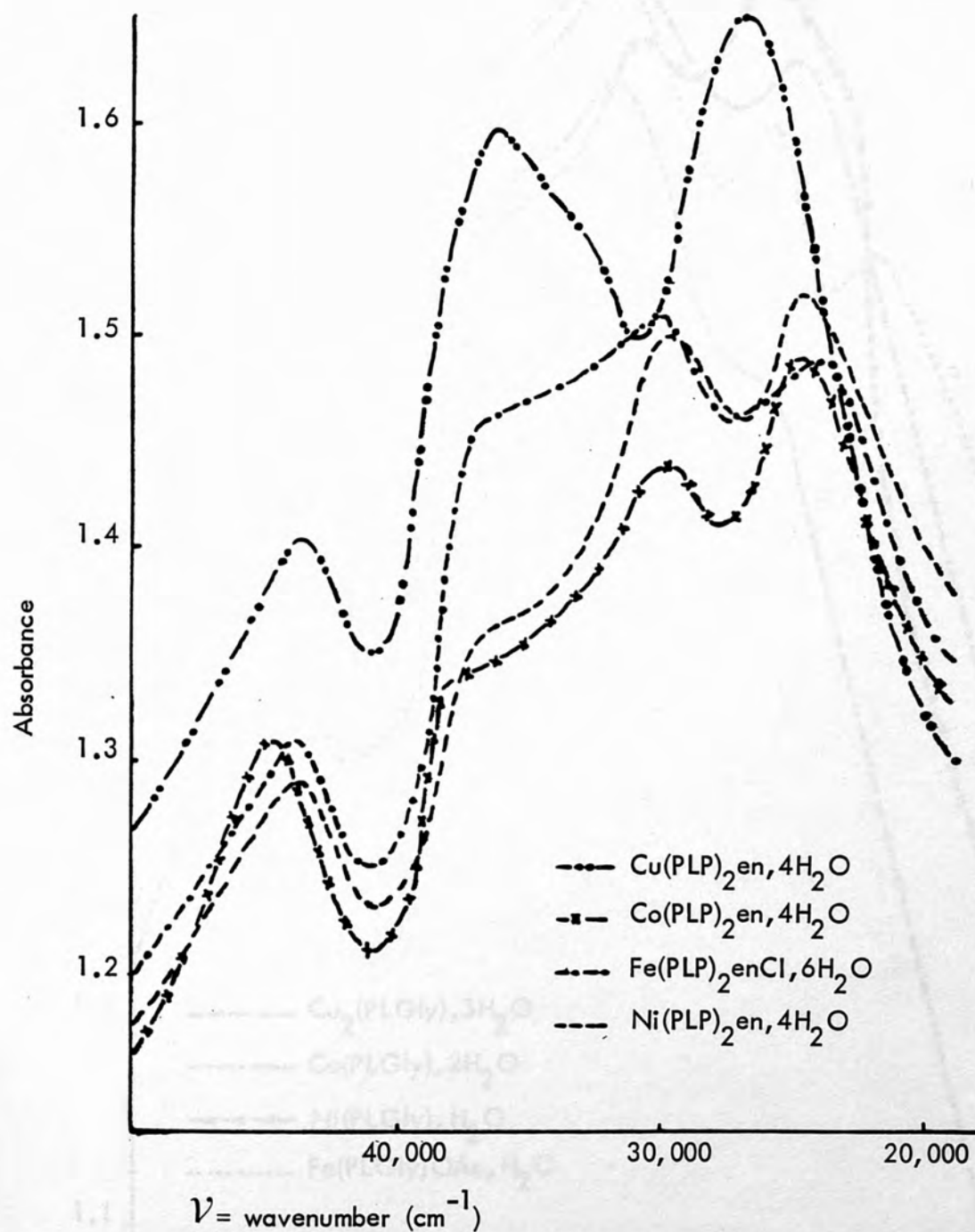


Fig. 4-2: Reflectance electronic spectra of metal-pyridoxal phosphate Schiff base complexes

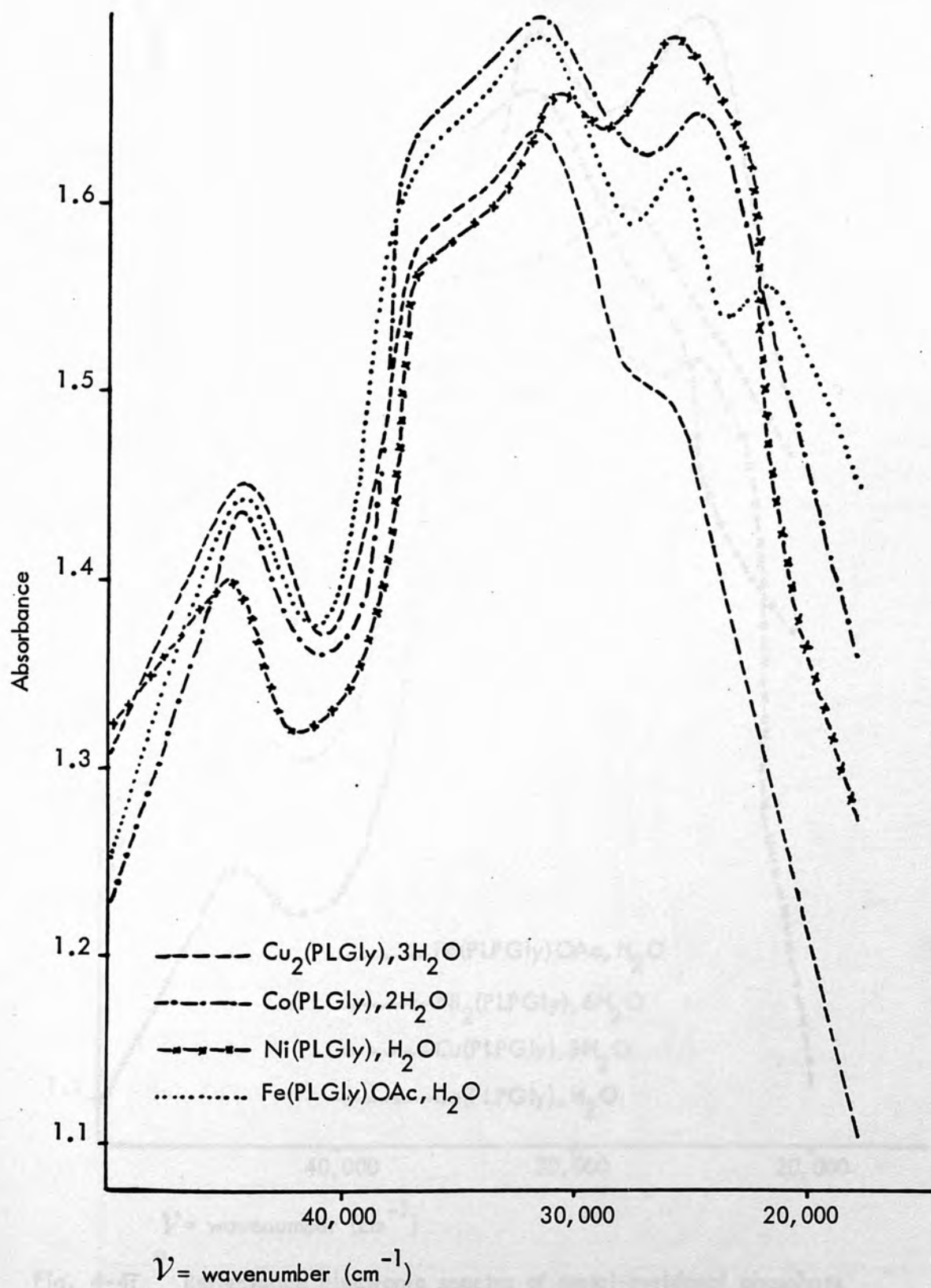


Fig. 4-3: Reflectance electronic spectra of metal-pyridoxal Schiff base complexes

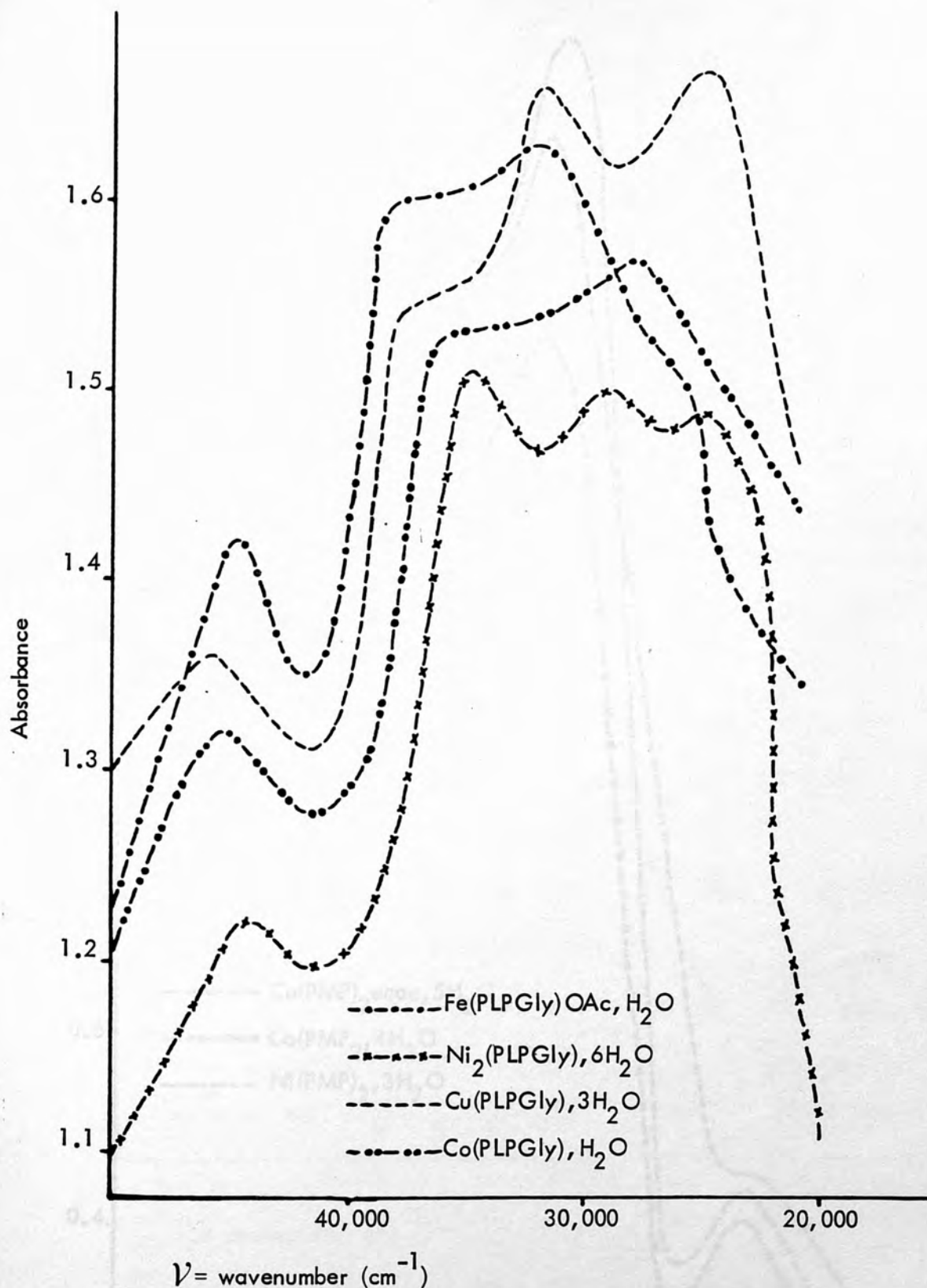


Fig. 4-4: Reflectance electronic spectra of metal-pyridoxal phosphate Schiff base complexes

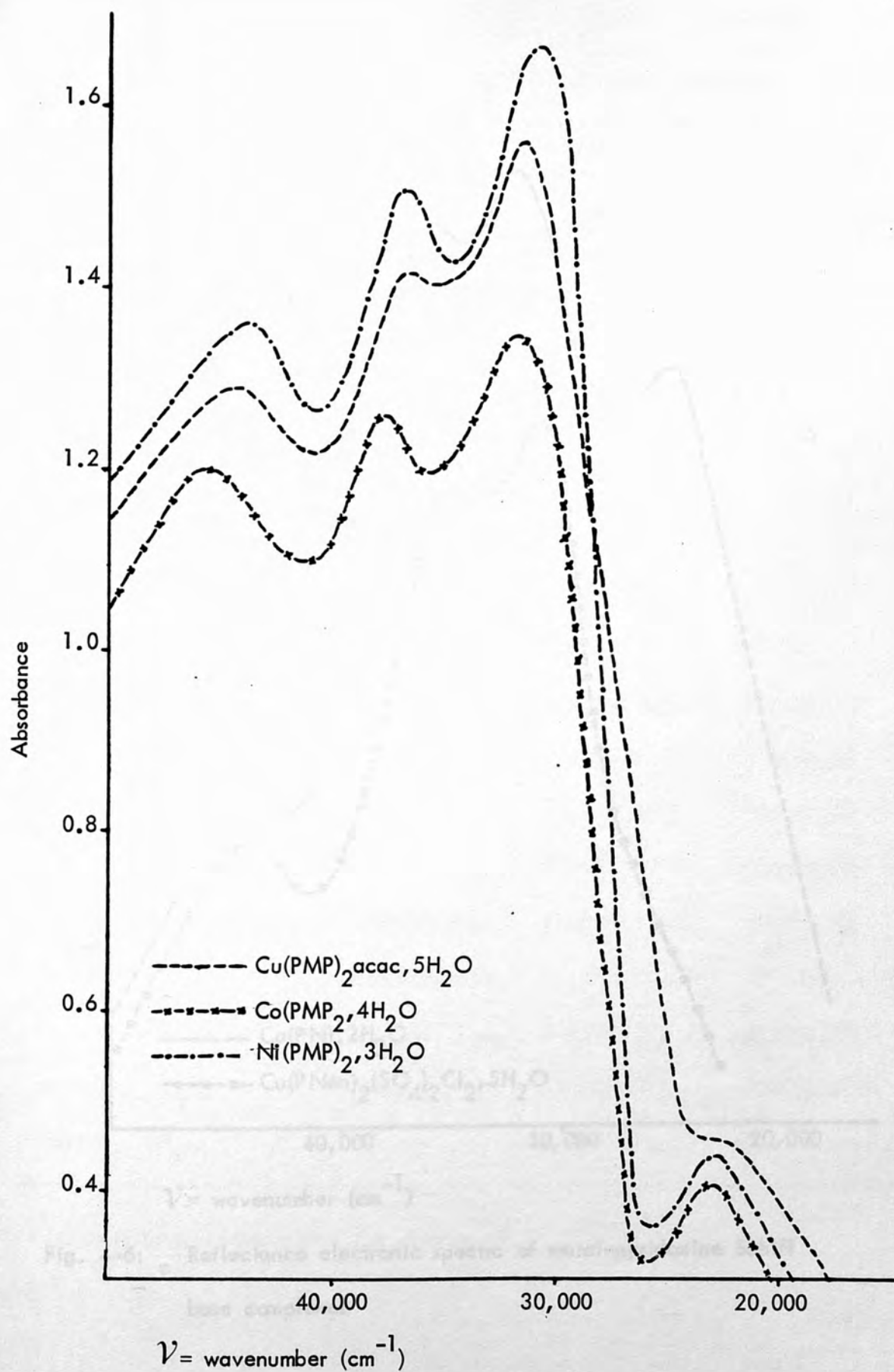


Fig. 4-5: Reflectance electronic spectra of metal-pyridoxamine phosphate Schiff base complexes

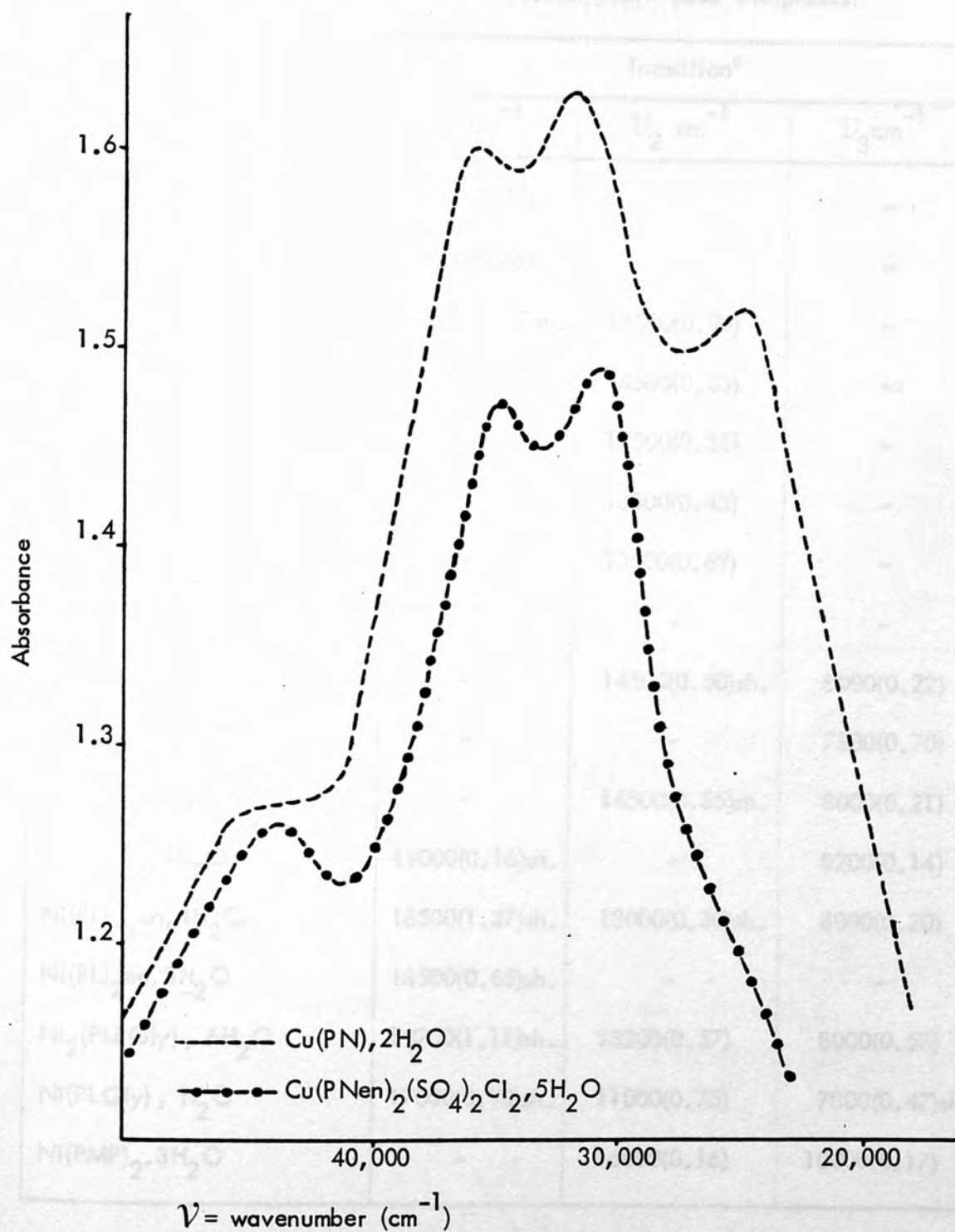


Fig. 4-6: Reflectance electronic spectra of metal-pyridoxine Schiff base complexes

Table 4-6: Main d-d Band Maxima of Metal-Schiff-Base Complexes:

Complexes	Transition*		
	$\nu_1 \text{ cm}^{-1}$	$\nu_2 \text{ cm}^{-1}$	$\nu_3 \text{ cm}^{-1}$
$\text{Cu(PLP)}_2\text{en}, 4\text{H}_2\text{O}$	16500(0.74)	-	-
$\text{Cu(PL)}_2\text{en}, \text{H}_2\text{O}$	18200(0.86)	-	-
$\text{Cu(PLPGly)}, 3\text{H}_2\text{O}$	19500(1.45)sh.	13000(0.96)	-
$\text{Cu}_2(\text{PLGly}), 3\text{H}_2\text{O}$	-	14500(0.63)	-
$\text{Cu(PMP)}_2, \text{acac}, 5\text{H}_2\text{O}$	-	15500(0.35)	-
$\text{Cu(PNen)}_2(\text{SO}_4)_2\text{Cl}_2, 5\text{H}_2\text{O}$	-	13500(0.45)	-
$\text{Cu(PN)}, 2\text{H}_2\text{O}$	-	13500(0.69)	-
$\text{Co(PLP)}_2\text{en}, 4\text{H}_2\text{O}$	-	-	-
$\text{Co(PL)}_2\text{en}, 2\text{H}_2\text{O}$	-	14500(0.50)sh.	8000(0.22)
$\text{Co(PLPGly)}, \text{H}_2\text{O}$	-	-	7500(0.70)
$\text{Co(PLGly)}, 2\text{H}_2\text{O}$	-	14500(0.35)sh.	8000(0.21)
$\text{Co(PMP)}_2, 4\text{H}_2\text{O}$	19000(0.16)sh.	-	8200(0.14)
$\text{Ni(PLP)}_2\text{en}, 4\text{H}_2\text{O}$	18500(1.37)sh.	13000(0.30)sh.	8000(0.20)
$\text{Ni(PL)}_2\text{en}, 3\text{H}_2\text{O}$	18500(0.65)sh.	-	-
$\text{Ni}_2(\text{PLPGly}), 6\text{H}_2\text{O}$	19700(1.11)sh.	13200(0.57)	8000(0.58)
$\text{Ni(PLGly)}, \text{H}_2\text{O}$	17000(0.90)sh.	11000(0.75)	7800(0.47)sh.
$\text{Ni(PMP)}_2, 3\text{H}_2\text{O}$	-	16000(0.16)	10000(0.17)

*Numbers in parantheses give the absorbances

sh: shoulder

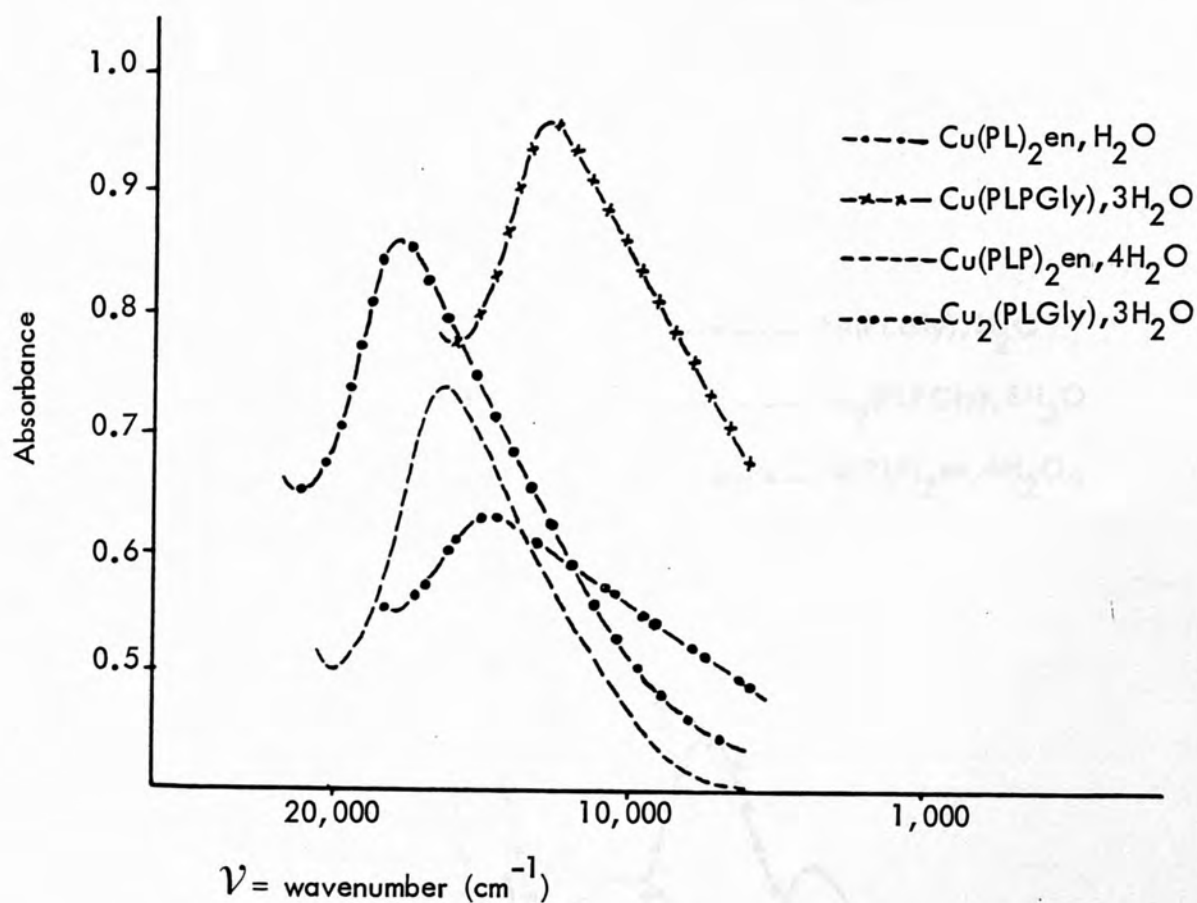


Fig. 4-7: Reflectance electronic spectra of Copper^{II}-Schiff base complexes

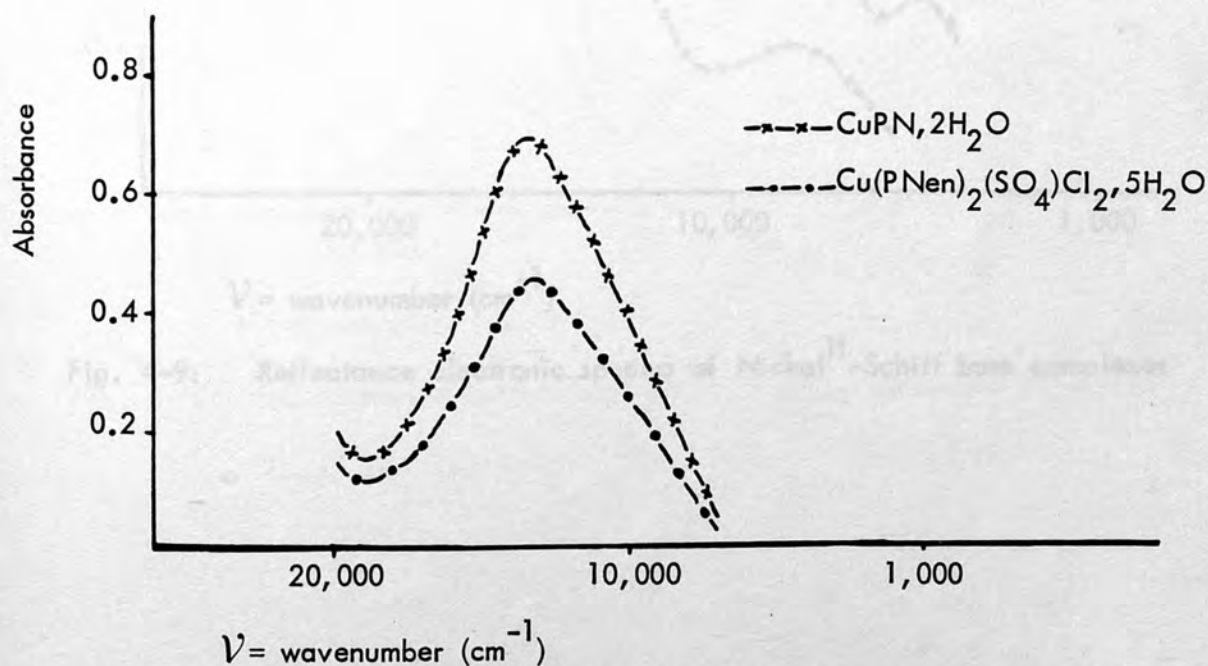


Fig. 4-8: Reflectance electronic spectra of Copper^{II}-pyridoxine Schiff base complexes

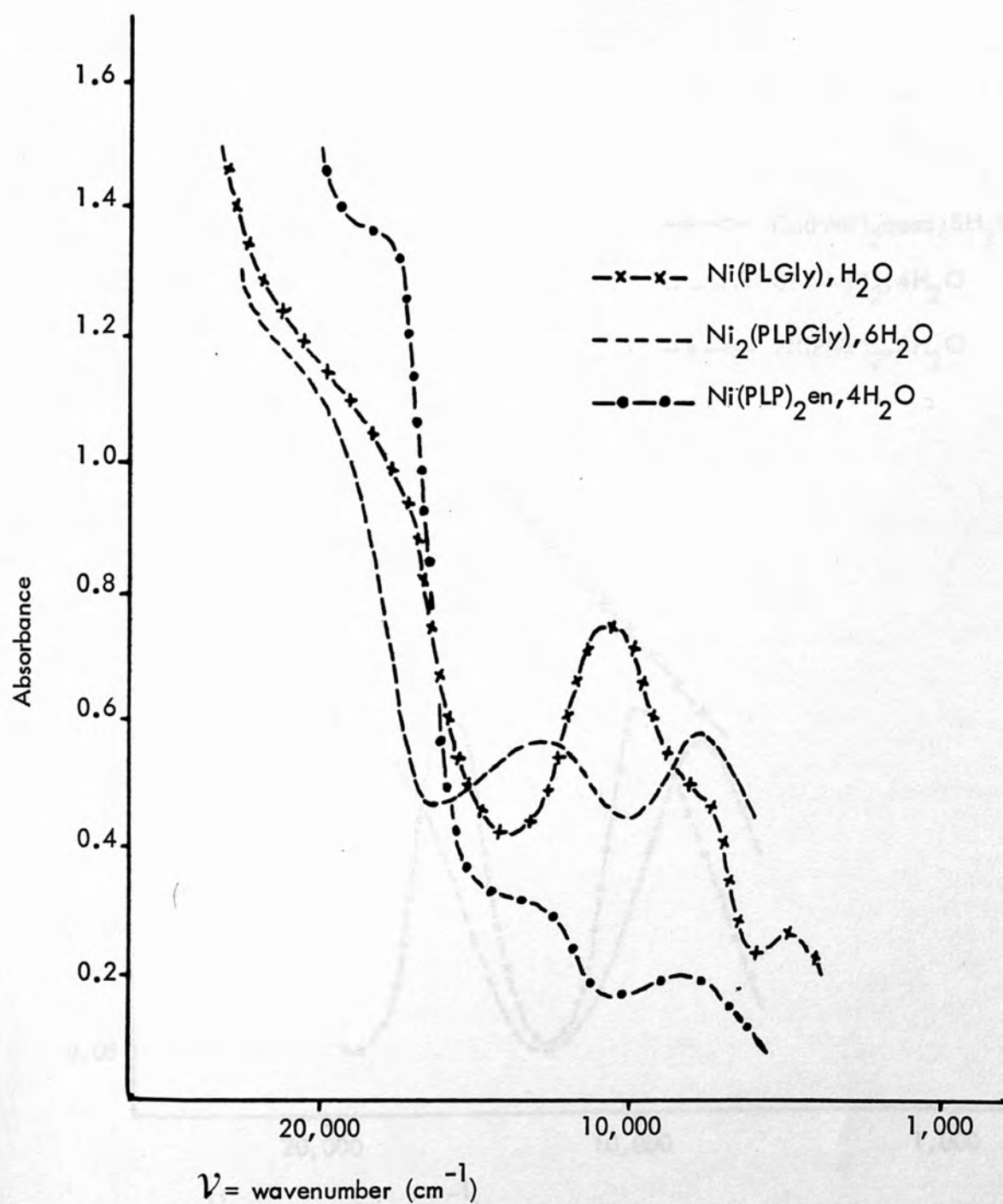


Fig. 4-9: Reflectance electronic spectra of Nickel^{II}-Schiff base complexes

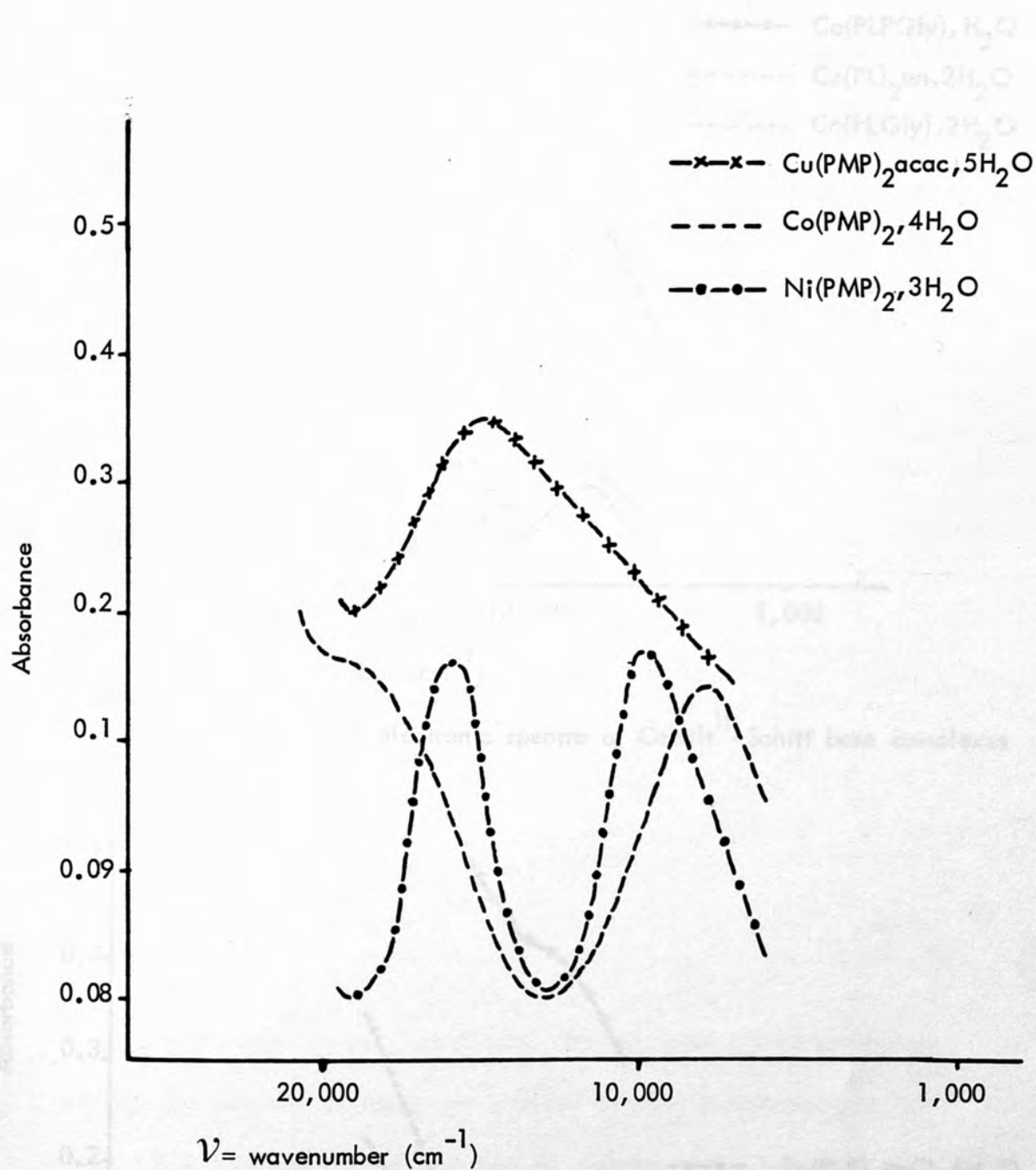


Fig. 4-10: Reflectance electronic spectra of metal-pyridoxamine phosphate Schiff base complexes

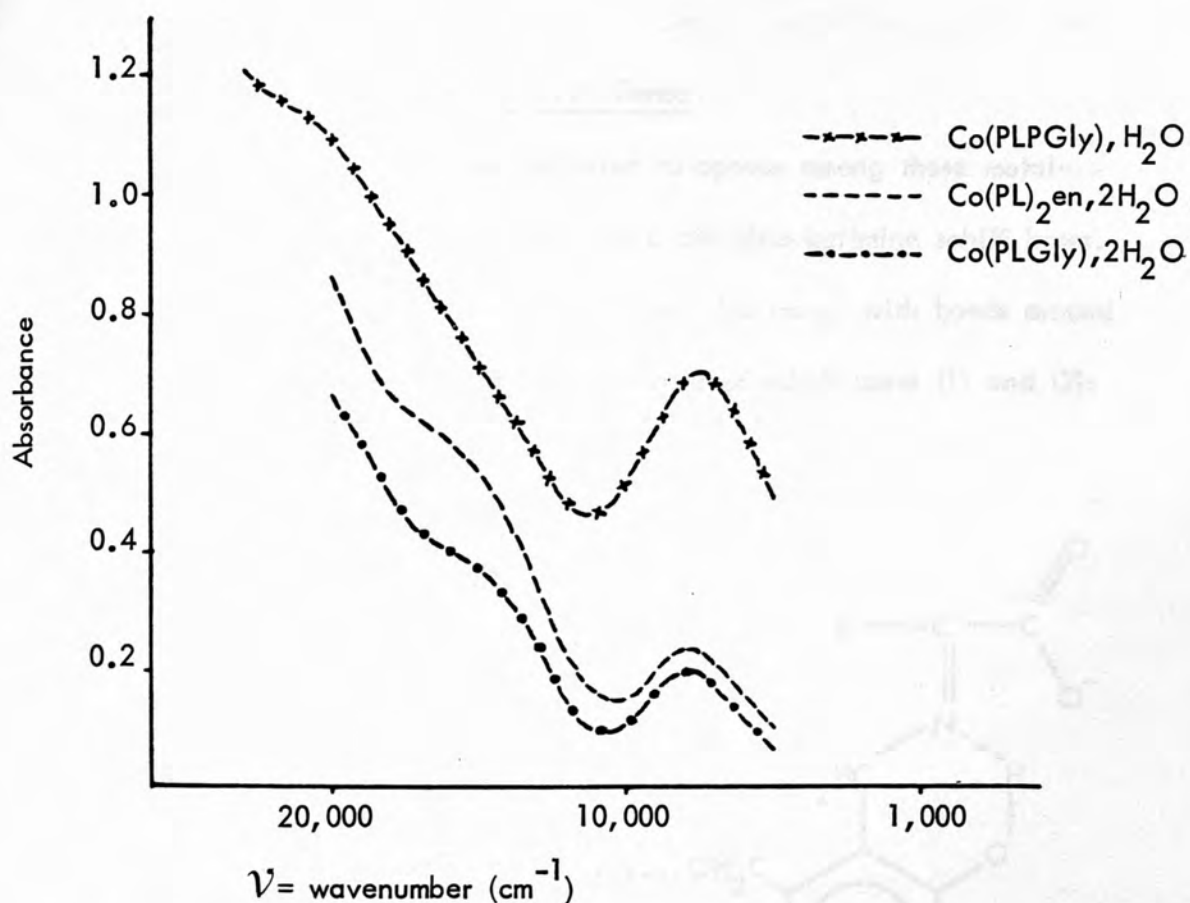


Fig. 4-11: Reflectance electronic spectra of Cobalt^{II}-Schiff base complexes

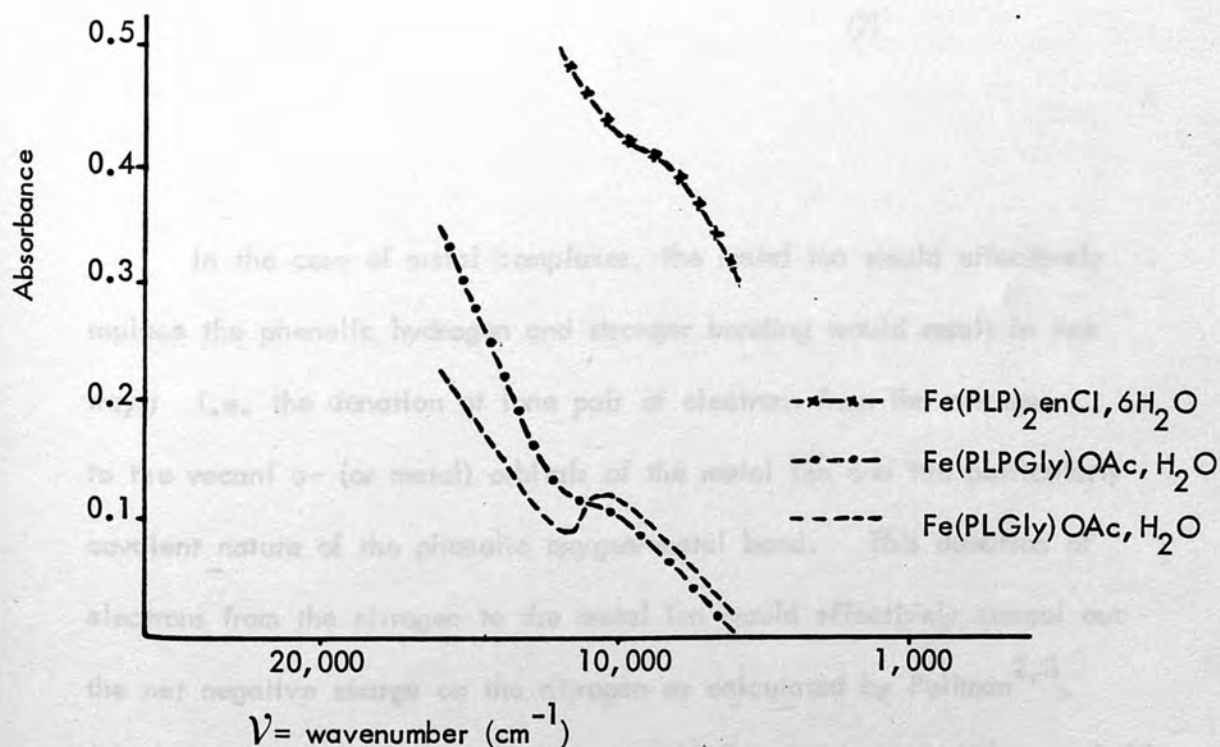
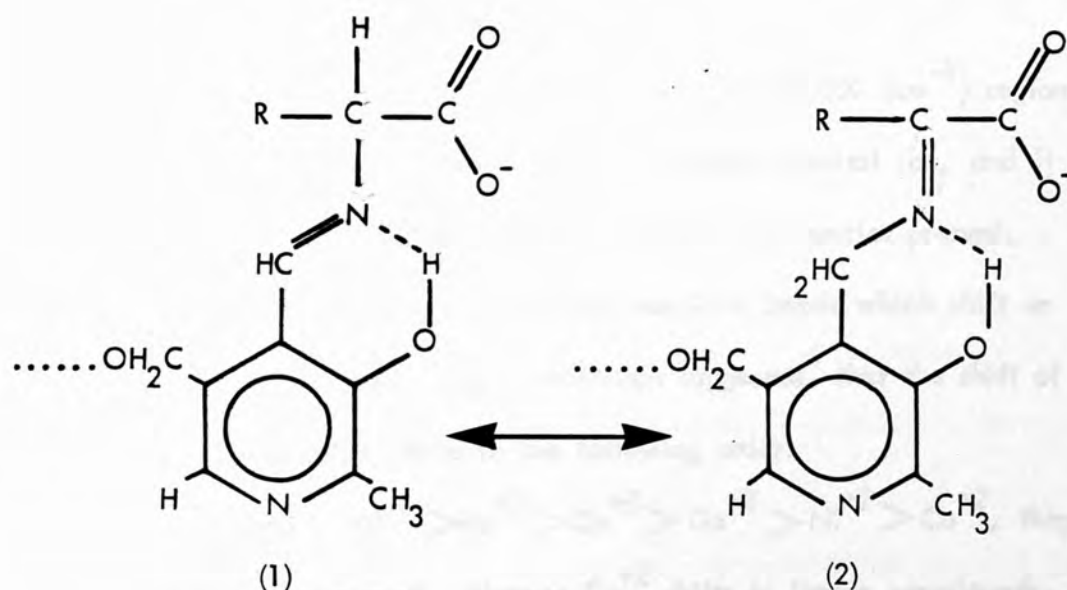


Fig. 4-12: Reflectance electronic spectra of Iron^{III}-Schiff base complexes

4.3 Discussion

(a) Assignment of the U.V. Bands

The species which are expected to appear among these metal-schiff base complexes are the tautomeric aldimine-ketimine schiff bases. This tautomeric mixture occurred¹ in the solid state, with bands around $26,000 \text{ (cm}^{-1}\text{)}$ attributable to the two forms of schiff bases (1) and (2):



In the case of metal complexes, the metal ion would effectively replace the phenolic hydrogen and stronger bonding would result in two ways; i.e. the donation of lone pair of electrons from the nitrogen to the vacant d- (or metal) orbitals of the metal ion and the particularly covalent nature of the phenolic oxygen-metal bond. This donation of electrons from the nitrogen to the metal ion would effectively cancel out the net negative charge on the nitrogen as calculated by Pullman^{2,3}. A rearrangement of electronic charge would therefore ensue with a probable

electron sink⁴ and a shift to shorter wavelength would be expected because of the protonation of the pyridine-nitrogen.

By comparison of the various Schiff-base chelates with the simple metal-amine complexes, it was clear that the "imine" band around 25,000 (cm^{-1}) and the band around 44,000 (cm^{-1}) both shifted to shorter wavelengths (longer wavenumber). This factor could be taken as an indication that there is a greater degree of chelation and stability in the Schiff-base metal complexes.

However, it was found that in the 40,000-30,000 (cm^{-1}) region, the maxima do appear to vary with the chelation of metal ion, and it is this region which one hopes will indicate the ionic species present.

Pyridoxamine phosphate has four transition bands which shift on co-ordination with metal ions. McMillan suggested⁴ that the shift of $\pi-\pi^*$ bands takes place in the following order:

$\pi-\pi_1^*$ band: $\text{Al}^{+3} > \text{Fe}^{+3} > \text{Zn}^{+2} > \text{Ga}^{+3} > \text{Ni}^{+2} > \text{Co}^{+2}$, they shift to shorter wavelength, whereas Cu^{+2} shifts to longer wavelength.

$\pi-\pi_2^*$ band: $\text{Zn}^{+2} > \text{Al}^{+3} > \text{Ga}^{+3} > \text{Cu}^{+2} > \text{Co}^{+2} > \text{Ni}^{+2}$, they shift to longer wavelength.

In the present work $\pi-\pi_1^*$ band shifts to longer wavelength (shorter wavenumber), whereas the $\pi-\pi_2^*$ band shifts to shorter wavelength:

Table 4-7: Shift of the $\pi - \pi^*$ bands in PMP and its Complexes:

bands	PMP	M^{+2} -PMP
$\pi - \pi_1^*$	24,000 cm^{-1}	23,000 cm^{-1}
$\pi - \pi_2^*$	31,000 cm^{-1}	32,000 cm^{-1}
"	34,000 cm^{-1}	37,000 cm^{-1}
"	44,000 cm^{-1}	45,000 cm^{-1}

(b) Assignment of d-d Bands

Electronic transitions for transition metal ions are expected in the visible region of spectrum when d-d electron transfers take place. The nature of the ligands, the stereochemical configuration of the molecule and the multiplicity all affect the energy of the transition and the position of the absorption band.

The most common stereochemistries for the metal ions are octahedral or tetrahedral. Splitting of the d-electron shell into subshells has been shown as in the following energy level diagram⁵:

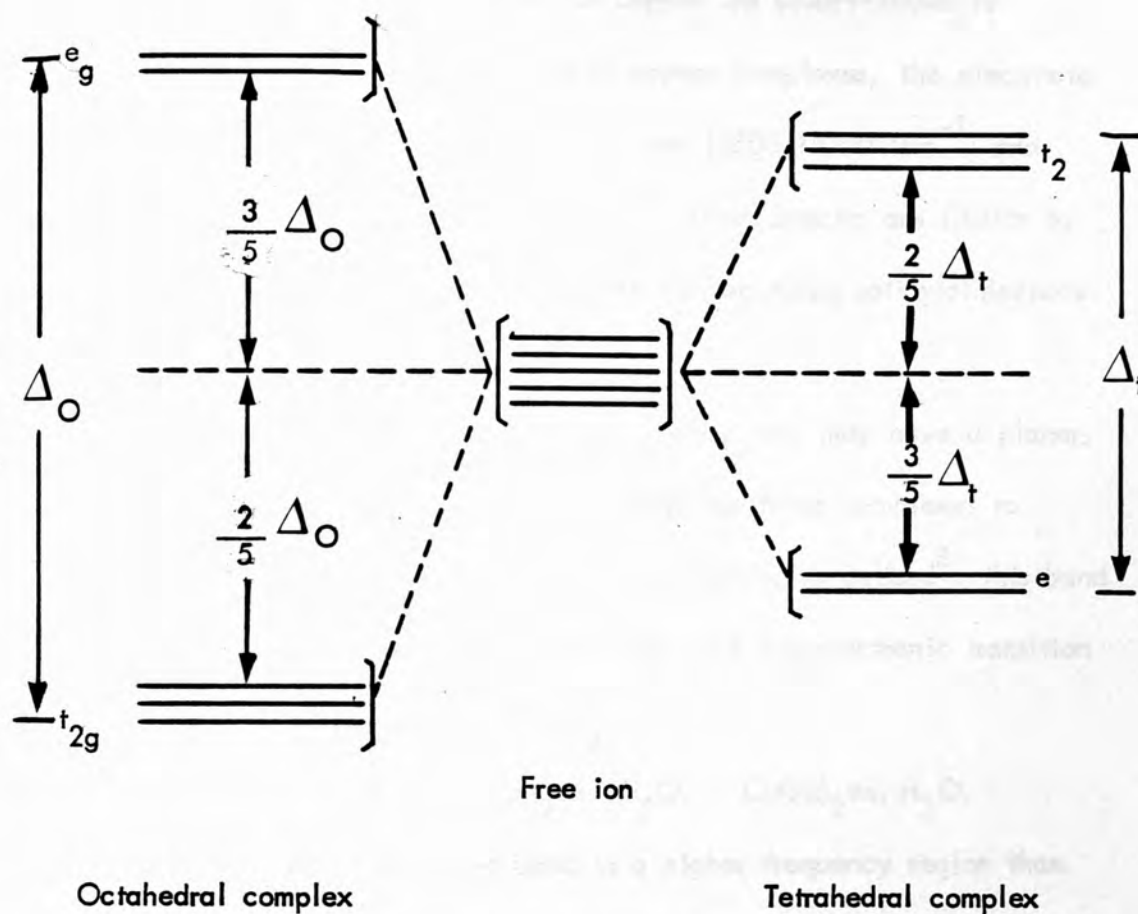


Fig. 4-13: Splitting of d-orbital in Octahedral and Tetrahedral Complexes

Any distortion from these two regular symmetry configurations will result in a probable splitting of the subshells and the rearrangement of the specific d-orbitals ($d_{x^2-y^2}$; d_{xy} , etc.) Distortion of the octahedral configuration includes that of the tetragonal (lengthening of the d_z axis) and square configurations (removal of the d_z ligands to infinity). The Jahn-Teller theory⁵ predicts distortions for unstable electronic states, which will lower the symmetry of the molecule and split the degenerate state. The results of the d-d band assignment are as follows:

Cu-Schiff Base Complexes:

The most common structures for copper are square-planar or distorted octahedral. In this series of copper complexes, the electronic spectra show that the d-d bands arise in the 13500-15500 (cm^{-1}) and 16500-20000 (cm^{-1}) regions (Table 4-6). These spectra are similar to each other and also to the spectra of the corresponding salicylaldiminate complexes^{6,7}.

It is considered that these copper^{II} complexes may have a planar configuration. One band only was expected for these complexes to appear around 14000 cm^{-1} (Table 4-6). According to Belford⁸, this band would imply a $d_{xy} \rightarrow d_{x^2-y^2}$ transition, and the electronic transition can be assigned to ${}^2T_{2g} \leftarrow {}^2E_g$.

On the contrary, $\text{Cu}(\text{PLP})_2\text{en}, 4\text{H}_2\text{O}$, $\text{Cu}(\text{PL})_2\text{en}, \text{H}_2\text{O}$, $\text{Cu}(\text{PLPGly}), 3\text{H}_2\text{O}$ have a d-d band in a higher frequency region than the others. These complexes most probably have a configuration distorted from a square-planar to a distorted octahedral arrangement.

Copper-pyridoxamine phosphate shows a very intense band at 15500 cm^{-1} which is very good evidence for mixed nitrogen-oxygen co-ordination. This has been confirmed by Farago et al⁹ and Jorgensen¹⁰ (CuGly_2 has a band at 15800 cm^{-1}).

Absorption maxima (cm^{-1}) in all complexes slightly shifted to higher or lower frequency and this can be expected because of:

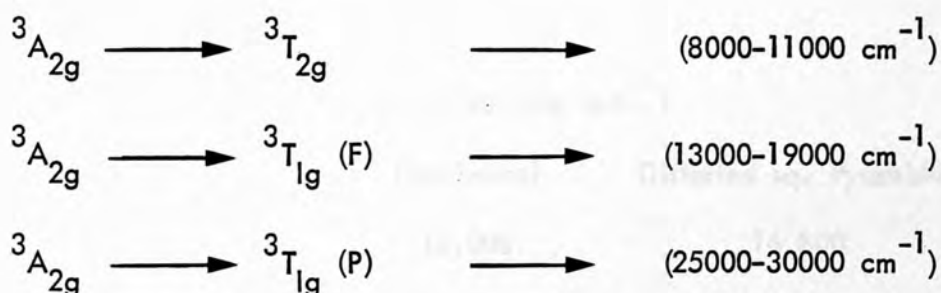
- 1) The different substituent chain on the amino acid (imine).
- 2) The fact that pyridine-nitrogen might not be bonded to the metal ion.

- 3) The phosphate group has not been expected to bond in pyridoxal phosphate-amino acid chelates, this co-ordination position could be occupied by either a water molecule or a second amino acid molecule.

Ni^{II}-Schiff Base Complexes:

An octahedral configuration has been found to occur for nickel most frequently in biological systems.

Electronic spectra of the Ni^{II}-Schiff base complexes show three d-d bands which can be attributed to the three expected transitions of Ni⁺²:



In the case of Ni(PMP)₂·3H₂O, the $\nu_1 = {}^3A_{2g} \longrightarrow {}^3T_{1g} (P)$ transition appeared to be obscured by another band which was more intense.

The complex Ni(PL)₂en·3H₂O has been found to have a different configuration from the others. Yamada et al¹¹ proved that this compound is a diamagnetic compound and its electronic spectrum in the solid state is typical of the spectra of four-co-ordinate, planar Ni^{II} complexes showing a d-d band as a shoulder at about 18500 cm⁻¹ and 17000 (cm⁻¹) respectively (Table 4-6, ~~Figure 4-6~~). The band at 17,000 (cm⁻¹) was masked by the 18,500 (cm⁻¹) band which is slightly more intense.

Co-Schiff Base Complexes:

Octahedral and tetrahedral are the most common configurations for cobalt complexes, but there are a fair number of square-planar¹² cases as well as some which are five co-ordinate¹³.

The d^7 electronic configuration of Co^{II} ion, in its high spin form, gives rise to a quartet state⁵, with a Jahn-Teller distortion due to the t_{2g}^5 configuration. The d-d band maxima of these cobalt complexes lie at nearly the same frequencies as the band maxima of the corresponding salicylaldehyde Schiff base complexes occurred. These absorption maxima in various configurations were suggested by Sacconi¹⁴ and are shown below:

Absorption Maxima (cm^{-1})		
Octahedral	Tetrahedral	Distorted sq. Pyramidal
15,600	18,000	16,800
11,000	11,200	11,400
9,300	7,700	6,700

The position of the bands in the 15,000–18,000 (cm^{-1}) region will indicate the nature of the configuration of the complexes. In all cobalt-Schiff base complexes which have been prepared, there is no distinctive band in this region, although the strong band in the 23,000–27,000 (cm^{-1}) region could overshadow it and envelop it as a shoulder at around 14,000–15,000 (cm^{-1}) region. There is, however, no band in the 11,000 (cm^{-1}) region. The only common band which appeared in all complexes is the band at 8000 (cm^{-1}) (Table 4-6). This band may correspond to the tetrahedral nature of the complexes (Sacconi¹⁴).

The Zn^{+2} , Cd^{+2} and Ag^{+} Schiff-base complexes did not show any d-d transition in the visible region.

The iron^{III} complexes $Fe^{III}(PLPGly)OAc, H_2O$ and $Fe^{III}(PLGly)OAc, H_2O$ showed a low-intensity d-d transition at approximately $11,000\text{ (cm}^{-1}\text{)}$ which may be assigned¹⁵ to a ligand-field transition. Although the proper assignment for these absorption maxima is uncertain, it appears to be a common feature of five-coordinate iron^{III} complexes.

10. C.K. Jørgensen, "Absorption Spectra and Chemical Bonding in Complexes", Pergamon, Oxford, (1962), 286.
11. S. Yamada, Y. Kuge, T. Yamayoshi and H. Kuroki, *Inorg. Chem. Acta.*, (1974), 11, 253.
12. S. Yamada, H. Kuroki and K. Yamayoshi, *Inorg. Chem. Acta.*, (1974), 10, 151.

References

1. D. Heinert and A.E. Martell, *JACS*, (1959), 81, 3933.
2. B. Pullman, *Proc. Int. Union Biochem.*, Rome (1966).
3. B. Pullman, A.M. Perault and C. Valdemoro, *Biochem. Biophys. Acta.*, (1961), 46, 555.
4. M. McMillan, M. Phil. Thesis, Bedford College, University of London, (1967).
5. F.A. Cotton and G. Wilkinson, *Advanced Inorganic Chemistry*, New York, Interscience Publishers, (1972).
6. S. Yamada and H. Nishikawa, *Bull. Chem. Soc., Japan*, (1963), 36, 755.
7. L. Sacconi, "Essay in Coordination Chemistry", W. Schneider, G. Anderegg and R. Gut, Ed., Birkhauser Verlag, Basel, (1964), 148.
8. R.L. Belford, M. Calvin and G. Belford, *J. Chem. Phys.*, (1957), 26, 1165.
9. M.E. Farago, M. McMillan and S. Sabir, *Inorg. Chem. Acta.*, (1975), 14, 207.
10. C.K. Jorgensen, "Absorption Spectra and Chemical Bonding in Complexes", Pergamon, Oxford, (1962), 286.
11. S. Yamada, Y. Kuge, T. Yamayoshi and H. Kuma, *Inorg. Chem. Acta.*, (1974), 11, 253.
12. S. Yamada, H. Kuma and K. Yamanouchi, *Inorg. Chem. Acta.*, (1974), 10, 151.

13. L. Sacconi, *J. Chem. Soc., A.*, (1970), 248.
14. L. Sacconi, *Coord. Chem. Revs.*, (1966), 1, 192.
15. M. Gerloch, F.E. Mabbs, J. Lewis and A. Richards, *J. Chem. Soc. A.*, (1968), 112.

CHAPTER 5

Infra-Red Study of Metal-Schiff Base Complexes

... which are most or less shifted ...
... As the metal-ligand bond becomes ...
... the frequencies increase. Further ...
... the symmetry of the ligand, forbidden ...
... on the parallel and degenerate vibrations are ...
... the metal-ligand bond, the larger the splitting of ...
... Therefore, frequency shifts, the negative of ...
... the intensity of newly permitted bands are used as a ...
... of the effect of co-ordination and in the assignment of the bands.

In the present infra-red study of metal-schiff base complexes, the free ligands (5,8.) were not isolated as pure compounds. Therefore, the assignment of the bands on the basis of shifts in band position upon complexation was not possible.

Wyrobek et al.¹ and McMillan² with similar ligands have, however, indicated that the position of several infrared bands is indicative of the mode of co-ordination. These observations include asymmetric C-N stretch (1310cm^{-1}), the phenolic C-O stretch (1260cm^{-1}), and

5.1. Introduction

Studies of the effect of co-ordination on the infrared spectra of the metal-schiff base complexes afford valuable information on the nature of the metal-ligand bonding.

Co-ordination often causes:

- 1) The appearance of new bands and splitting of the degenerate modes due to lowering of the symmetry.
- 2) Frequency shifts of the bands.
- 3) Intensification of the spectra.

By co-ordination, all the fundamentals are more or less shifted according to their modes of vibration. As the metal-ligand bond becomes stronger, the shifts to lower or higher frequencies increase. Furthermore, when co-ordination lowers the symmetry of the ligand, forbidden vibrations of the free ion are permitted and degenerate vibrations are split. The stronger the metal-ligand bond, the larger the splitting of the degenerate mode. Therefore, frequency shifts, the magnitude of the splitting and the intensity of newly permitted bands are useful as a measure of the effect of co-ordination and in the assignment of the bands.

In the present infrared study of metal-schiff base complexes, the free ligands (S.B.) were not isolated as pure compounds. Therefore, the assignment of the bands on the basis of shifts in band position upon complexation was not possible.

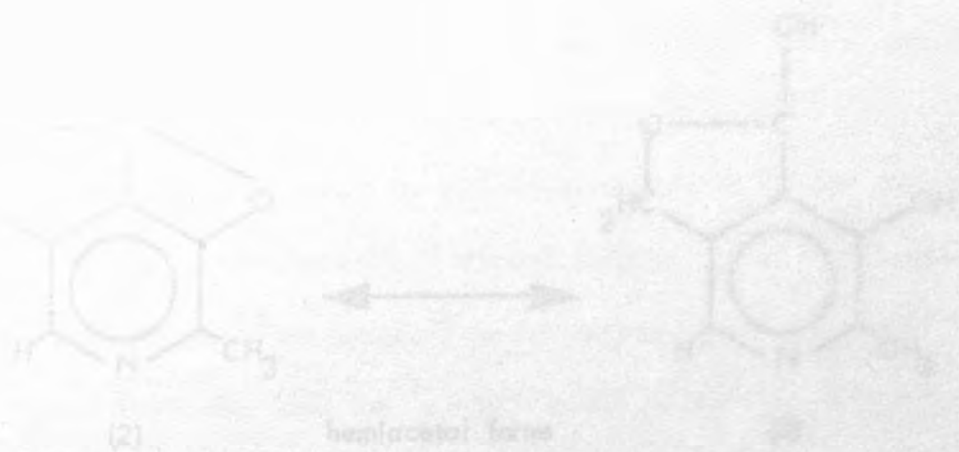
Wroblewski et al¹ and McMillan² with similar ligands have, however, indicated that the position of several infrared bands is indicative of the mode of co-ordination. These absorptions include azomethine C=N stretch (ν_{CN}), the phenolic carbon-oxygen stretch (ν_{CO}), and

the asymmetric carboxyl stretch (ν_{COO}) in the PLPGly and PLGly complexes.

In this series of Schiff-base complexes, however, all the bands have been assigned and the shift of the bands for various metals have been discussed.

5.2 Experimental

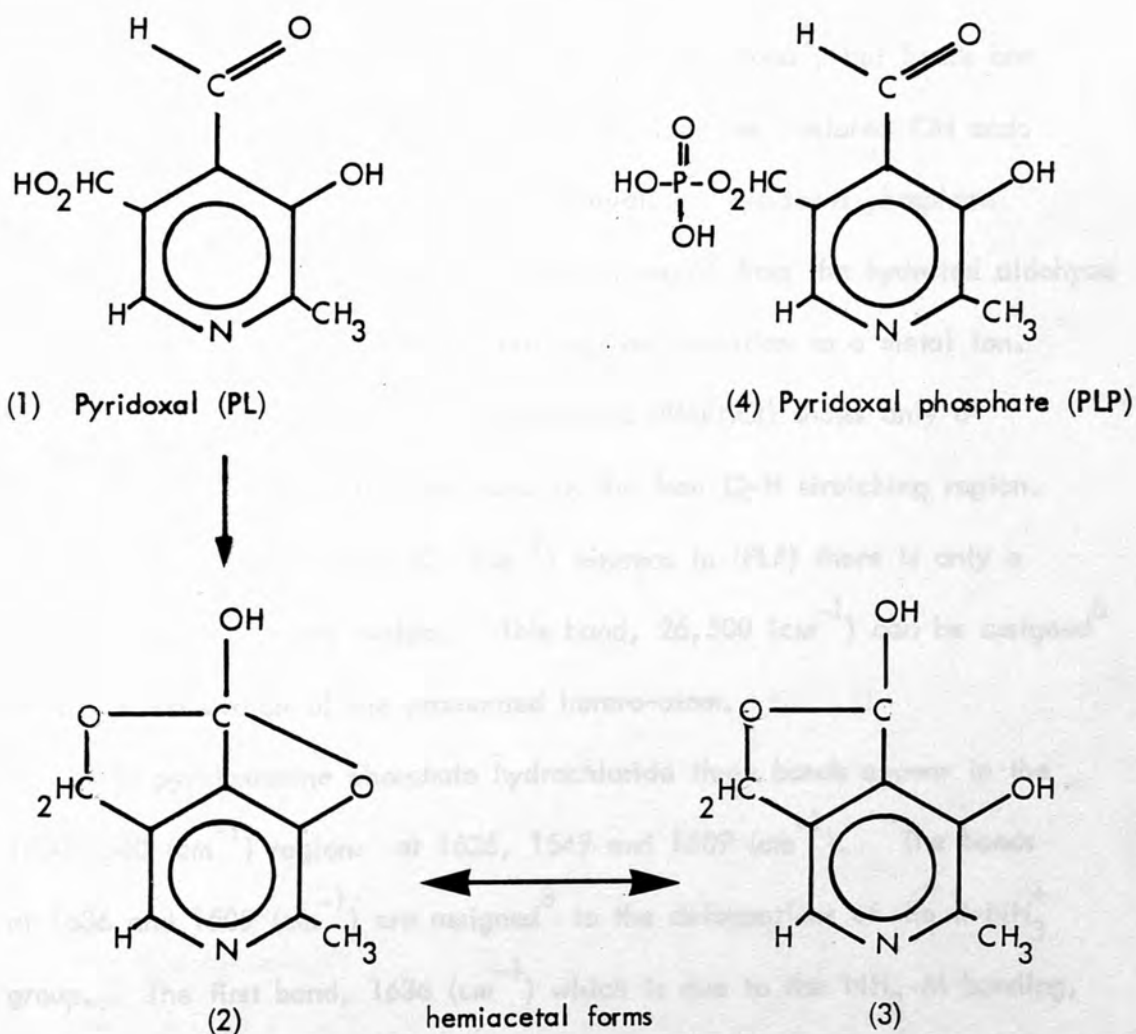
The infra-red absorption spectra were recorded on a Perkin Elmer 197 spectrophotometer. The spectra were taken as a dispersion in Nujol in 4000-600 (cm^{-1}) region. However, in the case of $\text{Ni}_2(\text{PLPGly}), 6\text{H}_2\text{O}$ this was difficult as the compound tended to hydrolyse and become rather sticky on mulling, and a KBr disc proved unsatisfactory. Sulphate and phosphate groups interfered in the 900-1200 (cm^{-1}) region and tended to envelop the resolution and other bands in the region.



The suggested structure has been largely confirmed by investigation of the crystals⁴. The pyridonal hydrochloride has shown a cyclic hemiacetal and a protonated ring nitrogen.

5.3 Results and Discussion

The infrared spectrum of pyridoxal (PL) has been discussed by Heinert and Martell³, who noted that in the solid state the C=O stretching band is absent due to the predominance of the hemi-acetal form:



The suggested structure has been largely confirmed by investigation of the crystals⁴. The pyridoxal hydrochloride was shown to contain hemi-acetal and a protonated ring nitrogen.

In the case of pyridoxal-5'-phosphate (PLP) hemi-acetal formation is prevented by the presence of the 5'-phosphate group (4). In the dihydrate PLP, the ring nitrogen is protonated⁴ by one hydrogen atom attached to the phosphate group.

In pyridoxamine phosphate (PMP) and pyridoxine (PN) the ring nitrogen is reported^{5,6,7} to be protonated.

In pyridoxal there is no free OH stretching band³, but bands are assigned at 3180-3100 (cm^{-1}) and 2735 (cm^{-1}) to the chelated OH and intermolecular O-H.....N bands respectively. Pyridoxal phosphate shows two sharp bands in the OH stretching region from the hydrated aldehyde at 3250 and 3420 (cm^{-1}); these disappear on chelation to a metal ion.

Pyridoxamine phosphate hydrochloride (PMPHCl) shows only a shoulder at 3200 (cm^{-1}) and no bands in the free O-H stretching region. A strong band occurs at 26 50 (cm^{-1}) whereas in (PLP) there is only a broad absorption in this region. This band, 26,500 (cm^{-1}) can be assigned⁸ to the $\text{N}^+\text{-H}$ stretch of the protonated hetero-atom.

In pyridoxamine phosphate hydrochloride three bands appear in the 1500-1640 (cm^{-1}) region: at 1636, 1549 and 1509 (cm^{-1}). The bands at 1636 and 1509 (cm^{-1}) are assigned⁸ to the deformations of the R-NH_3^+ group. The first band, 1636 (cm^{-1}) which is due to the $\text{NH}_2\text{-M}$ bonding, shifts to a lower wavelength (larger wavenumber) on chelation to metal ion; $\text{Co}^{+2} = 1655$ (cm^{-1}), $\text{Ni} = 1660$ (cm^{-1}). In the case of $\text{Cu(PMP)}_2\text{acac}, 5\text{H}_2\text{O}$, this band completely disappeared because of the non-existence of $\text{NH}_2\text{-M}$ bonding. The 1549 (cm^{-1}) band is likely to be the C=C/C=N stretching which shifts to longer wavelength on co-ordination.

The pyridoxamine phosphate and pyridoxine metal complexes exhibit several peaks in the 1450-1650 (cm^{-1}) region, which is the region for HOH bending and NH_2 deformation modes as well as ring breathing frequencies of pyridine⁹.

In all metal complexes of pyridoxamine phosphate and pyridoxine, the ligand exists as a zwitterion with the ring nitrogen protonated⁵.

Figure (5-1) summarizes the solid state structures, and schematically shows the changes which occur in ligands upon deprotonation and complexation:

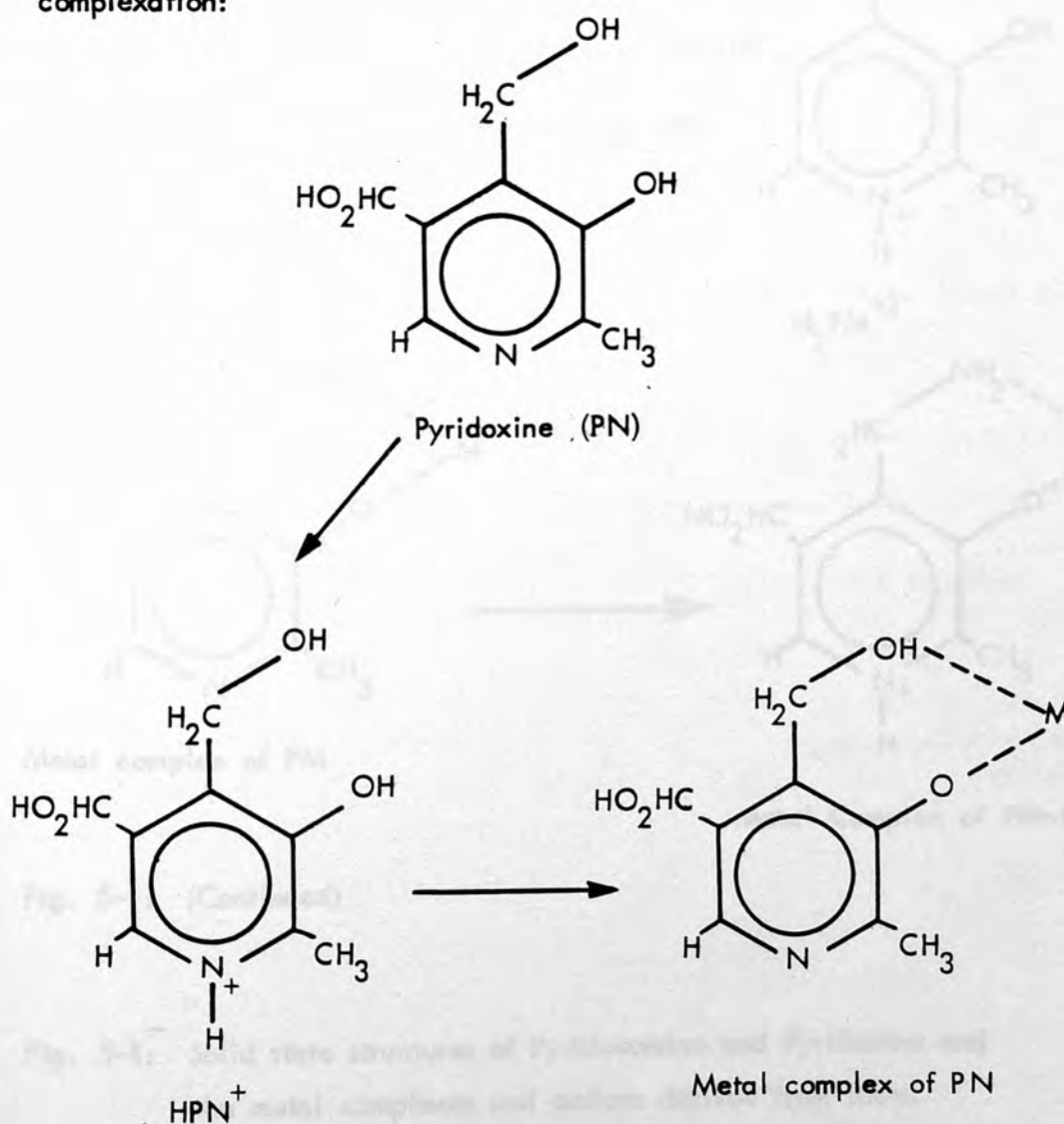


Fig. 5-1: Solid state structures of pyridoxamine (PM) and pyridoxine (PN) and the metal complexes and cations derived from them.

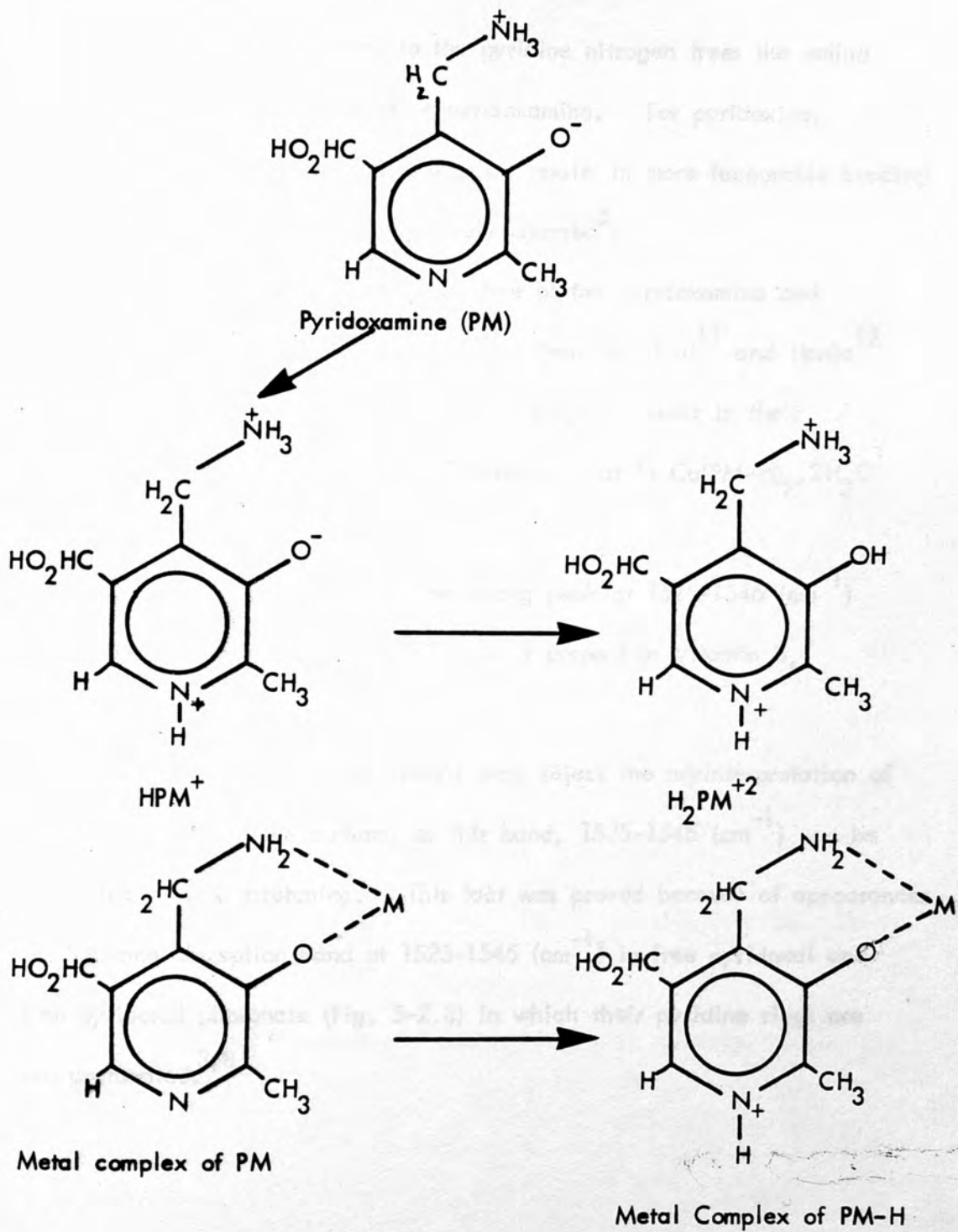


Fig. 5-1: (Continued)

Fig. 5-1: Solid state structures of Pyridoxamine and Pyridoxine and the metal complexes and cations derived from them.

The shift of the proton to the pyridine nitrogen frees the amino group for chelation in the case of pyridoxamine. For pyridoxine, shifting the proton from the phenol group results in more favourable bonding because the liganding site is negatively charged⁵.

The crystal structure study of some of the pyridoxamine and pyridoxine complexes by Mosset et al¹⁰, Franklin et al¹¹ and Hanic¹² have in fact established that a pyridinium ring is present in their complexes, whereas Franklin et al¹³ revealed that in $\text{Cu}(\text{PM-H})_2 \cdot 2\text{H}_2\text{O}$ the pyridine ring is not protonated.

They suggested¹¹⁻¹³ that the strong peak at 1525-1545 (cm^{-1}) indicates that a protonated ring nitrogen is present in Vitamin B₆ derivatives.

Farago et al⁸ and the present work reject the misinterpretation of this band by the above authors, as this band, 1525-1545 (cm^{-1}) can be attributed to C=C stretching. This fact was proved because of appearances of the same absorption band at 1525-1545 (cm^{-1}) in free pyridoxal and free pyridoxal phosphate (Fig. 5-2,3) in which their pyridine rings are not protonated.^{3,8}

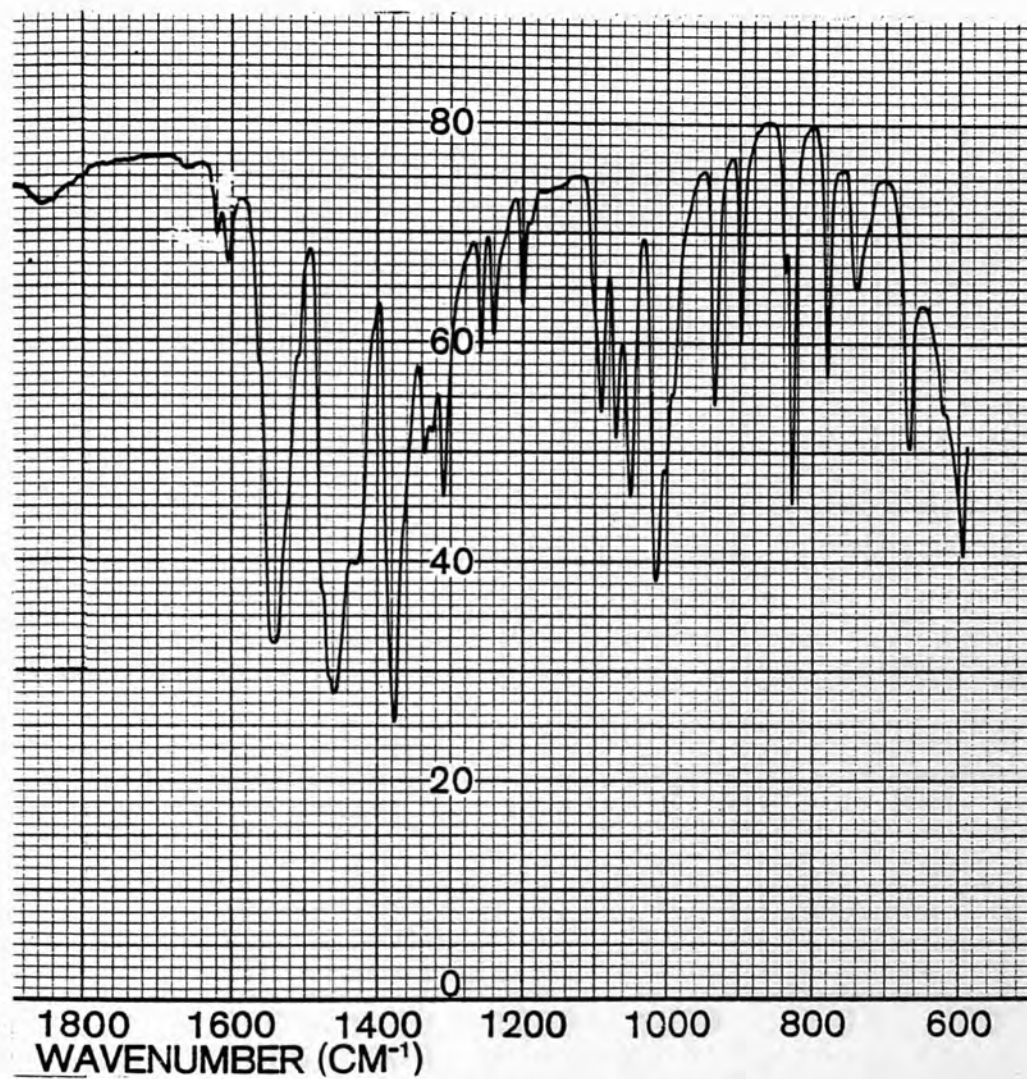


Fig. 5-2: Infrared Spectrum of free Pyridoxal (PL) in Nujol

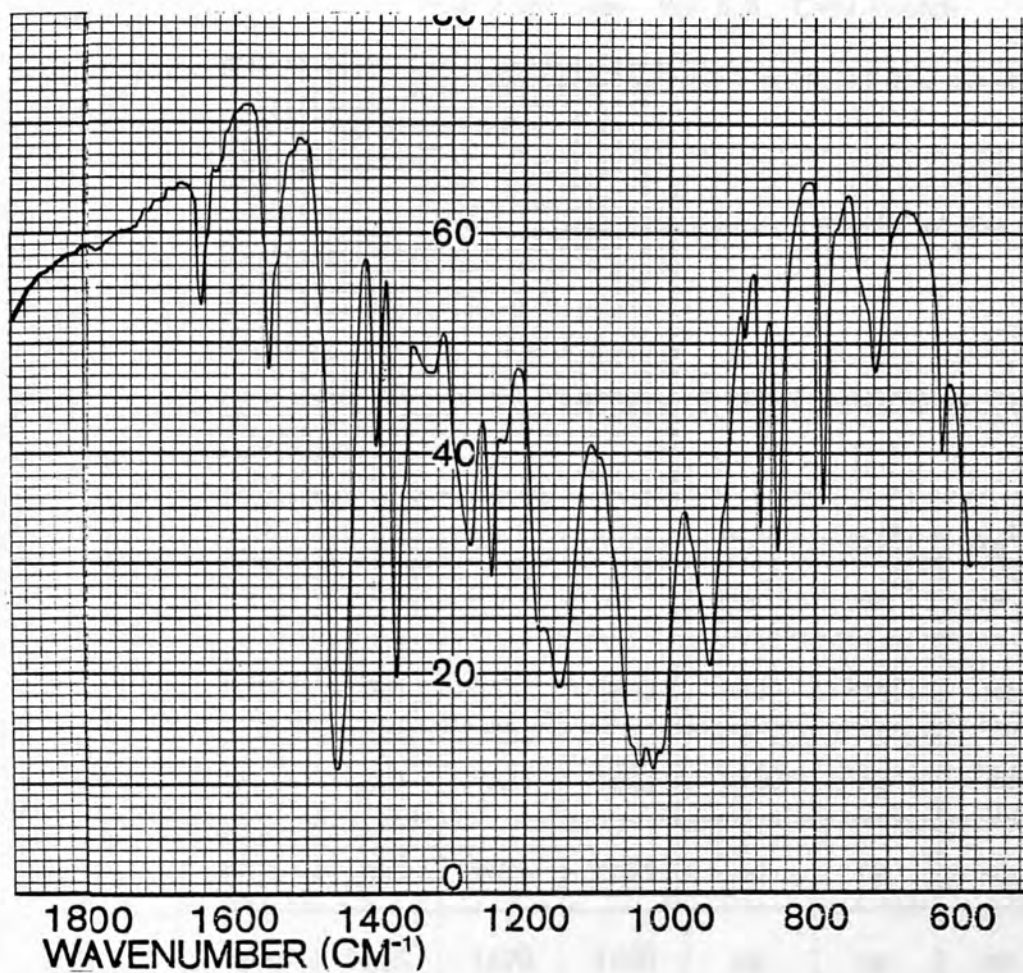


Fig. 5-3: Infrared Spectrum of Pyridoxal Phosphate (PLP) in Nujol

In the case of schiff base complexes, the most important region is 1500-1650 (cm^{-1}).

In this series of schiff base complexes, the S.B. C=N stretch frequency commonly occurred at 1600-1650 (cm^{-1}). Shifts of the bands are expected to vary according to the metal ion and the strengths of the nitrogen and phenolic-oxygen bonds with the metal ion. Results of the band shift are shown in Table (5-1):

Table 5-1: Bands (cm^{-1}) of the C=N stretching of Metal Schiff Base Complexes

S.B.	Fe ^{III} cm^{-1}	Co ^{II} cm^{-1}	Ni ^{II} cm^{-1}	Cu ^{II} cm^{-1}	Zn ^{II} cm^{-1}	Cd ^{II} cm^{-1}	Ag ^I cm^{-1}
(PLP) ₂ en	1630	1638	1612 _w	1645	1650	1645	np
(PL) ₂ en	np	1608	1635	1642	1650	np	1640
PLPGly	1635	1635	1630	1635	np	np	np
PLGly	1640	1625	1620	1640	np	np	np

w = weak

np = not prepared

The maximum shift was noticed in $\text{Co(PL)}_2\text{en}, 2\text{H}_2\text{O}$ (1608 cm^{-1}). No band was found in this region in other complexes, but a similar band was found at 1612 cm^{-1} in the $\text{Ni(PLP)}_2\text{en}, 4\text{H}_2\text{O}$ complex. This would seem to confirm the opinion that the metal co-ordination tended to shift the imine band (C=N) to longer wavelength (smaller wave number).

In PLPGly and PLGly complexes, the asymmetric carboxyl (ν_{COO}) stretching absorption is found¹⁴ around $1570 \text{ (cm}^{-1}\text{)}$ and varies according to the metal ion used. This band was not distinctly observed in all complexes, and almost overlapped with the ring C=C stretching band which occurred in the $1500\text{--}1550 \text{ (cm}^{-1}\text{)}$ region.

The (C-O⁻) frequency was quoted by Martell¹⁵ to occur at $1410 \text{ (cm}^{-1}\text{)}$ in free pyridoxal-5'-phosphate and the pyridoxal molecule.

This band was absent in all Schiff-base complexes. The disappearance of this band proved that the co-ordination takes place between the phenolic oxygen and metal ion.

The C-O stretching band which occurs in the $1300\text{--}1350 \text{ (cm}^{-1}\text{)}$ region is due to the bonding of phenolic-oxygen to metal ion (C-O-M) and has been assigned by Kovacic¹⁶.

Frequency of this band varies according to the metal ions used.

Results of shifting of the frequency are shown in Table (5-2):

Table 5-2: Bands (cm^{-1}) of C-O str. of the Metal-Schiff Base Complexes

S.B.	Fe ^{III} cm^{-1}	Co ^{II} cm^{-1}	Ni ^{II} cm^{-1}	Cu ^{II} cm^{-1}	Zn ^{II} cm^{-1}	Cd ^{II} cm^{-1}	Ag ^I cm^{-1}
(PLP) ₂ en	1318 _w	1310	1315	1330	1322	1315	np
(PL) ₂ en	np	1325	1328	1320	1318	np	1318
PLPGly	1310	1318 _w	1338 _w	1340	np	np	np
PLGly	1324	1324 _w	1310 _w	1316	np	np	np
(PNen) ₂	np	np	np	1305	np	np	np
PN	np	np	np	1308	np	np	np
(PMP) ₂	np	1330	1335	1315	np	np	np

w = weak

np = not prepared

The (C-O-M) band in the PLP, PL and PMP complexes occurs at 1324 and 1328 (cm^{-1}) respectively. The following order is suggested for the shift of this band in (PLP)₂en and PMP upon complexation:

i) In the (PLP)₂en complexes:

shift to longer wavelength: $\text{Co}^{\text{II}} > \text{Ni}^{\text{II}} = \text{Cd}^{\text{II}} > \text{Fe}^{\text{III}} = \text{Ag}^{\text{I}} > \text{Zn}^{\text{II}}$

shift to shorter wavelength: Cu^{II}

ii) In the PMP complexes:

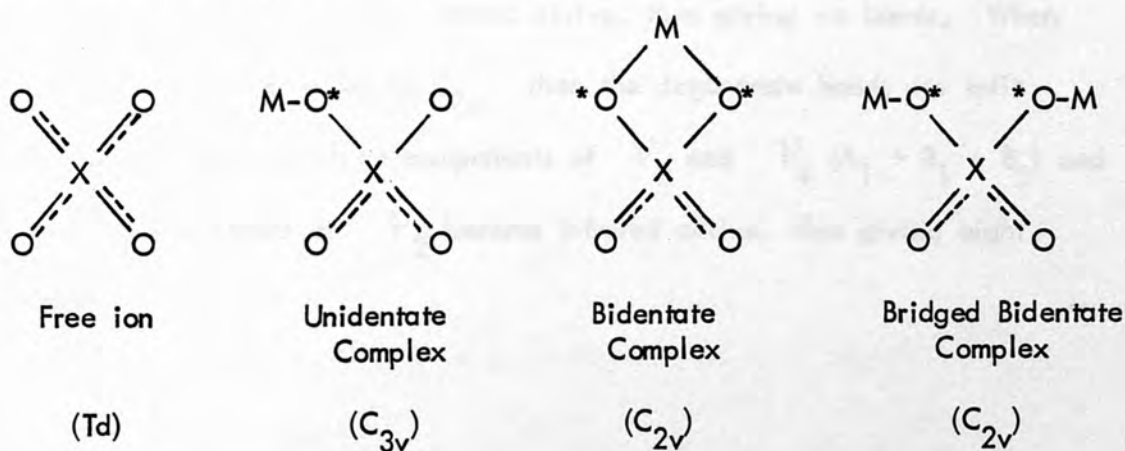
shift to shorter wavelength: $\text{Co}^{\text{II}} > \text{Ni}^{\text{II}}$

shift to longer wavelength: Cu^{II}

In the 900-1200 (cm^{-1}) region, the spectra of the phosphorylated Vitamin B₆ compounds and their derivatives are dominated by bands from the phosphate group. This region (900-1200 cm^{-1}) has been studied and largely discussed by Farago et al.⁸. The sulphate group (SO_4^{--}) also appears in the same region (900-1200 cm^{-1}) and it has been discussed by Nakamoto¹⁹. The free phosphate ion (PO_4^{3-}), like the sulphate ion (SO_4^{2-}) belongs to the symmetry group Td.

On bonding one of the oxygen atoms of the phosphate group its symmetry is lowered to C_{3v} and this would apply to the fully ionised 5'-phosphate group of the phosphorylated Vitamin B₆ compounds.

The lowering of symmetry caused by co-ordination is different for the unidentate (C_{3v}) and bidentate (C_{2v}):



This lowering of symmetry splits the degenerate vibrations and activates infrared inactive vibrations as Table 5-3 shows:

Table 5-3: Correlations between T_d , C_{3v} and C_{2v}

Group	ν_1	ν_2	ν_3	ν_4
T_d	$A_1(R)$	$E(R)$	$F_2(I, R)$	$F_2(I, R)$
C_{3v}	$A_1(I, R)$	$E(I, R)$	$A_1(I, R)+E(I, R)$	$A_1(I, R)+E(I, R)$
C_{2v}	$A_1(I, R)$	$A_1(I, R) +$ $A_2(R)$	$A_1(I, R)+B_1(I, R)$ $+ B_2(I, R)$	$A_1(I, R)+B_1(I, R)$ $+ B_2(I, R)$

In the free phosphate ion both stretching (ν_3) and bending (ν_4) are infrared active and triply degenerate. In symmetry C_{3v} each of these is split into two bands ($A_1 + E$) and $\nu_1(A_1)$ and $\nu_2(E)$ vibrations become infrared active, thus giving six bands. When the symmetry is lowered to C_{2v} then the degenerate bands are split completely and the three components of ν_3 and ν_4 ($A_1 + B_1 + B_2$) and the A_1 component of ν_2 become infrared active, thus giving eight bands.

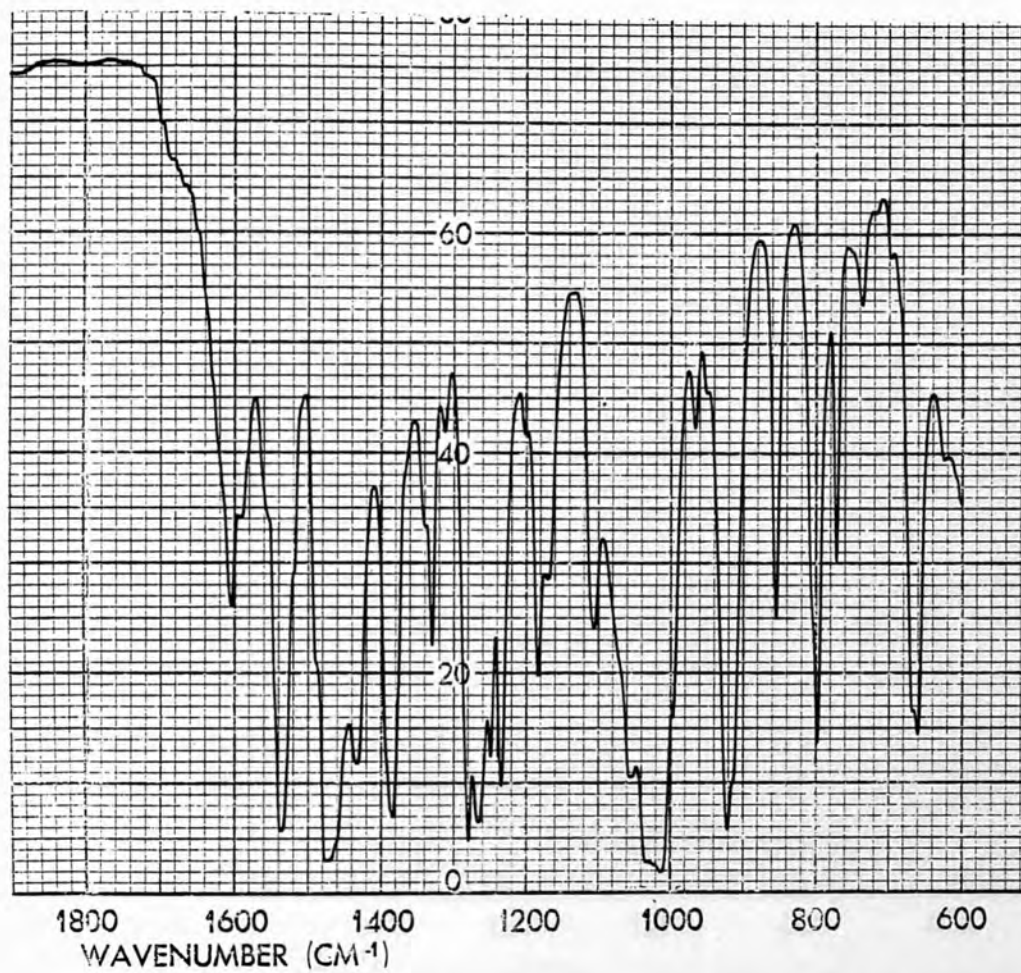


Fig. 5-4: Infrared Spectrum of $\text{Cu(PMP)}_2\text{acac}, 5\text{H}_2\text{O}$ in Nujol

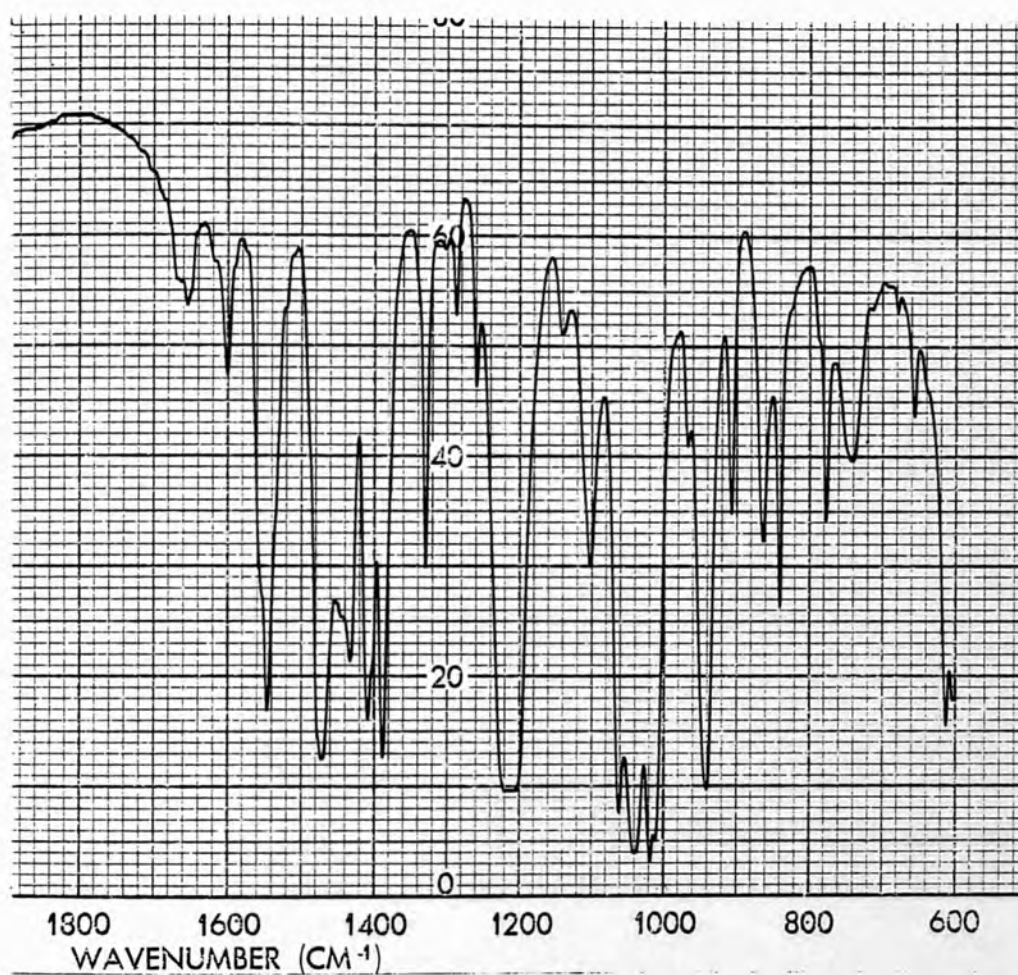


Fig. 5-5: Infrared Spectrum of $\text{Co(PMP)}_2 \cdot 4\text{H}_2\text{O}$ in Nujol

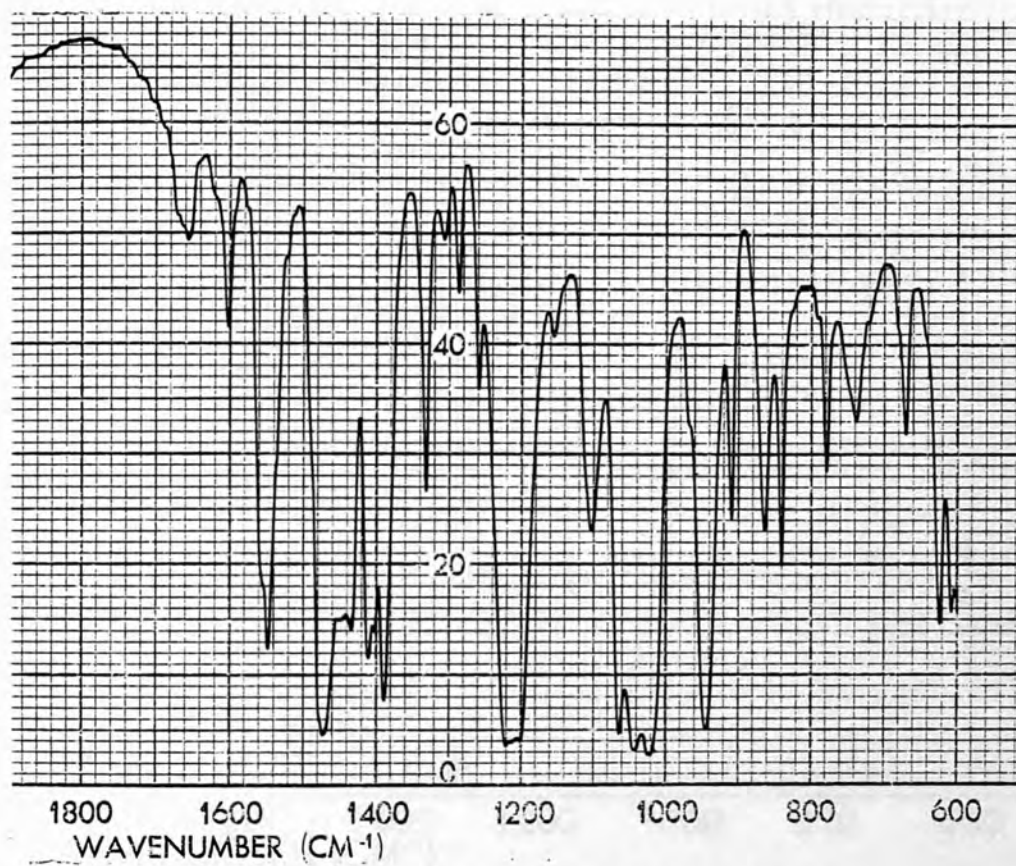


Fig. 5-6: Infrared Spectrum of $\text{Ni(PMP)}_2 \cdot 3\text{H}_2\text{O}$ in Nujol

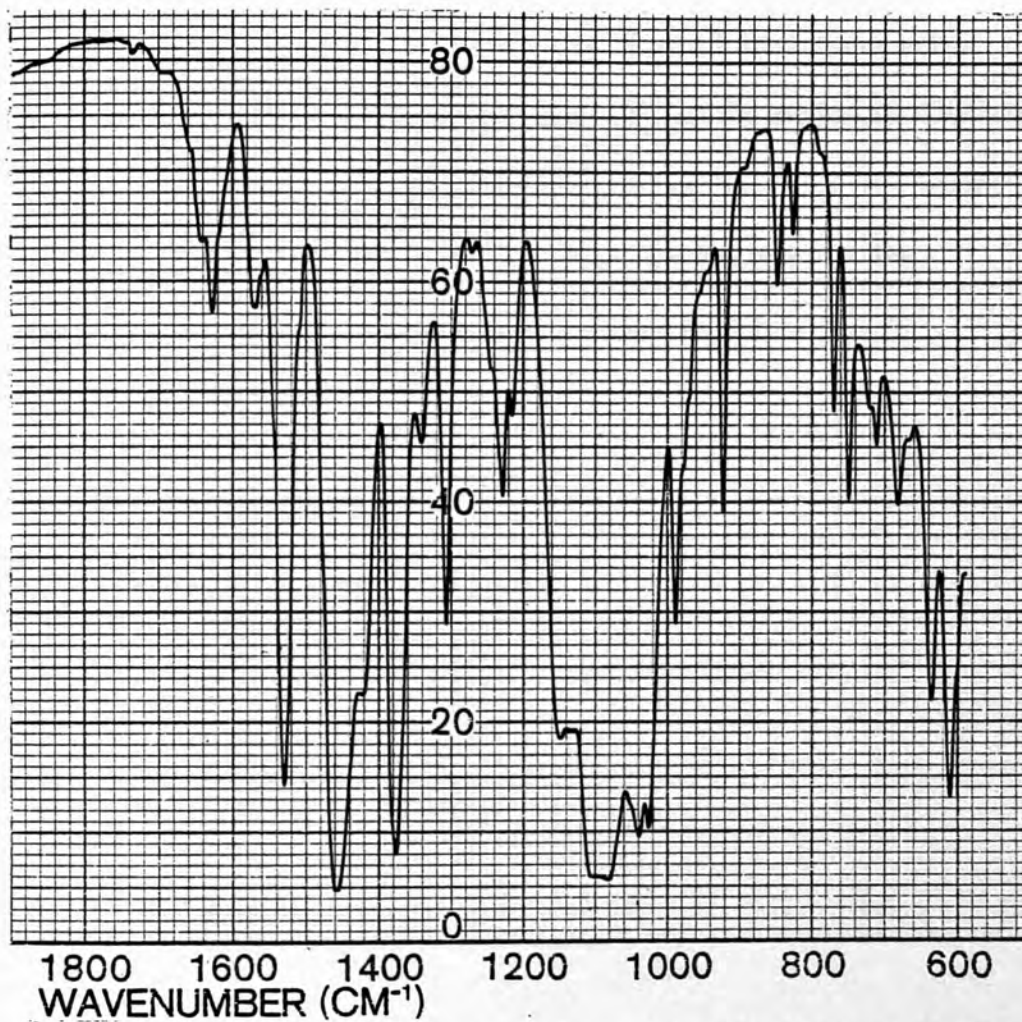


Fig. 5-7: Infrared Spectrum of $\text{Cu}(\text{PNen})_2(\text{SO}_4)_2(\text{Cl})_2 \cdot 5\text{H}_2\text{O}$ in Nujol

In phosphate (Fig. 5-4,5,6) and sulphate (Fig. 5-7) ν_1 appears around 900-1000 (cm^{-1}), ν_2 under 600 (cm^{-1}) (below 600 (cm^{-1}) has not been studied for these series of schiff base complexes), ν_3 in the 1000-1200 (cm^{-1}) region, and ν_4 in the region of 630-700 (cm^{-1}). Interpretations of the spectra along these lines must be treated with caution since site symmetry is not taken into account. The bands assigned to the phosphate group are shown in Tables 5-4,5:

Table 5-4: Bands (cm^{-1}) assigned to the Phosphate Group in PMP and its Metal Complexes

Complexes	ν_1 cm^{-1}	ν_2 cm^{-1}	ν_3 cm^{-1}	ν_4 cm^{-1}	Symm. of PO_4^{3-} PO_4
PMPHCl	920-940	1130	-	680	C_{2v}
		1070	-	620	
		1038	-	605	
		985	-		
$\text{Cu(PMP)}_2\text{acac}, 5\text{H}_2\text{O}$	920	1180	-	690	C_{2v}
		1105	-	660	
		1055	-		
		1040-1010	-		
		970	-		
$\text{Co(PMP)}_2, 4\text{H}_2\text{O}$	940	1140	-	680	C_{2v}
		1100	-	660	
		1060	-		
		1040	-		
		1020	-		
		970	-		
$\text{Ni(PMP)}_2, 3\text{H}_2\text{O}$	942	1155	-	670	C_{2v}
		1105	-	640 _{sh}	
		1065	-		
		1045	-		
		1025	-		
		970 _{sh}	-		

Table 5-5: Bands (cm^{-1}) assigned to the Phosphate Group in PLP and its Metal-Schiff Base Complexes

Complexes	ν_1 cm^{-1}	ν_2 cm^{-1}	ν_3 cm^{-1}	ν_4 cm^{-1}	Symm. of PO_4^{3-}
PLP	945	1010-1040 1150-1180	- -	600 625	C_{3v}
$\text{Cu}(\text{PLP})_2\text{en}, 4\text{H}_2\text{O}$	940	1025 1075 1170-1190	- - -	628 645 662 _w	C_{3v}
$\text{Cu}(\text{PLPGly}), 3\text{H}_2\text{O}$	900	1038 1110 1160 _{sh}	- - -	625 _{sh} 660	C_{3v}
$\text{Ni}(\text{PLP})_2\text{en}, 4\text{H}_2\text{O}$	930	1030 1115 1170	- - -	640 _w 665 _w	C_{3v}
$\text{Ni}_2(\text{PLPGly}), 6\text{H}_2\text{O}$	930	1030 1080 _{sh} 1160	- - -	640 670	C_{3v}
$\text{Co}(\text{PLP})_2\text{en}, 4\text{H}_2\text{O}$	920	1020 1105 1160	- - -	645 660	C_{3v}
$\text{Co}(\text{PLPGly}), \text{H}_2\text{O}$	930	1030 1080 _{sh} 1170-1150	- - -	638 668	C_{3v}

Table 5-5 (continued)

Complexes	ν_1 cm ⁻¹	ν_2 cm ⁻¹	ν_3 cm ⁻¹	ν_4 cm ⁻¹	Symm. of PO ₄ ³⁻
Fe(PLP) ₂ en, (Cl) ₃ , 6H ₂ O	980	1040	-	630	C _{3v}
		1090 _{sh}	-	670	
		1160 _{sh}	-		
Fe(PLPGly)OAc, H ₂ O	960	1010	-	640	C _{3v}
		1060-1100	-	680	
		1160			
Cd(PLP) ₂ en(Cl) ₃ , 6H ₂ O	910	1000	-	650	C _{3v}
		1060	-	680	
		1160	-		
Zn(PLP) ₂ en(Cl) ₂ , 2H ₂ O	940	1005	-	660	C _{3v}
		1100-1120	-	680	
		1160 _{sh}			

Phosphate in

The band pattern of ν PLP (Fig. 5-3) is similar to that of sulphate¹⁹ in $[\text{Co}(\text{NH}_3)_5\text{SO}_4]^+$, suggesting full protonation of the phosphate group.

The bands which have been assigned to the sulphate group in

$\text{Cu}(\text{PNen})_2(\text{SQ})_2(\text{Cl})_2, 5\text{H}_2\text{O}$ appears at: (Fig. 5-7)

$$\nu_1 = 920 \text{ (cm}^{-1}\text{)}$$

$$\nu_3 = 1150, 1080-1110, 1040, 1022, 990 \text{ (cm}^{-1}\text{)}$$

$$\nu_4 = 680, 640 \text{ (cm}^{-1}\text{)}$$

In the 800-900 (cm⁻¹) region, two bands commonly occurred, which can be attributed to C-H deformation:

$$\text{PLP} = 850 \text{ (cm}^{-1}\text{)} \text{ and } 880 \text{ (cm}^{-1}\text{)}$$

$$\text{PL} = 840 \text{ (cm}^{-1}\text{)} \text{ and } 880 \text{ (cm}^{-1}\text{)}$$

$$\text{PMP} = 830 \text{ (cm}^{-1}\text{)} \text{ and } 870 \text{ (cm}^{-1}\text{)}$$

$$\text{PN} = \text{-----} 890 \text{ (cm}^{-1}\text{)}$$

In all of these Schiff base complexes, these two bands (850 cm⁻¹ and 880 cm⁻¹) shift either to higher or lower frequency and the bands are very weak or almost absent. The results are shown below in Table 5-6:

Table (5-6): Bands (cm⁻¹) Assigned to the C-H Deformation

S.B.	Fe ^{III} cm ⁻¹	Co ^{II} cm ⁻¹	Ni ^{II} cm ⁻¹	Cu ^{II} cm ⁻¹	Zn ^{II} cm ⁻¹	Cd ^{II} cm ⁻¹	Ag ^I cm ⁻¹
(PLP) ₂ en	840 _w	840	840	860	850	850	np
(PL) ₂ en	np	882	890	885	890	np	845
PLPGly	860 _w	840	840	897	np	np	np
PLGly	860 _w	870	860	860	np	np	np
(PNen) ₂	np	np	np	850	np	np	np
PN	np	np	np	850	np	np	np
(PMP) ₂	np	865	865	860	np	np	np

w = weak

np = not prepared

The most common mode to all the Schiff base complexes is the C-H out-of-plane deformation¹⁸ of the pyridine ring which occurs at 720 (cm^{-1}). This band is shifted by ± 5 (cm^{-1}) (except: Zn, Ni(PL)₂en and Co, Cu(PLGly)₁) and it is therefore thought that this mode must be a basic one which is attributable only to the ring system. If this is the case, then it would not be affected by consequent chelation of the ring system to the metal ion. The results are shown below (Table 5-7):

Table 5-7: Bands (cm^{-1}) assigned to the C-H out-of-plane Deformation

S.B.	Fe ^{III} cm^{-1}	Co ^{II} cm^{-1}	Ni ^{II} cm^{-1}	Cu ^{II} cm^{-1}	Zn ^{II} cm^{-1}	Cd ^{II} cm^{-1}	Ag ^I cm^{-1}
(PLP) ₂ en	725	722	722	725	720	725	np
(PL) ₂ en	np	728	740	726	740	np	720
PLPGly	724	725	724	724	np	np	np
PLGly	715	730	725	735	np	np	np
(PNen) ₂	np	np	np	718	np	np	np
PN	np	np	np	715	np	np	np
(PMP) ₂	np	718 _w	720	718	np	np	np

w = weak

np = not prepared

An important feature in the infrared spectra of these schiff base complexes is the presence of a most strong band in 600-630 (cm^{-1}) region which can be assigned²⁰ to the co-ordinated water. Table (5-8) shows the results:

Table 5-8: Bands (cm^{-1}) assigned to the Co-ordinated Water

S.B.	Fe ^{III} cm^{-1}	Co ^{II} cm^{-1}	Ni ^{II} cm^{-1}	Cu ^{II} cm^{-1}	Zn ^{II} cm^{-1}	Cd ^{II} cm^{-1}	Ag ^I cm^{-1}
(PLP) ₂ en	600	625	630	610	615	610	np
(PL) ₂ en	np	612	618	622	618	np	612
PLPGly	618	625	600	620	np	np	np
PLGly	630	618	615	615	np	np	np
(PNen) ₂	np	np	np	612	np	np	np
PN	np	np	np	610	np	np	np
(PMP) ₂	np	612	622	622 _w	np	np	np

w = weak

np = not prepared

The absorption near 400 (cm^{-1}) which is characteristic of the metal to water oxygen stretching (M-OH_2) was not, however, observed. The presence of a large number of ligand absorptions below 600 (cm^{-1}) precludes the assignment of metal-ligand absorption bands even when KBr discs were used. This region is therefore not discussed further.



Fig. 5-8: Infrared Spectrum of $\text{Cu(PL)}_2\text{en}\cdot\text{H}_2\text{O}$ in Nujol

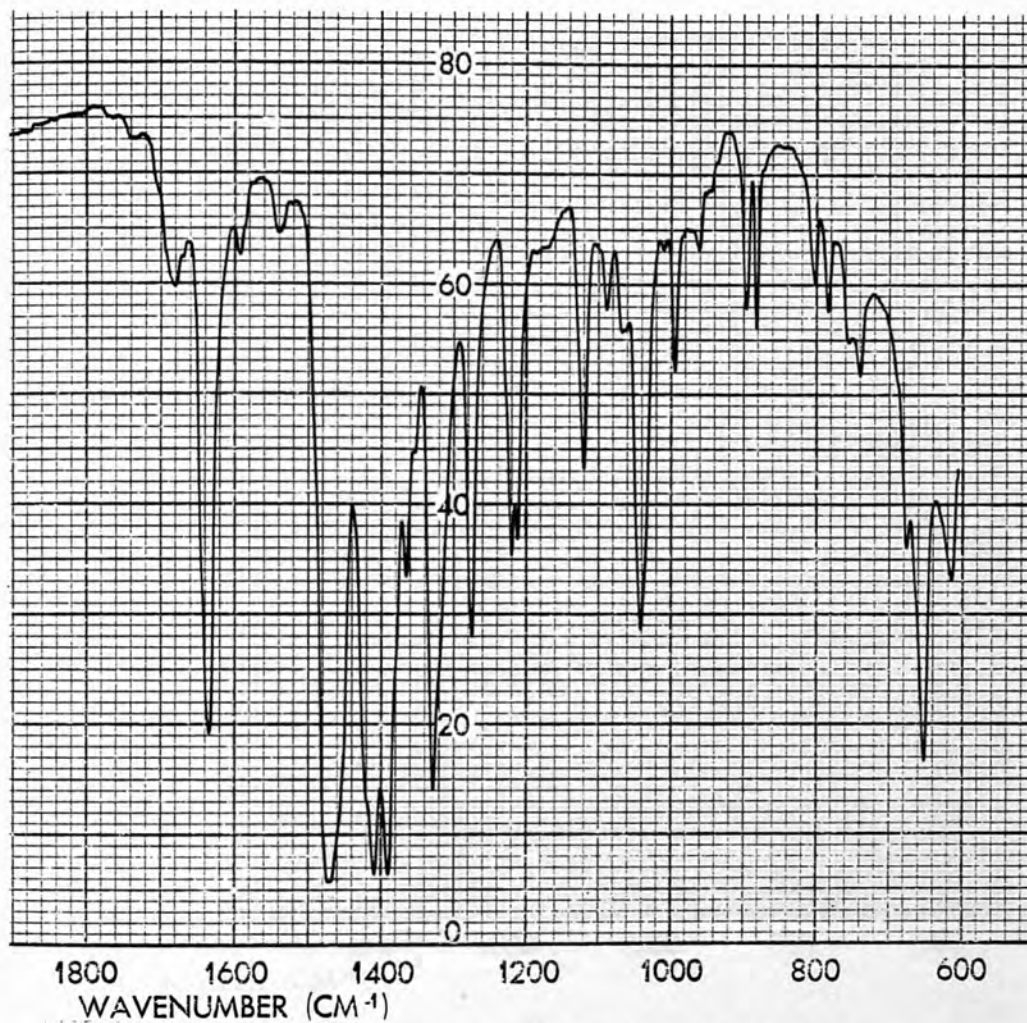


Fig. 5-9: Infrared Spectrum of $\text{Ni(PL)}_2\text{en}, 3\text{H}_2\text{O}$ in Nujol

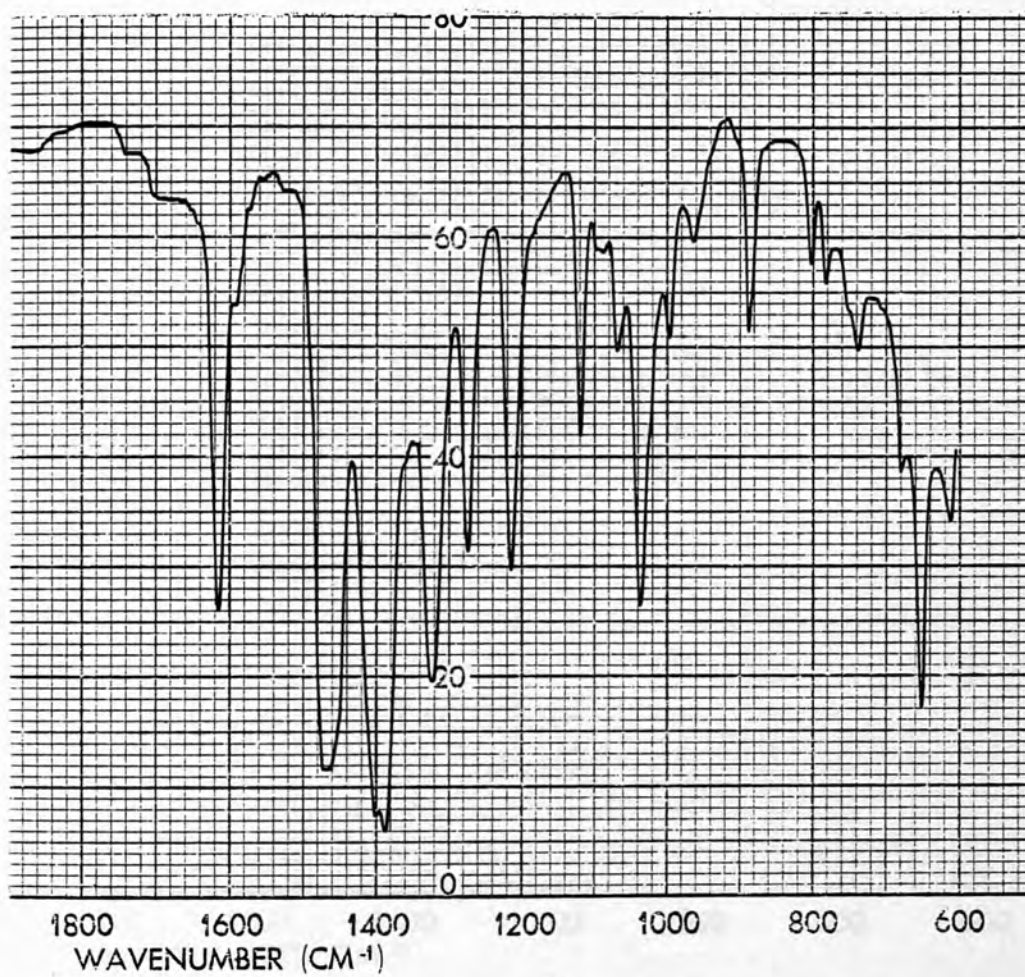


Fig. 5-10: Infrared Spectrum of $\text{Co}^{\text{II}}(\text{PL})_2\text{en}, 2\text{H}_2\text{O}$ in Nujol

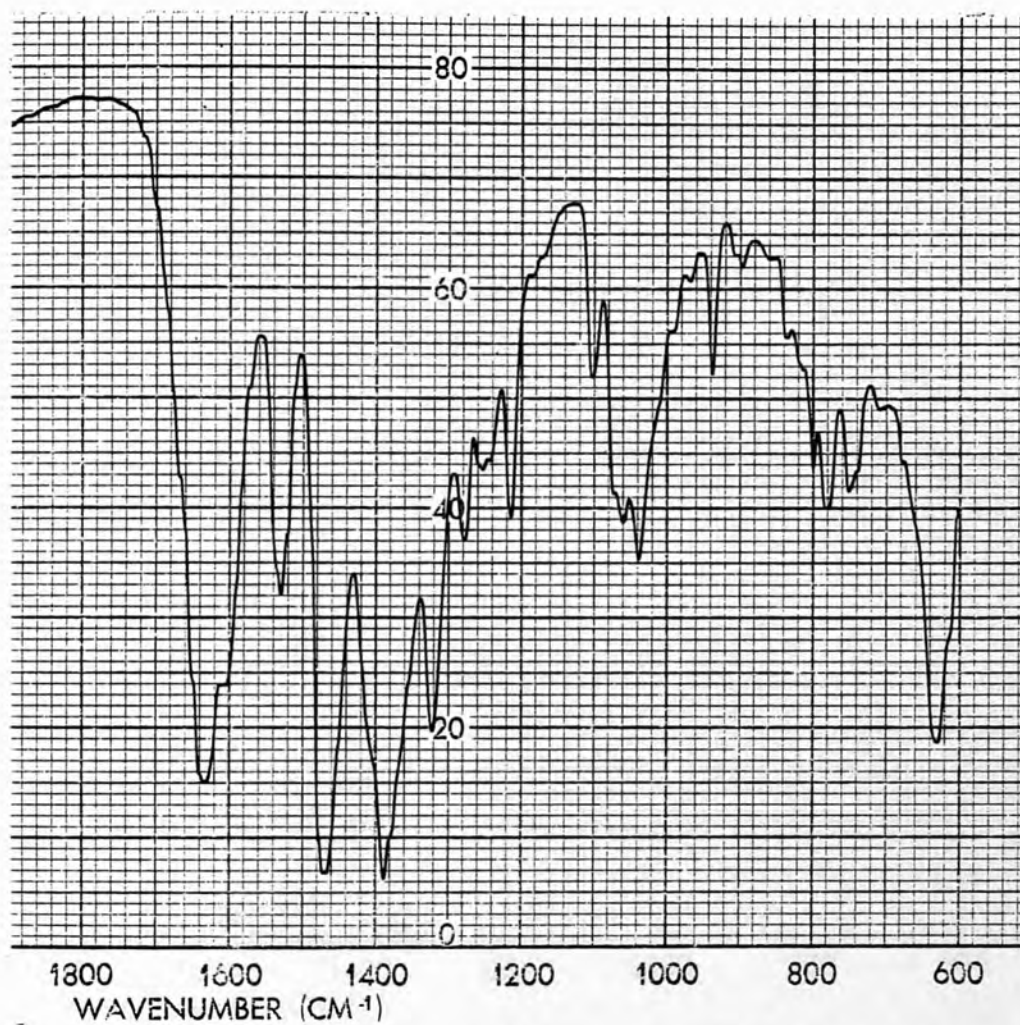


Fig. 5-11: Infrared Spectrum of Fe^{III} (PLGly) (OAc), H₂O in Nujol

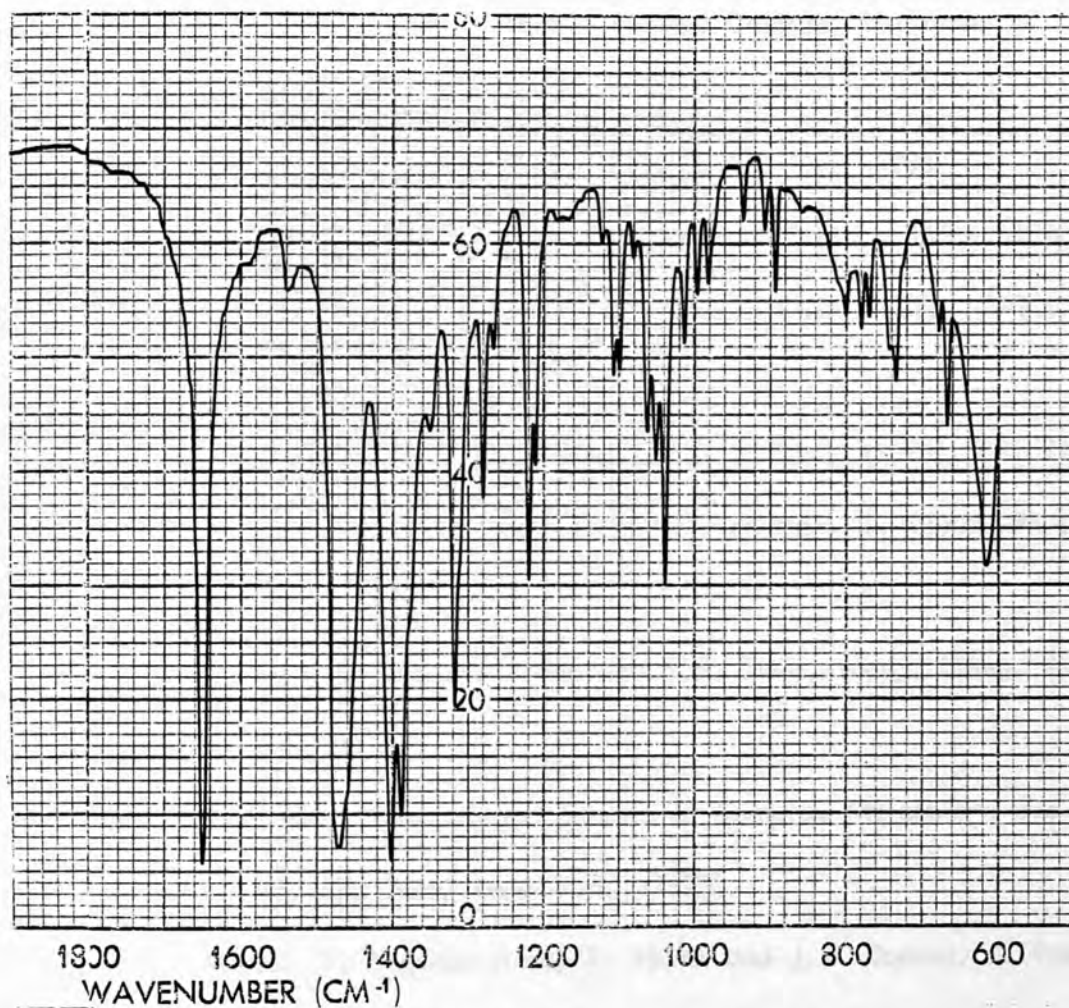


Fig. 5-12: Infrared Spectrum of $Zn(PL)_2en, 2H_2O$ in Nujol

1. J.L. Hooley and M.F. Richardson, *J. Chem. Soc. Chem. Commun.* (1975), 2.
2. J.L. Hooley, *Chem. Commun.* (1975), 2.
3. J.L. Hooley and M.F. Richardson, *Chem. Commun.* (1975), 2.
4. J.L. Hooley and D.J. Long, *Chem. Commun.* (1975), 2.
5. J.L. Hooley and A.J. Marshall, *JACS*, (1975), 2.
6. J.L. Hooley, *Chem. Commun.* (1975), 2.
7. A.J. Marshall, *JACS*, (1975), 2.

REFERENCES

1. J.T. Wroblewski and G.J. Long, *Inorg. Chem.*, (1977), 16, 2752.
2. M. McMillan, M. Phil. Thesis, Bedford College, University of London, 1967.
3. D. Heinert and A.E. Martell, *JACS*, (1959), 81, 3933.
4. T. Fujiwara, Y. Zumi and K. Tomita, *Acta Cryst.*, (1972), A28, S49.
5. T.A. Franklin and M.F. Richardson, *Inorg. Chem. Acta*, (1980), 46, 191.
6. E.C. Kelusky and J.S. Hartman, *Can. J. Chem.* (1979), 57, 2118.
7. L. Asso, M. Asso, J. Mossoyan and D. Benlian, *J. Chem. Phys.*, (1978), 75, 561.
8. M.E. Farago, M.M. McMillan and S.S. Sabir, *Inorg. Chem. Acta.*, (1975), 14, 207.
9. L.J. Bellamy, "The Infrared Spectra of Complex Molecule", 3rd ed., John Wiley and Sons, New York, (1975).
10. A. Mosset, F. Nepveu-Juras, R. Haran and J.J. Bonnet, *J. Inorg. Nucl. Chem.*, (1978), 40, 1259.
11. K.J. Franklin and M.F. Richardson, *J. Chem. Soc. Chem. Comm.*, (1978), 97.
12. F. Hanic, *Acta Crystal.*, (1966), 21, 332.
13. K.J. Franklin and M.F. Richardson, *Inorg. Chem.* (1980), 19, 2107.
14. J.T. Wroblewski and G.J. Long, *Inorg. Chem. Acta*, (1979), 36, 155.
15. D. Heinert and A.E. Martell, *JACS*, (1959), 81, 3933.
16. J.E. Kavacic, *Spectrochim. Acta*, (1967), 23, 183.
17. A.I. Popov, J.C. Marshall, F.B. Stute and W.B. Person, *JACS*, (1961), 83, 3586.

18. C.H. Kline and J. Turkevich, *J. Chem. Phys.*, (1953), 21, 1170.
19. K. Nakamoto, "Infrared Spectra of Inorganic and Co-ordination Compounds", Wiley, N.Y., (1968).
20. K. Nakamoto, "Infrared Spectra of Inorganic and Co-ordination Compounds", 3rd ed., Wiley, Interscience, New York, (1978), 227.

CHAPTER 6

Mass Spectrometric Study of Metal-Schiff Base Complexes

Mass spectrometry was used for the analysis of metal-schiff base complexes. The study of chemical elements, their compounds, and their reactions is a fast and accurate way of analysis. Schiff base complexes and inorganic chemists. The mass spectrum may be molecular ions, fragment ions, rearrangement ions, multiply-charged ions, monocharged ions, positive or negative ions, ions formed by ion-molecule interaction.

In the electric field the potential energy (eV) of an ion is equal to its kinetic energy ($\frac{1}{2}mv^2$) after complete acceleration.

$$eV = \frac{1}{2}mv^2 \quad (1)$$

- where e = electric charge,
- V = potential used to accelerate the ion,
- m = mass of the ion,
- v = velocity of the ion.

6.1 Introduction

The fundamental principle of mass spectrometry, the separation and recording of atomic masses, was demonstrated many years ago. In 1898 Wein found that positive rays could be deflected in electric and magnetic fields, and in 1912 Thompson was able to demonstrate the existence of two isotopes of neon, masses 20 and 22 using a magnetic instrument. Accurate mass measurements were made by Dempster and Aston (1918 and 1919) using a photographic plate on to which the ions were then focused (hence the term "spectrograph").

Until 1940 the mass spectrometer was used only for the analysis of gases and for the determination of the stable isotopes of chemical elements. Recently, mass spectrometry has become a fast and accurate way of analysis of complex mixtures for both organic and inorganic chemists.

The ions that appear in the mass spectrum may be molecular ions, isotopic ions, fragment ions, rearrangement ions, multiply-charged ions, metastable ions, positive or negative ions, ions formed by ion-molecule interaction.

In the electric field the potential energy (eV) of an ion is equal to its kinetic energy ($\frac{1}{2} mv^2$) after complete acceleration:

$$eV = \frac{1}{2} mv^2 \quad (1)$$

where e = electric charge,

V = potential used to accelerate the ion.

m = mass of the ion,

v = velocity of the ion.

In the magnetic field the ion is subject to two forces in equilibrium, the centripetal force (Hev) and the centrifugal force (mv^2/R).

$$Hev = \frac{mv^2}{R} \quad (2)$$

where e , v , and m are as in (1),

H = intensity of the magnetic field,

R = radius of curvature of the path of the ion.

Rearranging equation (2) and substituting v for the value in equation (1):

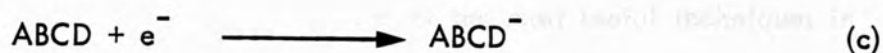
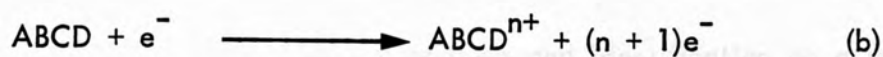
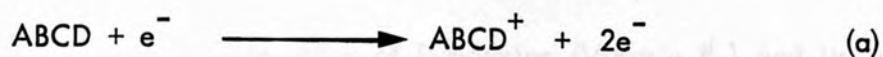
$$m/e = \frac{H^2 R^2}{2V} \quad (3)$$

Equation (3) is the most fundamental equation of mass spectrometers of the magnetic deflection type.

From this equation we can see that a mass spectrometer can be maintained at constant H , with V varied (electric scanning), or V can be maintained constant and H varied (magnetic scanning). The latter is the usual mode of operation.

When a molecule of the sample, in the vapour phase in the high vacuum of the instrument (10^{-6} mm Hg), is bombarded with electrons of suitable energy, there are two types of primary process it can undergo:

- i) The extraction of one or more electrons from the molecule (reactions (a) and (b)).
- ii) The absorption of an electron by the molecule (reaction (c)).



The ion ABCD^+ is called the positive molecular ion and is indicated by M^+ . In instruments of normal design negative ions do not enter the magnetic field, and can therefore be ignored.

The ionisation process (a) is greatly favoured in normal modern instruments, but the formation of ABCD^+ may not consume all the energy obtained from the collision of e^- with ABCD. Subsequent very rapid decompositions, rearrangements, etc. continue while the primary ion is still in the ion source before it receives its electric and magnetic accelerations. A whole pattern of ions is therefore derived from one original molecular species, and is highly characteristic of that species.

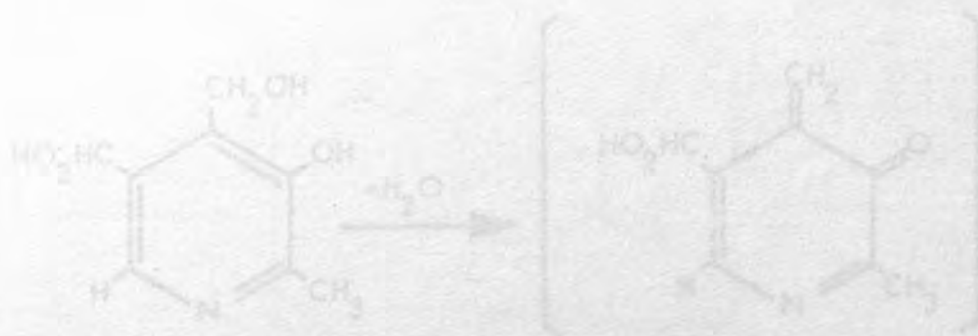


Fig. 4-1: Abstraction of water molecule from pyrimidine and formation of molecular ion.

6.2 Mass Spectrometry Study of Pyridoxine (Vitamin B₆) and its Analogues

Its suitability for structural analysis and identification on a small scale makes mass spectrometry one of the most useful techniques in many chemical and biological studies. In studies of the biosynthesis of Vitamin B₆, the characteristic mass spectra can be used to establish the position and quantitative analysis of stable isotopes, without resorting to complex procedures. The mass spectra of pyridoxine and its derivatives are especially interesting in relation to electron-impact fragmentation mechanisms, since these compounds can be viewed from different standpoints as substituted pyridines.

In 1966 pyridoxine, pyridoxal and similar compounds were studied by means of mass spectrometry by DeJongh¹. The initial event was found to be abstraction of a water molecule followed by rearrangement of the resulting ion (Fig. 6-1):

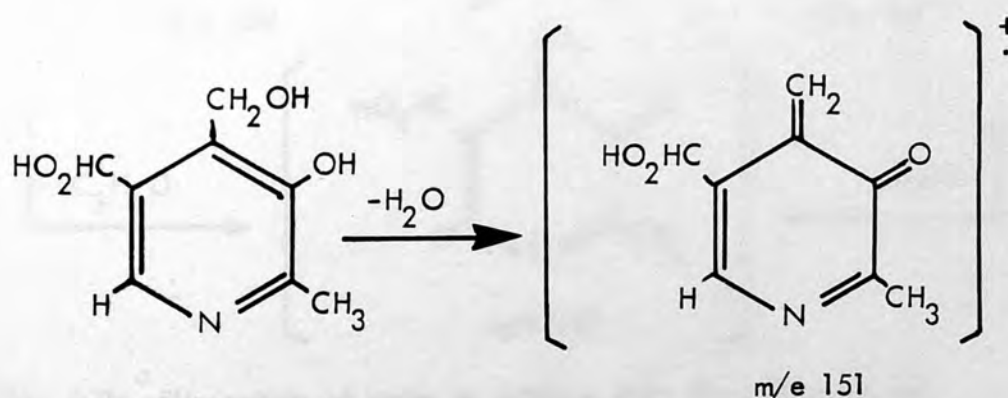


Fig. 6-1: Abstraction of water molecule from pyridoxine and formation of molecular ion.

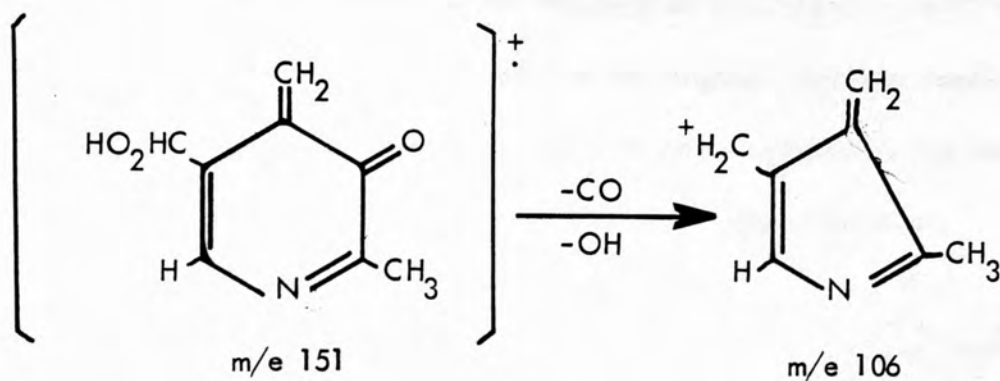


Fig. 6-1: (Continued)

or formation of an orthoquinonoid structure resulting from the elimination of either water or acetone from the molecular ion (Fig. 6-2):

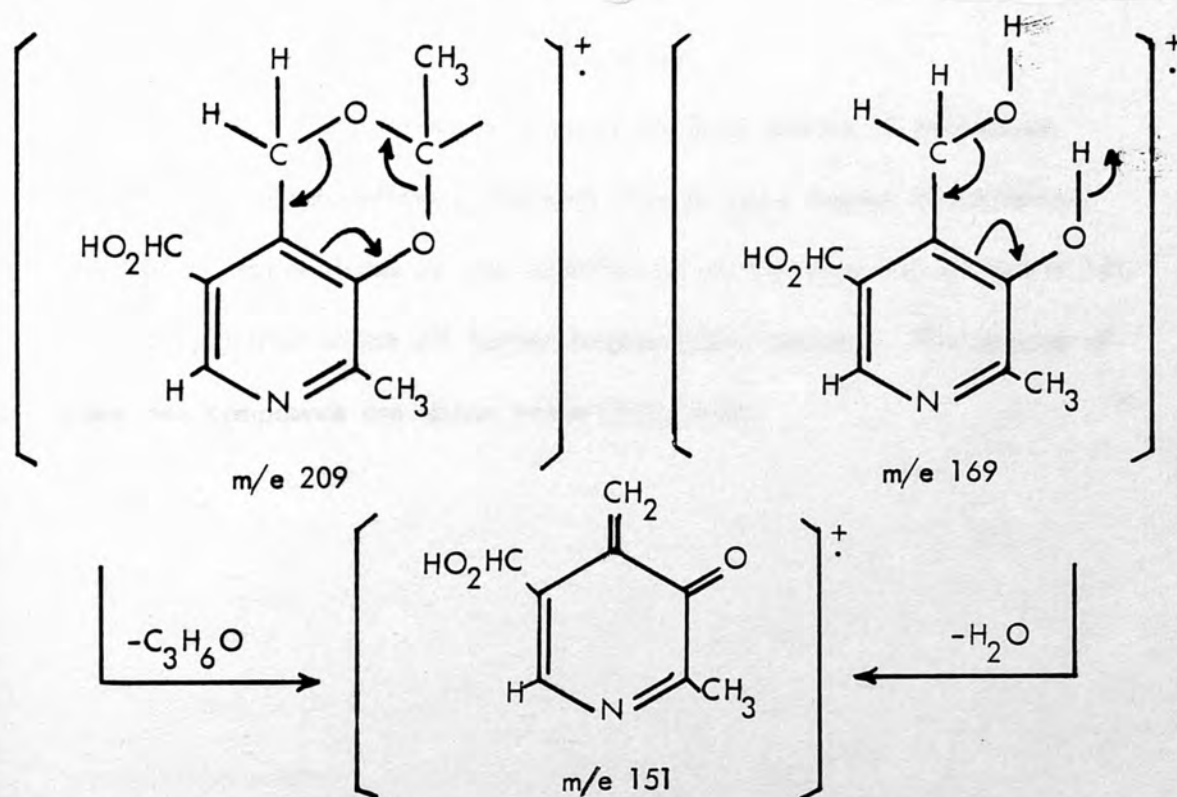
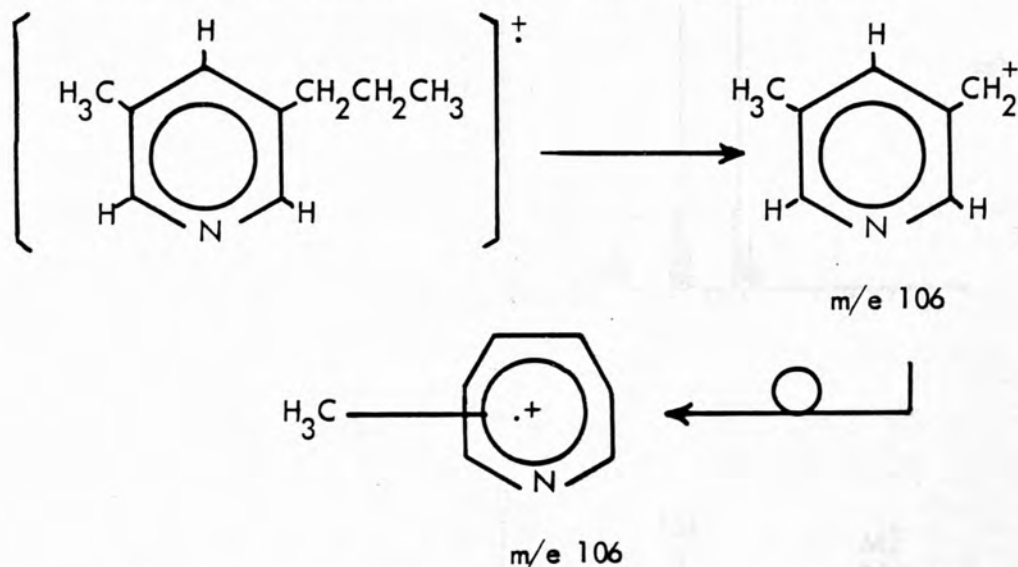


Fig. 6-2: Elimination of water or acetone from the molecular ion.

The structure shown for the fragment at m/e 106 (Fig. 6-1) should be used only to visualize which part of the original molecule remains. It is possible that this 106 fragment undergoes ring expansion as has been suggested¹ for the fragmentation of 3-methyl-5-n-propylpyridine:



According to DeJongh's research the mass spectra of pyridoxine and $\alpha^4,3$ -O-isopropylidene-pyridoxine show a large degree of similarity. This can be rationalized by the formation of an identical ion at $m/e = 151$ (Fig. 6-1,2) from which all further fragmentation occurs. The spectra of these two compounds are shown below (Fig. 6-3):

Fig. 6-3- The mass spectra of pyridoxine (a) and $\alpha^4,3$ -O-isopropylidene-pyridoxine (b).

There is an intermediate of m/e 122 from which C_7H_7 (or possibly the phenolic oxygen) is lost.

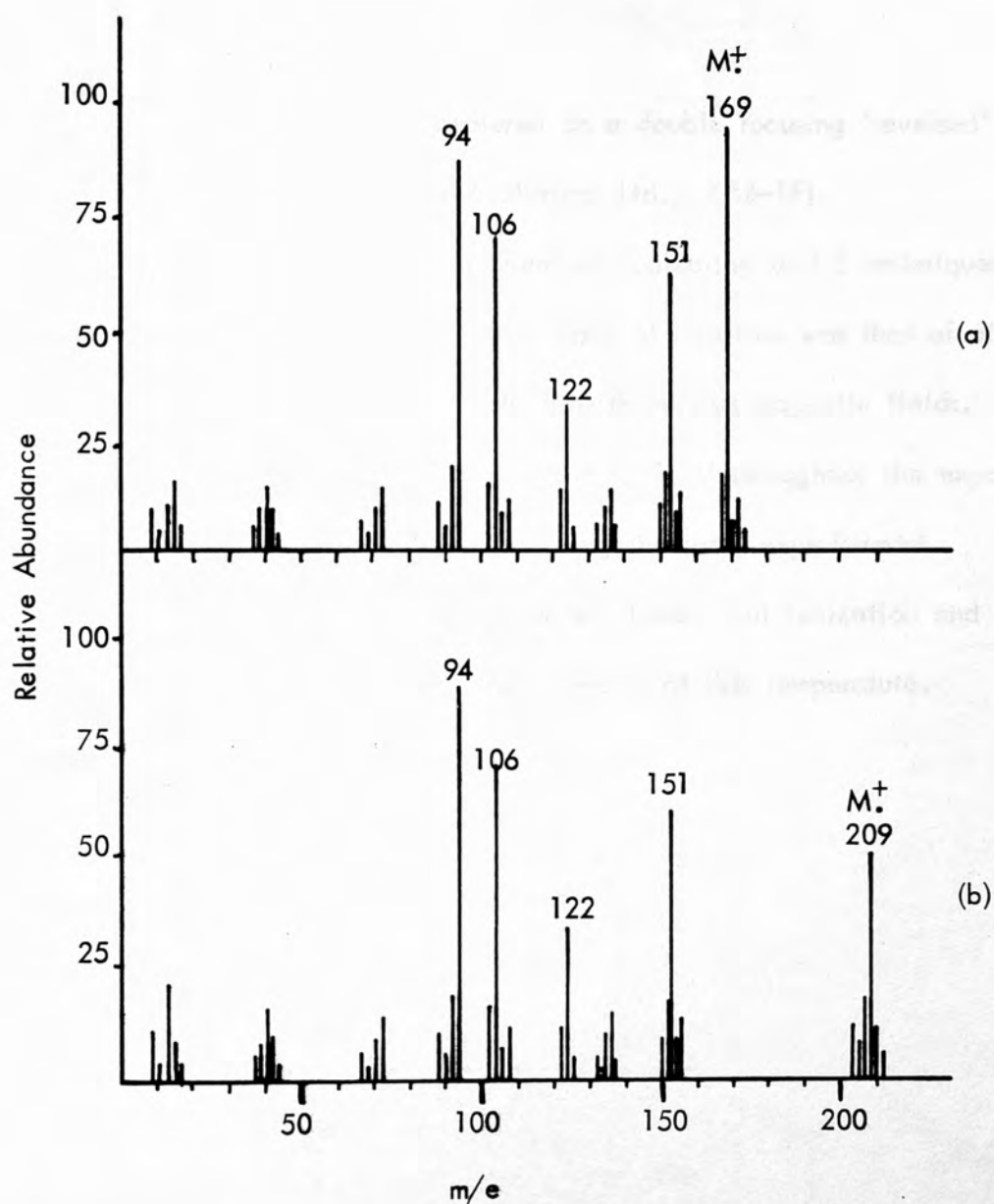


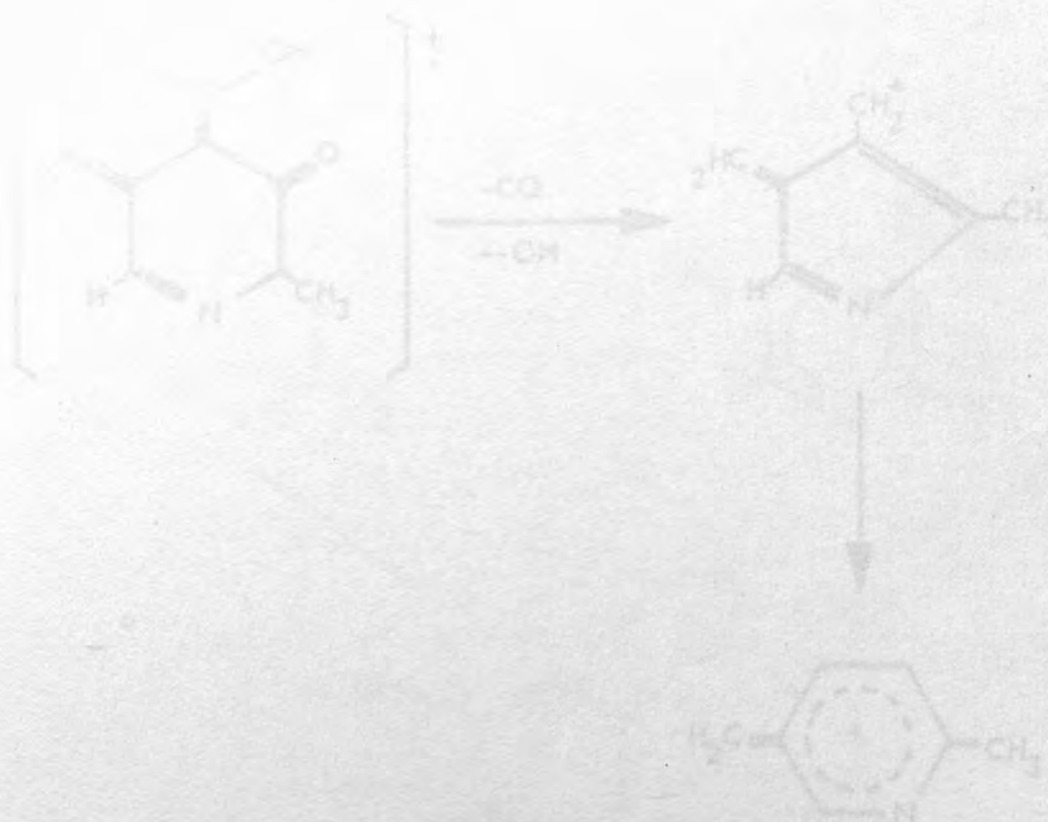
Fig. 6-3: The mass spectra of pyridoxine (a) and $\alpha^4,3$ -O-isopropylidene-pyridoxine (b).

There is an intermediate of m/e 122 from which CH_2 (or just possibly the phenolic oxygen) is lost.

6.3 Experimental

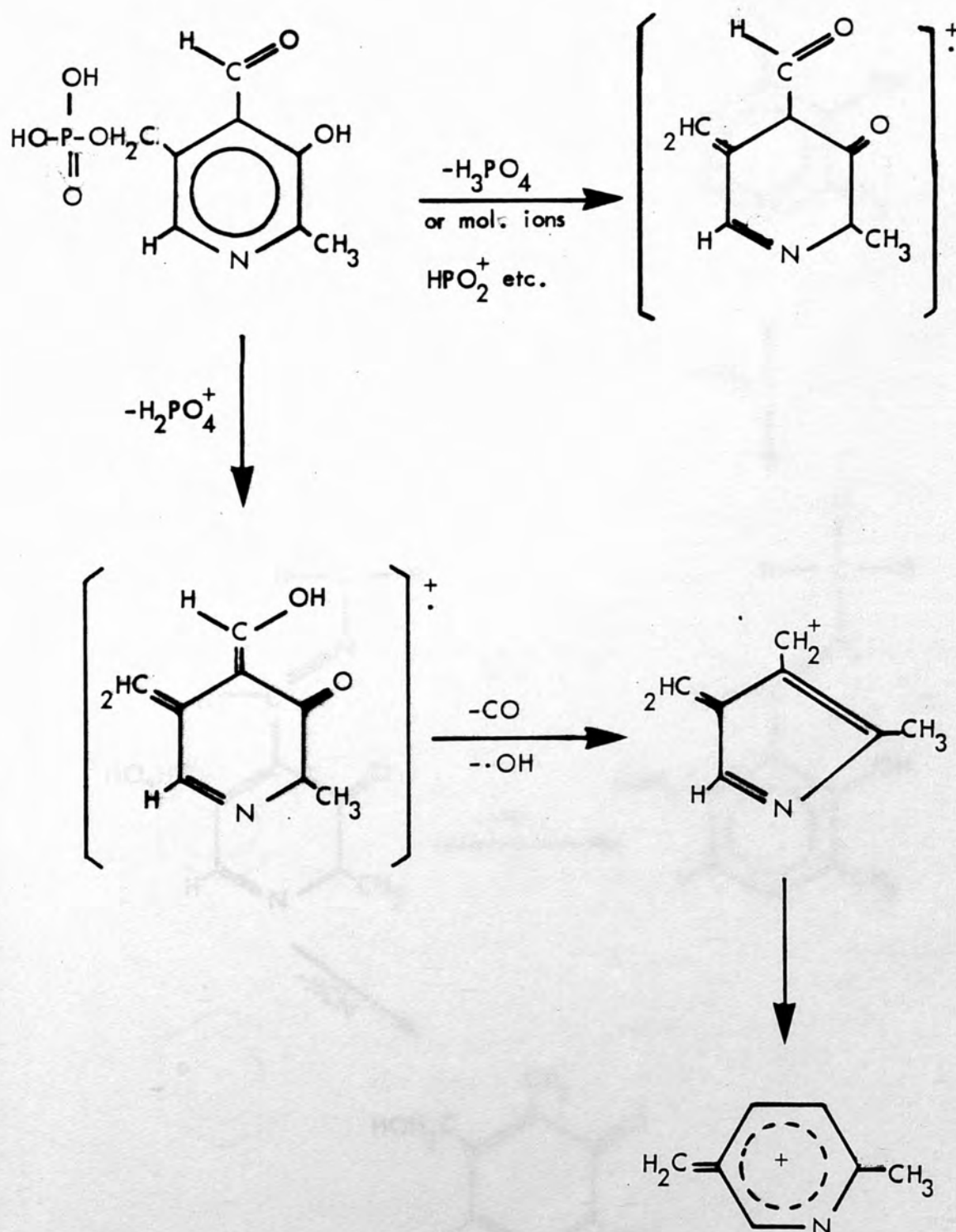
The mass spectra were measured on a double focusing 'reversed' geometry mass spectrometer (VG Analytical Ltd., ZAB-1F).

Electron impact (e.i.) and chemical ionization (c.i.) techniques were used throughout the work. The mode of insertion was that of direct insertion at a temperature of 250–280°C with various magnetic fields. The ionization potential was kept constant at 70 V throughout the experiments. Preliminary spectra were run using the same experimental conditions, except that the temperature was lower, but ionization and fragmentation took place in very low intensity at this temperature.

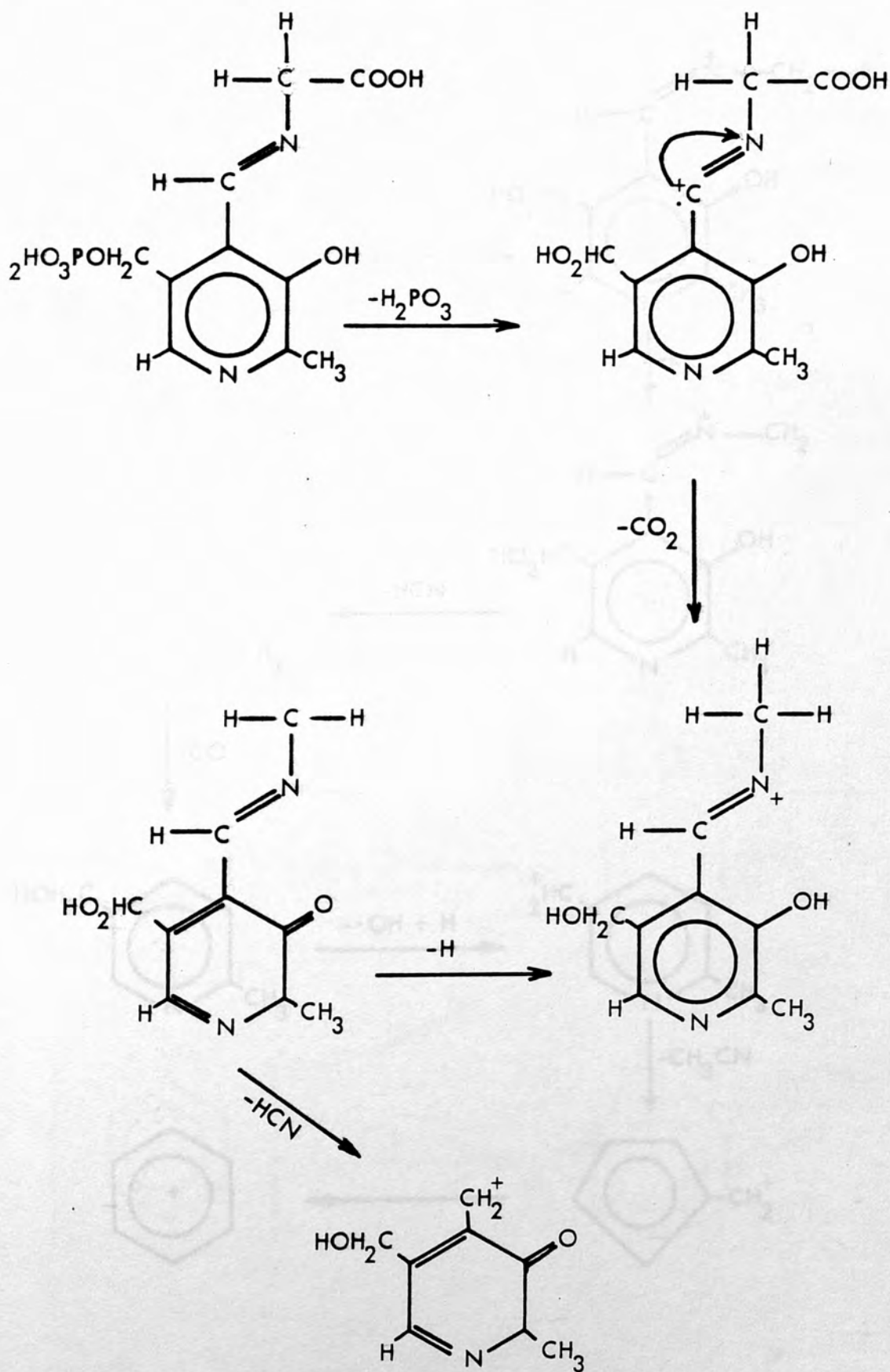


6.4 Schemes for the Dissociation and Fragmentation of PL, PLP, PMP, PN and their Metal-Schiff Base Complexes by Mass Spectrometry

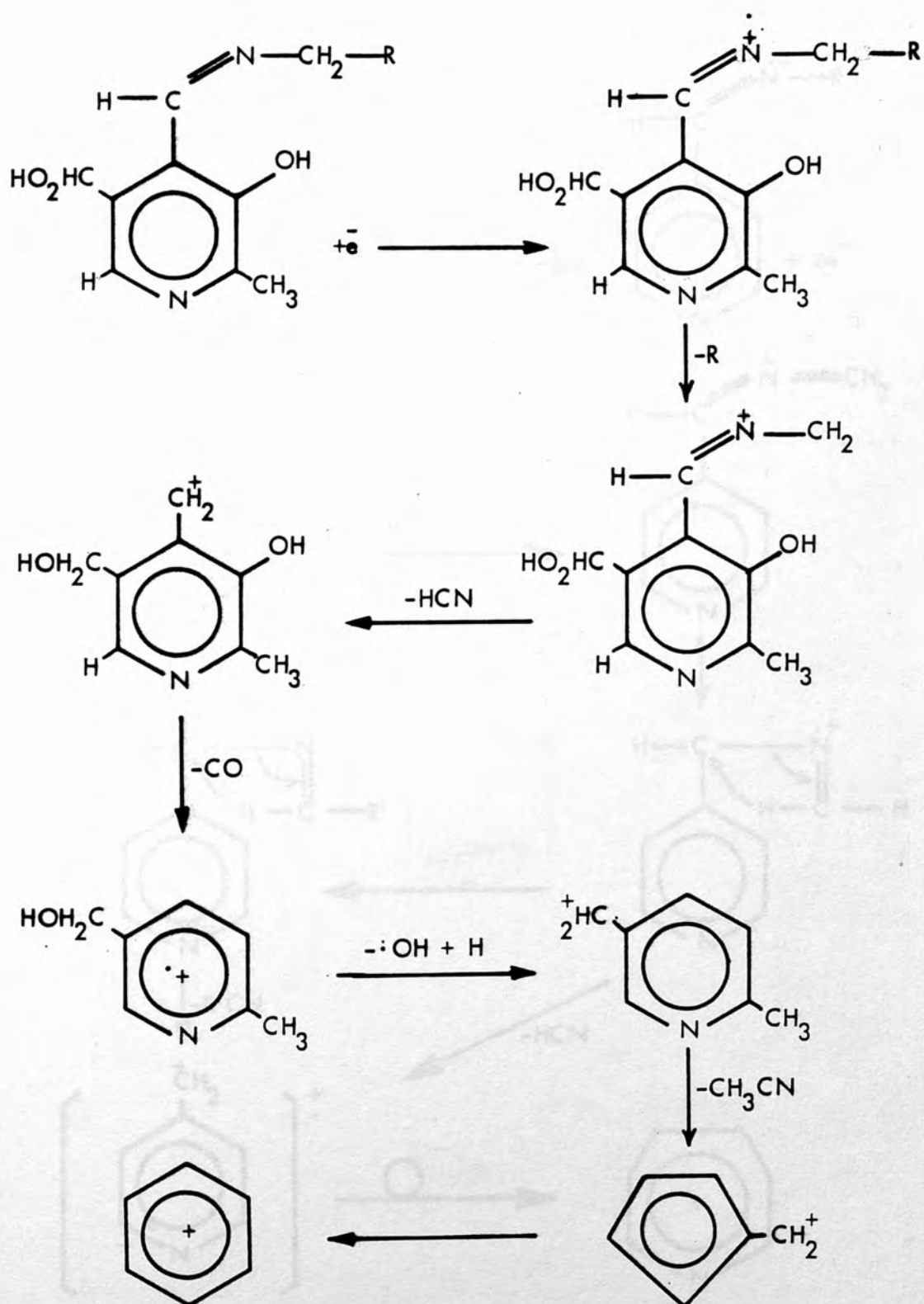
a) Pyridoxal-5'-Phosphate (PLP)

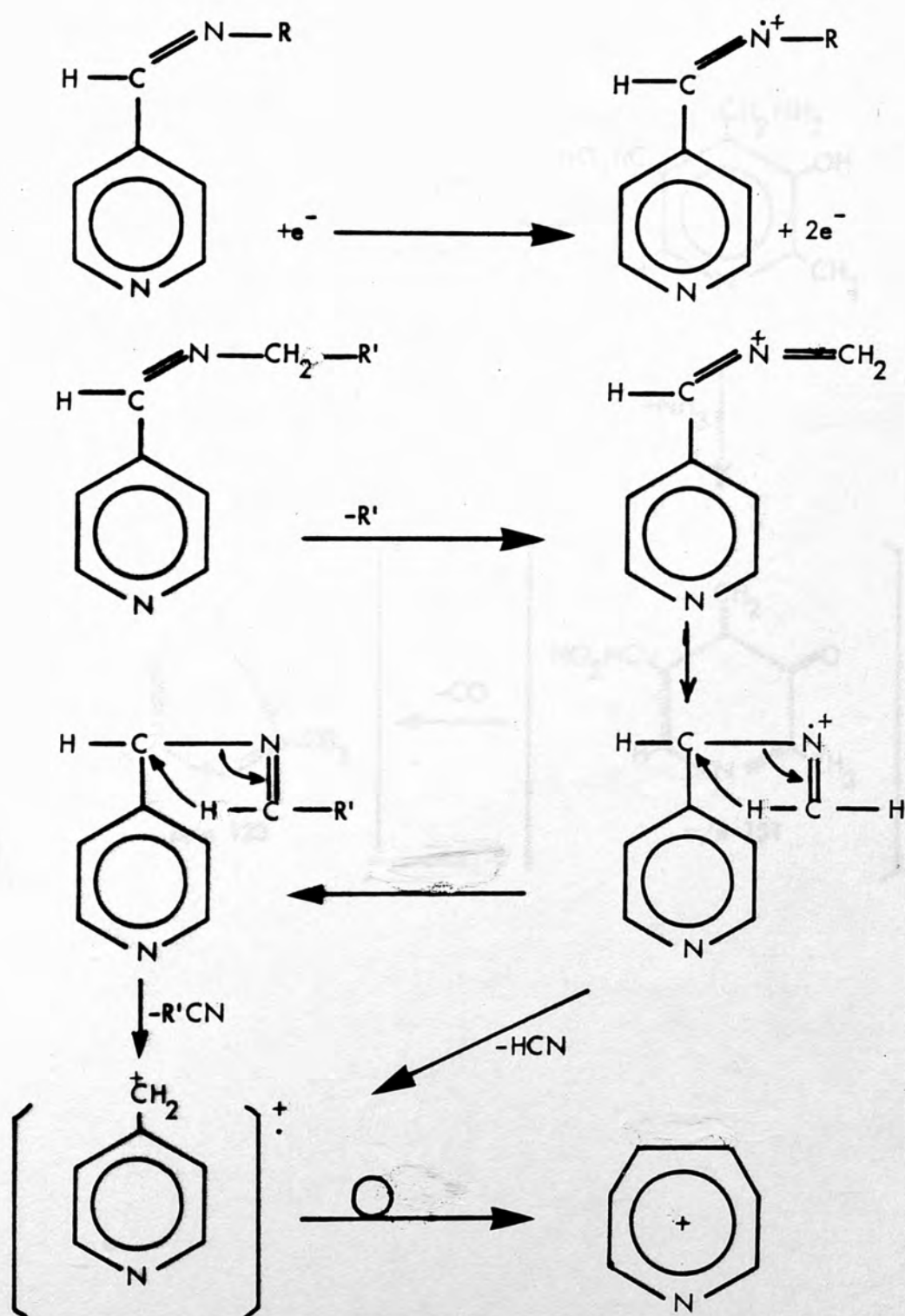


b) Pyridoxal Phosphate-Amino Acid Schiff Bases

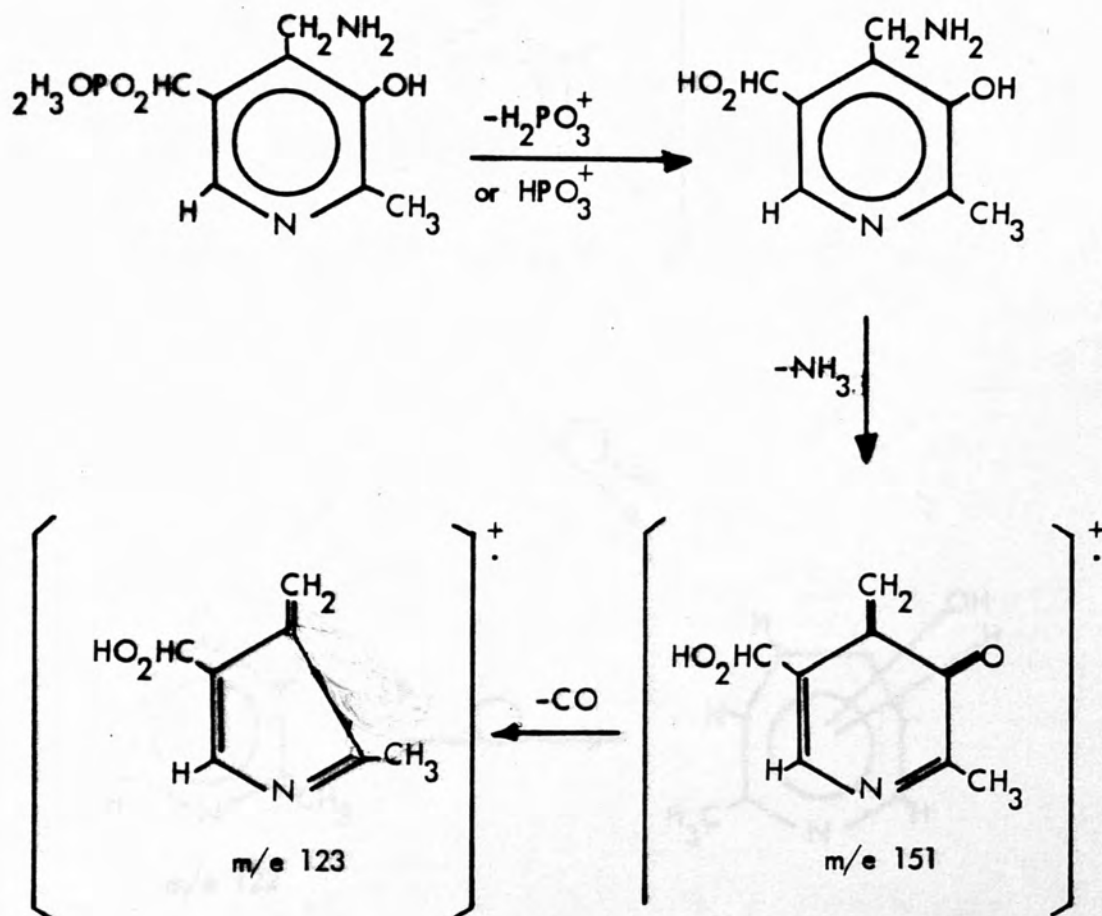


c) Schiff-Base of Pyridoxal

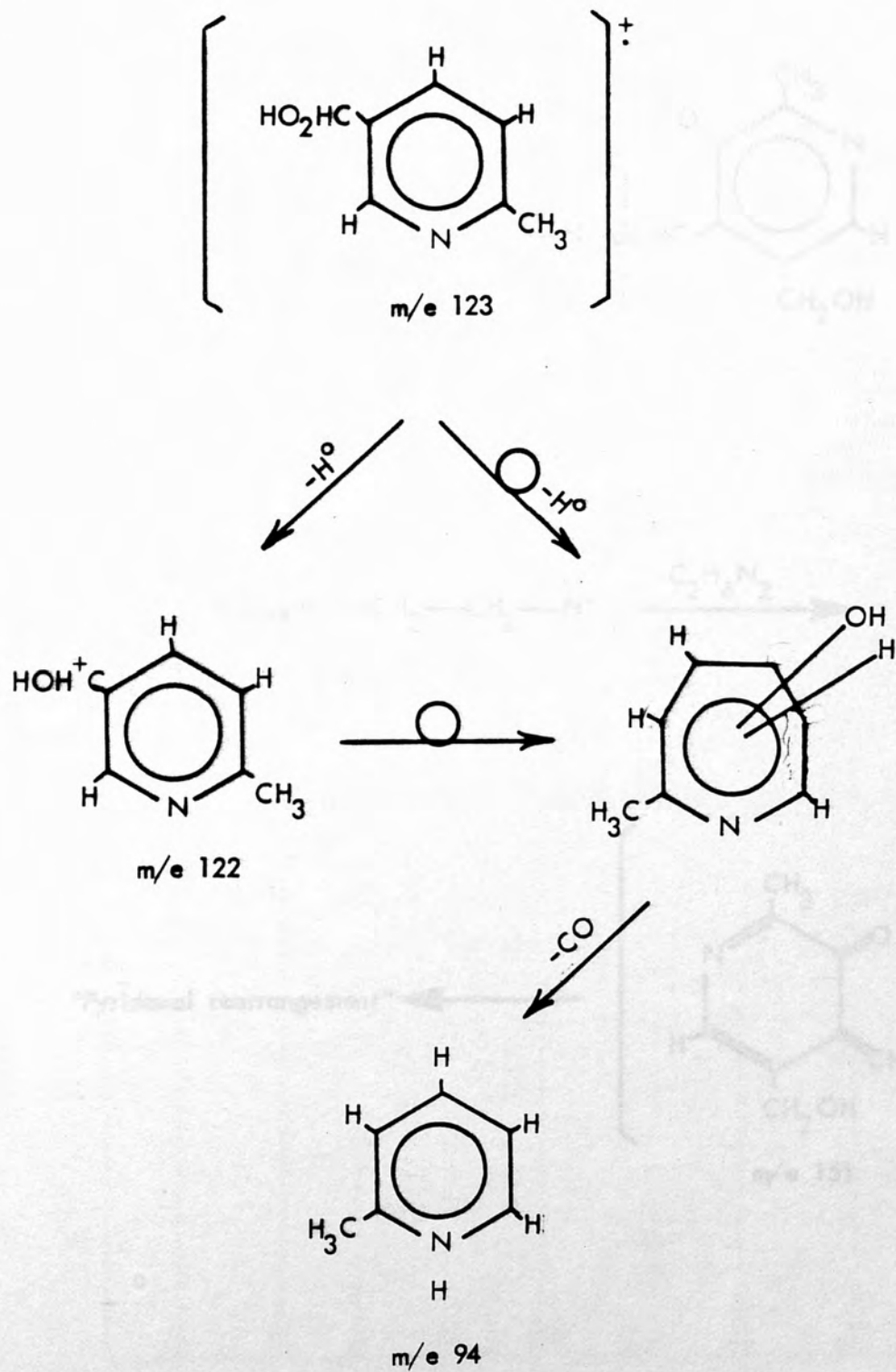


d) Schiff-Base of Pyridine-4-Aldehyde

e) Pyridoxamine-5'-Phosphate (PMP):



e) PMP (continued)



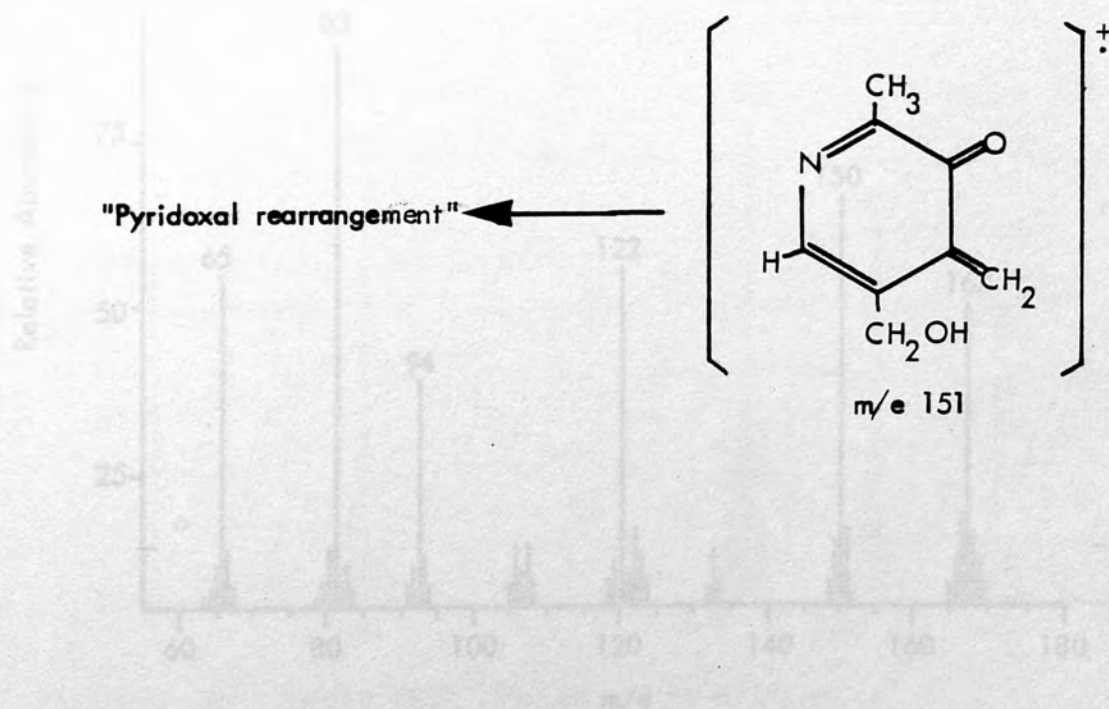
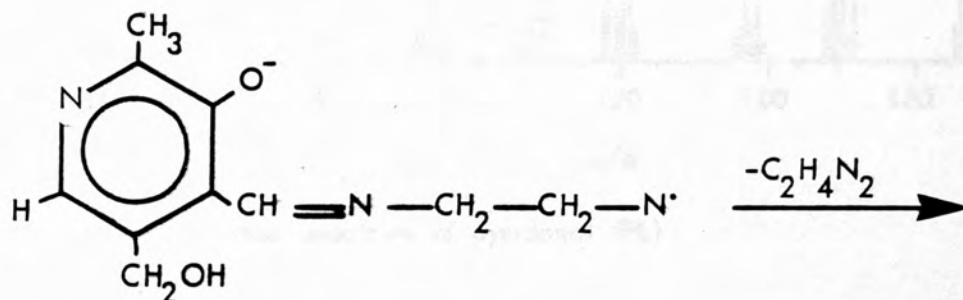
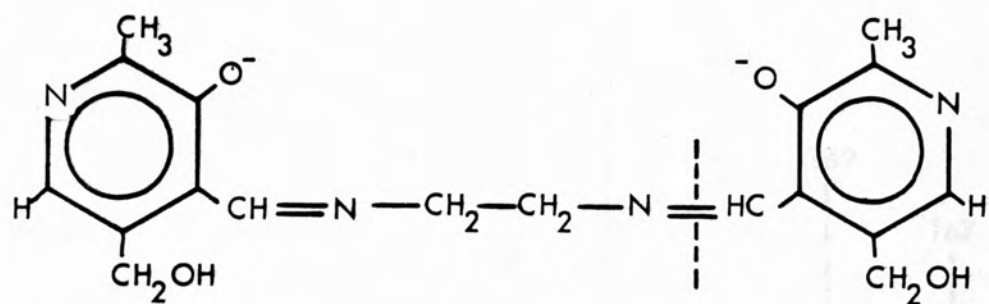
f) Phosphopyridoxylidene-Ethylenediamine:

Fig. 3-5: Mass spectrum of pyridoxal phosphate (PLP)

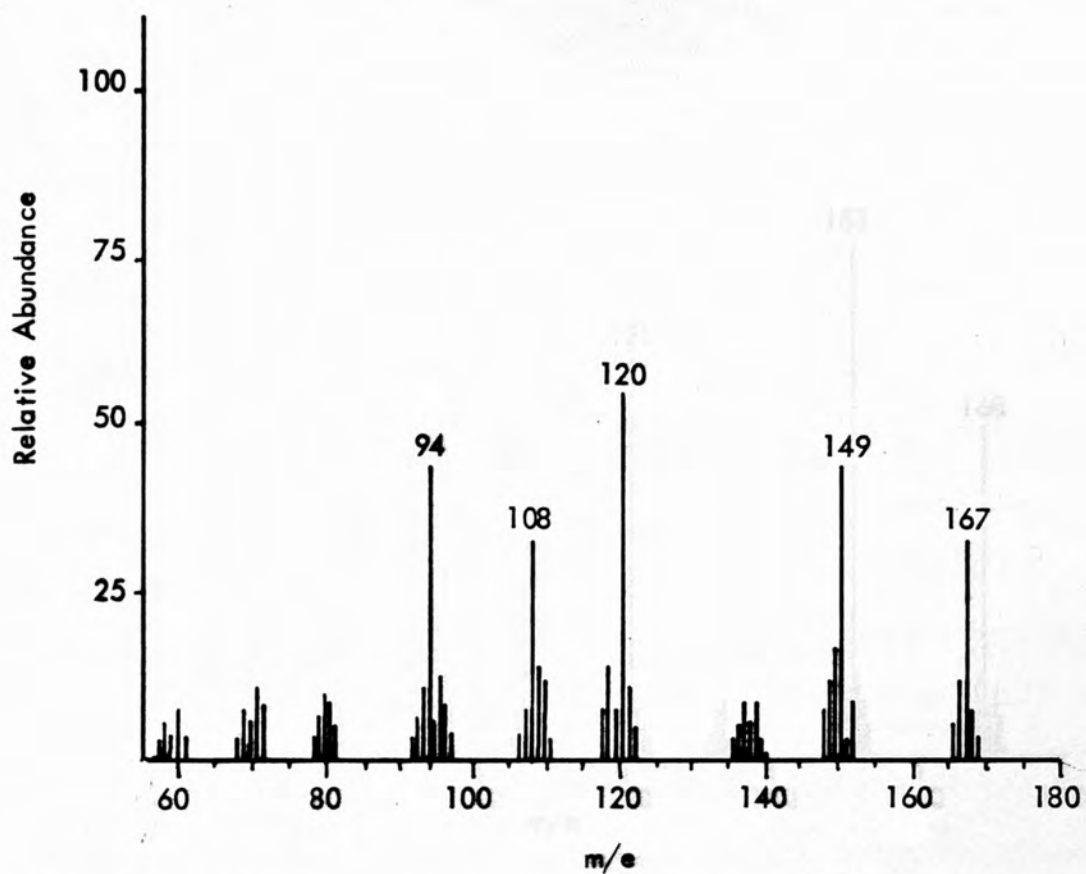


Fig. 6-4: Mass spectrum of pyridoxal (PL)

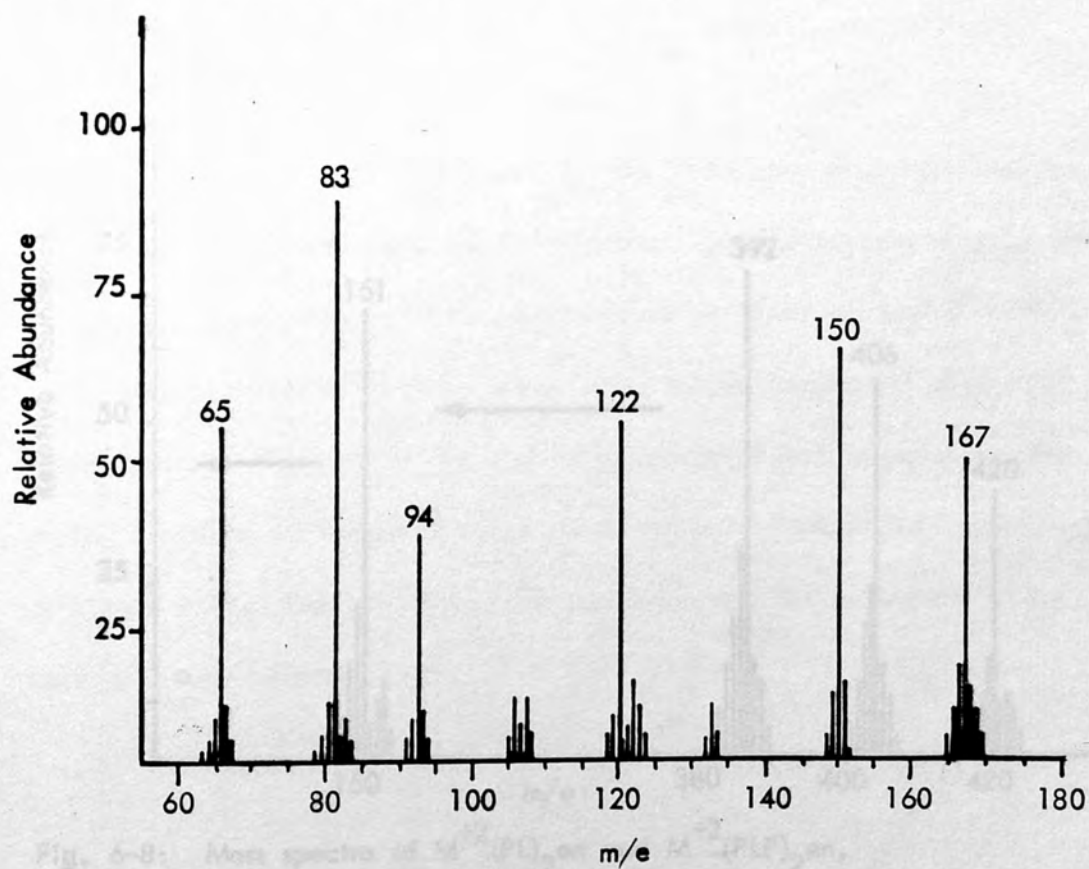


Fig. 6-5: Mass spectrum of pyridoxal phosphate (PLP)

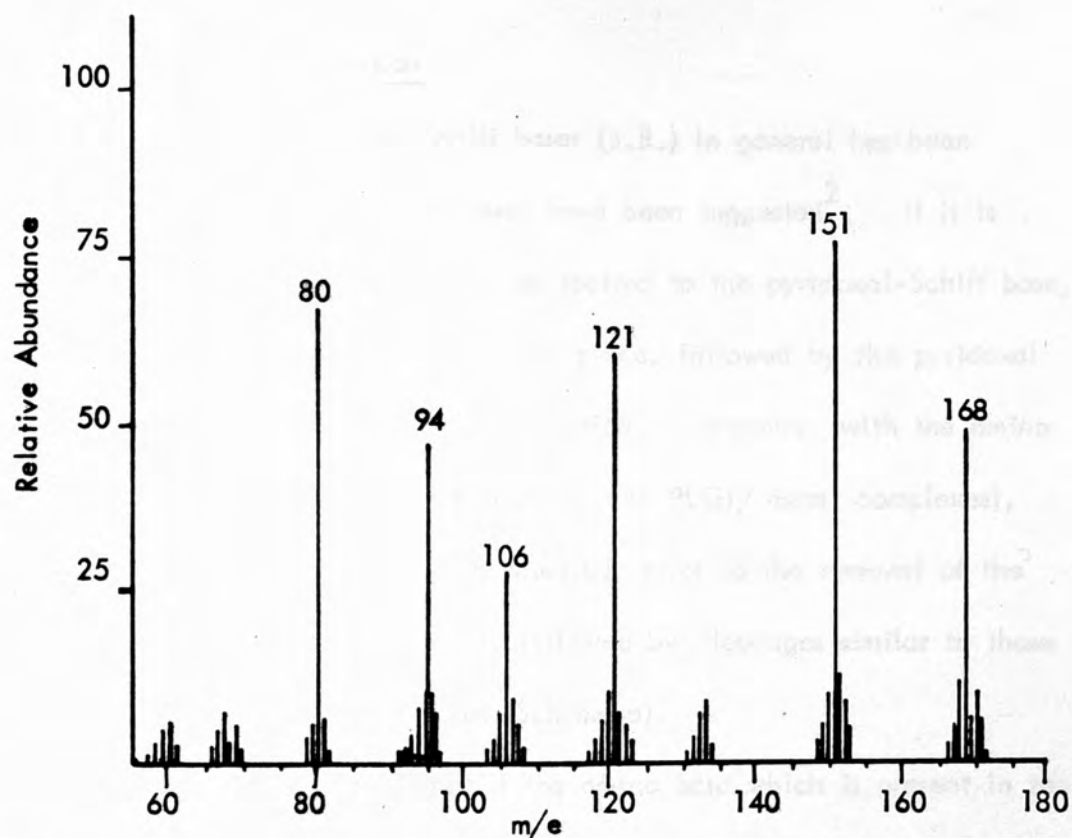


Fig. 6-6: Mass spectrum of pyridoxamine phosphate (PMP)

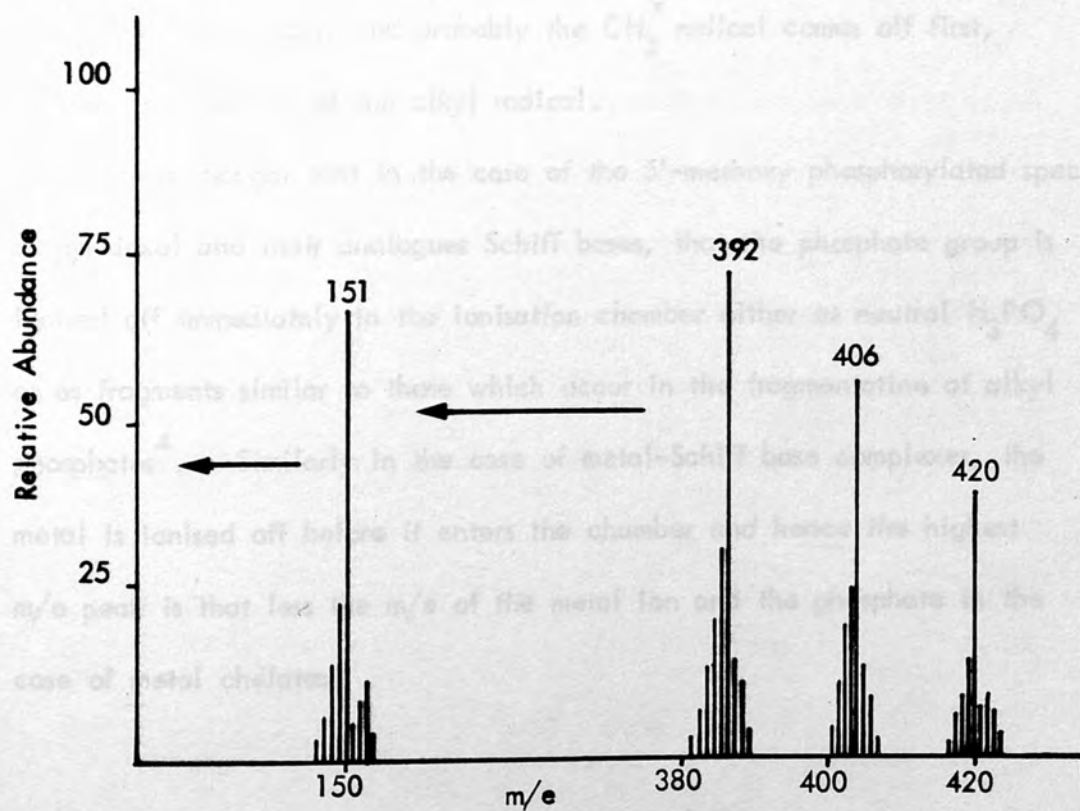


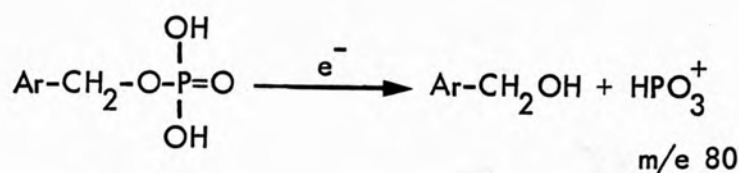
Fig. 6-8: Mass spectra of $M^{+2}(PL)_2en$ and $M^{+2}(PLP)_2en$,
 $M^{+2} = Cu^{II}, Co^{II}, Ni^{II}$

6.5 Results and Discussion

Mass spectrometry of Schiff bases (S.B.) in general has been discussed and fragmentation processes have been suggested². If it is assumed that similar reasoning can be applied to the pyridoxal-Schiff base, then the imine fragmentation will take place, followed by the pyridoxal rearrangement, and subsequent fragmentation. However, with the amino acid present in the species (e.g. PLPGly and PLGly metal complexes), carbon dioxide would probably be released, prior to the removal of the other fragments of the amino acid, followed by cleavages similar to those discussed for pyridine Schiff bases (Scheme d).

McMillan suggested³ that if the amino acid which is present in the complexes has a straight chain like glutamate, the CO_2 is lost first followed by removal of $\text{CH}_2=\text{CH}_2$, but for valine, fragmentation is more difficult due to the branched chain, and probably the CH_3^\bullet radical comes off first, followed by the rest of the alkyl radical.

It is thought that in the case of the 5'-methoxy phosphorylated species of pyridoxal and their analogues Schiff bases, that the phosphate group is ionised off immediately in the ionisation chamber either as neutral H_3PO_4 or as fragments similar to those which occur in the fragmentation of alkyl phosphates⁴. Similarly in the case of metal-Schiff base complexes, the metal is ionised off before it enters the chamber and hence the highest m/e peak is that less the m/e of the metal ion and the phosphate in the case of metal chelates.



The other fragments are:

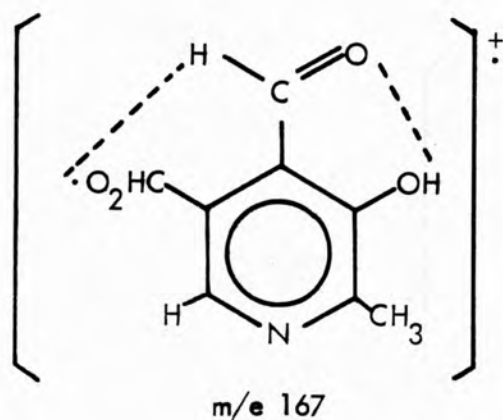


Pyridoxal and related compounds were found to lose a molecule of water first, to form a molecular ion-radical. Rearrangement and further radical abstraction followed the pattern with m/e peaks at 167, 149, 120, 108 and 94 as shown in Figure 6-4.

The rearrangement of pyridoxal-5'-phosphate is expected to follow a similar pattern to that of pyridoxal (Fig. 6-5: m/e peaks, 167, 150, 122, 94 and 83). A peak occurs at $m/e = 65$, which can be attributed to the HPO_2^+ ion, which would therefore leave the 5-methoxy group as an entity to rearrange as in the case of pyridoxal. The peak which appeared at m/e 167 could be accounted for by the following ion:



Fig. 6-7: Fragmentation of pyridoxal phosphate.



Internal rearrangement of the above ion ($m/e = 167$) would then allow the molecule to lose a molecule of water to form the ion with $m/e = 149$, as found in the mass spectrum (Fig. 6-1,2). Other peaks of consequence are those at m/e ratios of 122, 106, 94 and a strong peak at m/e 83.

Investigation of the fragmentation of pyridoxamine phosphate seems to show the same type of pattern (Fig. 6-6 m/e peaks 168, 149, 121, 106, 94 and 80). After ionisation of the phosphate group, elimination of ammonia (NH_3) would occur (m/e 151), followed by a pyridoxal rearrangement as shown in Fig. 6-7:

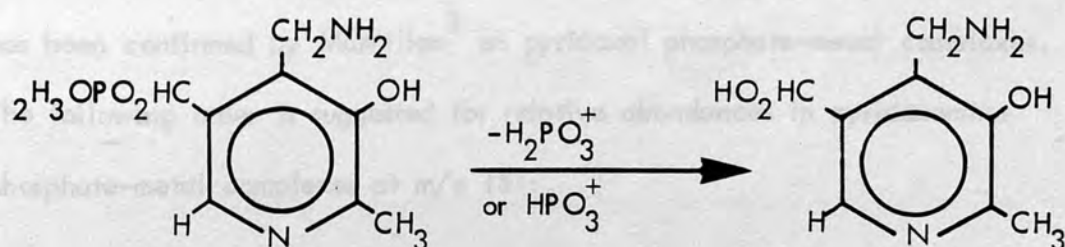
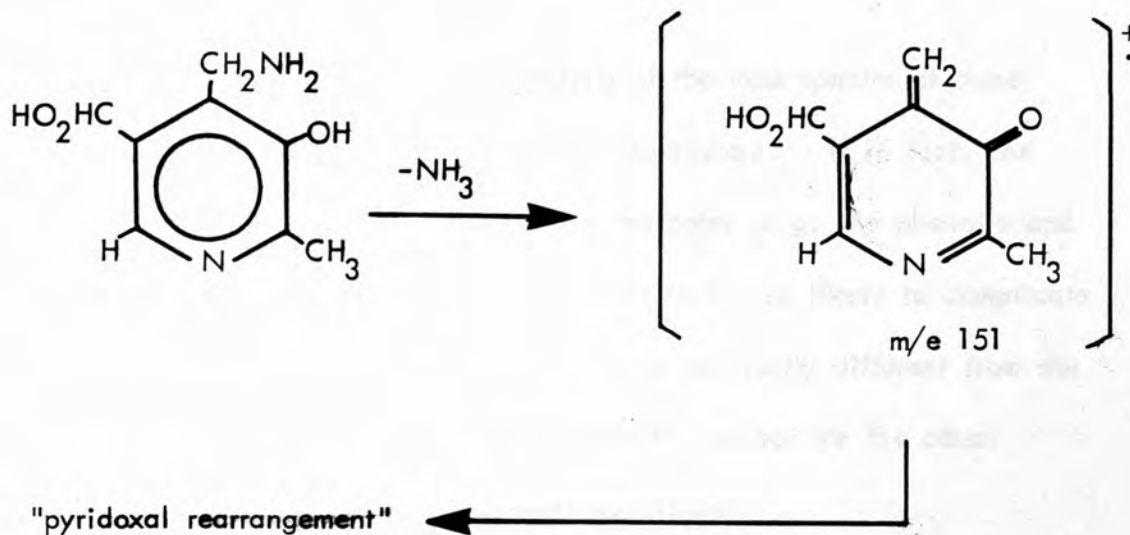


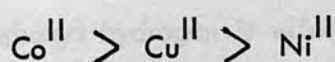
Fig. 6-7: Fragmentation of pyridoxamine phosphate.



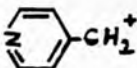
$m/e \ 121, 106, 94$

Fig. 6-7: (Continued)

The pyridoxamine phosphate metal complexes (PMP-M) have similar peaks to pyridoxamine phosphate (PMP) and therefore the fragmentation and bond cleavage, followed by rearrangement, is essentially the same. The peak at $m/e \ 151$ in pyridoxamine phosphate (PMP) is much stronger than that given by the bonded pyridoxamine phosphate (PMP-M) and so it is assumed that the breaking of the metal-ligand bonds facilitates a greater abundance of the ion fragment at that m/e ratio. This assumption has been confirmed by McMillan³ on pyridoxal phosphate-metal complexes. The following order is suggested for relative abundances in pyridoxamine phosphate-metal complexes at $m/e \ 151$:



The fragmentation and rearrangement is upheld by the results of mass spectra for both pyridoxamine phosphate, pyridoxal phosphate and their respective metal complexes.

Complications arise in the analysis of the mass spectra of these Schiff base complexes because of certain assumptions. If in fact, the Schiff base rearranges as in Scheme (d), the other (e.g. the phenolic and 5-methoxy groups) are neglected and if considered are likely to complicate the issue. The  molecular ion is not vastly different from the ion suggested for the "pyridoxal rearrangement", except for the other substituent groups (phenolic and 5-methoxy groups).

It is thus easy to assume that in the case of phosphopyridoxylidene-glycine (PLPGly) and pyridoxylidene-glycine (PLGly) Schiff bases the usual rearrangement will take place as in Scheme (b,c). Korytnyk¹ pointed out that if the 5-methoxy group was substituted to an aldehyde, then expulsion of the CH_3CN group from the nucleus of the pyridine ring would take place prior to the expulsion of CO . Either way, rearrangement and fragmentation would eventually lead to an m/e ratio of 61 which is present in all the spectra of the compounds investigated.

The only rearrangement foreign to that of the amine-aldehyde of pyridoxal-pyridoxamine is the migration of the phenolic hydrogen, not to be extracted as a neutral molecule but to promote the cleavage of the formyl-C=N bond and supply the necessary charge for the formation of a CH_2^+ ion.

The elimination of carbon dioxide from the amino acid is set out in scheme (b), the carboxyl hydrogen is effectively donated to the

α -carbon atom of the Schiff base which is then effectively negatively charged. The fragmentation of the Schiff base is then similar to scheme (c).

Beiman and his co-workers⁵ have suggested that in pyridoxal and pyridoxal phosphate-amino acid Schiff bases, rupture of the $\text{H}_2\text{C}-\overset{\text{N}}{\parallel}{\text{C}}-\text{R}$ bond depends on the nature of R. If R is a simple straight chain, the cleavage will take place in one step, but if it includes a branched chain then the fragmentation of R will follow a different pattern. McMillan³ studied the fragmentation of valinate and glutamate and came to the same conclusion and added to this the idea that since glutamate is a dicarboxylate group, it will evolve two volumes of CO_2 per Schiff base molecule and this does not complicate the mass spectrum as the acid is essentially a straight chain species.

The results obtained from the metal complexes of phosphopyridoxylidene-glycine and pyridoxylidene-glycine showed that the relative intensities of the m/e peaks are in the following order:



Considering just the mass spectra involving the commonest isotope of the metal in phosphopyridoxylidene-glycine metal complexes, ionisation of the phosphate group followed by extraction of CO_2 shows up at:

$\text{Cu}^{\text{II}} = m/e 221, 179$, $\text{Ni}^{\text{II}} = m/e 223, 178$, $\text{Co}^{\text{II}} = m/e 220, 176$ respectively. The removal of HCN then gives m/e 150 for Cu^{II} , m/e 151 for Ni^{II} , m/e 149 for Co^{II} , m/e 149 for Fe^{III} , and the subsequent rearrangements yield m/e 124, 108, 94 for Cu^{II} , m/e 119, 108, 95 for Ni^{II} ,

m/e 123, 109, 97 for Co^{II} , and m/e 121, 106, 97 for Fe^{III} , which are typical for the "pyridoxal cleavage" pattern.

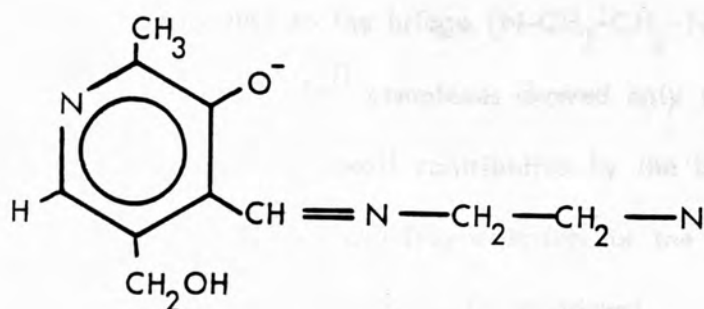
When PLPGly and PLGly metal complexes are studied the fragmentation patterns are almost identical, so one can assume that despite the stereochemical differences, the break-down processes of the complexes are closely similar.

The following process can be suggested for the dissociation and fragmentation of metal-pyridoxal phosphate-amino acid Schiff base complexes:

- 1) Ionisation of metal ion.
- 2) Removal of H_3PO_4 molecule or substituent ion.
- 3) Extraction of CO_2 from the amino acid.
- 4) Rearrangement and abstraction of HCN.
- 5) The remaining ion then rearranges as pyridoxine.

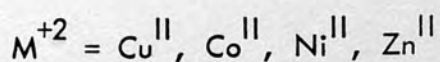
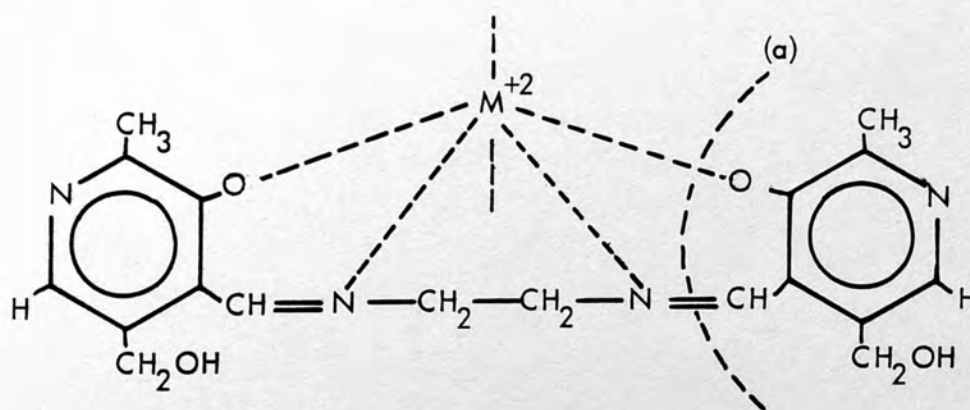
An additional step was suggested by McMillan³, namely that in metal-PLP-amino acid Schiff base complexes, fragmentation of the R-radical of the amino acid would occur after extraction of a molecule of CO_2 .

In the case of $(\text{PLP})_2\text{en}$ and $(\text{PL})_2\text{en}$ metal-Schiff base complexes, the fragmentation patterns are slightly different from those of glycine Schiff base complexes. Considering the fragmentation pattern of this series of complexes, the molecular ion peak occurs at m/e 420 (Fig. 6-8). The formation of the following fragment:



results from the elimination of H_2O and the metal ion from the molecular ion. The data in scheme (f) indicates that the above fragment gradually loses the bridge ($\text{N-CH}_2\text{-CH}_2\text{-N}$) to give a fragment at m/e 151. The "pyridoxal cleavage" then followed as was explained for glycine Schiff base complexes.

Considering the $\text{M}^{+2}(\text{PLP})_2\text{en}$ and $\text{M}^{+2}(\text{PL})_2\text{en}$ Schiff base complexes which have similar structures, the main breakage occurs at point (a) as follows:



The peak corresponding to the bridge ($\text{N-CH}_2\text{-CH}_2\text{-N}$) is not very intense. On the other hand, Zn^{II} complexes showed only the ligand fragment (i.e. pyridoxal system + small contribution by the bridge $\text{N-CH}_2\text{-CH}_2\text{-N}$ fragment). The main fragmentation for the Zn^{II} complexes then follows the same pattern as for pyridoxal.

In phosphopyridoxylidene-ethylenediamine metal complexes, the ionisation of metal ion and phosphate group takes place simultaneously to give an ion peak at m/e 420.

References:

1. D.C. DeJongh, S.C. Perricone, and W. Korytnyk, *JACS*, (1966), 88, 1233.
2. E. Schaucher and R. Taubenest, *Helv. Chim. Acta.* (1966), 49, 1455.
3. M. McMillan, M. Phil. Thesis, Bedford College, University of London, (1968).
4. D.A. Bafus, E.M. Gallegos and R.W. Kiser, *J. Phys. Chem.*, (1966), 70, 2614.
5. K. Bieman, J. Seibl and F. Gapp, *JACS*, (1961), 83, 3795.

CHAPTER 7

Electron Spin Resonance Study of Copper^{II}-Schiff Base Complexes

The electron spin resonance (ESR) study of the copper(II)-Schiff base complexes is a classic example of the application of the Zeeman effect to the study of the electronic structure of a paramagnetic complex. The copper(II) ion, with a d⁹ configuration, has a ground state with a spin quantum number S = 1/2. In the absence of an external magnetic field, the two degenerate spin states (α and β) are at the same energy level. The application of an external magnetic field splits these two states into two energy levels, corresponding to the alignment of the spin magnetic moment with the field. The two states are conventionally referred to as the α-state (parallel) and the β-state (antiparallel) of high energy and low energy, respectively. The splitting of degenerate energy levels by an external magnetic field is called the Zeeman effect (Scheme 7-1).

The electron may be promoted from lower to upper state by the absorption of energy corresponding to the exact difference in the energy levels of the two Zeeman states. Since the interaction energy between a magnetic dipole and a magnetic field is given by equation (1):

$$E = -\mu \cdot H \quad (1)$$

the energy difference between the two Zeeman levels may be written as:

$$\Delta E = g \beta H \quad (2)$$

7.1 Introduction

Electron spin resonance (e.s.r.) may be observed in a system containing unpaired electrons.

An electron in a magnetic field has a magnetic moment μ_S due to its intrinsic spin represented as:

$$\mu_S = -g_e \beta_e \hat{S} \quad (1)$$

β_e is the Bohr magneton (9.274×10^{-33}), g_e is the electronic g-factor (Lande's factor) equal to 2.0023 for a completely free electron, the notation $(\hat{\Lambda})$ represents a vector, S is the spin operator of $\frac{1}{2}(\frac{h}{2\pi})$ and h is Planck's constant (6.26×10^{-34} JS).

An electron placed in a magnetic field can occupy one of two quantized spin states with respect to a given field axis, corresponding to a parallel or anti-parallel alignment of the spin magnetic moment μ_S with the field direction. The two states are conventionally referred to as the α -state (anti parallel) of high energy and β -state (parallel) of lower energy and correspond to the Zeeman levels of unpaired electrons. The splitting of degenerate energy levels by an external magnetic field is called Zeeman effect (Scheme 7-1).

The electron may be promoted from lower to upper state by the absorption of energy corresponding to the exact difference in the energy levels of the two Zeeman states. Since the interaction energy between a magnetic dipole and a magnetic field is given by equation (2):

$$E = - \mu B \quad (2)$$

the energy difference between the two Zeeman levels may be written as:

$$\Delta E = g_e \beta_e B \quad (3)$$

Energy can be related to frequency by the Planck-Einstein equation

$E = h\nu$ and equation (3) may be rewritten as:

$$E = h\nu = g_e \beta_e B \quad (4)$$

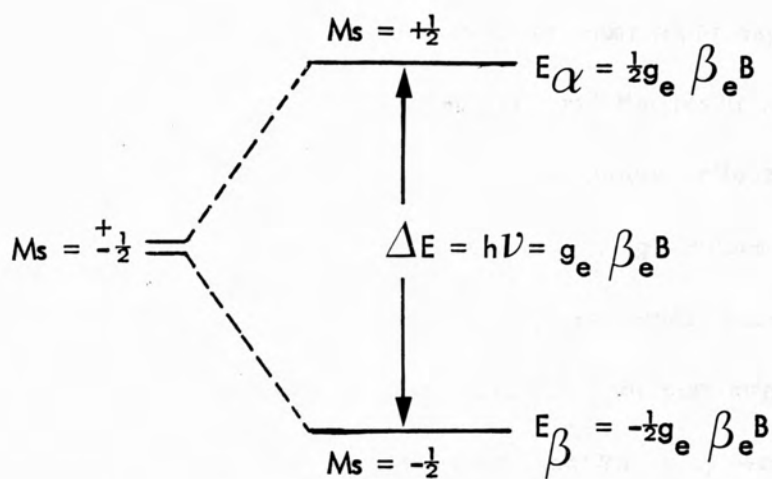
An electron in the presence of a static magnetic field B will absorb a quantum of electromagnetic radiation $h\nu$ and be promoted to the higher level. Similarly an electron in the upper level will be stimulated to emit radiation and drop to the lower level. Equation (3) is therefore known as the resonance equation.

In a macroscopic array of N electrons subjected to a magnetic field (B), a Boltzmann distribution exists between the two energy states at thermal equilibrium:

$$\frac{N_\alpha}{N_\beta} = \frac{\text{number of spins in } \alpha \text{ state}}{\text{number of spins in } \beta \text{ state}} = e^{\frac{-g \beta B}{KT}} = e^{\frac{-\Delta E}{KT}} \quad (5)$$

where K is the Boltzmann constant and T the absolute temperature.

Therefore, although emission and absorption of energy occurs with equal probability, a net absorption of energy occurs at resonance due to the unequal populations of the two states. This absorption may be detected spectroscopically and its observation forms the basis of an e.s.r. experiment.



Scheme 7-1 The energy levels of a single electron in a magnetic field (Zeeman energy levels)

7.2 The Practical Values of the E.S.R. Spectra of Cu^{II} Complexes

The e.s.r. spectra of copper^{II} complexes may be measured either as polycrystalline powders or as single crystals¹. Although the polycrystalline powder technique is the most rapid experimentally, it yields only approximate² "g" values, and the result may be subject to misinterpretations (due to exchange and dipolar effects). The single crystal technique yields the most accurate "g" values, and also gives their direction cosines relative to a given crystal face. However, since the spectra from dilute frozen solutions can largely overcome the limitations of polycrystalline powder spectra, they were used in this study to circumvent the problems inherent in growing single crystals.

Factors which determine the type of e.s.r. spectrum observed for a copper^{II} complex are:

- a) the nature of the electronic ground state
- b) the symmetry of the ligand field about the Cu⁺² ion
- c) The mutual orientation of the local molecular axes of the separate copper^{II} chromophores in the unit cell

7.3 Experimental

The e.s.r. measurements were made on a Decca X-3 spectrometer operating a frequency of 9270.301 MHz, equipped with a variable temperature unit and a proton resonance probe for accurate field determination and employing 100 KHz field modulation. Solution spectra were recorded from $\approx 10^{-3}$ M solutions in acetate buffer at pH 1-5.2 values since a general dependence of spectral features on pH was observed.

7.4 Results and Discussion

7.4.1 Powder Spectra

The powder spectra observed for these series of Cu^{II} -Schiff base complexes are insensitive to temperature down to $\approx 110\text{K}$ and may be classified into three main categories determined by their e.s.r. features:

- a) The spectrum of Cu^{II} -pyridoxine shows three definitive "g" values ($g_1 = 2.327$, $g_2 = 2.090$ and $g_3 = 2.048$) characteristic of rhombic symmetry to which this complex can therefore unambiguously be assigned. (Fig. 7-1,2)
- b) The spectra of $\text{Cu}(\text{PL})_2\text{en}, \text{H}_2\text{O}$; $\text{Cu}(\text{PNen})_2(\text{SO}_4)_2\text{Cl}_2, 5\text{H}_2\text{O}$; $\text{Cu}(\text{PLP})_2\text{enOAc}$; $\text{Cu}(\text{PL})_2\text{enOAc}$; $\text{Cu}_2(\text{PLGly}), 3\text{H}_2\text{O}$ and $\text{Cu}(\text{PMP})_2\text{acac}, 5\text{H}_2\text{O}$ show well defined features characteristic of ions with axially symmetric "g" tensor of appreciable anisotropy, i.e. $g_x = g_y = g_{\perp}$, $g_z = g_{\parallel}$ and $g_{\parallel} > g_{\perp}$ where the z axis is the principal symmetry axis (Fig. 7-3,4,5_a,5_b,5_c,6_a,6_b,6_c,7,8,9,10,11,12)*.
- c) In contrast to the above two cases (a,b) the spectra of $\text{Cu}(\text{PLP})_2\text{en}, 4\text{H}_2\text{O}$ and $\text{Cu}(\text{PLPGly}), 3\text{H}_2\text{O}$ are nearly isotropic, the "g" values not being definitive, although it is possible to extract tentative values for g_{\parallel} and g_{\perp} . These spectra (7-13,14,15,16) may suggest either that these complexes are $\text{Cu}^{\text{II}}(\text{L})_x$ chromophores of lower symmetry than octahedral or that they contain grossly misaligned tetragonal axes, which is the most common situation for the observation of isotropic spectra from powder samples (ignoring dynamic Jahn-Teller effects for these complexes).

Results of the "g" values obtained from the powder spectra are shown below (Table 7-1):

*Copper salts which were used:

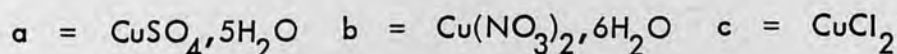


Table 7-1: Results of the "g" Values in Powder Spectra

Complexes	$g_{ }$ ± 0.01	g_{\perp} ± 0.01	g_1 ± 0.01	g_2 ± 0.01	g_3 ± 0.01
$\text{Cu(PLP)}_2\text{en}, 4\text{H}_2\text{O}^{\text{a}}$	2.16	2.05	-	-	-
$\text{Cu(PL)}_2\text{en}, \text{H}_2\text{O}$	2.17	2.04	-	-	-
$\text{Cu(PLPGly)}, 3\text{H}_2\text{O}^{\text{a}}$	2.30	2.07	-	-	-
$\text{Cu}_2(\text{PLGly}), 3\text{H}_2\text{O}$	2.20	2.05	-	-	-
$\text{Cu(PLP)}_2\text{en}, \text{OAc}$	2.23	2.04	-	-	-
$\text{Cu(PMP)}_2\text{acac}, 5\text{H}_2\text{O}$	2.26	2.05	-	-	-
$\text{Cu(PNen)}_2(\text{SO}_4)\text{Cl}_2, 5\text{H}_2\text{O}^{\text{b}}$	2.23	2.04	-	-	-
$\text{Cu(PNen)}_2(\text{SO}_4)\text{Cl}_2, 5\text{H}_2\text{O}^{\text{c}}$	2.226	2.039	-	-	-
$\text{Cu(PNen)}_2(\text{SO}_4)\text{Cl}_2, 5\text{H}_2\text{O}^{\text{d}}$	2.225	2.04	-	-	-
$\text{CuPN}, 2\text{H}_2\text{O}$	-	-	2.33	2.09	2.05

a = tentative values extracted from distorted spectra

Copper salts which were used:

b = $\text{CuSO}_4, 5\text{H}_2\text{O}$

c = $\text{Cu(NO}_3)_2, 6\text{H}_2\text{O}$

d = CuCl_2

Fig. 1-2. EPR spectra of $\text{CuPN}, 2\text{H}_2\text{O}$ at 110K

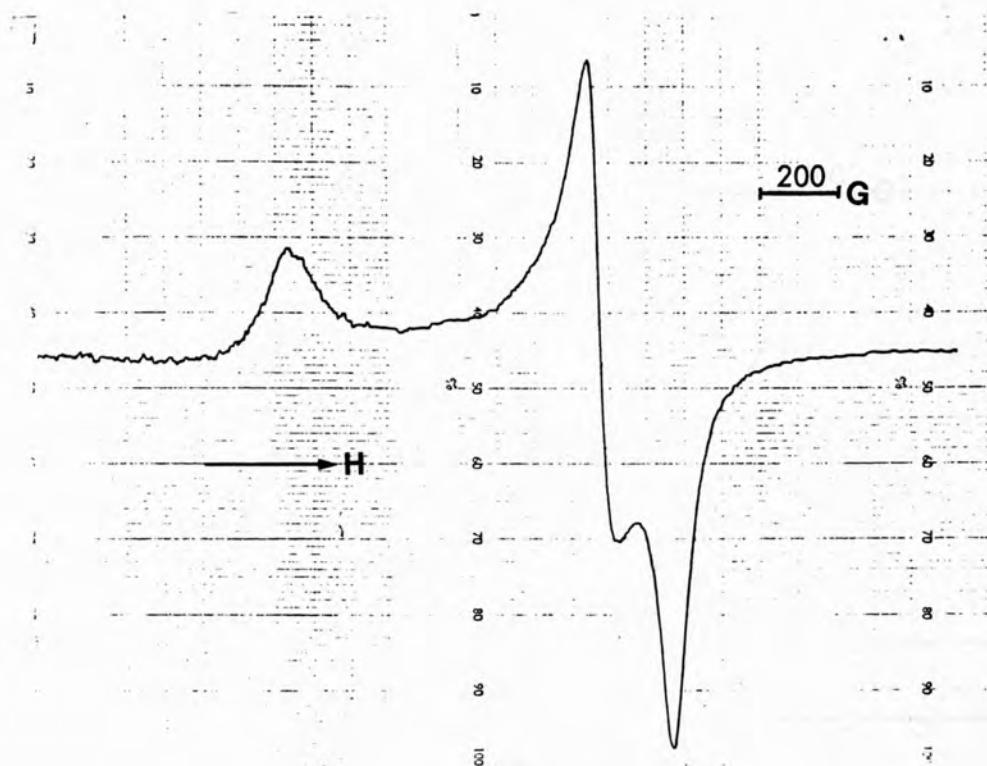


Fig. 7-1 E.s.r. spectrum of $\text{CuPN}, 2\text{H}_2\text{O}$ at room temperature

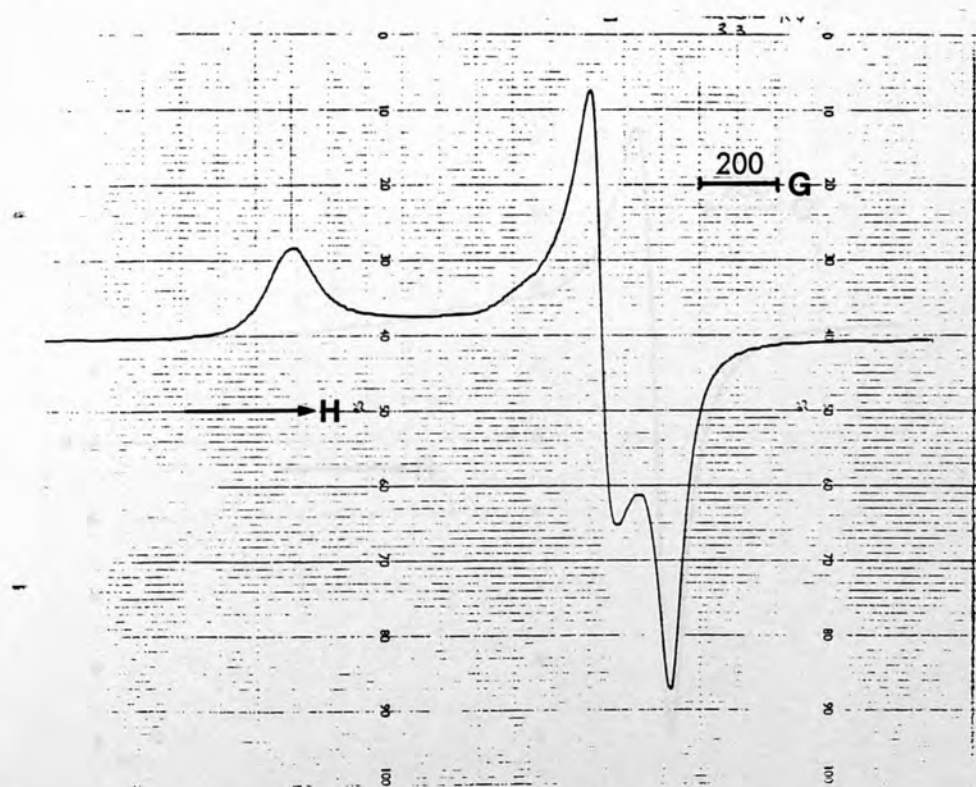


Fig. 7-2 E.s.r. spectrum of $\text{CuPN}, 2\text{H}_2\text{O}$ at 110K

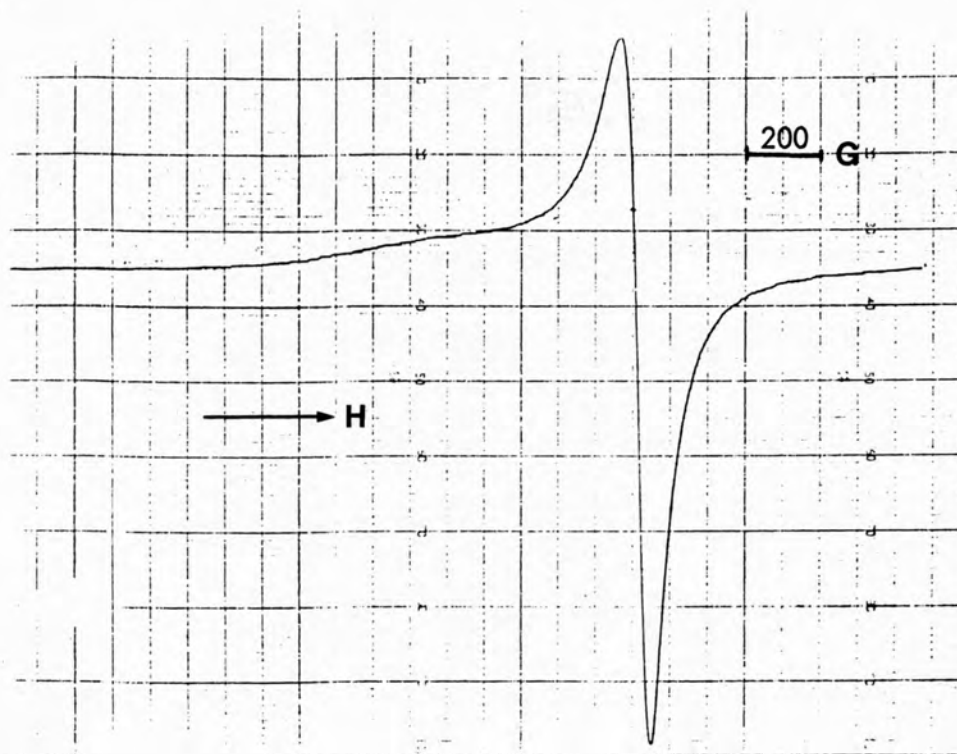


Fig. 7-3 E.s.r. spectrum of $\text{Cu(PL)}_2\text{en, H}_2\text{O}$ at room temperature

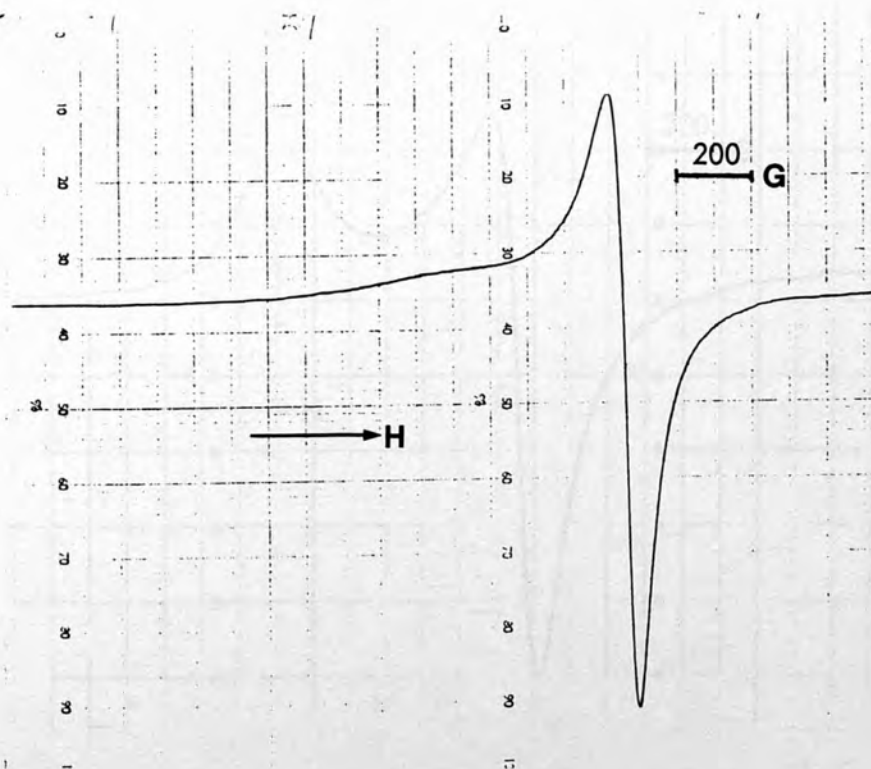


Fig. 7-4 E.s.r. spectrum of $\text{Cu(PL)}_2\text{en, H}_2\text{O}$ at 98K

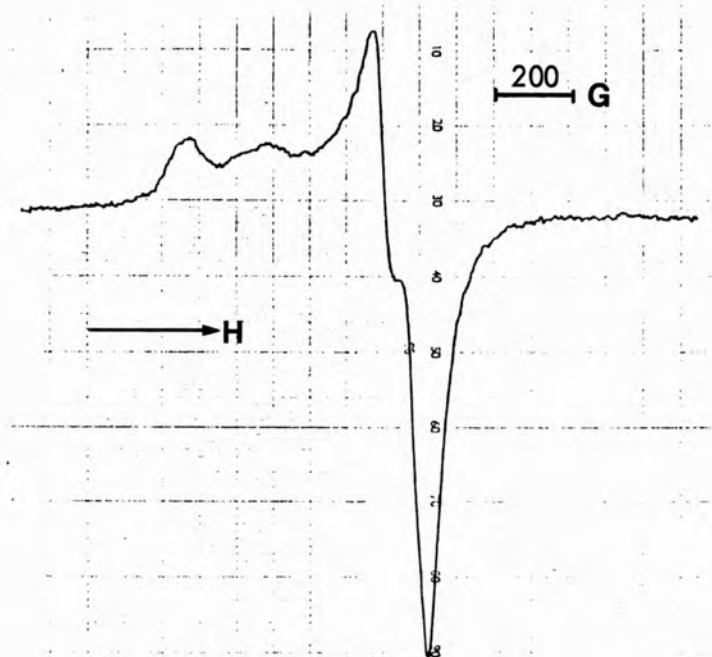


Fig. 7-5a E.s.r. spectrum of $\text{Cu}(\text{PNen})_2(\text{SO}_4)_2\text{Cl}_2, 5\text{H}_2\text{O}$
at room temperature

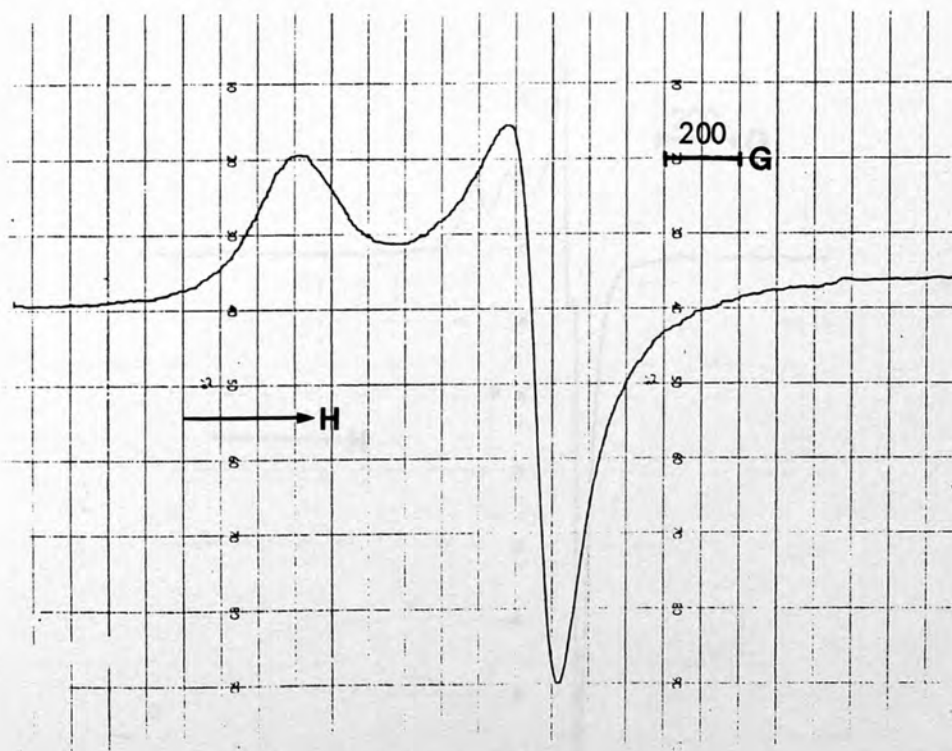


Fig. 7-5b E.s.r. spectrum of $\text{Cu}(\text{PNen})_2(\text{SO}_4)_2\text{Cl}_2, 5\text{H}_2\text{O}$
at room temperature

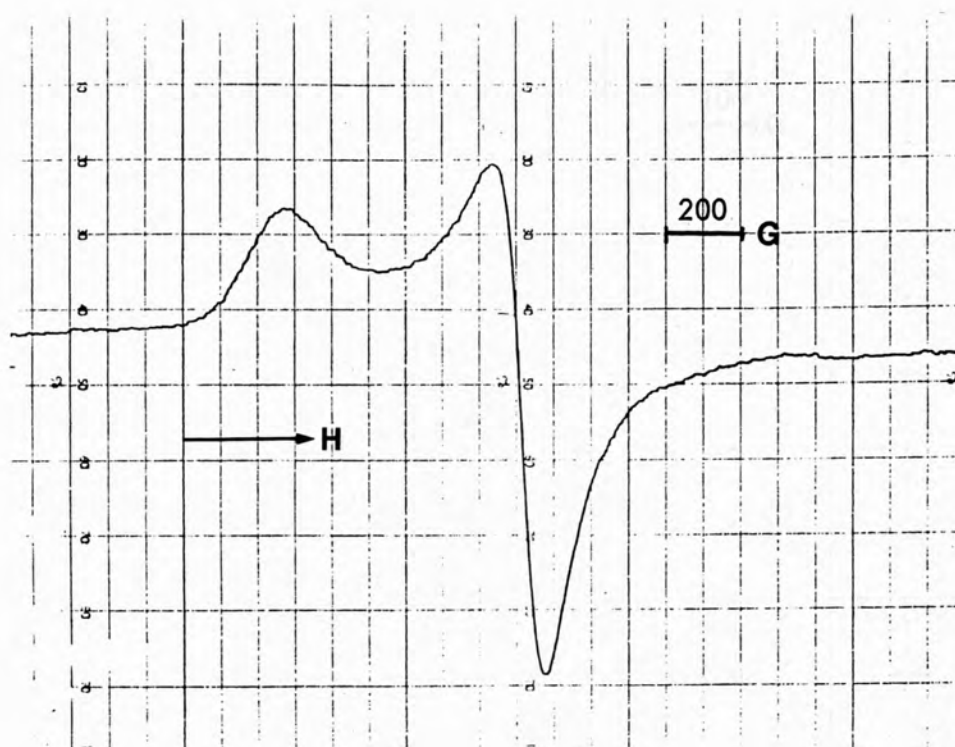


Fig. 7-5c E.s.r. spectrum of $\text{Cu}(\text{PNen})_2(\text{SO}_4)_2\text{Cl}_2 \cdot 5\text{H}_2\text{O}$
at room temperature

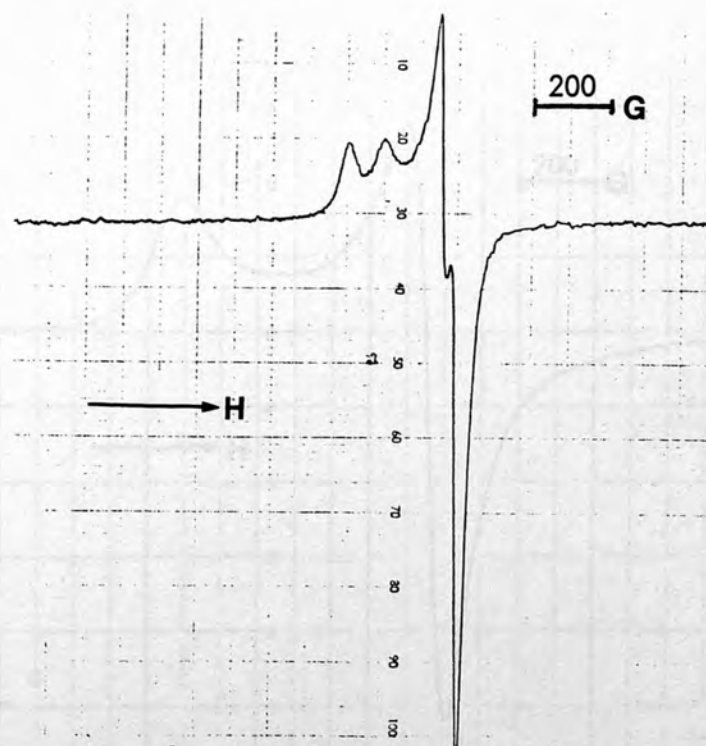


Fig. 7-6a E.s.r. spectrum of $\text{Cu}(\text{PNen})_2(\text{SO}_4)_2\text{Cl}_2 \cdot 5\text{H}_2\text{O}$ at 110K

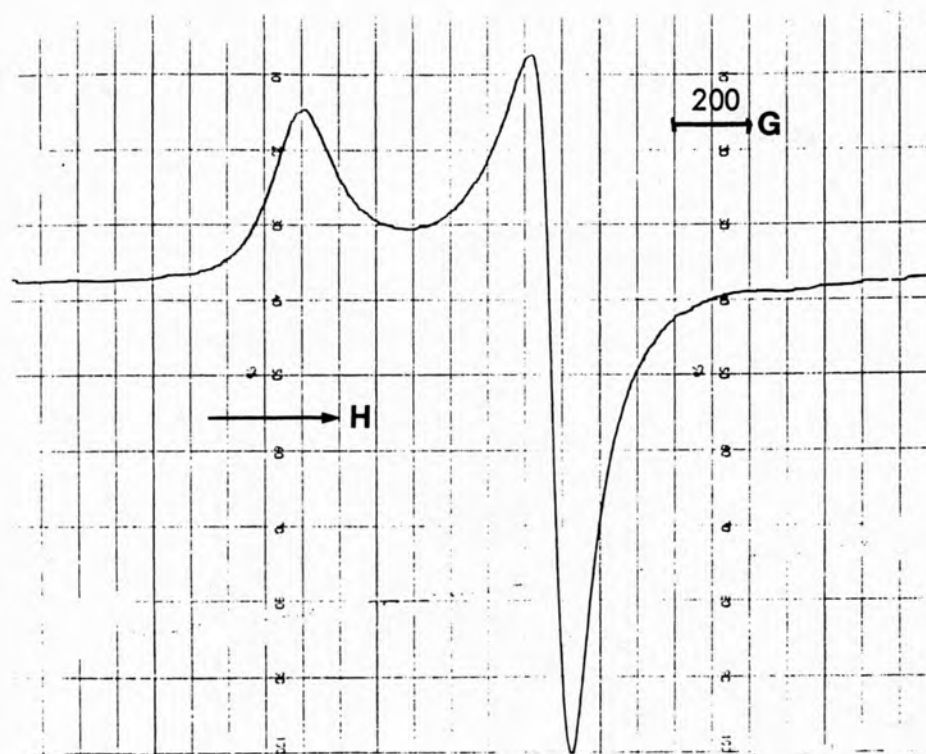


Fig. 7-6b E.s.r. spectrum of $\text{Cu}(\text{PNen})_2(\text{SO}_4)_2\text{Cl}_2 \cdot 5\text{H}_2\text{O}$ at 110K

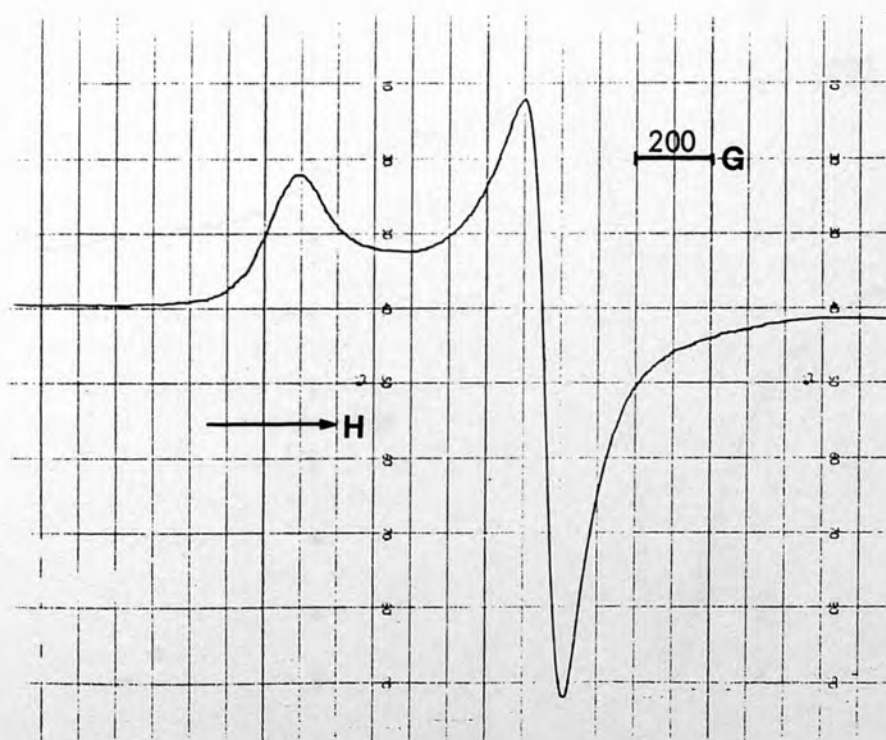


Fig. 7-6c E.s.r. spectrum of $\text{Cu}(\text{PNen})_2(\text{SO}_4)_2\text{Cl}_2 \cdot 5\text{H}_2\text{O}$ at 110K

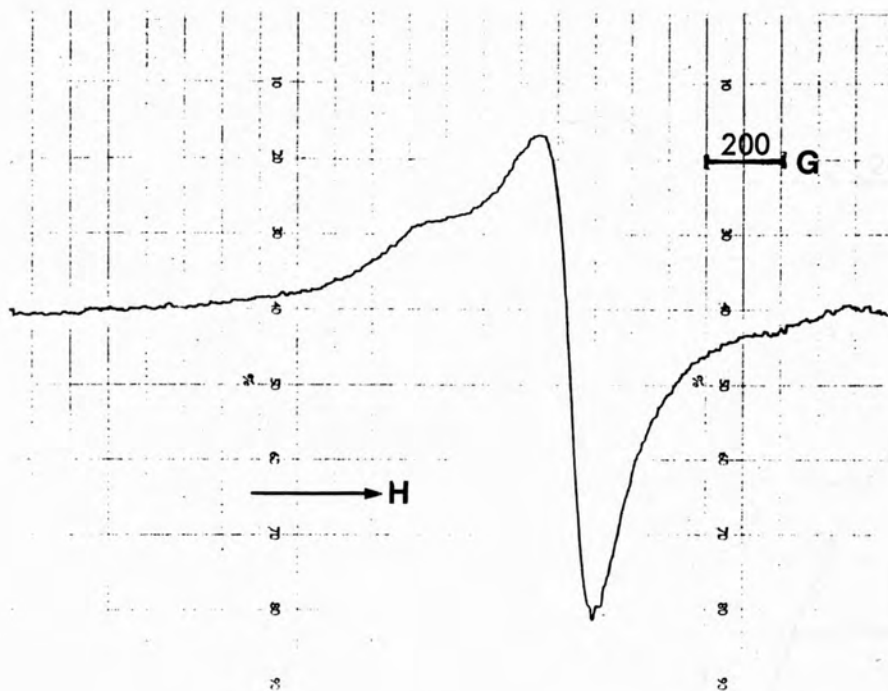


Fig. 7-7 E.s.r. spectrum of $\text{Cu(PLP)}_2\text{en OAc}$ at room temperature

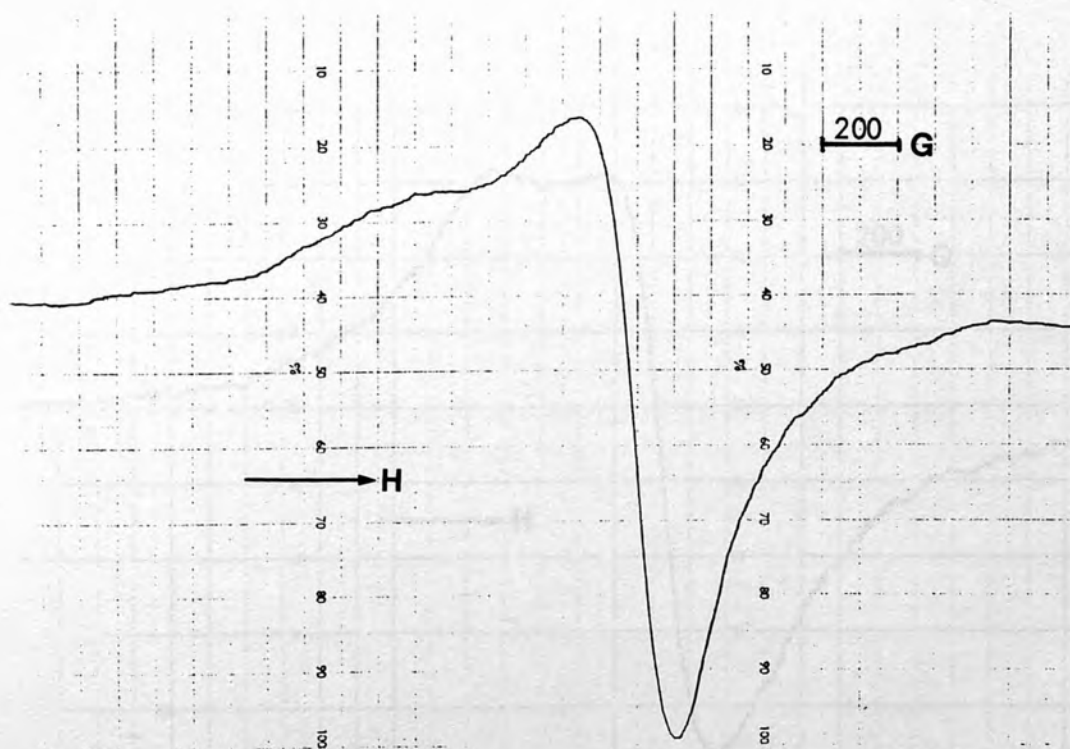


Fig. 7-8 E.s.r. spectrum of $\text{Cu(PLP)}_2\text{en OAc}$ at 110K

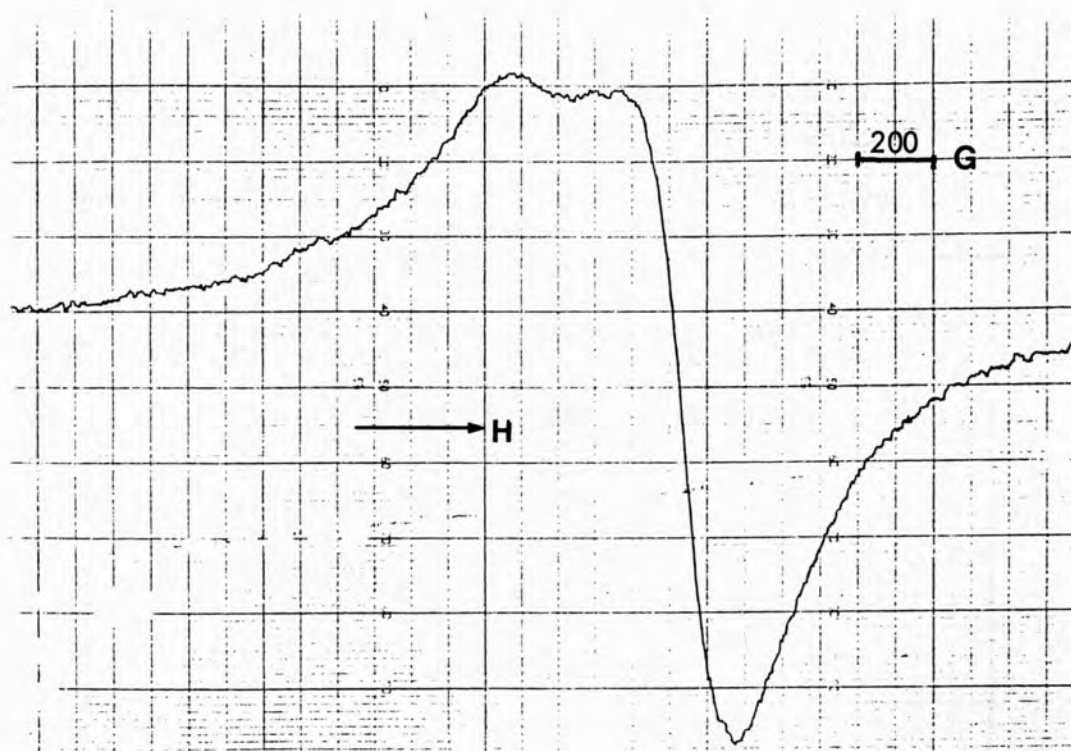


Fig. 7-9 E.s.r. spectrum of $\text{Cu}_2(\text{PLGly}), 3\text{H}_2\text{O}$ at room temperature

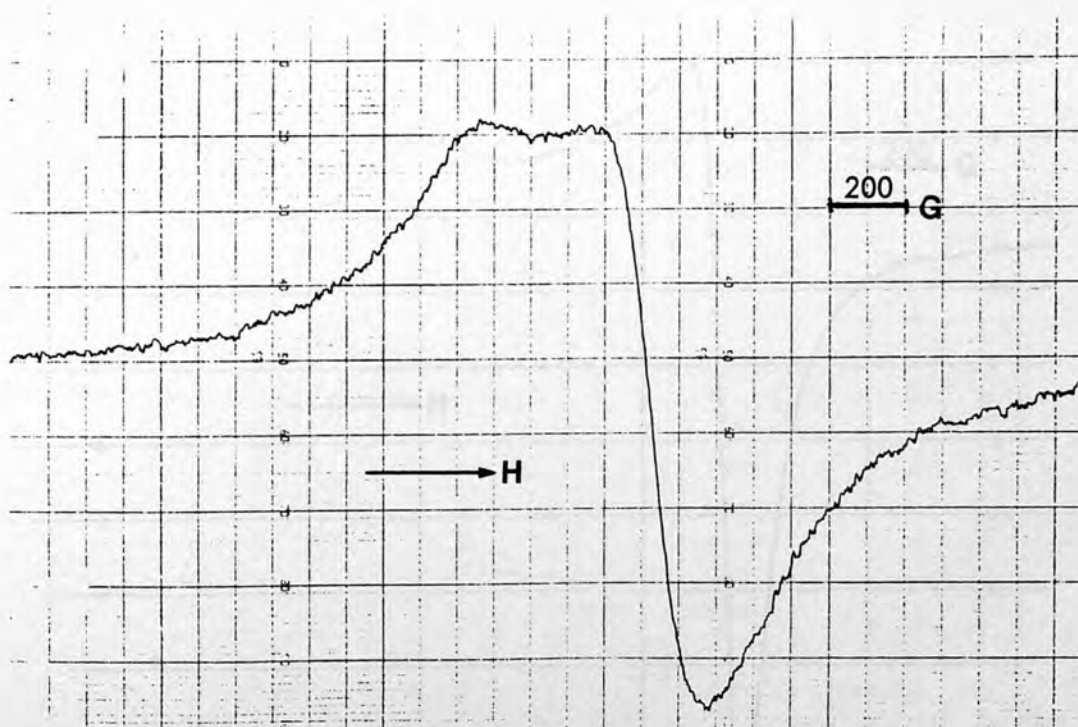


Fig. 7-10 E.s.r. spectrum of $\text{Cu}_2(\text{PLGly}), 3\text{H}_2\text{O}$ at 98K

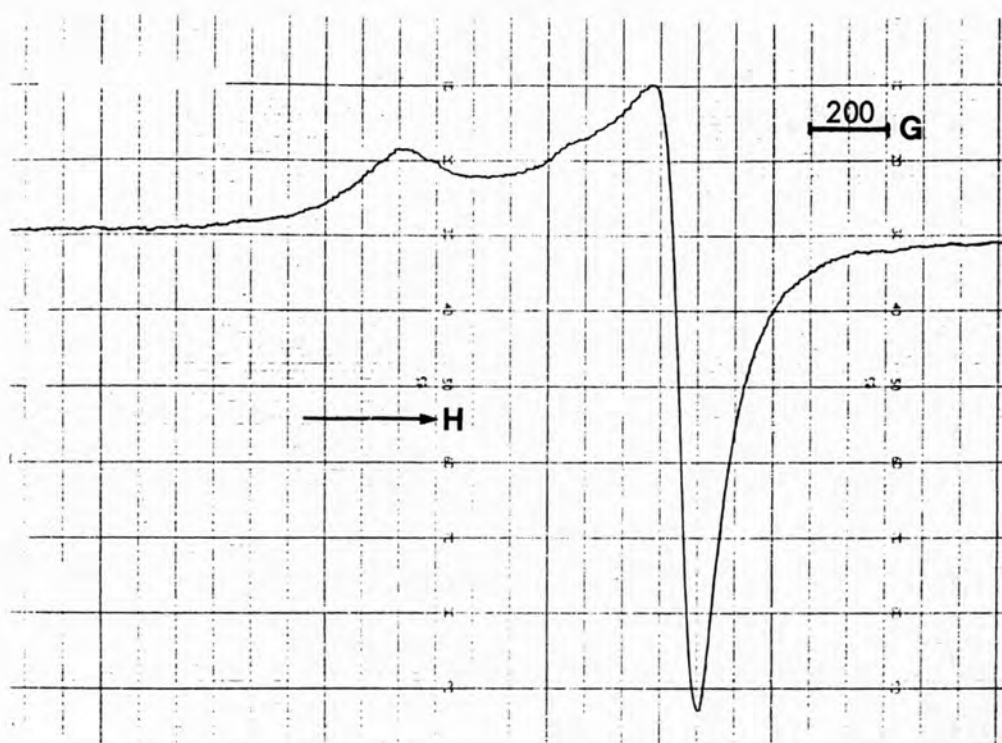


Fig. 7-11 E.s.r. spectrum of $\text{Cu}(\text{PMP})_2\text{acac}, 5\text{H}_2\text{O}$ at room temperature

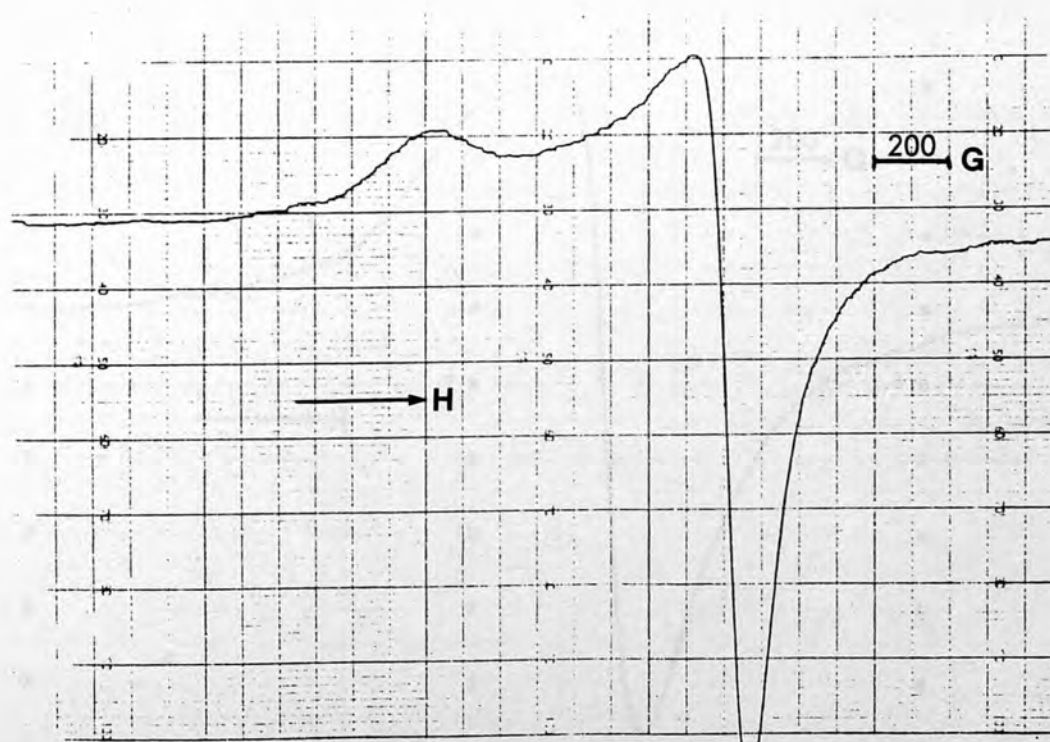


Fig. 7-12 E.s.r. spectrum of $\text{Cu}(\text{PMP})_2\text{acac}, 5\text{H}_2\text{O}$ at 98K

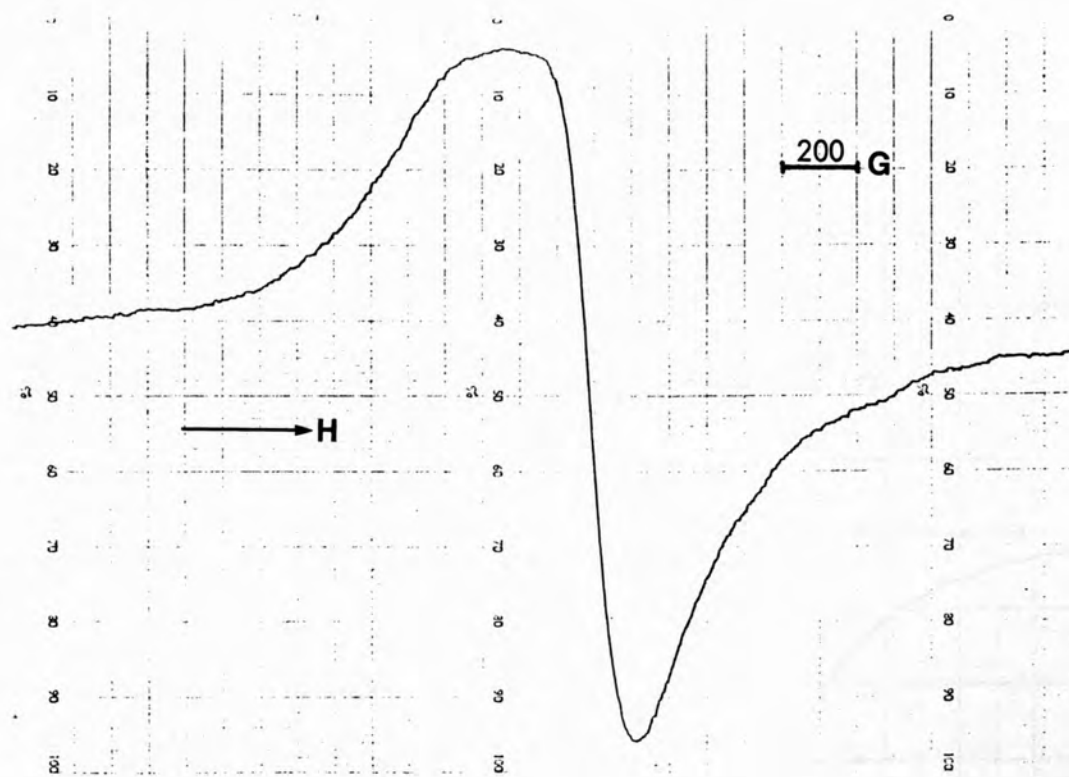


Fig. 7-13 E.s.r. spectrum of $\text{Cu(PLP)}_2\text{en}, 4\text{H}_2\text{O}$ at room temperature

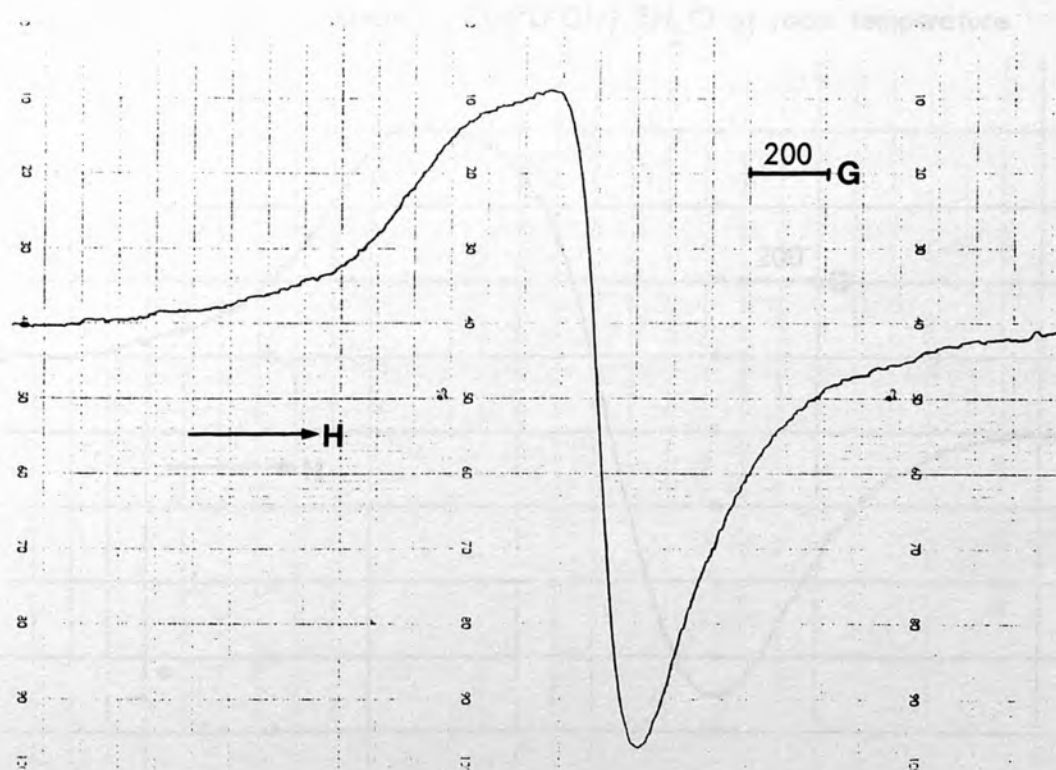


Fig. 7-14 E.s.r. spectrum of $\text{Cu(PLP)}_2\text{en}, 4\text{H}_2\text{O}$ at 98K

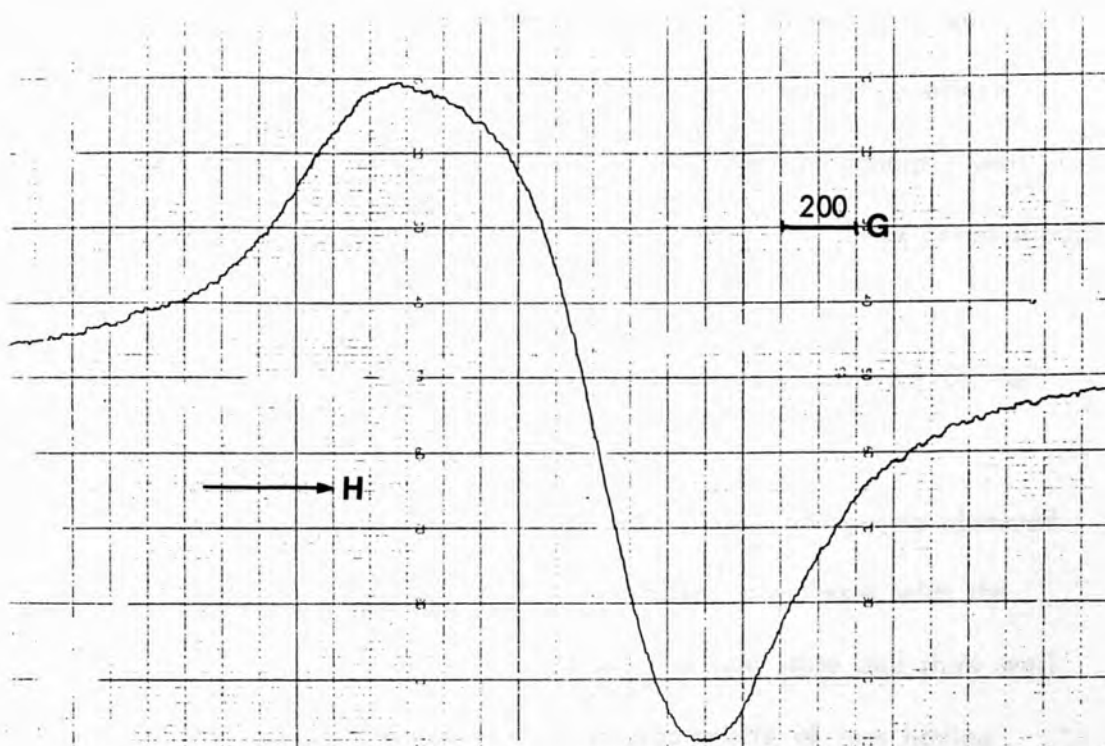


Fig. 7-15 E.s.r. spectrum of Cu(PLPGly),3H₂O at room temperature

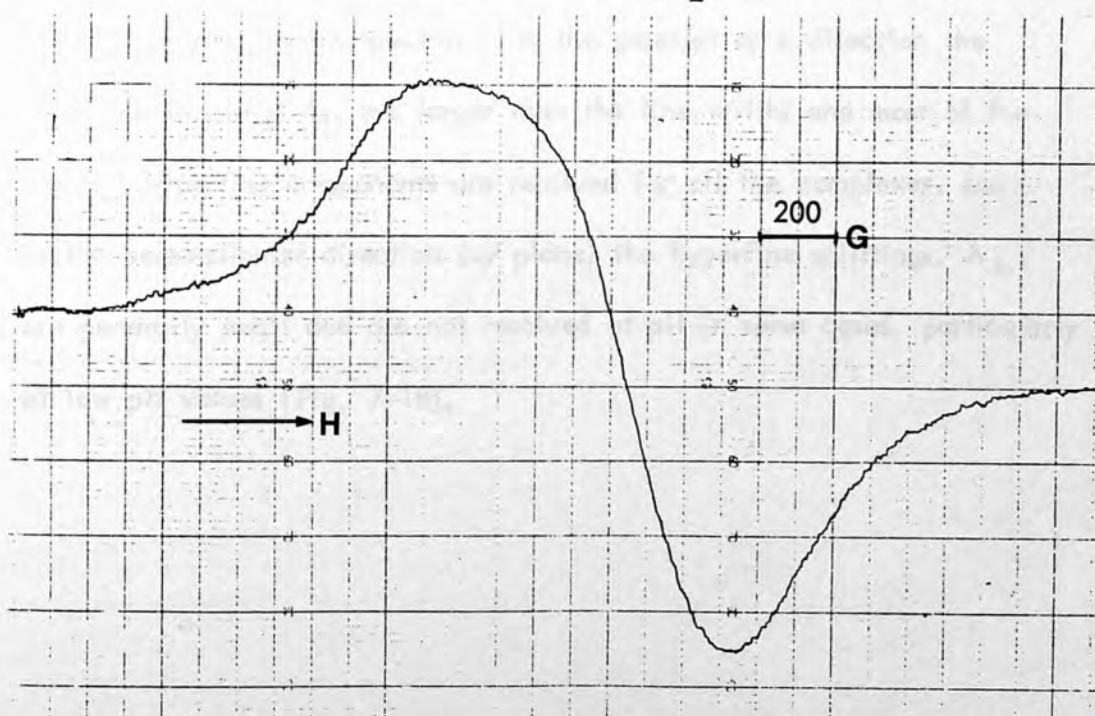


Fig. 7-16 E.s.r. spectrum of Cu(PLPGly),3H₂O at 98K

7.4.2 Solution Spectra

Solution spectra were obtained from acetate buffer (pH = 1-5.2) solutions having copper concentrations of $1-4 \times 10^{-3}$ M which is well below the range where ion-ion dipolar broadening or exchange effects can be significant. The fluid solution spectra show, in general, well resolved Cu^{+2} hyperfine structure at 273K from which A_{av} was determined. No superhyperfine splitting was detected.

The frozen solution technique was carried out at about 110K for almost all of the complexes.

In the case of $\text{Cu}(\text{PLP})_2\text{en}, 4\text{H}_2\text{O}$, frozen solution spectra observed at $\approx 110\text{K}$ (Fig. 7-17) are typical of copper^{II} complexes with the unpaired electron predominantly in a $d_{x^2-y^2}$ ground state and show well resolved hyperfine structure and features characteristic of ions having axially symmetric "g" and "A" tensors with $g_{||} > g_{\perp}$ as previously defined for the powder spectra. In the parallel or z direction the hyperfine splittings $A_{||}$ are larger than the line widths and most of the parallel hyperfine components are resolved for all the complexes, but in the perpendicular direction (xy plane) the hyperfine splittings, A_{\perp} , are generally small and are not resolved at all in some cases, particularly at low pH values (Fig. 7-18).

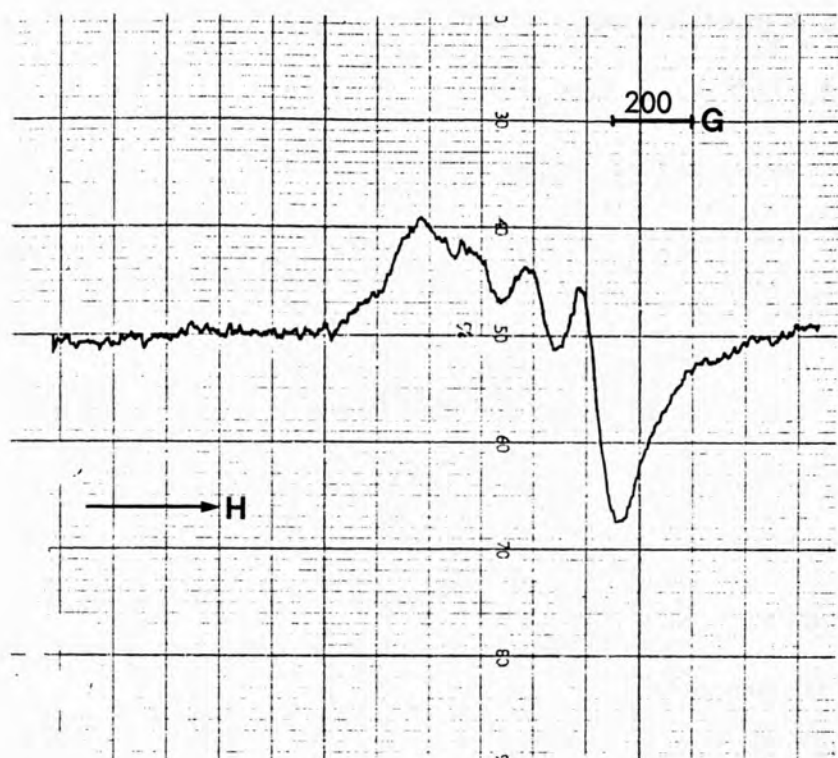


Fig. 7-17 E.s.r. spectrum of $\text{Cu(PLP)}_2\text{en}, 4\text{H}_2\text{O}$ in buffer pH=3 at 110K

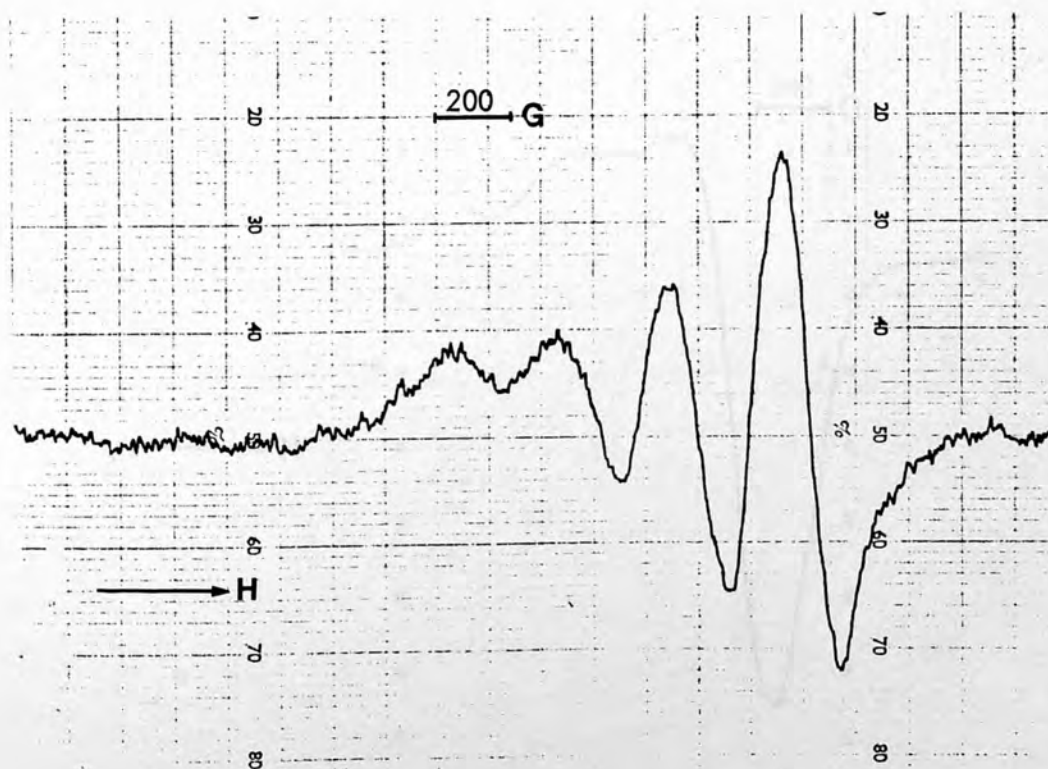


Fig. 7-18 E.s.r. spectrum of $\text{Cu(PLP)}_2\text{en}, 4\text{H}_2\text{O}$ in buffer pH=3 at room temperature

It is interesting to note that the spectral features and values of the parameters of "g" and "A" values, except for $\text{CuPN}, 2\text{H}_2\text{O}$ and $\text{Cu(PMP)}_2\text{acac}, 5\text{H}_2\text{O}$ depend markedly on the pH values used.

CuPLPen for example at a pH value of 5.2 has spectral parameters:

$g_{\parallel} = 2.240$, $g_{\perp} = 2.067$, $A_{\parallel} = 182\text{G}$ and $A_{\perp} = 21\text{G}$ ($\text{G} = \text{Gauss}$),
 A_{av} and g_{av} calculated³ from the equation (6):

$$A_{\text{av}} = \frac{1}{3} (A_{\parallel} + 2A_{\perp}) \quad (6)$$

All these parameters agree very well with the values observed from the fluid solution spectrum, indicating that rapid freezing does not significantly perturb the configuration of the complexes at room temperature.

At $\text{pH} = 1.09$ these parameters are: $g_{\parallel} = 2.332$, $g_{\perp} = 2.082$ and

$A_{\parallel} = 136\text{G}$ (Gauss), but A_{\perp} is not resolved at all (Fig. 7-19).

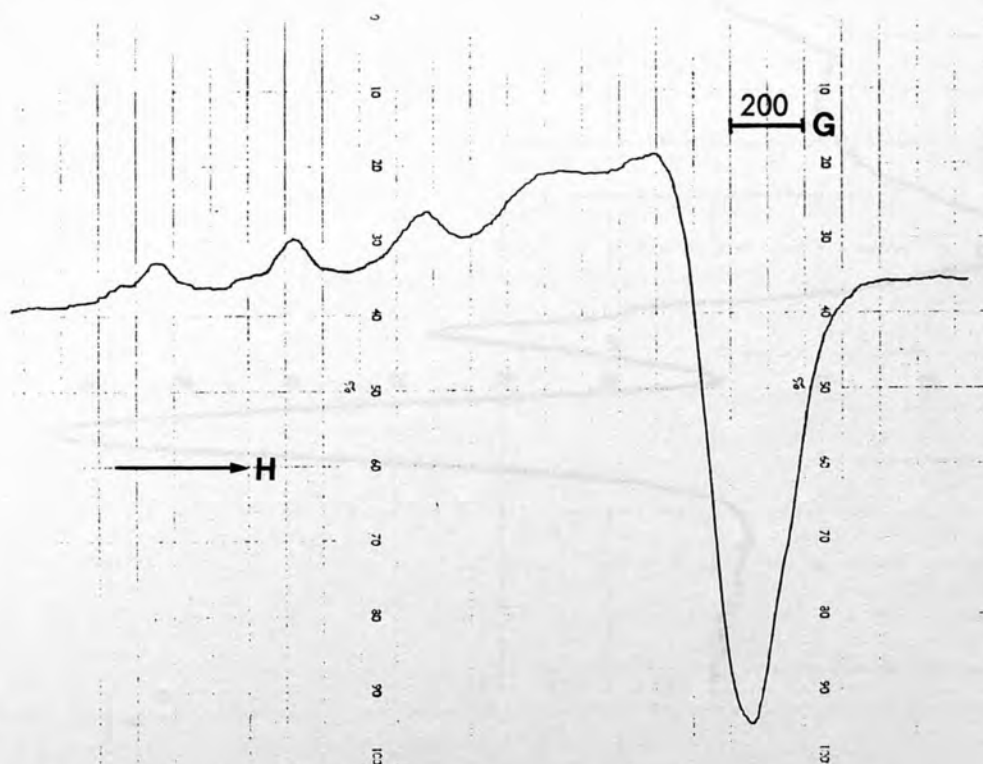
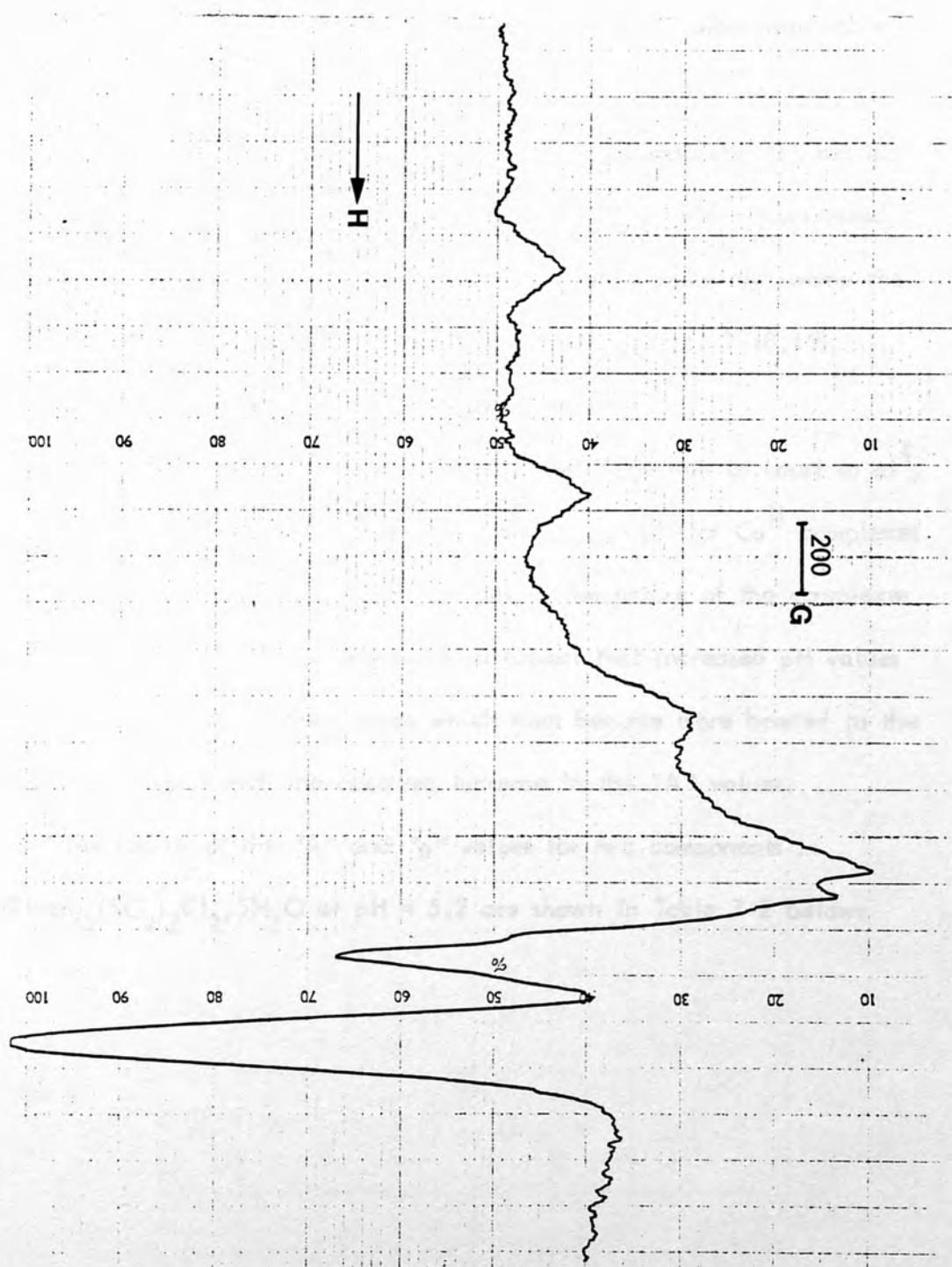
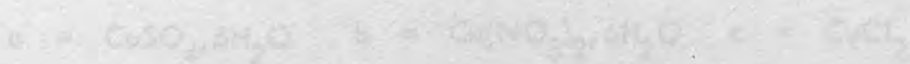


Fig. 7-19: E.s.r. spectrum of $\text{Cu(PLP)}_2\text{en}, 4\text{H}_2\text{O}$ in buffer $\text{pH} = 1.09$ at -10°C

Fig. 7-20: E.s.r. spectrum of $\text{Cu}(\text{PNen})_2(\text{SO}_4)\text{Cl}_2 \cdot 5\text{H}_2\text{O}$ in buffer pH = 1.09 at room temperature



* Copper salt which was used:



Other complexes such as $\text{Cu}(\text{PNen})_2(\text{SO}_4)_2\text{Cl}_2 \cdot 5\text{H}_2\text{O}$ at $\text{pH} = 1.09$ showed similar parameters to those observed for $\text{CuPN} \cdot 2\text{H}_2\text{O}$ (Fig. 7-20, 21, 22, 23, 24). But, at a higher pH value ($\text{pH} = 5.2$), other resolvable features are present which show that each spectrum is a mixture of two components (Fig. 7-25_a, 25_b, 25_c, 26_a, 26_b, 26_c)*. Component "1" has a higher g_{\parallel} and a lower A_{\parallel} value than component "2". It is considered that at even higher pH values component "2" would completely swamp the spectrum (analogous to the case of $\text{Cu}(\text{PLP})_2\text{en} \cdot 4\text{H}_2\text{O}$, Fig. 7-18, 19), although this was not investigated for those complexes.

These observations are in accord with the suggestion of Lauri et al⁴, who reported a similar dependence of A_{\parallel} and g_{\parallel} on pH for Cu^{II} complexes and could be explained in terms of changes in the nature of the complexes as the pH is varied. It is reasonable to expect that increased pH values lead to deprotonation of the ligands which then become more bonded to the copper^{II}, consistent with the observed increase in the "A" values.

The results of the "A" and "g" values for two components in $\text{Cu}(\text{PNen})_2(\text{SO}_4)_2\text{Cl}_2 \cdot 5\text{H}_2\text{O}$ at $\text{pH} = 5.2$ are shown in Table 7-2 below:

Component	A_{\parallel}	g_{\parallel}	A_{\perp}	g_{\perp}	A_{iso}	g_{iso}
1	0.12	2.05	0.08	2.00	0.10	2.02
2	0.15	2.00	0.10	2.05	0.12	2.03

*Copper salts which were used:

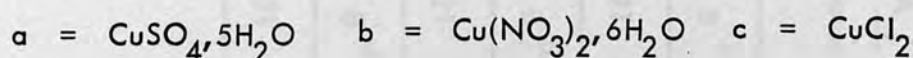
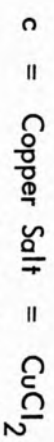
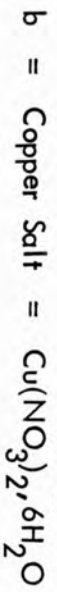
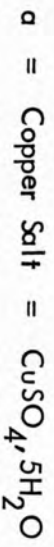


Table 7-2: Calculated "g" and "A" Values of $\text{Cu}(\text{P}(\text{Nen})_2(\text{SO}_4)_2\text{Cl}_2 \cdot 5\text{H}_2\text{O})$ at various pH Values

Complex*	Component	pH	$g_{\text{av}} \pm 0.005$	$g_{\text{II}} \pm 0.005$	$g_{\text{I}} \pm 0.005$	A_{av} Gauss	A_{II} Gauss	A_{I} Gauss
$\text{Cu}(\text{P}(\text{Nen})_2(\text{SO}_4)_2\text{Cl}_2 \cdot 5\text{H}_2\text{O})^{\text{d}}$	1	5.2	2.205	2.353	2.090	40	136	8 ^d
"	2	"	2.147	2.320	2.065	70	162	21
$\text{Cu}(\text{P}(\text{Nen})_2(\text{SO}_4)_2\text{Cl}_2 \cdot 5\text{H}_2\text{O})^{\text{b}}$	1	"	2.205	2.354	2.088	40	136	8 ^d
"	2	"	2.147	2.320	2.066	71	158	21
$\text{Cu}(\text{P}(\text{Nen})_2(\text{SO}_4)_2\text{Cl}_2 \cdot 5\text{H}_2\text{O})^{\text{c}}$	1	"	2.203	2.352	2.090	40	138	8 ^d
"	2	"	2.145	2.322	2.065	70	160	21

*The copper salts which were used:



d = was estimated from A_{II} and A_{av}

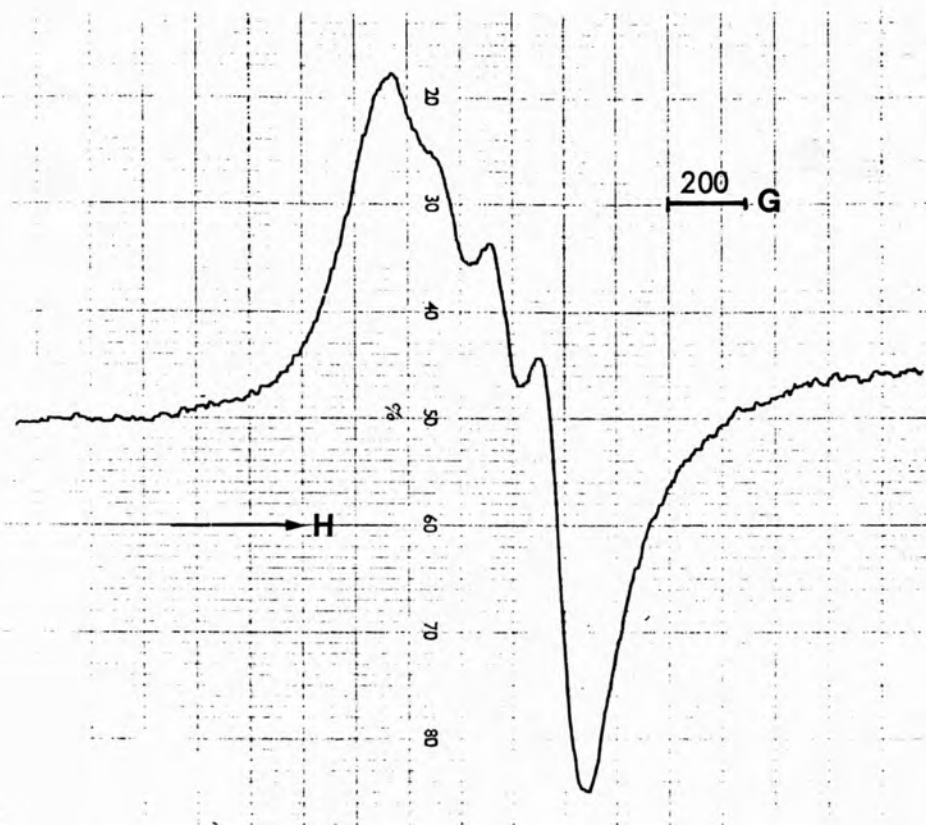


Fig. 7-21 E.s.r. spectrum of $\text{Cu}(\text{PNen})_2(\text{SO}_4)_2\text{Cl}_2 \cdot 5\text{H}_2\text{O}$ in buffer pH=1.09 at -5°C

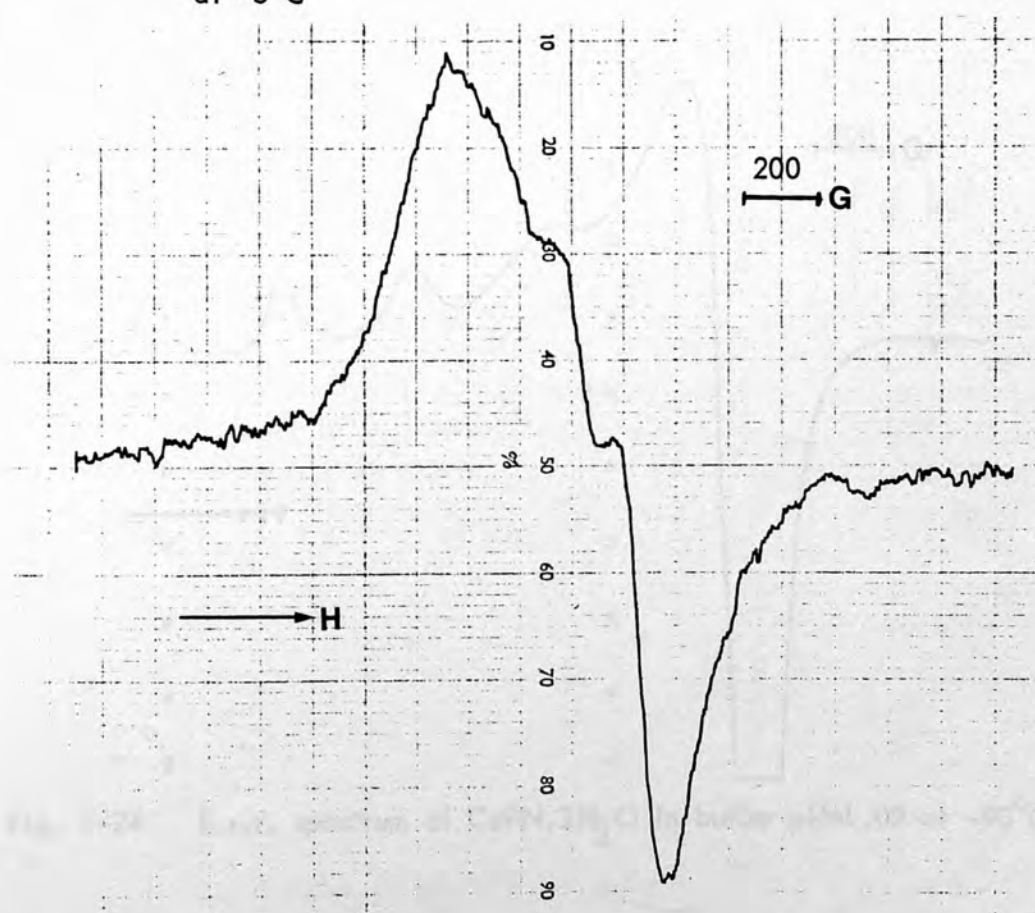


Fig. 7-22: E.s.r. spectrum of $\text{CuPN} \cdot 2\text{H}_2\text{O}$ in buffer pH = 1.09 at room temperature

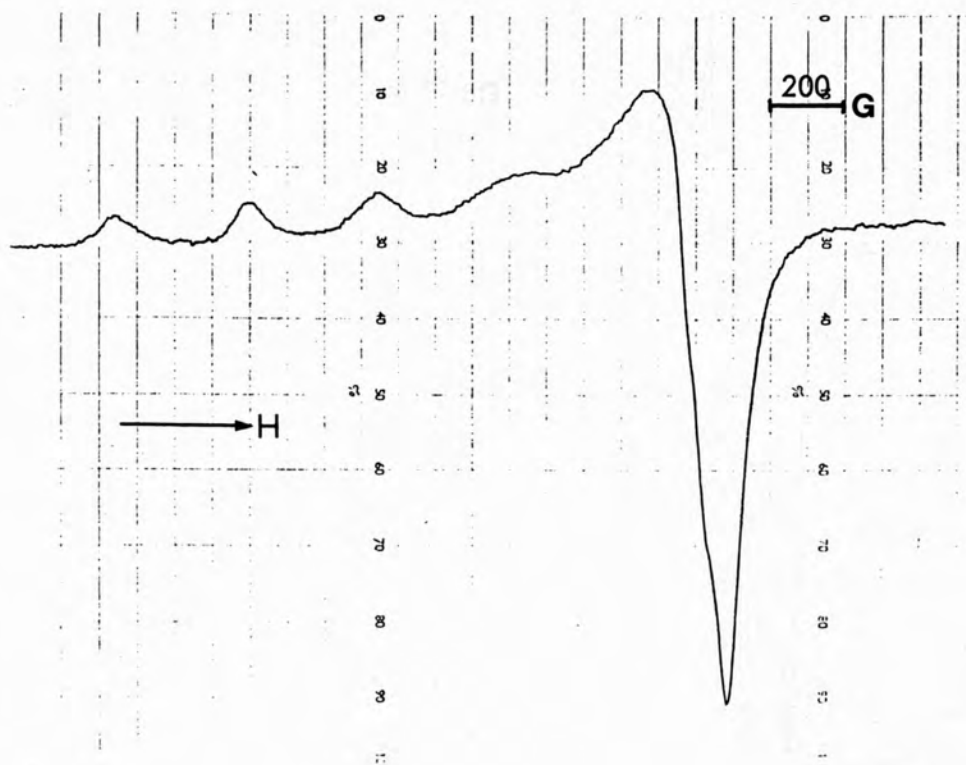


Fig. 7-23 E.s.r. spectrum of $\text{Cu}(\text{PNen})_2(\text{SO}_4)_2\text{Cl}_2 \cdot 5\text{H}_2\text{O}$ in buffer $\text{pH}=1.09$ at -90°C

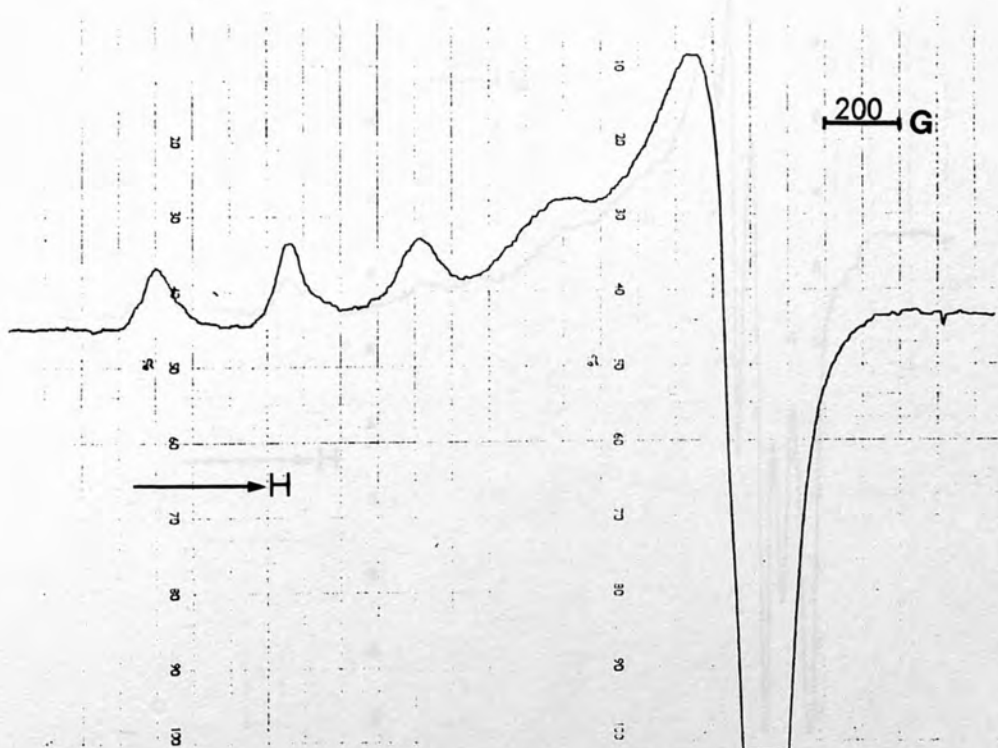


Fig. 7-24 E.s.r. spectrum of $\text{CuPN} \cdot 2\text{H}_2\text{O}$ in buffer $\text{pH}=1.09$ at -90°C

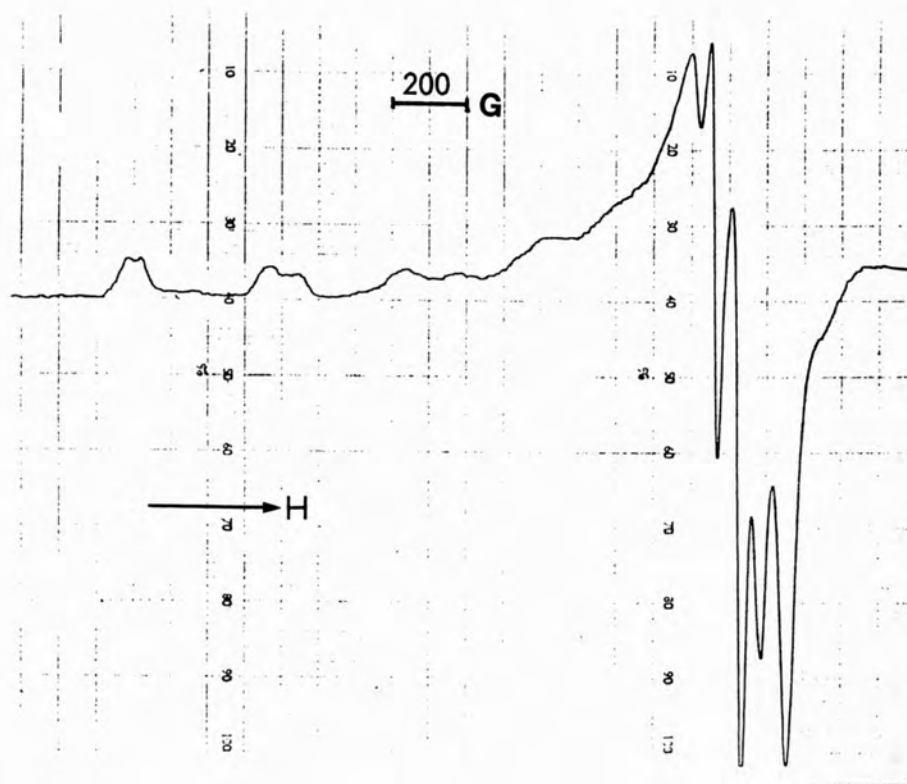


Fig. 7-25a E.s.r. spectrum of $\text{Cu}(\text{PNen})_2(\text{SO}_4)_2\text{Cl}_2 \cdot 5\text{H}_2\text{O}$ in buffer pH=5.20 at 110K

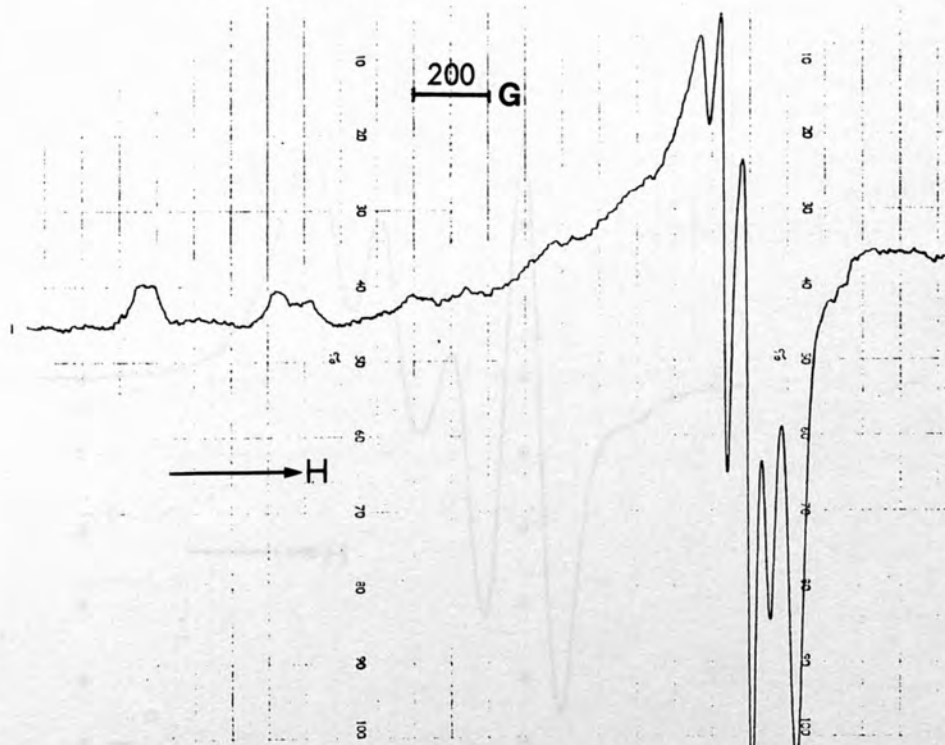


Fig. 7-25b E.s.r. spectrum of $\text{Cu}(\text{PNen})_2(\text{SO}_4)_2\text{Cl}_2 \cdot 5\text{H}_2\text{O}$ in buffer pH=5.20 at 110K

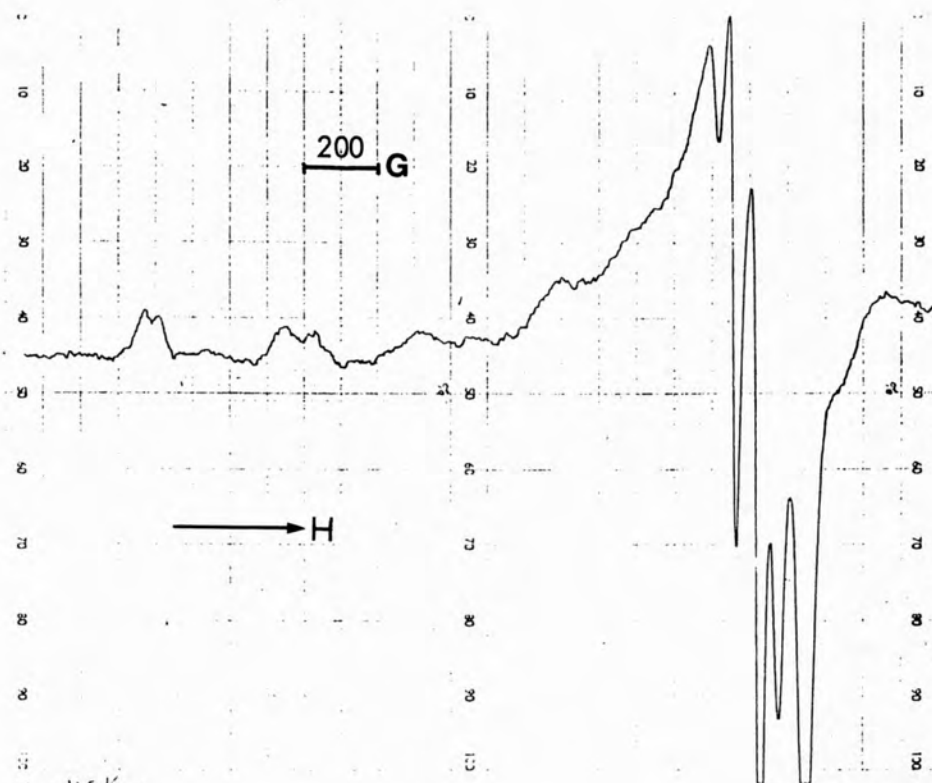


Fig. 7-25c E.s.r. spectrum of $\text{Cu}(\text{PNen})_2(\text{SO}_4)_2\text{Cl}_2 \cdot 5\text{H}_2\text{O}$ in buffer pH=5.20 at 110K

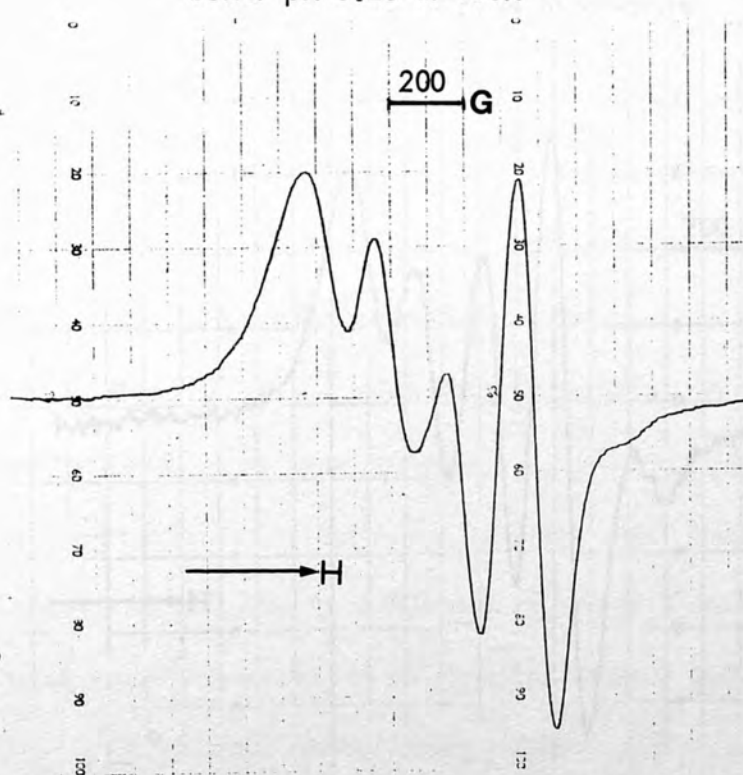


Fig. 7-26a E.s.r. spectrum of $\text{Cu}(\text{PNen})_2(\text{SO}_4)_2\text{Cl}_2 \cdot 5\text{H}_2\text{O}$ in buffer pH=5.20 at room temperature

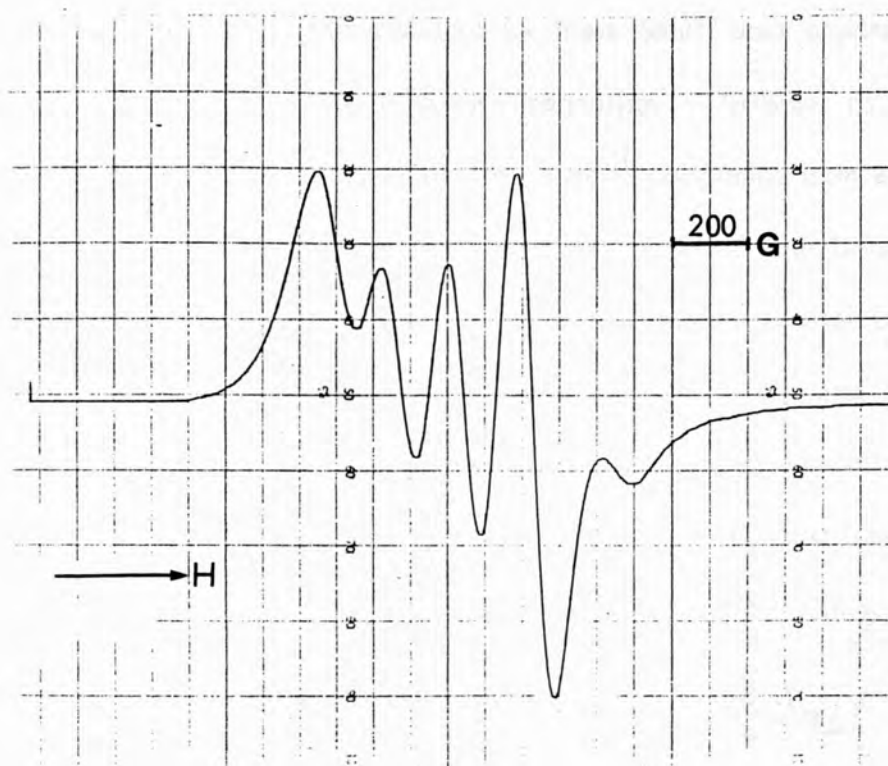


Fig. 7-26b E.s.r. spectrum of $\text{Cu}(\text{PNen})_2(\text{SO}_4)_2\text{Cl}_2 \cdot 5\text{H}_2\text{O}$ in buffer pH=5.20 at room temperature

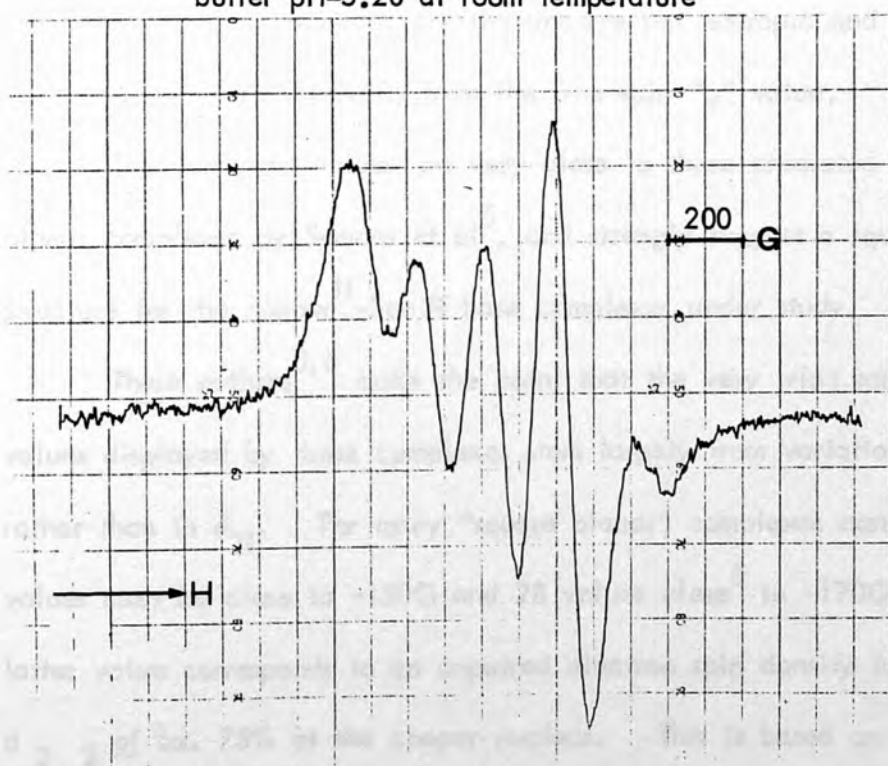


Fig. 7-26c E.s.r. spectrum of $\text{Cu}(\text{PNen})_2(\text{SO}_4)_2\text{Cl}_2 \cdot 5\text{H}_2\text{O}$ in buffer pH=5.20 at room temperature

It must be emphasized that for these Schiff base copper complexes $A_{iso} \neq A_{av}$, because of orbital magnetism. In order to determine the coordination environment of the copper^{II} complexes from e.s.r. parameters, the experimental data must be converted into isotropic and anisotropic parts (corrected for orbital magnetism) for orbital population calculations. Two similar procedures by Symons et al⁵ and Giordano et al⁶ were adopted. The corrected data (following Symons' approach) which are shown in Table 7-3,4,5 are obtained from equations (7) and (8) which are derived from standard equations for the d^9 ($d_{x^2-y^2}$) case:

$$A_{||} \text{ (experimental)} = A + 2B(1 - \frac{7}{4} \Delta g_{||} - \frac{3}{4} \Delta g_{\perp}) \quad (7)$$

$$A_{\perp} \text{ (experimental)} = A - B(1 + \frac{11}{4} \Delta g_{\perp}) \quad (8)$$

A and 2B parameters are the uncorrected isotropic and anisotropic parts and Δg are the shifts from the free-spin "g" value.

The corrected values are very close to those predicted for square planar complexes by Symons et al⁵, and strongly suggest a square planar structure for the copper^{II}-Schiff base complexes under study.

These authors^{5,6} make the point that the very wide range of "A" values displayed by these complexes stem largely from variations in $\Delta g_{||}$ rather than in $A_{||}$. For many "square planar" complexes corrected A_{iso} values must be close to -150G and 2B values close⁵ to -170G. The latter value corresponds to an unpaired electron spin density in the $d_{x^2-y^2}$ of ca. 75% at the copper nucleus. This is based on a calculated value of 235G (for 2B) for unit population, as estimated from the wave functions for copper^{II} by Froese⁷.

However, since the e.s.r. spectra of copper^{II} complexes are especially informative, if ligand nuclei also exhibit hyperfine coupling to the unpaired electron, the absence of any such interaction from the calculated data (Table 7-3,4,5) probably limits further clarified information deducible from these results.

Giordano et al⁶ suggest that identification of the bonding groups may be obtained from the "P" value which is calculated from equation (9):

$$P = (A_{\parallel} - A_{\perp}) / \left[(g_{\parallel} - 2) - \frac{5}{14} (g_{\perp} - 2) - \frac{6}{7} \right] \quad (9)$$

i.e. for bonding to four sulphur atoms, these authors⁶ found that "P" lies in the range of 0.020-0.016 cm⁻¹ and for bonding to two nitrogens and two oxygens P = 0.026 cm⁻¹. Values of "P" calculated in the present study (Table 7-5) show a considerable variation.

	1.09	2.202	2.329	2.061
	1.09	2.203	2.331	2.076
	1.2	2.120	2.231	2.059
	1.2	2.110	2.215	2.059
	1.09	2.193	2.305	2.073
	1.09	2.206	2.331	2.067
	1.2	2.205	2.354	2.077

Error in measurement: $\delta g = \pm 0.005$

Table 7-3: Calculated "g" values in Cu^{II}-Schiff Base Complexes

Complexes	pH	g_{av} ± 0.005	$g_{ }$ ± 0.005	g_{\perp} ± 0.005
Cu(PLP) ₂ en, 4H ₂ O	1.09	2.206	2.332	2.082
"	5.2	2.129	2.240	2.067
Cu(PL) ₂ en, H ₂ O	1.09	2.204	2.332	2.084
"	5.2	2.112	2.212	2.061
Cu(PNen) ₂ (SO ₄) ₂ Cl ₂ , 5H ₂ O	1.09	2.203	2.332	2.090
"	5.2	2.205	2.353	2.090
"	5.2	2.147	2.320	2.065
Cu(PLPGly), 3H ₂ O	1.09	2.202	2.329	2.081
Cu ₂ (PLGly), 3H ₂ O	1.09	2.203	2.331	2.078
Cu(PLP) ₂ enOAc	5.2	2.120	2.231	2.069
Cu(PL) ₂ enOAc	5.2	2.110	2.215	2.059
CuPN, 2H ₂ O	1.09	2.193	2.335	2.075
Cu(PMP) ₂ acac, 5H ₂ O	1.09	2.206	2.331	2.077
"	5.2	2.205	2.334	2.078

Error in measurement $\delta g = \pm 0.005$

Table 7-4: Calculated "A" values in Cu^{II}-Schiff Base Complexes:

Complexes	pH	A _{av} ± 5G	A ± 5G	A _⊥ ± 5G
Cu(PLP) ₂ en, 4H ₂ O	1.09	40	136	8*
"	5.2	76	182	21
Cu(PL) ₂ en, H ₂ O	1.09	40	135	8*
"	5.2	85	198	26
Cu(PNen) ₂ (SO ₄) ₂ Cl ₂ , 5H ₂ O	1.09	40	136	10*
"	5.2	40	136	8*
"	5.2	70	162	21
Cu(PLPGly), 3H ₂ O	1.09	40	138	10*
Cu ₂ (PLGly), 3H ₂ O	1.09	40	136	10*
Cu(PLP) ₂ enOAc	5.2	76	186	20
Cu(PL) ₂ enOAc	5.2	85	194	30
CuPN, 2H ₂ O	1.09	52	135	10*
Cu(PMP) ₂ acac, 5H ₂ O	1.09	38	140	12
"	5.2	40	138	10*

*estimated from A_{||} and A_{av}

Error in measurement $\delta A = \pm 5$ Gauss

Table 7-5: E.S.R. Spectral Parameters of Cu^{II} -Schiff Base Complexes

Complexes	pH	corrected value*		orbital population	P cm ⁻¹
		A _{iso} G	2B G		
$\text{Cu}(\text{PLP})_2\text{en}, 4\text{H}_2\text{O}$	1.09	- 97	-172	0.73	0.0281
"	5.2	-117	-163	0.69	0.0267
$\text{Cu}(\text{PL})_2\text{en}, \text{H}_2\text{O}$	1.09	- 97	-170	0.72	0.0279
"	5.2	-122	-165	0.70	0.0269
$\text{Cu}(\text{PNen})_2(\text{SO}_4)_2\text{Cl}_2, 5\text{H}_2\text{O}$	1.09	- 98	-173	0.74	0.0283
"	5.2	-102	-178	0.76	0.0291
"	5.2	-120	-169	0.72	0.0277
$\text{Cu}(\text{PLPGly})_2, 3\text{H}_2\text{O}$	1.09	- 95	-174	0.74	0.0287
$\text{Cu}_2(\text{PLGly})_2, 3\text{H}_2\text{O}$	1.09	- 97	-174	0.74	0.0285
$\text{Cu}(\text{PLP})_2\text{enOAc}$	5.2	-118	-164	0.70	0.0268
$\text{Cu}(\text{PL})_2\text{enOAc}$	5.2	-122	-160	0.68	0.0259
$\text{CuPN}, 2\text{H}_2\text{O}$	1.09	-105	-166	0.70	0.0272
$\text{Cu}(\text{PMP})_2\text{acac}, 5\text{H}_2\text{O}$	1.09	- 97	-181	0.77	0.0296
"	5.2	- 97	-178	0.76	0.0291

*Corrected for orbital magnetism as described in the text according to the magnitude of A_{av} .

G = Gauss

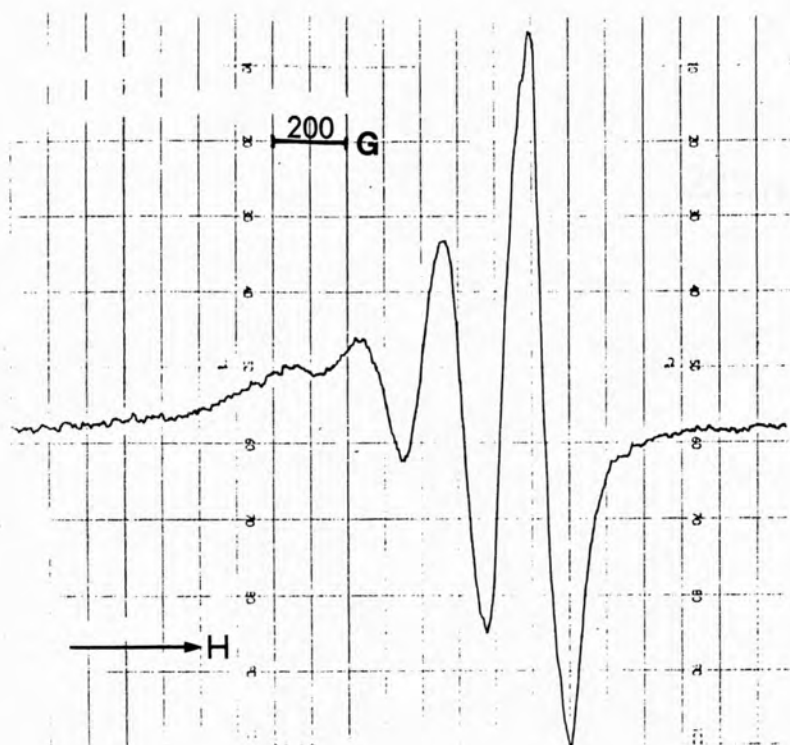


Fig. 7-27 E.s.r. spectrum of $\text{Cu(PL)}_2\text{en, H}_2\text{O}$ in buffer $\text{pH}=1.09$
at room temperature

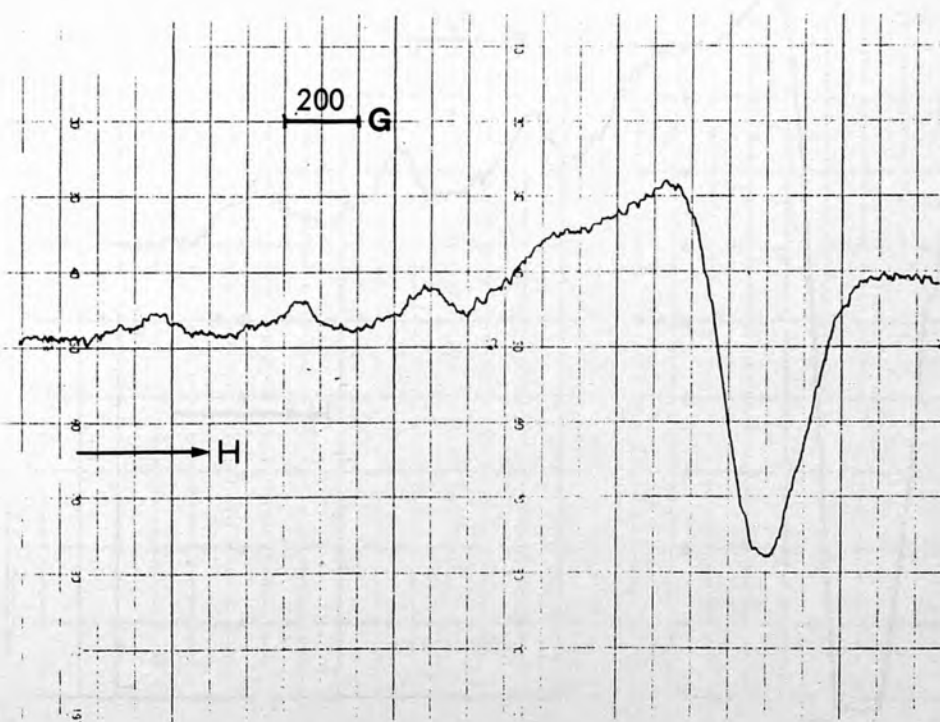


Fig. 7-28 E.s.r. spectrum of $\text{Cu(PL)}_2\text{en, H}_2\text{O}$ in buffer $\text{pH}=1.09$
at 110K

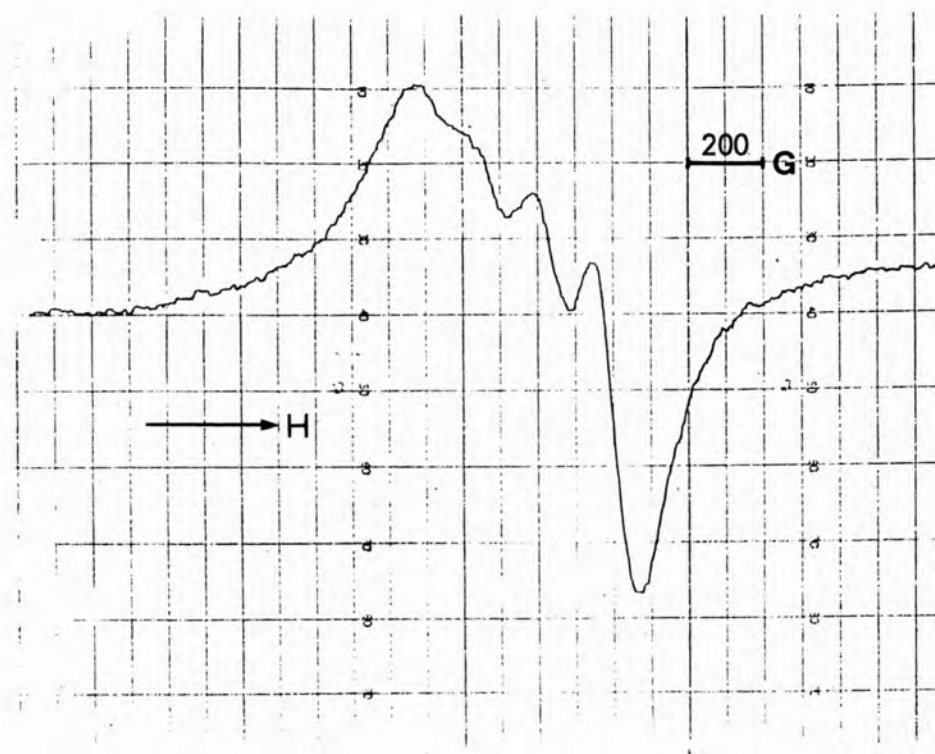


Fig. 7-29 E.s.r. spectrum of $\text{Cu}(\text{PLPGly}), 3\text{H}_2\text{O}$ in buffer $\text{pH}=1.09$
at -10°C

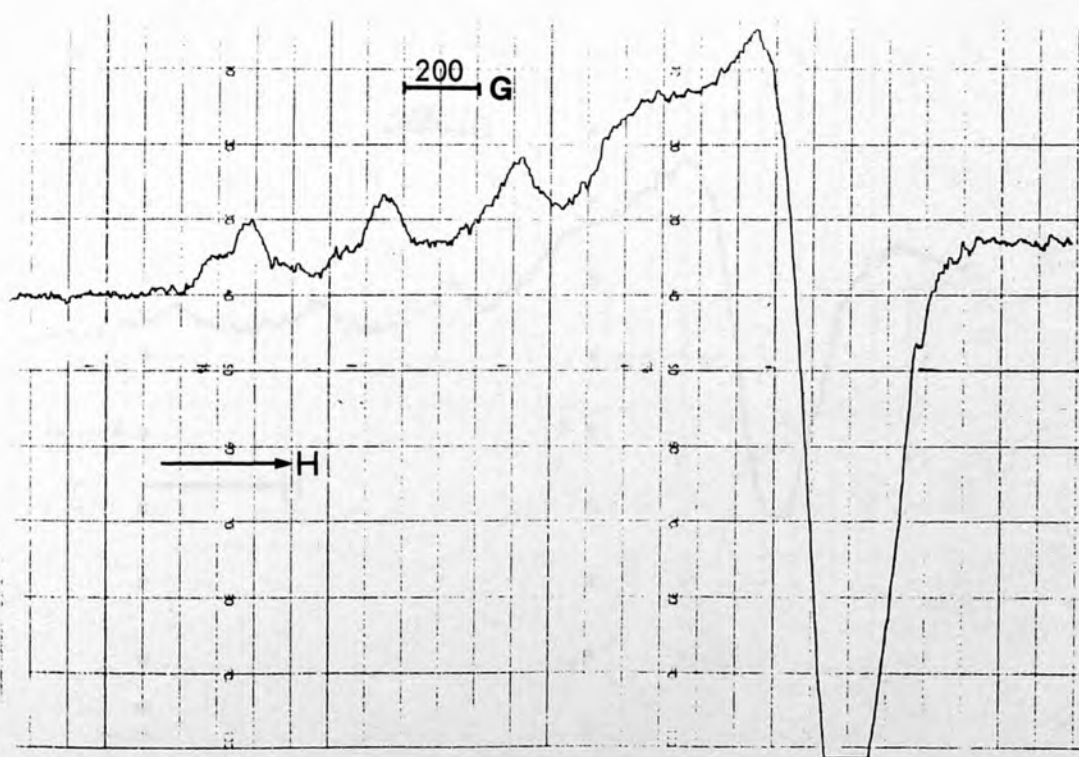


Fig. 7-30 E.s.r. spectrum of $\text{Cu}(\text{PLPGly}), 3\text{H}_2\text{O}$ in buffer $\text{pH}=1.09$
at 110K

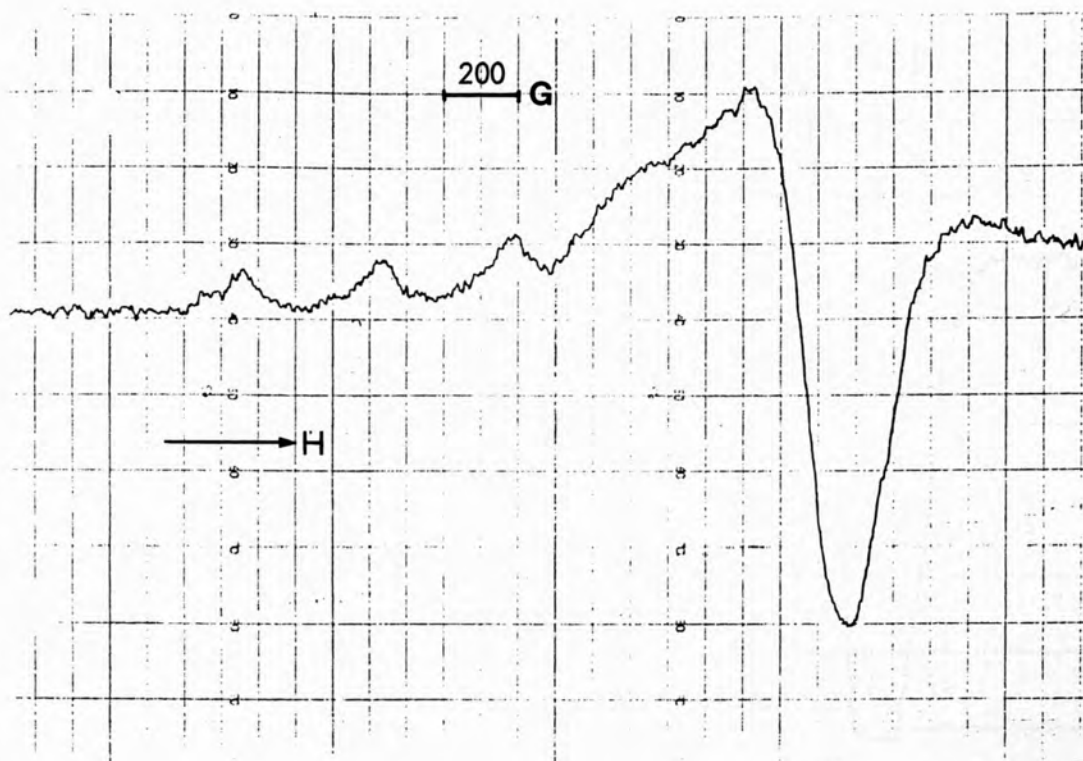


Fig. 7-31 E.s.r. spectrum of $\text{Cu(PMP)}_2\text{acac}, 5\text{H}_2\text{O}$ in buffer pH=1.09 at 110K

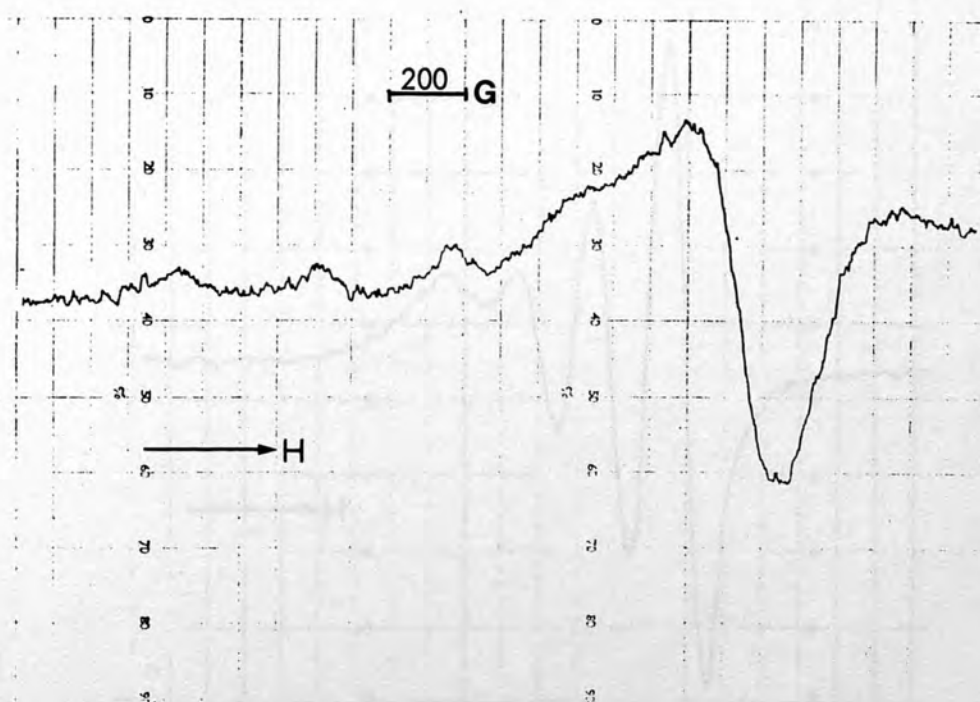


Fig. 7-32 E.s.r. spectrum of $\text{Cu(PMP)}_2\text{acac}, 5\text{H}_2\text{O}$ in buffer pH=5.20 at 110K

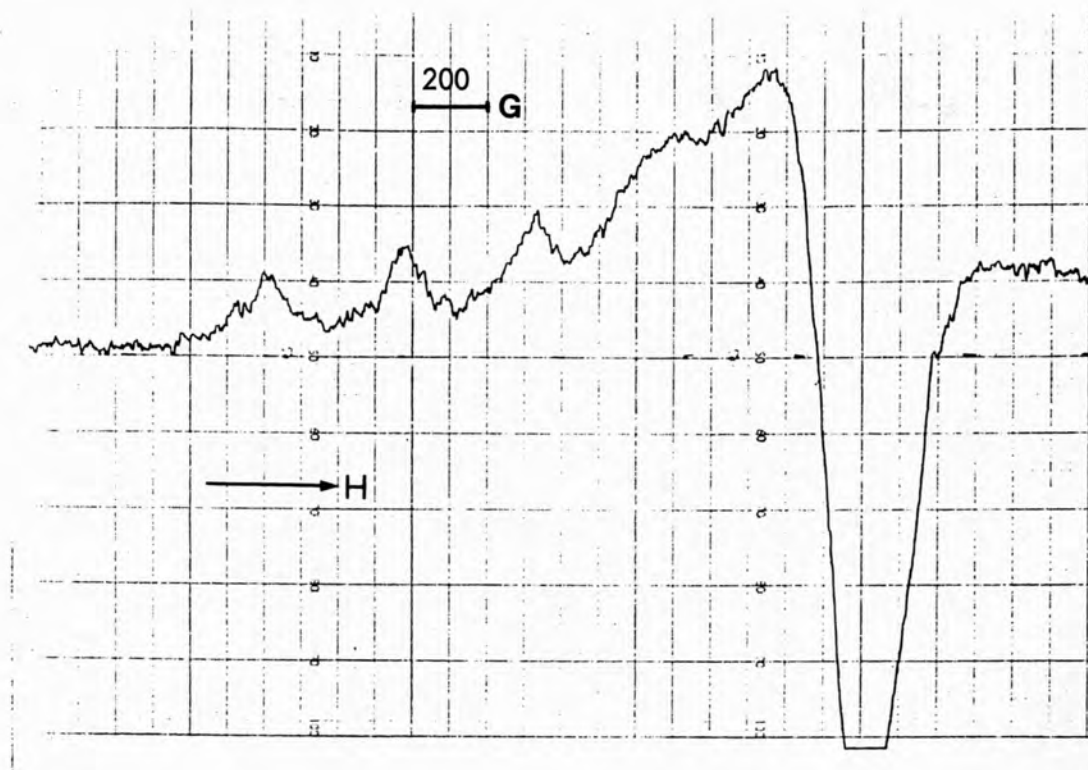


Fig. 7-33 E.s.r. spectrum of $\text{Cu}_2(\text{PLGly})_3 \cdot 3\text{H}_2\text{O}$ in buffer pH=1.09 at 110K

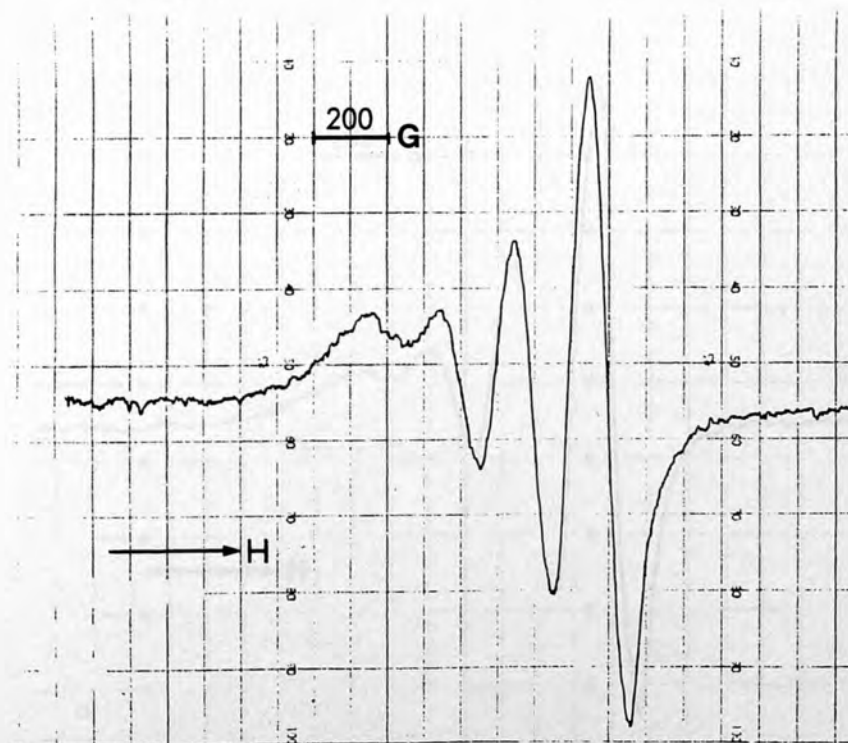


Fig. 7-34 E.s.r. spectrum of $\text{Cu}(\text{PLP})_2 \cdot \text{en} \cdot \text{OAc}$ in buffer pH=1.09 at room temperature

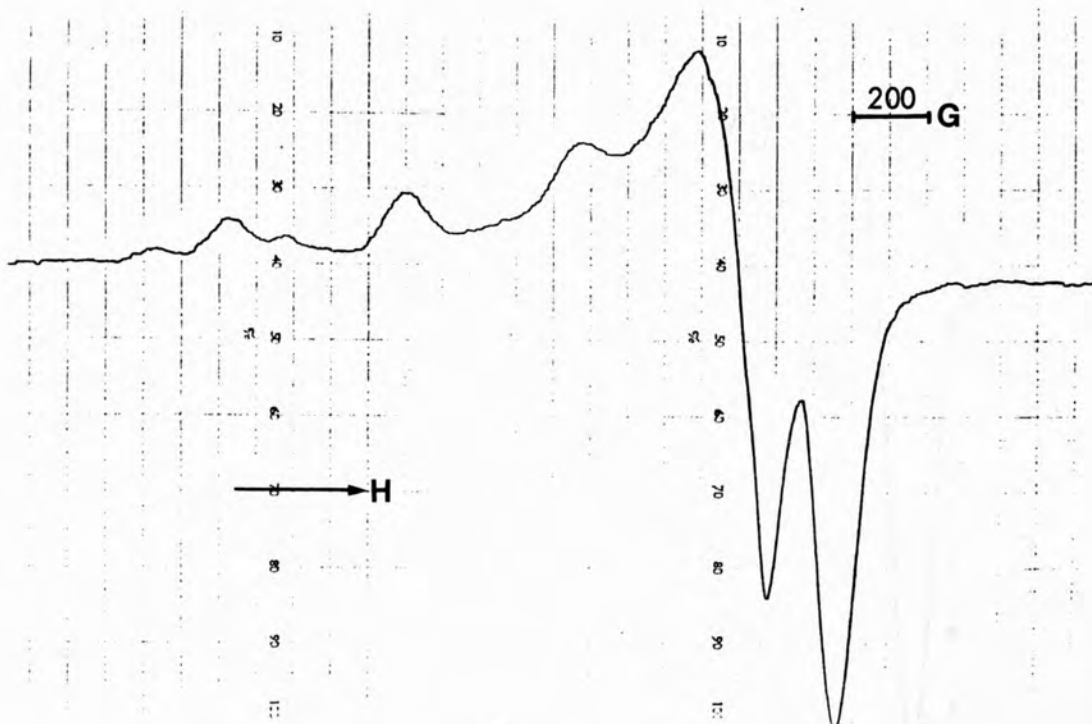


Fig. 7-35 E.s.r. spectrum of $\text{Cu(PLP)}_2\text{en OAc}$ in buffer $\text{pH}=1.09$ at 110K

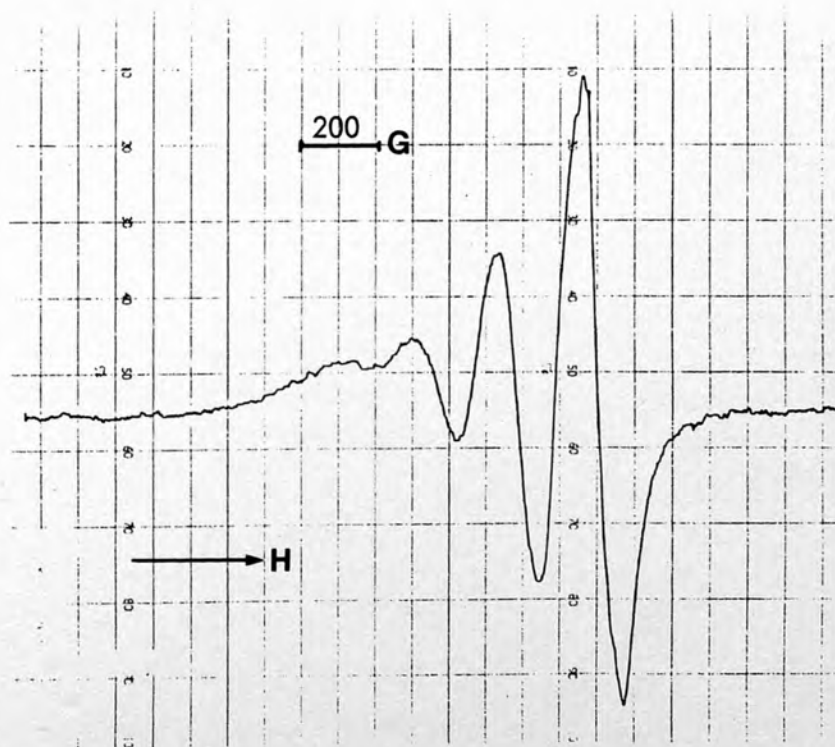


Fig. 7-36 E.s.r. spectrum of $\text{Cu(PL)}_2\text{en OAc}$ in buffer $\text{pH}=1.09$ at room temperature

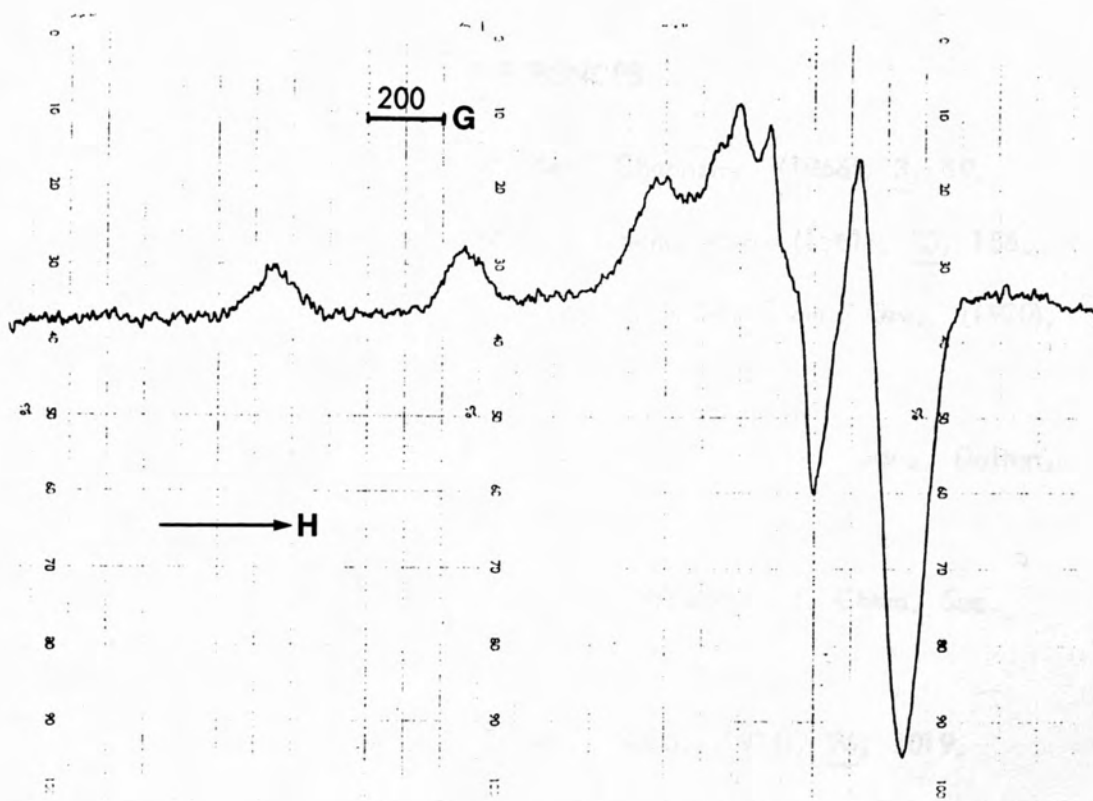


Fig. 7-37 E.s.r. spectrum of $\text{Cu(PL)}_2\text{en OAc}$ in buffer $\text{pH}=1.09$ at 110K

REFERENCES

1. B.R. McGarvey, *Transition Metal Chemistry*, (1966), 3, 89.
2. R. Neiman and D. Kivelson, *J. Chem. Phys.* (1961), 35, 156.
3. B.G. Hathaway and D.E. Billing, *Coordin. Chem. Rev.*, (1970), 5, 143-207.
4. S.H. Laurie, T. Lund and J.B. Raynor, *J. Chem. Soc., Dalton*, (1975), 1389.
5. M.C.R. Symons, D.X. West, J.G. Wilksons, *J. Chem. Soc. Dalton*, (1975), 1696.
6. R.S. Giordano and R.D. Berman, *JACS*, (1974), 96, 1019.
7. C. Froese, *J. Chem. Phys.*, (1966), 45, 1417.

CHAPTER 8

Kinetics of Transamination Reactions

The reaction of α -ketoglutarate with these metals is... with the copper reaction. The reaction is followed by a slower one to give spectrum (3). The species responsible for spectrum (3) is, as yet, unidentified. No spectra comparable to (3) appeared in reaction mixtures containing metal ions other than copper^{II} (Fig. 8-3, 4, 5).

The reference cell for these reactions was made up to contain the same concentration of α -ketoglutaric acid (α -KG) as in the reaction mixtures in order to compensate for its slight absorption.

Apparently sharp isobestic points were observed at "A" and "B" and another less sharp one at "C" (Fig. 8-1, 3).

¹Preliminary work on this reaction has been done by J. Matthews.

8.1 Reaction between Pyridoxamine Phosphate and α -Ketoglutaric Acid in the Presence of Copper^{II} Ion*

By the addition of pyridoxamine phosphate solution to a buffered solution containing α -ketoglutaric acid (α -KG) and copper^{II} ion in suitable concentration, two consecutive changes in spectrum took place (Fig. 8-1,2):

- a) The first change was from pyridoxamine phosphate alone to give the different species (2) and took place in about two hours.
- b) The second change was from spectrum (2) to spectrum (3), and took place over a period of twenty four hours.

This experiment has been carried out with some other metal ions (Fig. 8-3,4,5). The extent of the reactions with these metals is insufficient for their comparison with the copper reaction.

The initial reactions are followed by a slower one to give spectrum (3) (Fig. 8-1,2). The species responsible for spectrum (3) is, as yet, unidentified. No spectra comparable to (3) appeared in reaction mixtures containing metal ions other than copper^{II} (Fig. 8-3,4,5).

The reference cell for these reactions was made up to contain the same concentration of α -ketoglutaric acid (α -KG) as in the reaction mixtures in order to compensate for its slight absorption.

Apparently sharp isosbestic points were observed at "A" and "B" and another less sharp one at "C" (Fig. 8-1,2).

*Preliminary work on this reaction has been done by T. Matthews.¹

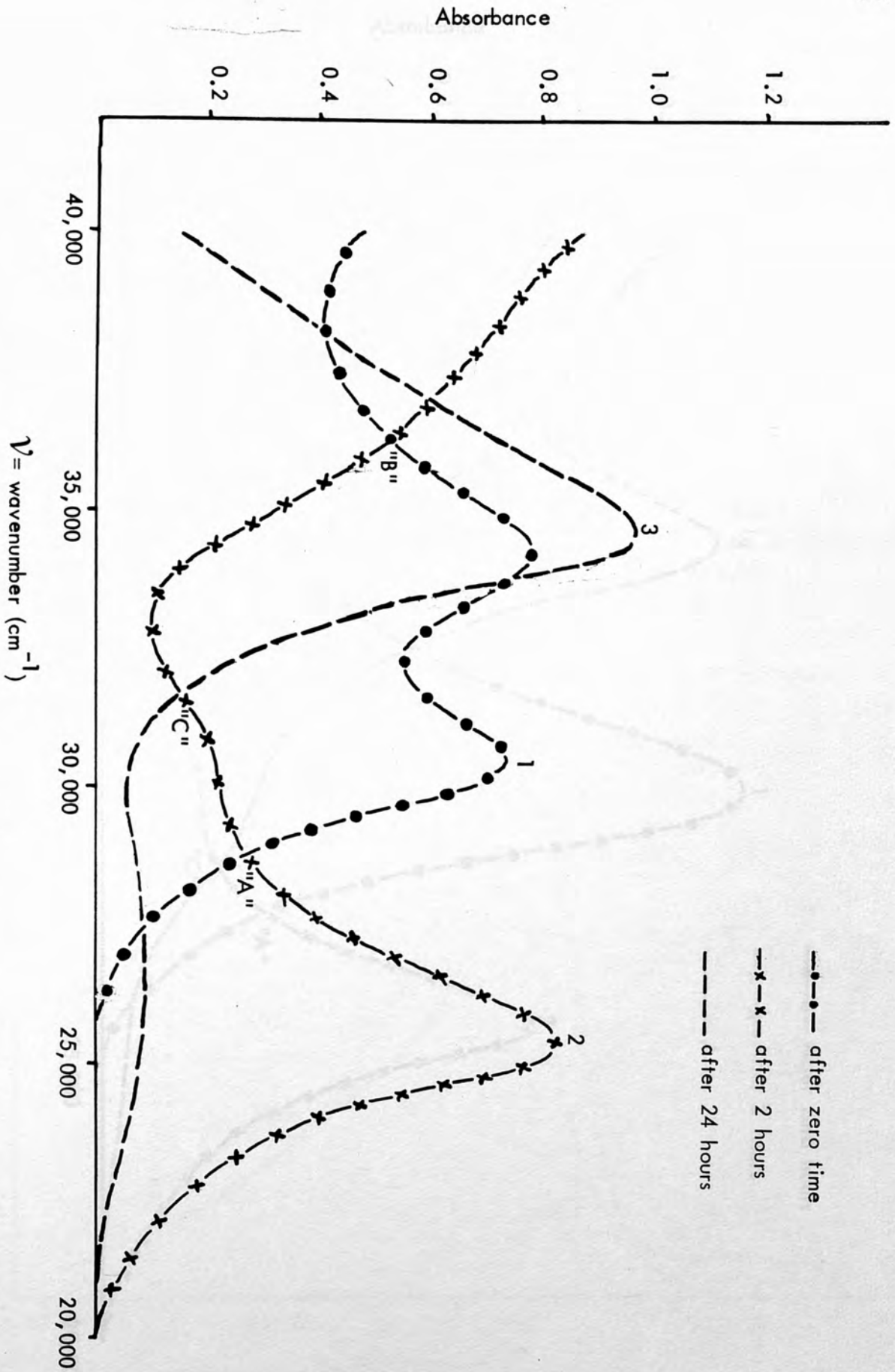


Fig. 8-1: Electronic absorption spectra of Cu^{II} -PMP-QKG in acetate buffer (pH = 3.98)

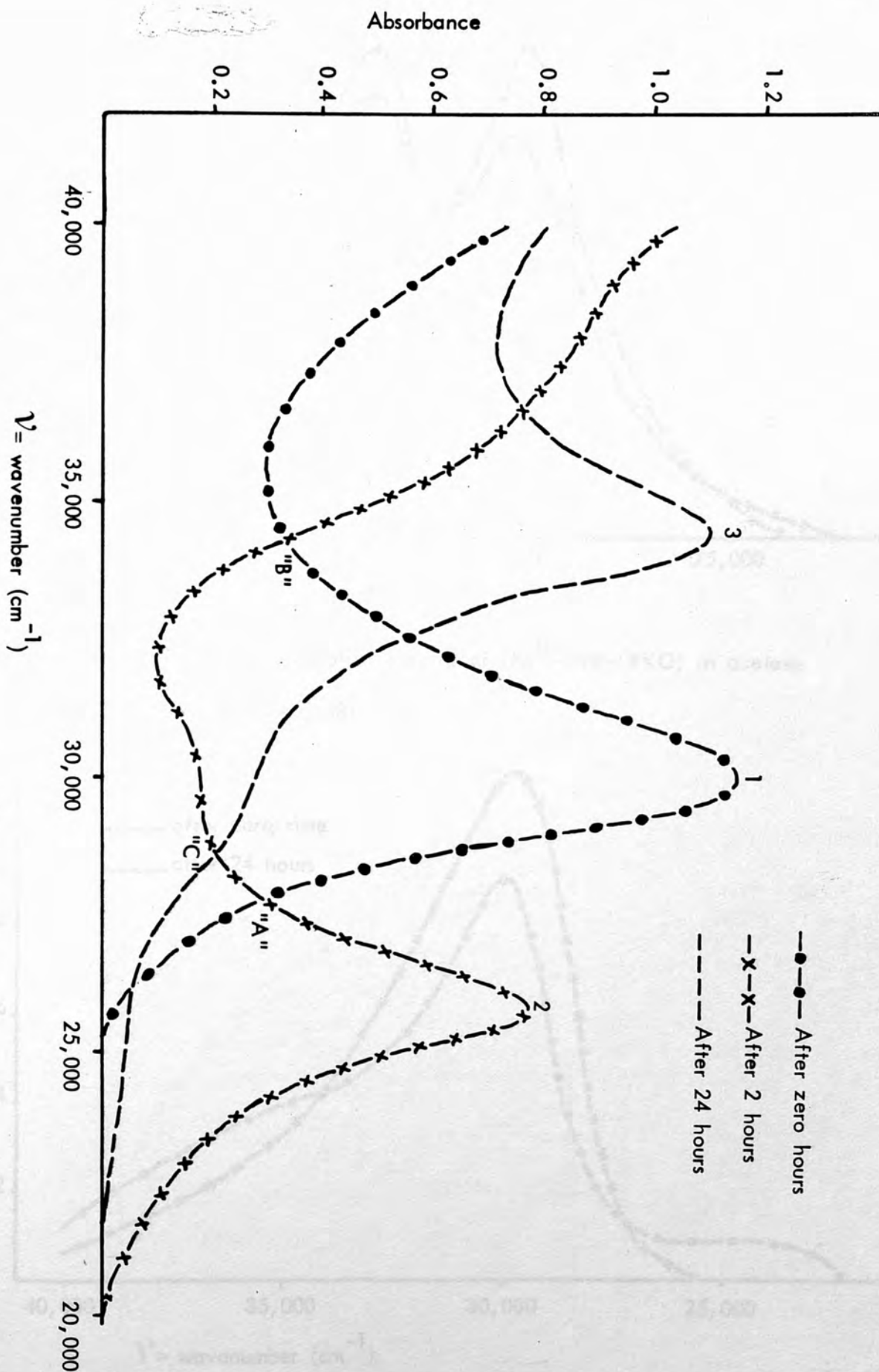


Fig. 8-2: Electronic absorption spectra of Cu^{II} -PMP-QKG in acetate buffer (pH = 5.20)

Fig. 8-4: Electronic absorption spectra of Cu^{II} -PMP-QKG in acetate buffer (pH = 5.20)

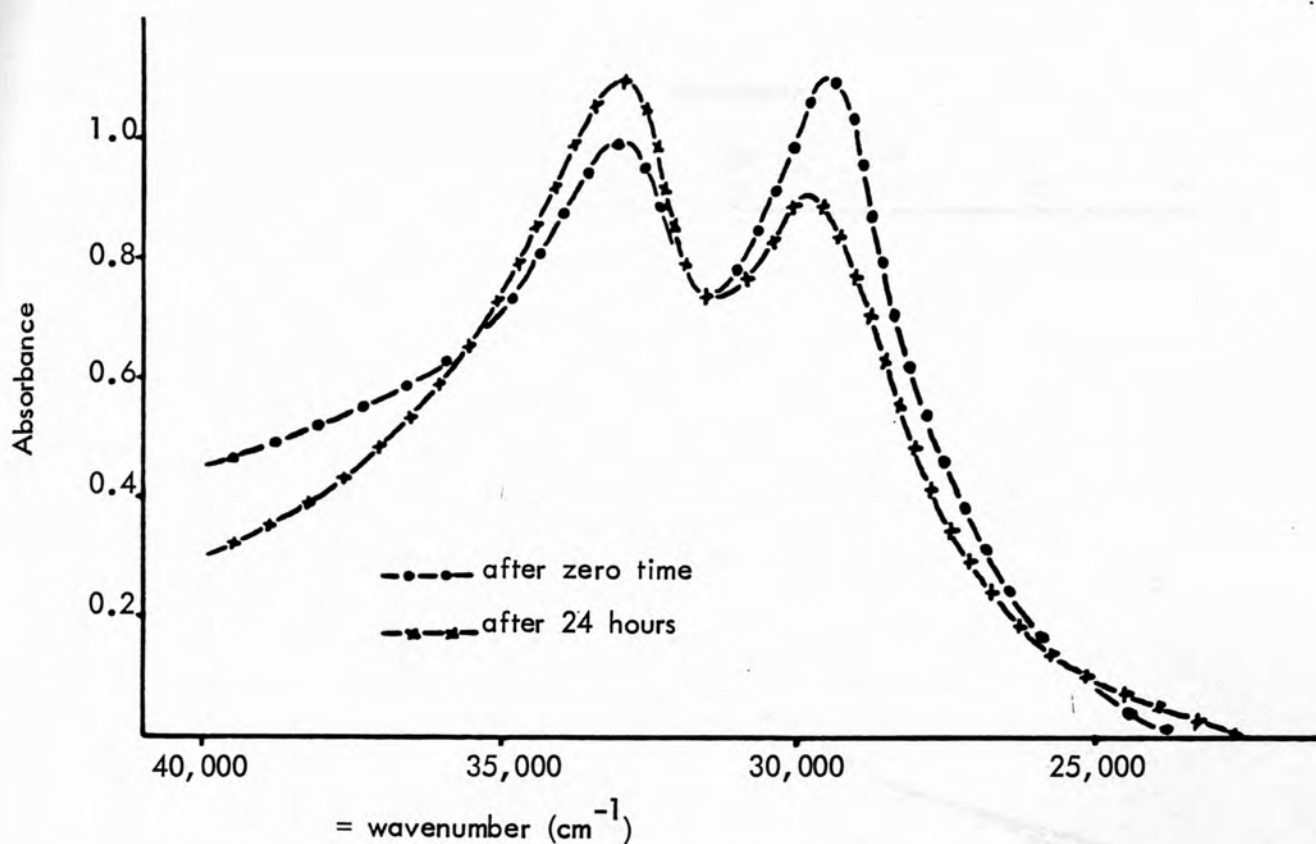


Fig. 8-3: Electronic absorption spectra of $(\text{Ni}^{\text{II}}\text{-PMP-}\alpha\text{KG})$ in acetate buffer (pH = 3.98)

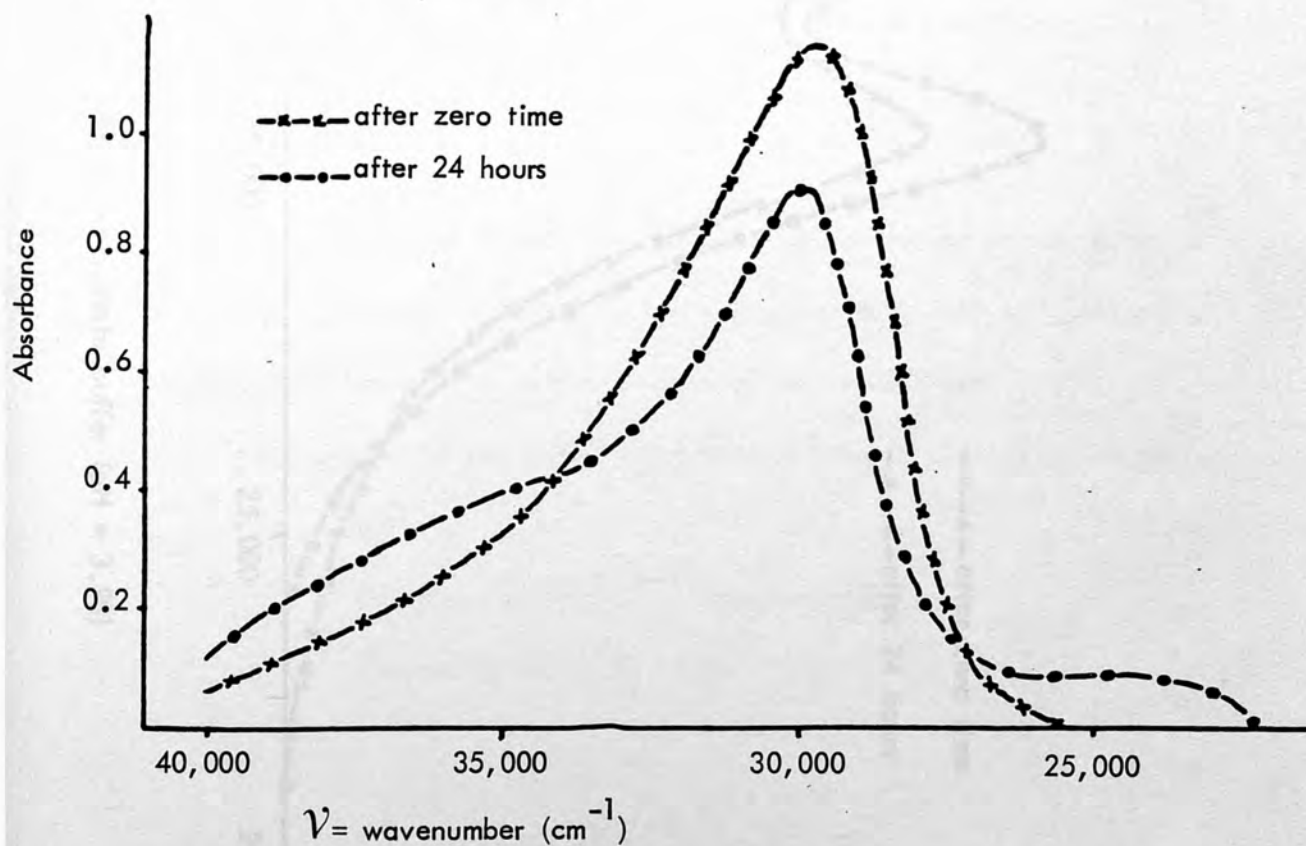


Fig. 8-4: Electronic absorption spectra of $(\text{Ni}^{\text{II}}\text{-PMP-}\alpha\text{KG})$ in acetate buffer (pH = 5.2)

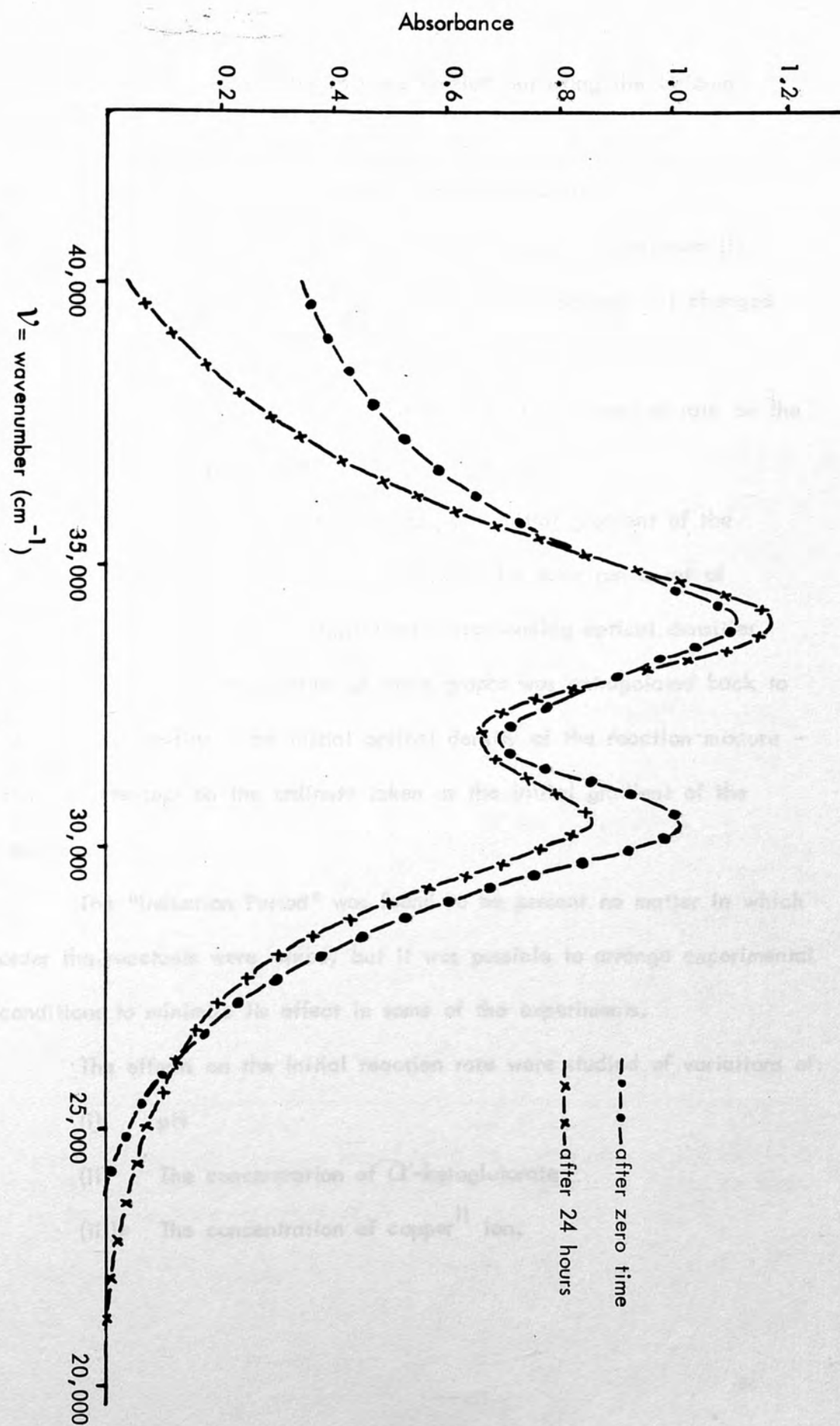


Fig. 8-5: Electronic absorption spectra of $(\text{Co}^{\text{II}}\text{-PMP-QKG})$ in acetate buffer ($\text{pH} = 3.98$)

8.2 Experimental

Single wavelength studies were carried out using the Unicam SP8-100 spectrophotometer.

Two main points were shown during the reaction:

- a) The first was an "Induction Period" during which spectrum (1) remained almost constant for a few minutes before spectrum (1) changed to spectrum (2).
- b) The second was an unusual dependence of the reaction rate on the concentration of copper ion.

Because of the "Induction Period" the initial gradient of the reaction was difficult to measure directly, so for each run a set of values dD/dt were plotted against their corresponding optical densities (D). The straight line portion of these graphs was extrapolated back to zero optical density - the initial optical density of the reaction mixture - and the intercept on the ordinate taken as the initial gradient of the reaction.

The "Induction Period" was found to be present no matter in which order the reactants were mixed, but it was possible to arrange experimental conditions to minimise its effect in some of the experiments.

The effects on the initial reaction rate were studied of variations of:

- (i) pH
- (ii) The concentration of α -ketoglutarate
- (iii) The concentration of copper^{II} ion.

8.2.1 The Effect of Variation of the pH on the Initial Reaction Rate

The concentrations* of the reactants were α -KG = 16 mM, PMP = 0.3 mM and Cu^{II} = 0.6 mM. The pH was varied from 2.4-5.2 using acetate buffer and 5.2-12.5 using the reactants and sodium hydroxide as buffer.

Typical plots of dD/dt against D are shown in Fig. 8-6, the intercepts of which have the initial reaction gradients. These were plotted against pH in Fig. 8-7.

A rate maximum was observed at about pH = 5, and a minimum at about pH 10.5, followed by a further increase in rate up to pH 13.0.



*Note: These concentrations should be the concentration of the reactants in the cell, therefore the concentration of the reactants should be made up ten times more concentrated.

Fig. 8-6. Graph of dD/dt against optical density at various pH values.

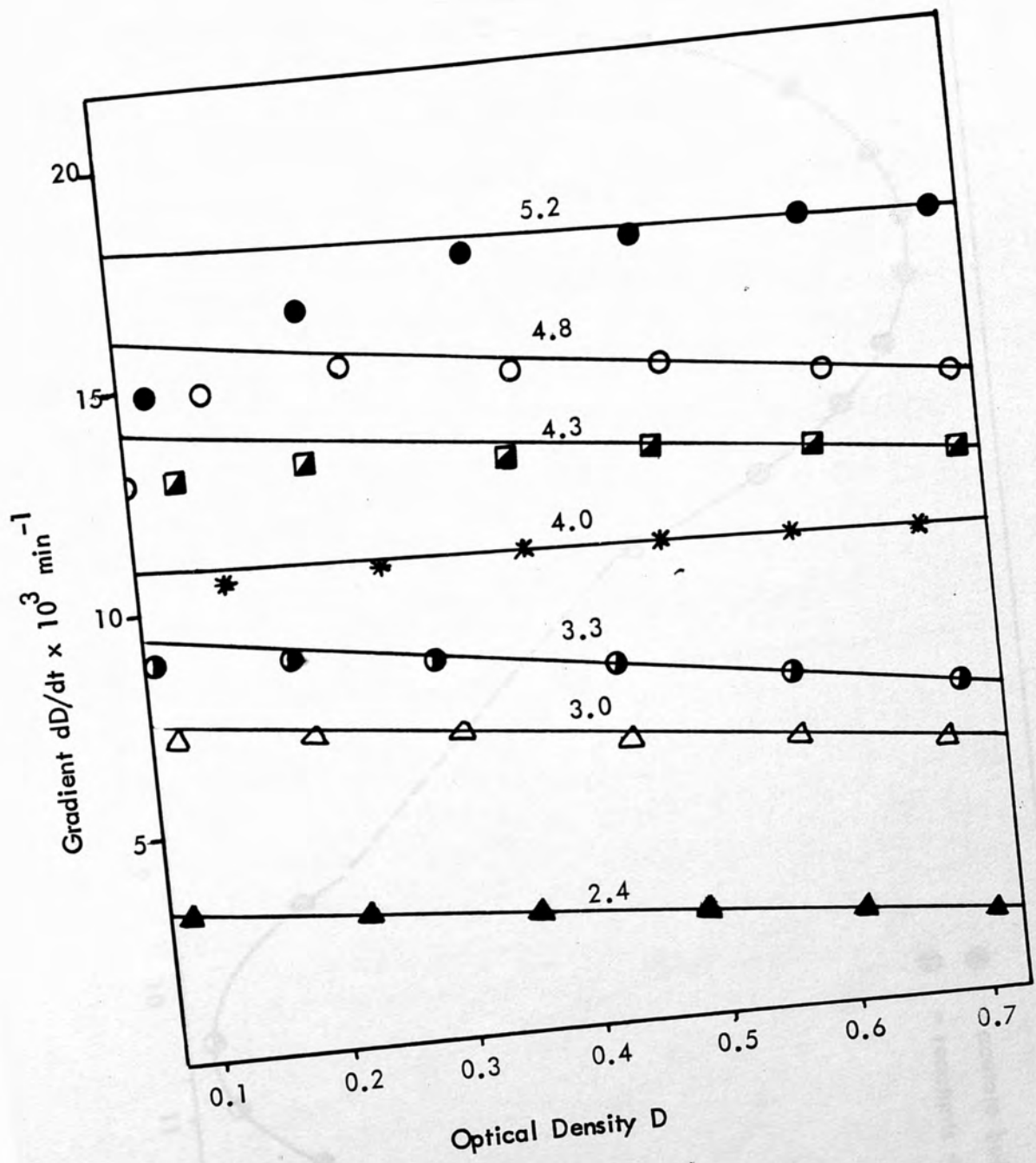


Fig. 8-6 Graph of dD/dt against optical density at various pH values

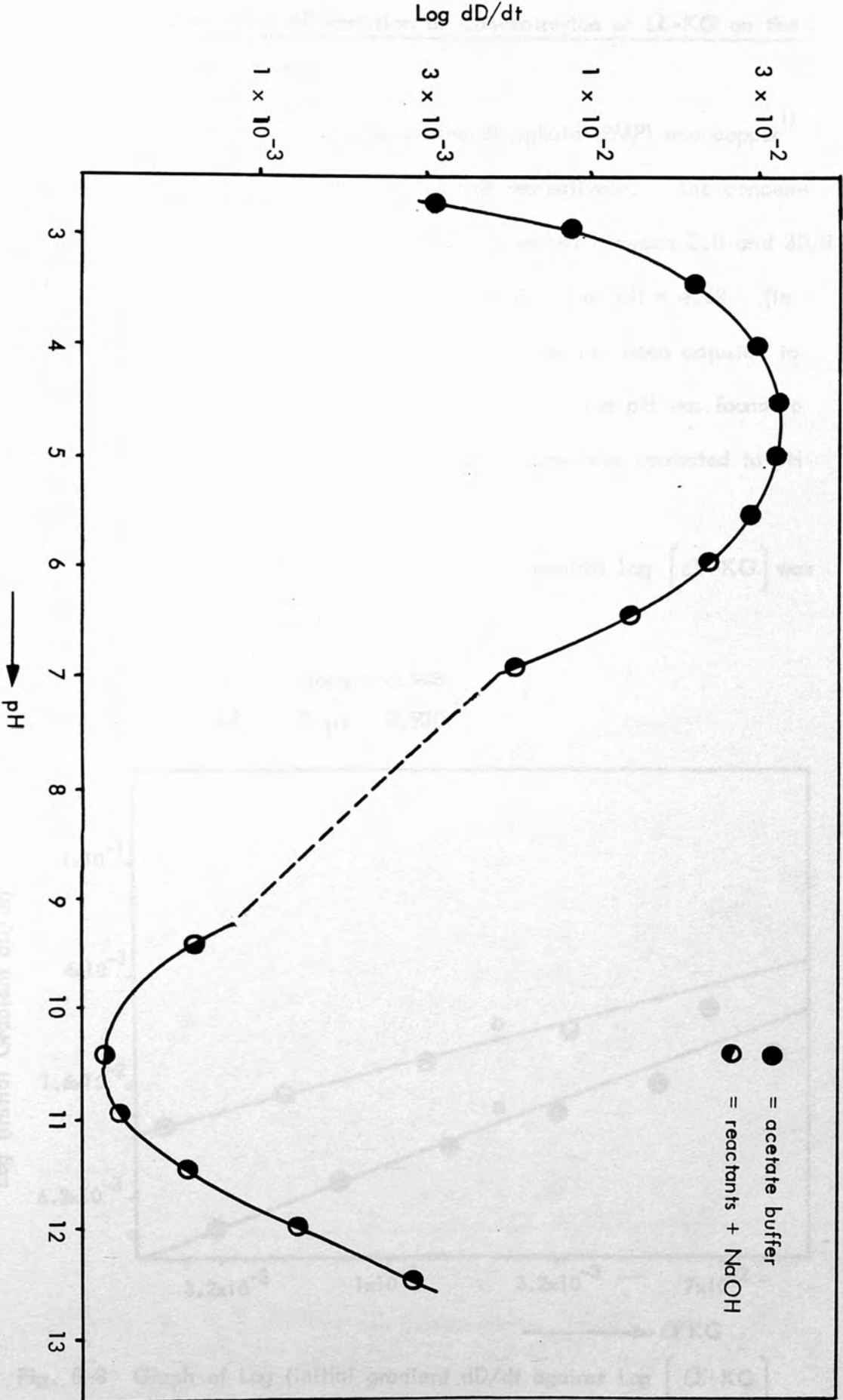


Fig. 8-7: Graph of Log Initial Gradient/pH

8.2.2 The Effect of Variation of Concentration of α -KG on the Initial Reaction Rate

The concentrations of pyridoxamine phosphate (PMP) and copper^{II} were kept constant at 0.3 mM and 0.6 mM respectively. The concentration of α -ketoglutaric acid (α -KG) was varied between 2.0 and 20.0 mM at pH = 3.98 and between 3.2 and 100.0 mM at pH = 4.62. (In the former case the pH of the α -KG solution had not been adjusted to that of the buffer and so in some reaction mixtures the pH was found to have changed. In these cases the initial gradient was corrected to pH 3.98 (Fig. 8-7).

A graph of Log (initial gradient dD/dt) against Log [α -KG] was plotted at each pH (Fig 8-8):

$$a = \text{pH } 3.98 \quad \text{Slope} = 0.948$$

$$b = \text{pH } 4.62 \quad \text{Slope} = 0.930$$

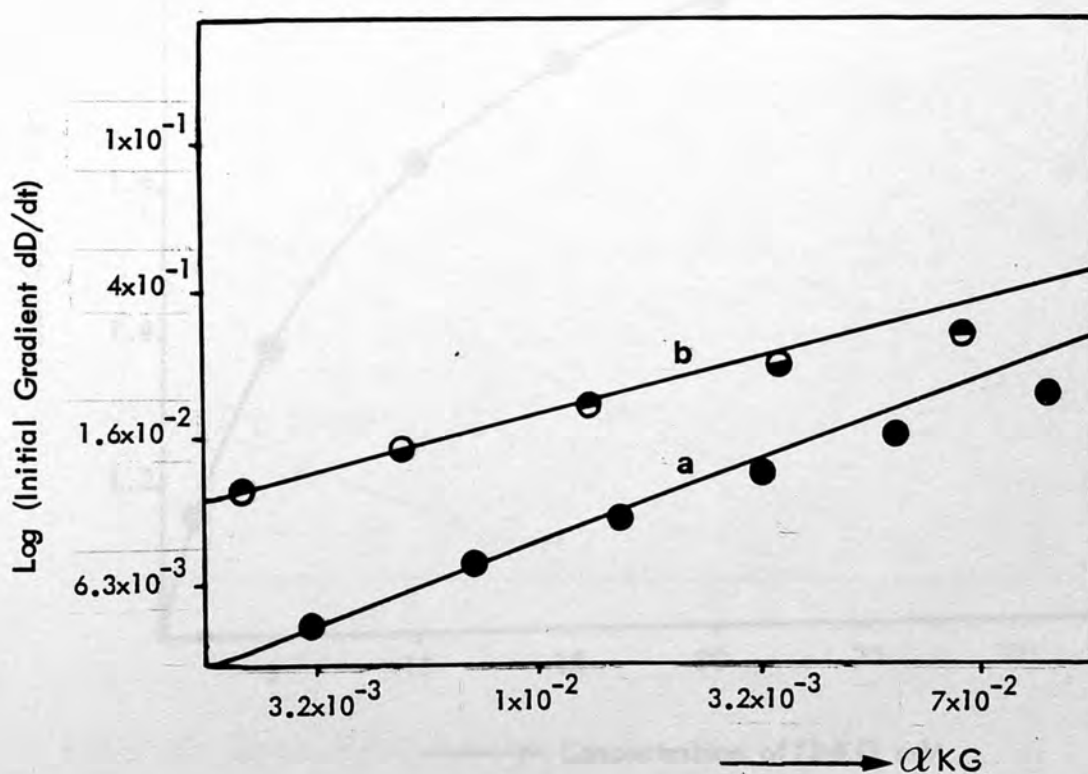


Fig. 8-8 Graph of Log (initial gradient dD/dt) against Log [α -KG]

The slopes of these graphs were 0.95 at pH 3.98 and 0.93 at pH 4.62. The points at higher concentration can be seen to fall increasingly short of the straight line relationship for those at low concentrations of α -KG. This reflects the co-ordination of the copper by the α -KG at low Cu^{+2}/α -KG ratios.

The final optical density of the reaction mixture was very dependent on the concentration of α -KG, indicating that an equilibrium is involved. A graph of final optical density against concentration of α -KG is shown below (Fig. 8-9) for the runs at pH 3.98.

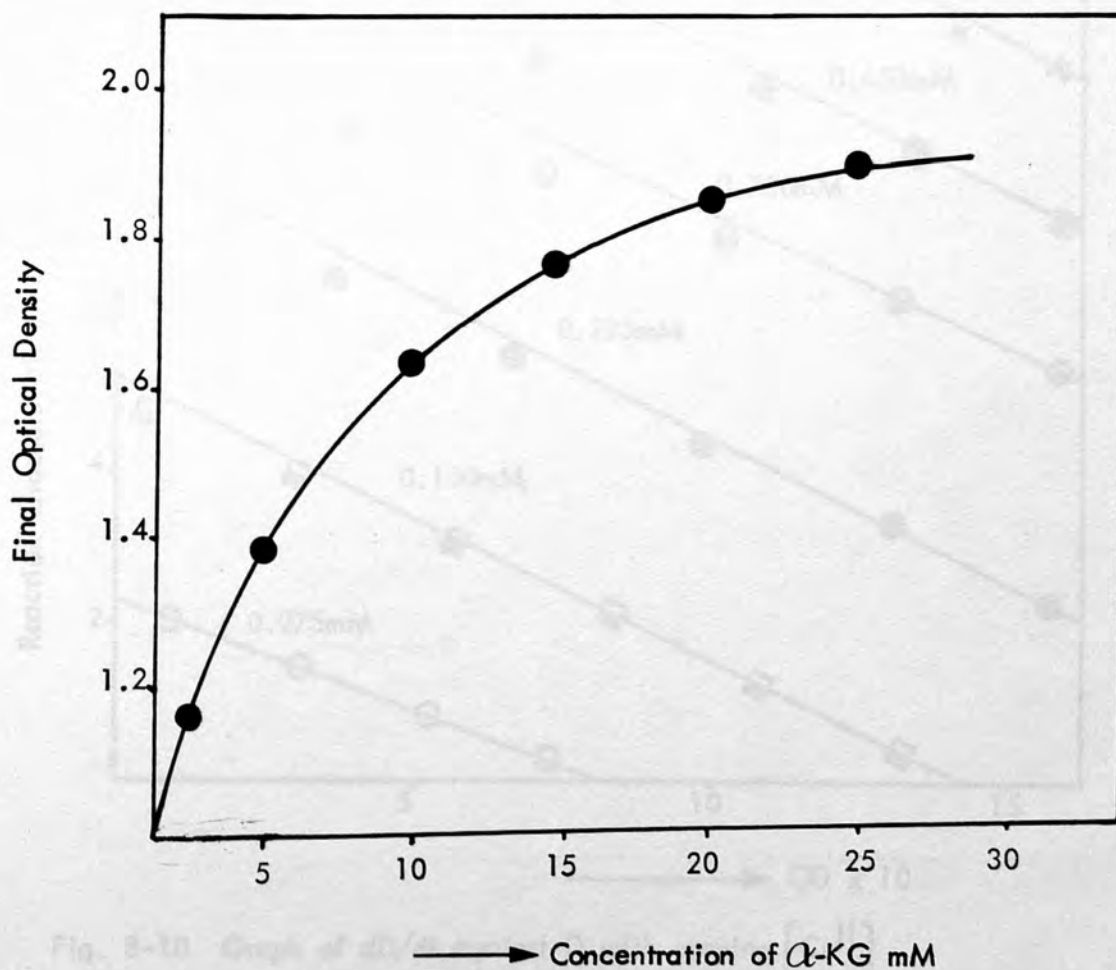


Fig. 8-9 Graph of final OD against $[\alpha\text{-KG}]$

8.2.3 The Effect of Variation of the Concentration of Copper^{II}

Ion on the Initial Reaction Rate:

At the beginning of this experiment it was very difficult to find out the exact amount of the concentration of pyridoxamine phosphate (PMP) and the α -ketoglutaric acid (α -KG) which can minimise the interference of the "Induction Period" over a wide range of copper^{II} concentration. The effect on the graphs of dD/dt against D of too high concentration of pyridoxamine phosphate (3.0 mM) is shown in Fig. 8-10. The concentration of α -ketoglutarate was 8.0 mM and the pH = 4.50.

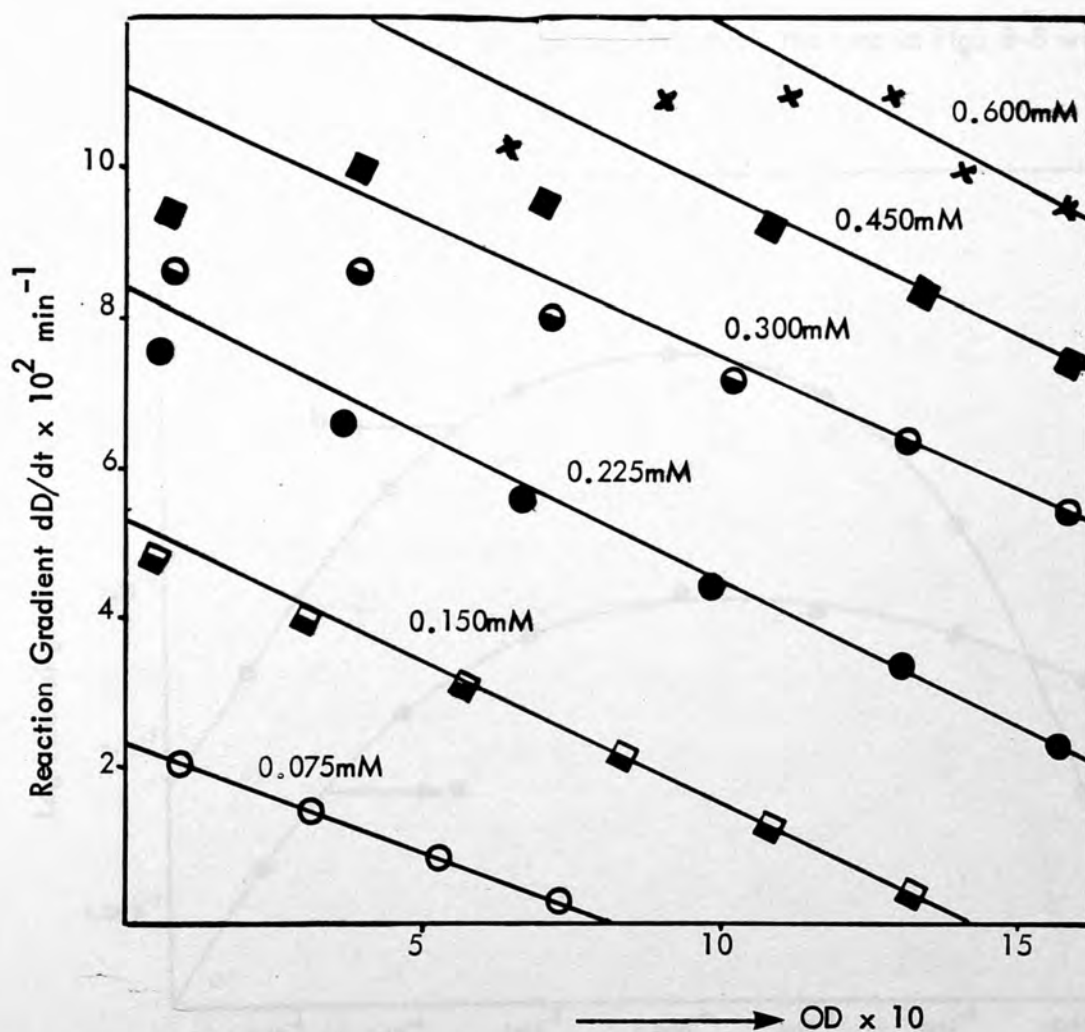


Fig. 8-10 Graph of dD/dt against D with varying $[Cu^{II}]$

At higher concentrations of Cu^{II} than 0.3 mM the induction period became very important in that no straight line portion of the graph dD/dt against D was observed (Fig. 8-10) before the next stage of the reaction became apparent.

However, satisfactory results were obtained for the two sets of experimental conditions:

- a) 0.3 mM PMP and 16 mM α -KG at pH = 4.22
- b) 0.3 mM PMP and 8 mM α -KG at pH = 4.42

A graph of $\text{Log}(\text{initial gradient } dD/dt)$ against $\text{Log}[\text{Cu}^{\text{II}}]$ was plotted and it was found that the maximum occurs at Cu^{II} concentration corresponding to a ratio of PMP: Cu^{II} of 1:2. This was the ratio at which the runs in Fig. 8-8 were carried out.

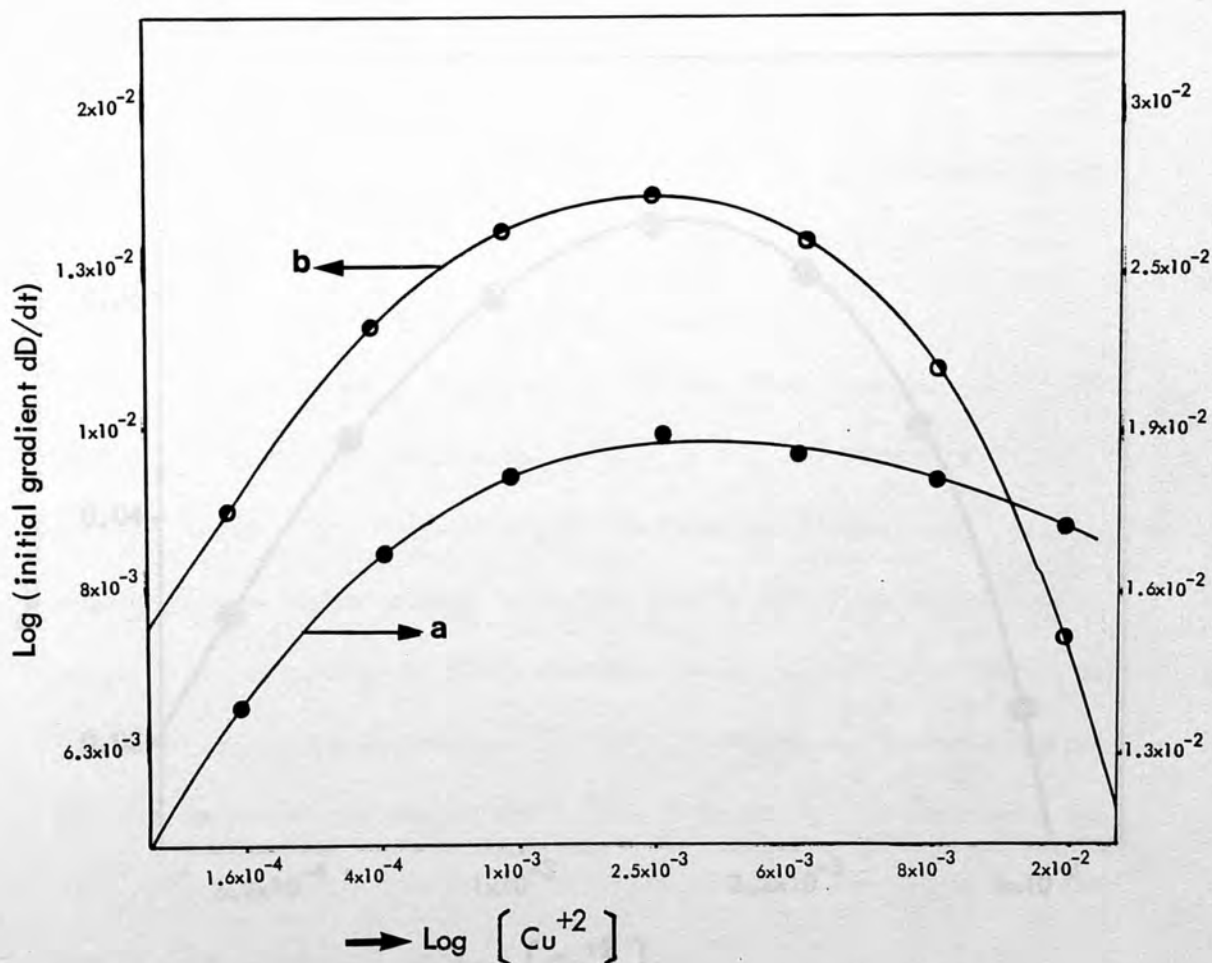


Fig. 8-11 Graph of $\text{Log}(\text{initial gradient } dD/dt)$ against $\text{Log}[\text{Cu}^{+2}]$

8.3 Kinetics of the Isosbestic Point

At low concentrations of pyridoxamine phosphate (PMP) it is possible to get three isosbestic points (Fig. 8-1,2). Two sharp isosbestic points "A" and "B" and another less sharp one at "C". Here, isosbestic point "A" was studied more closely at a single wavelength and it was found that the optical density first decreased by a small amount before finally becoming steady. The time taken for this initial decrease corresponded closely to that of the induction period, indicating some relationship between the two. The extent of decrease depended on the concentration of Cu^{II} . The relationship is shown in Fig. 8-12. The concentration of PMP = 0.6 mM, α -KG = 8.0 mM and pH = 3.96.

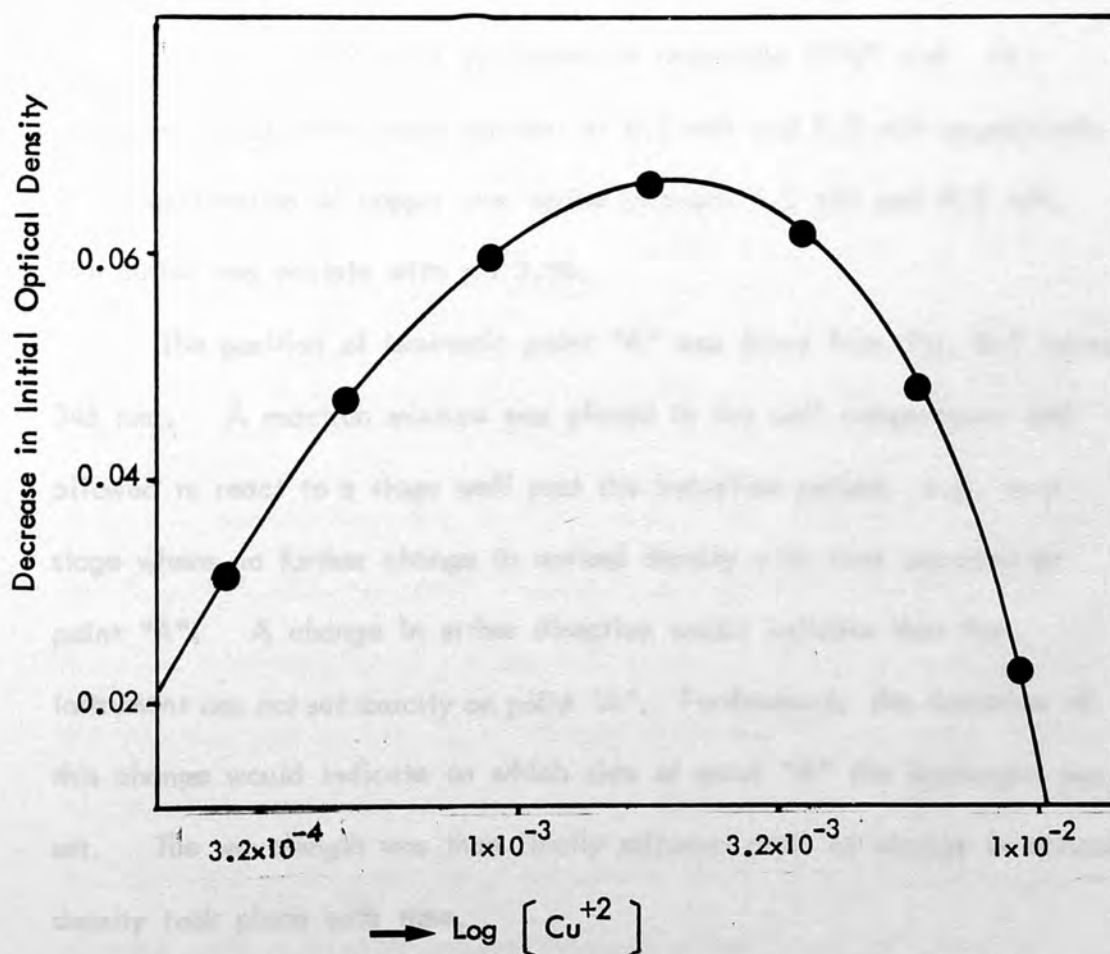


Fig. 8-12 Graph of Decrease in Initial OD at Isosbestic Point "A" against Log [Cu²⁺]

There is an obvious similarity between Fig. 8-11 and Fig. 8-12. In both cases maxima occur at a ratio of Cu:PMP of 2:1.

It was found that the extent of decrease in absorbance was also dependent upon the concentration of α -KG. By studying the change in absorbance at point "A" during the "Induction Period" as a function of α -KG concentration, it was found, however, that the changing concentration of α -KG affects the isosbestic point and caused a slight movement in the position of "A", so that there was interference from the transamination step. The quantitative interpretation of these results was therefore prevented.

The measurements at isosbestic point "A" were carried out as described below:

The concentrations of pyridoxamine phosphate (PMP) and α -ketoglutaric acid were kept constant at 0.6 mM and 8.0 mM respectively. The concentration of copper was varied between 0.2 mM and 9.0 mM. The buffer was acetate with pH 3.96.

The position of isosbestic point "A" was found from Fig. 8-1 (about 345 nm). A reaction mixture was placed in the cell compartment and allowed to react to a stage well past the induction period; e.g. to a stage where no further change in optical density with time occurred at point "A". A change in either direction would indicate that the instrument was not set exactly on point "A". Furthermore, the direction of this change would indicate on which side of point "A" the instrument was set. The wavelength was then finally adjusted until no change in optical density took place with time.

The results are shown in Table 8-1. The initial optical density of the reactions mixtures was recorded. The initial optical densities are compared with the calculated initial optical densities found from a set of readings on solutions 0.6 mM pyridoxamine phosphate (PM) and various concentrations of Cu^{II} . To these readings were added the optical density of an 8.0 mM solution of α -ketoglutaric acid (OD of 8.0 mM α -KG = 0.145)(pH = 3.96).

Table 8-1 Optical Density of Cu^{II} at various concentrations

Cu^{II} M. $\times 10^4$	Initial OD D_o	Final OD D	$D_o - D$	Calc. Initial OD D'_o	$D'_o - D$
0.00	1.702	1.696	0.006	1.745	0.043
2.0	1.683	1.658	0.025	1.724	0.041
4.0	1.668	1.630	0.038	1.698	0.030
8.0	1.634	1.589	0.045	1.653	0.019
12.0	1.610	1.551	0.059	1.622	0.012
30.0	1.481	1.443	0.038	1.460	-0.021
60.0	1.359	1.335	0.024	1.310	-0.049
90.0	1.284	1.275	0.009	1.202	-0.082

A maximum occurs in $D_o - D$ at a Cu^{II} :PMP ratio of 2:1 (Fig. 8-12). By comparison with Fig. 8-11 it would seem that this ratio gave the maximum concentration of the reactive species. The concentration of this reactive species must be a function of the equilibrium constant of its formation and of the concentration of the reactants. Also, this equilibrium constant (and hence the concentration of the reactive species) must be small to account for the observed linear relationship between the

reaction rate and the concentration of α -KG (Fig. 8-8). The departure from linearity at higher concentrations of α -KG supports this view.

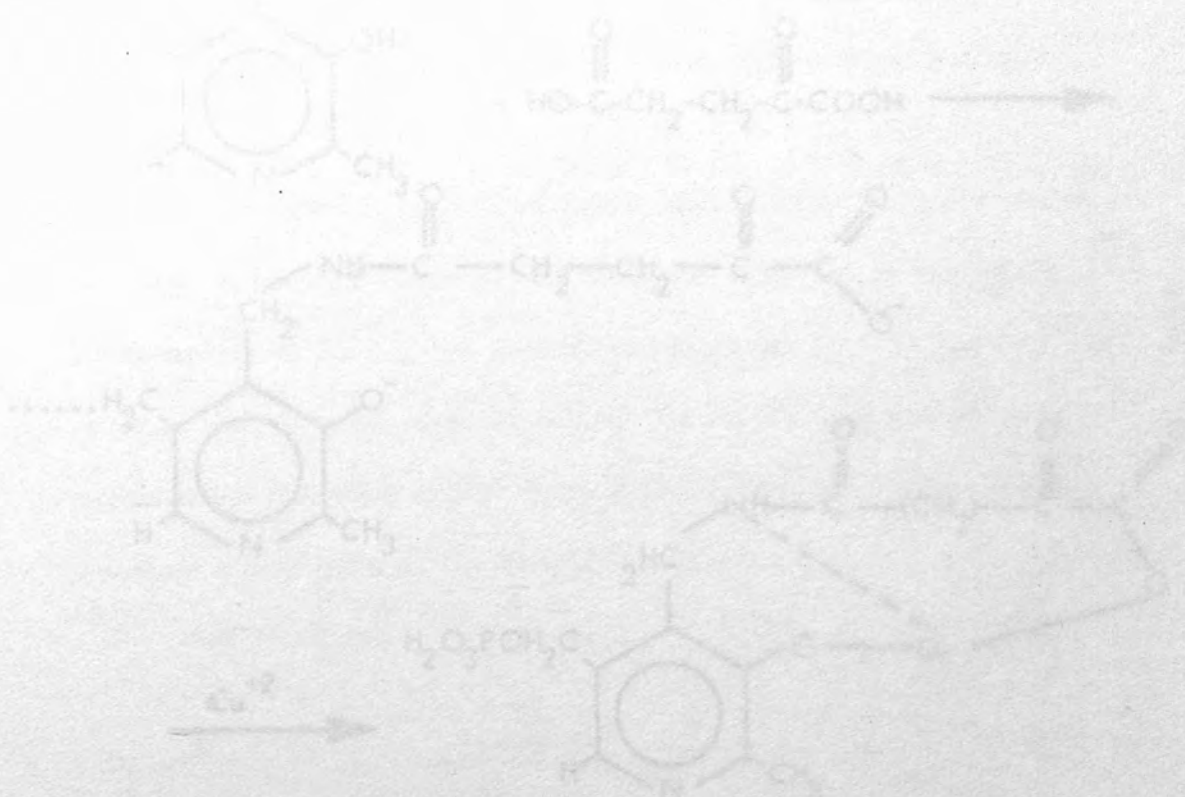


Fig. 8-13: Reaction between Pyridoxamine Phosphate and α -Ketoglutaric Acid in the presence of Ca^{2+} ion.

8.4 Discussion

When pyridoxamine phosphate (PMP), α -ketoglutaric acid and copper^{II} ions are mixed in aqueous solution, the spectrum changes from that of PMP (1) to that of a new species (2) which is identified with a copper-Schiff base complex, (spectral change 1 \longrightarrow 2 in Fig. 8-1,2). This change, which takes place in 2 hours and shows sharp isosbestic points at "A" and "B", is followed by a slower one (2 \longrightarrow 3) which takes place over 24 hours and shows a less sharp isosbestic point at "C". The species responsible for the spectrum (3) in Fig. 8-1,2 is as yet unidentified. All three reactants (PMP + α -KG + Cu^{+2}) are necessary to give the required products, absence of any one of the reactants leads to the formation of different products.

A possible reaction which takes place is as follows:

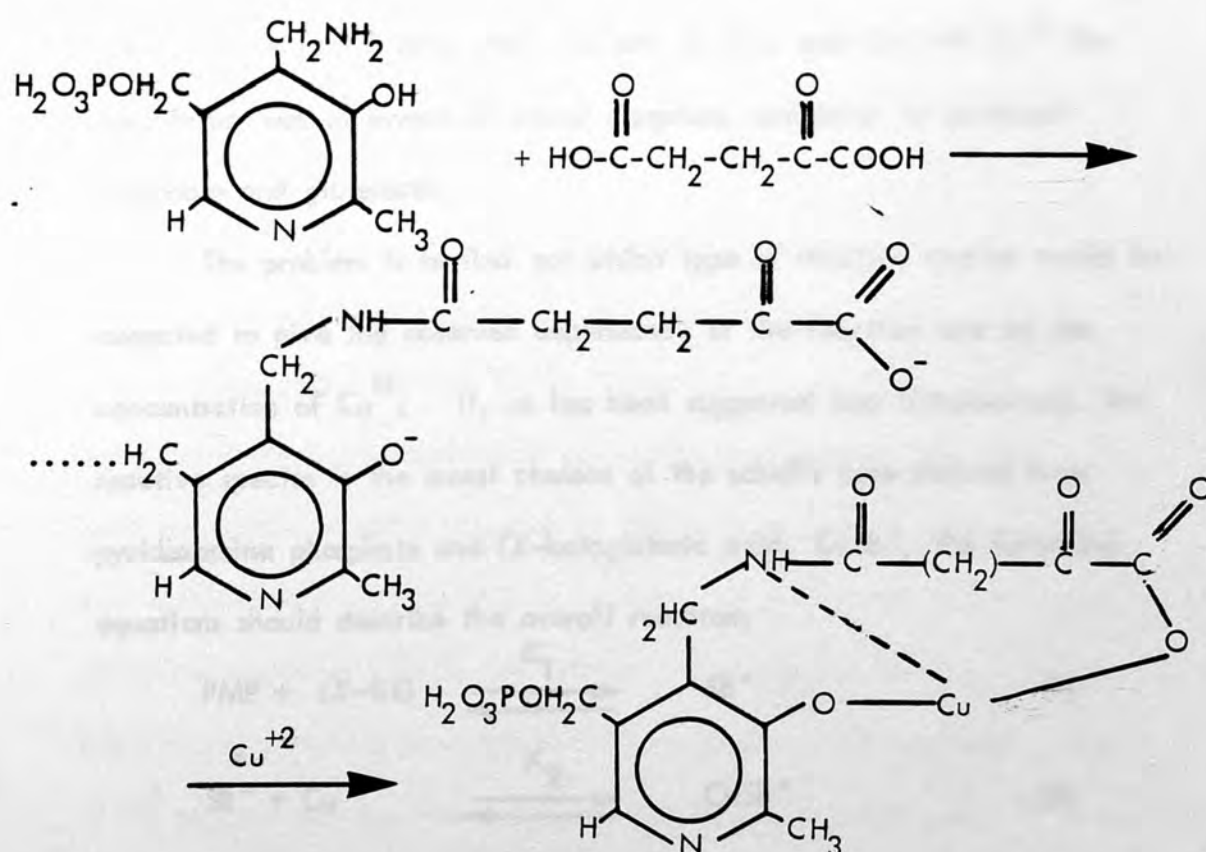


Fig. 8-13: Reaction between Pyridoxamine Phosphate and α -Ketoglutaric Acid in the presence of Cu^{II} Ion.

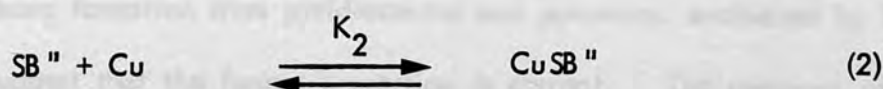
In the above figure (8-13) Cu^{II} is involved only as a trap for the schiff base (S.B.)

According to the results which were explained earlier (the ratio of PMP:Cu is 1:2), the second copper most likely attaches to the ring nitrogen.

The dependence of the rate of formation of the species on the concentration of Cu^{II} also indicates that copper acts as a reaction-promoting species. If so, Cu^{II} is much more active than any other metal ions used as no spectrum comparable to (3) appeared when Ni^{II} , Co^{II} and Zn^{II} were present (Fig. 8-3,4,5).

Copper^{II} ion was found to promote strongly the transamination reaction of pyridoxamine phosphate and α -ketoglutaric acid. With reactant concentrations of 0.3 mM. PMP, 16 mM α -KG, and 0.6 mM Cu^{II} the equilibrium was in favour of almost complete conversion to pyridoxal phosphate and glutamate.

The problem is to find out which type of reactive species would be expected to give the observed dependence of the reaction rate on the concentration of Cu^{II} . If, as has been suggested (see Introduction), the reactive species is the metal chelate of the schiff's base derived from pyridoxamine phosphate and α -ketoglutaric acid, CuSB^{II} , the following equations should describe the overall reaction:



If these are the only equilibria to be considered, either equation (1) or (2) must account for the observed behaviour at isosbestic "A" preceding the reaction shown in equation (3).

The absence of any appreciable spectral change before that due to transamination (Fig. 8-1,2) would indicate either that the species CuSB^{II} was present in low concentrations, or that its spectrum was similar to that of pyridoxamine phosphate.

It is unlikely that the attainment of equilibrium in equation (2) would be slow enough to be observed. Consequently the changes observed at "A" cannot be caused by the reaction shown in equation (2). The rate determining step for the changes observed at the isosbestic point must therefore be that shown in equation (1). This would be followed by the rapid and almost complete reaction (2) with which the spectral change is probably associated. If the reactive species, CuSB^{II} was present in only low concentration, as was concluded above, this must be caused by an unfavourable equilibrium constant K_1 in equation (1).

The equilibrium constant K_1 for schiff's base formation from pyridoxamine phosphate and α -ketoglutarate is unknown. Attempts to evaluate it spectrophotometrically were made by Matthews¹, but the results have not been successful, because of the small changes in optical density. This indicates again either that K_1 is very low or that the spectra of SB^{II} and pyridoxamine phosphate are similar. The equilibrium constants for schiff's base formation from pyridoxamine and pyruvate, evaluated by Banks et al² suggest that the former suggestion is correct. The presence of Cu^{II} ions in the system would not favour as great a stabilisation of the schiff's base from PMP and α -KG as it did for the schiff's base from PLP and

glutamate. It may be expected therefore that some optimum concentration of Cu^{II} exists at which $[\text{CuSB}^{\text{II}}]$ has a maximum value.

Defining the equilibrium constants K_1 and K_2 from equations (1) and (2):

$$\text{as } K_1 = [\text{SB}^{\text{II}}] / [\text{P}^{3-}] [\text{G}^{2-}] \quad (4)$$

$$\text{and } K_2 = [\text{CuSB}^{\text{II}}] / [\text{Cu}^{2+}] [\text{SB}^{\text{II}}] \quad (5)$$

or, multiplying together (4) and (5):

$$K_1 K_2 = [\text{CuSB}^{\text{II}}] / [\text{Cu}^{+2}] [\text{P}^{3-}] [\text{G}^{2-}] \quad (6)$$

rearranging (6) gives:

$$[\text{CuSB}^{\text{II}}] = K_1 K_2 [\text{Cu}^{2+}] [\text{P}^{3-}] [\text{G}^{2-}] \quad (7)$$

and differentiating w.r.t. the total Cu^{II} concentration, C_m ,

$$d[\text{CuSB}^{\text{II}}]/dC_m = K_1 K_2 [\text{G}^{2-}] \left([\text{P}^{3-}] \bullet d[\text{Cu}^{2+}]/dC_m + [\text{Cu}^{+2}] \bullet d[\text{P}^{3-}]/dC_m \right) \quad (8)$$

as α -KG was in considerable excess derivatives of $[\text{G}^{2-}]$ were taken

as zero. For a maximum concentration of CuSB^{II} , $d[\text{CuSB}^{\text{II}}]/dC_m = 0$

$$\text{or } [\text{P}^{3-}] \bullet d[\text{Cu}^{+2}]/dC_m = -[\text{Cu}^{+2}] \bullet d[\text{P}^{3-}]/dC_m \quad (9)$$

The successive stability constants of Cu^{II} and PMP are given by:

$$K_1 = [\text{CuP}^-] / [\text{Cu}^{+2}] [\text{P}^{3-}] \quad (10)$$

$$\text{and } K_2 = [\text{CuP}_2^{4-}] / [\text{CuP}^-] [\text{P}^{3-}] \quad (11)$$

Summing the concentrations of all the species,

$$C_p = [\text{CuP}^-] + 2 [\text{CuP}_2^{4-}] + A [\text{P}^{3-}] + [\text{CuSB}^{\text{II}}] \quad (12)$$

where A is the ratio (total free PMP)/anionic PMP). The concentration of

free SB^{II} is taken as zero in equation (12)

$$C_m = [\text{CuP}^-] + [\text{CuP}_2^{4-}] + [\text{Cu}^{+2}] + [\text{CuSB}^{\text{II}}] \quad (13)$$

Substituting equations (4), (5), (6), (7) and (10) in (12) and (13):

$$C_p = K_1 Cu \bullet P + 2K_1 K_2 Cu \bullet P^2 + AP + K_1 K_2 Cu \bullet P \bullet G =$$

$$P(K_1 Cu + 2K_1 K_2 Cu \bullet P + A + K_1 K_2 Cu \bullet G) \quad (14)$$

$$\text{and } C_m = K_1 Cu \bullet P + K_1 K_2 Cu \bullet P^2 + Cu + K_1 K_2 Cu \bullet P \bullet G =$$

$$Cu(K_1 P + K_1 K_2 P + 1 + K_1 K_2 P \bullet G) \quad (15)$$

where $P = [P^{3-}]$ etc. for simplicity

Differentiating (14) and (15) w.r.t. C_m gives:

$$0 = (K_1 Cu + 2K_1 K_2 Cu \bullet P^2 + K_1 K_2 Cu \bullet G + 1) \bullet dP/dC_m +$$

$$P([K_1 + 2K_1 K_2 P + K_1 K_2 G] \bullet dCu/dC_m + 2K_1 K_2 Cu \bullet dP/dC_m) \quad (16)$$

$$1 = (K_1 P + K_1 K_2 P^2 + K_1 K_2 P \bullet G + 1) \bullet dCu/dC_m +$$

$$(K_1 + 2K_1 K_2 P + K_1 K_2 G) \bullet Cu \bullet dP/dC_m \quad (17)$$

Putting $-P \bullet dCu/dC_m$ for $Cu \bullet dP/dC_m$ (equation (19) in (17):

$$dCu/dC_m = 1/(1 - K_1 K_2 P^2) \quad (18)$$

and, from (9)

$$dP/dC_m = -P/(1 - K_1 K_2 P^2) \bullet Cu \quad (19)$$

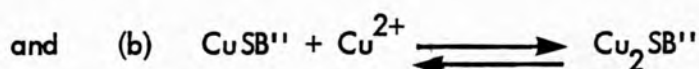
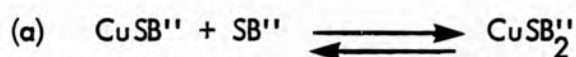
Substituting (18) and (19) into (16) gives:

$$A/Cu + 2K_1 K_2 P = 0$$

This condition cannot be fulfilled for positive concentrations of Cu and P. The physical interpretation of this is that the concentration of the species $CuSB''$ can not have a finite maximum value of

concentrations if the only equilibria involved are those shown in equation (1) to (3). This view is supported by figures in column 6 on Table (8-1) which show the differences between the theoretical and experimental optical densities at isobestic "A" immediately upon mixing the reactants. These results would indicate the presence of another species, the concentration of which increased with that of Cu^{II} throughout the experimental range.

The mathematical treatment above indicates that at least one other equilibrium must exist in the reaction mixtures for it to be possible for CuSB'' to have a maximum value. The two most probable equilibria are:



Of these, suggestion (a) seems the most probable in view of the number of species of type $\text{M}(\text{SB})_2$ reported in the literature (see Introduction). Mathematical treatment of suggestion (a) shows that the addition of this extra equilibrium does indeed cause the term $[\text{CuSB}'']$ to go through a maximum value, but at an expected ratio $\text{Cu}^{\text{II}}:\text{PMP}$ of 1:2 and not 2:1 as required.

Similar treatment of suggestion (b) is rather more complex unless several assumptions are made. These are,

1) That a negligible amount of Cu-PMP co-ordination takes place at the pH of the experiment (3.98);

and

2) that the concentrations of CuSB'' and $\text{Cu}_2\text{SB}''$ are small compared with the total concentration of Cu^{II} and PMP.

The first of these assumptions is justifiable by Matthews'¹ inspection of the stability constant. Assumption (2) is merely a restatement of what was said earlier (page 284). Thus introducing K_4 :

$$\text{where } K_4 = \frac{[\text{CuSB}^{II}]}{[\text{Cu}^{2+}][\text{CuSB}^{II}]}$$

The total concentrations of Cu^{II} and PMP become:

$$C_m = \text{Cu} \bullet (1 + K_1 K_2 P \bullet G + 2K_1 K_2 K_4 \text{Cu} \bullet PG) \quad (20)$$

$$\text{and } C_p = P \bullet (A + K_1 K_2 \text{Cu} \bullet G + K_1 K_2 K_4 \text{Cu}^2 G) \quad (21)$$

Differentiating (20) w.r.t. C_m gives,

$$0 = (K_1 K_2 \text{Cu} \bullet G + K_1 K_2 K_4 \text{Cu}^2 G + A) \bullet dP/dC_m + \\ (K_1 K_2 G + 2K_1 K_2 K_4 \text{Cu} \bullet G) \bullet P \bullet d\text{Cu}/dC_m \quad (22)$$

Substituting equation (9) into equation (22) and simplifying gives,

$$A - K_1 K_2 K_4 \text{Cu} \bullet G = 0 \\ \text{or } \text{Cu} = A/K_1 K_2 K_4 G \quad (23)$$

Substituting equation (23) into (20) and (21) and dividing equation (20) by (21):

$$\frac{C_m}{C_p} = \frac{\text{Cu} + A \bullet P/K_4 + 2 \text{Cu} \bullet A \bullet P}{A \bullet P + A \bullet P/K_4 + \text{Cu} \bullet A \bullet P} \quad (24)$$

The desired ratio of C_m/C_p is 2, therefore this in equation (24) and simplifying gives:

$$\text{Cu} = A \bullet P \bullet (2 + 1/K_4)$$

If K_4 is sufficiently large, this becomes:

$$Cu = 2A \bullet P \quad (25)$$

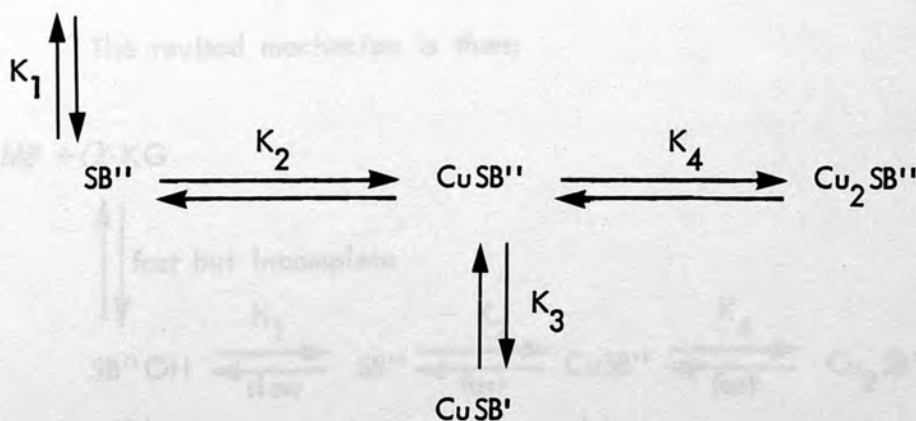
Now $A \bullet P$ is the total concentration of free PMP, therefore if the concentrations of free copper ion (Cu in the above derivation) is comparable to the total concentration of copper, C_m , (see assumption (2) above) then equation (25) becomes:

$$C_m = 2C_p$$

This means that, if the above assumptions hold, the concentration of the species $CuSB''$ has a maximum value at a ratio of $C_m/C_p = 2$. It also means that the concentrations of the proposed complex are small compared with the concentrations of the other reactants. (This is presumably only true at low pH values)

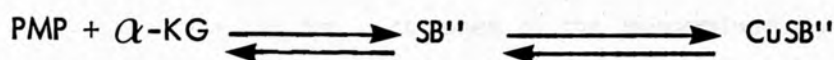
The proposed mechanism is shown diagrammatically below:

PMP + α -KG



K_1 is assumed to be very small and K_2 and K_4 are assumed to be very large.

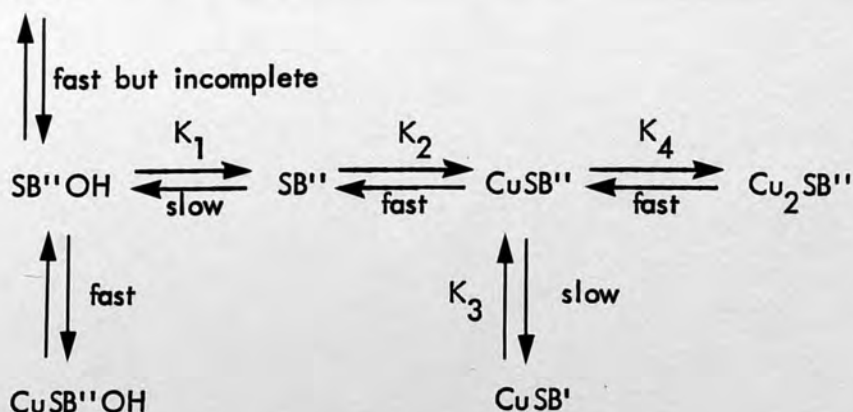
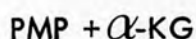
Then the mechanism implies that the steps:



are responsible for the decrease in optical density observed at the isosbestic point "A".

However, these equilibria alone do not account for all the experimental observations. Column 6 in Table 8-1 exhibits a steady change with increasing Cu^{II} concentration which cannot be caused by the species $\text{Cu}_2\text{SB}''$ postulated here as the values $D'_o - D_o$ are those for the reaction mixture immediately upon mixing, whereas the complexes CuSB'' and $\text{Cu}_2\text{SB}''$ are not formed until after the slow SB'' formation step. This phenomenon was suggested¹ to be very similar to the PLP/Glu system (carbinolamine complex proposal). Such complexes could possibly exist in the present system without the need for drastic alteration of the mechanism already put forward. These carbinolamine complexes could not themselves be the reactive species as Column 6 of Table 8-1 exhibits no maximum or minimum to parallel the maximum which appears in Column 4.

The revised mechanism is then:



For further support of the occurrence of the transamination, paper chromatographic technique was used. Two hours after mixing the reactants in acetate buffer, just at the end of the second stage of the reaction (when spectrum (2) becomes apparent, Fig. 8-1,2) the mixture was spotted on Whatman No. 1 paper. The solvent used was a mixture of n-butanol, acetic acid and water in the ratio of 12:3:5. The dried paper was viewed under ultra-violet light, then was exposed to ammonia vapour and viewed again under ultra-violet light. Finally the paper was sprayed successively with ninhydrin and dithiazone (0.05% chloroform). The colour spots were marked and the Rf values were obtained. The Rf values and the colours produced under certain conditions are shown in Table (8-2):

Spot	Color	Rf	Notes
1	White	0.15	
2	White	0.25	
3	White	0.35	
4	U.V.	0.45	
5	White	0.55	
6	White	0.65	

Table 8-2 Results obtained from Paper Chromatography for the reaction
of PMP + α -KG + Cu^{+2}

Reaction	Condition	Colour	Compound	Rf x 100
PMP + α KG + Cu^{+2}	U.V.	blue	PLP	93.6
	U.V.	purple	PMP	92.4
	U.V.	purple	PM	96.0
	visible	yellow	PLP	93.6
	ninhydrin	orange	PMP	92.4
PMP	U.V.	purple	PMP	94.2
	visible	colourless	PMP	
	ninhydrin	orange	PMP	
PLP	U.V.	blue	PLP	91.7
	visible	yellow	PLP	
	ninhydrin	colourless	PLP	
α -KG	U.V.	colourless	α -KG	89.1
	visible	colourless	α -KG	
	ninhydrin	yellow	α -KG	

From the results it is clear that for the first 30 minutes after mixing the reactants either no transamination reaction occurred or that the amount of pyridoxal phosphate (PLP) formed³ is so small that no blue spot was visible under U.V. light. After the first two hours, transamination was almost complete, because of the appearance of the blue spot under the ultra-violet light which indicates the formation of pyridoxal phosphate. The reverse reaction (PLP + Glu $\xrightleftharpoons{Cu^{+2}}$ PMP + α -Ketoglutarate) has been largely investigated by the same technique at various pH values with different metals by Mastrantonis⁴.

The most interesting result from the chromatographic studies is the appearance of an unusual spot when the mixture (after 30 min.) was spotted and viewed under U.V. light. This spot, which was purple under U.V. light, can be attributed to dephosphorylated pyridoxamine phosphate, as pyridoxamine gives a similar spot but with a slightly higher Rf value. If this was the case then the metal dephosphorylation would be suggested. This suggestion was confirmed by Mastrantonis⁴ and Farago et al⁵.

REFERENCES

1. T. Matthews, Ph.D Thesis, Bedford College, University of London, (1966).
2. B.E.C. Banks, A.A. Diamantis and C.A. Vernon, J.C.S. (1961), 4235.
3. J.B. Longenecker and E. Snell, JACS, (1957), 79, 142.
4. J. Mastrantonis, Ph.D Thesis, Bedford College, University of London, (1982).
5. M.E. Farago, M.M. McMillan and S.S. Sabir, Inorg. Chem. Acta, (1975), 14, 207.

APPENDIX 1

Rate Measurements of Formation of Metal-Schiff-Base Complexes

The rate of formation of metal-Schiff base complexes of pyridoxal phosphate, glycine in the presence of five metal ions, namely Cu^{++} , Co^{++} , Cd^{++} , Mn^{++} and Al^{+3} were measured under the same experimental conditions as was explained in Chapter 3.

The rate of change of absorbance at $25,500 \text{ cm}^{-1}$ when the concentration of (1) hydrogen ion, (2) glycine, (3) pyridoxal phosphate, and (4) metal ion were varied was observed. Rate constants were calculated from plots of $\log (A_{\infty} - A_t)$ versus time, where A_{∞} is optical density at infinity and A_t optical density at time t .

The concentrations of stock reactants were: PLP = $2 \times 10^{-3} \text{ M}$, Glycine = $8 \times 10^{-2} \text{ M}$, Metal ions = $4 \times 10^{-2} \text{ M}$, and the pH range was 1.68-5.25. The reactions were carried out at 25°C in matched silica cells (1 cm = 3 ml). The results are shown in table 1, 2 and 3.

Table 1 - Results obtained from the reaction between PLP and Gly in the presence of different metal ions at various pH values

pH	Rate Constant K/sec^{-1}				
	Cu^{++}	Cd^{++}	Co^{++}	Mn^{++}	Al^{++}
1.68	3×10^{-4}	-	1.4×10^{-3}	-	1.8×10^{-4}
3.02	3.9×10^{-4}	-	1.9×10^{-3}	-	3.7×10^{-4}
5.25	1.1×10^{-3}	-	2.4×10^{-3}	-	6.9×10^{-4}

Pyridoxal phosphate = 0.4 ml
 Glycine = 0.3 ml
 Metal ions = 0.3 ml
 Buffer = 2.0 ml

Table 2 - Results obtained from the reaction between PLP and Gly in the presence of different metal ions at various pH values

pH	Rate Constant K/sec^{-1}				
	Cu^{++}	Cd^{++}	Co^{++}	Mn^{++}	Al^{+3}
1.68	2.7×10^{-4}	-	1.8×10^{-3}	-	2.1×10^{-4}
3.02	4.6×10^{-4}	-	2.4×10^{-3}	-	4.3×10^{-4}
5.25	1.2×10^{-3}	-	3.2×10^{-3}	-	8.2×10^{-4}

Pyridoxal phosphate = 0.3 ml
 glycine = 0.4 ml
 Metal ions = 0.3 ml
 Buffer = 2.0 ml

Table 3 - Results obtained from the reaction between PLP and Gly in the presence of different metal ions at various pH values

pH	Rate Constant K/sec^{-1}				
	Cu^{++}	Cd^{++}	Co^{++}	Mn^{++}	Al^{+3}
1.68	2.3×10^{-4}	-	1.2×10^{-3}	-	2.6×10^{-4}
3.02	4×10^{-4}	-	1.9×10^{-3}	-	5.3×10^{-4}
5.25	9.8×10^{-4}	-	2.2×10^{-3}	-	7×10^{-4}

Pyridoxal phosphate = 0.3 ml
 Glycine = 0.3 ml
 Metal ions = 0.4 ml
 Buffer = 2.0 ml

Discussion:

The observed rates of the reactions (Fig. 1) of PLPGly and Cu^{++} , Co^{++} , Cd^{++} , Mn^{++} and Al^{+3} (Table 1, 2, 3), showed that these reactions are first order because of the linearity of the plots of $\log (A_{\infty} - A_t)$ versus time.

The slope of each line has been used for determination of the rate constant (K) values from the following relation:

$$K = \frac{2.303}{60} \times \text{slope}$$

because the time scale used in the plots is minutes.

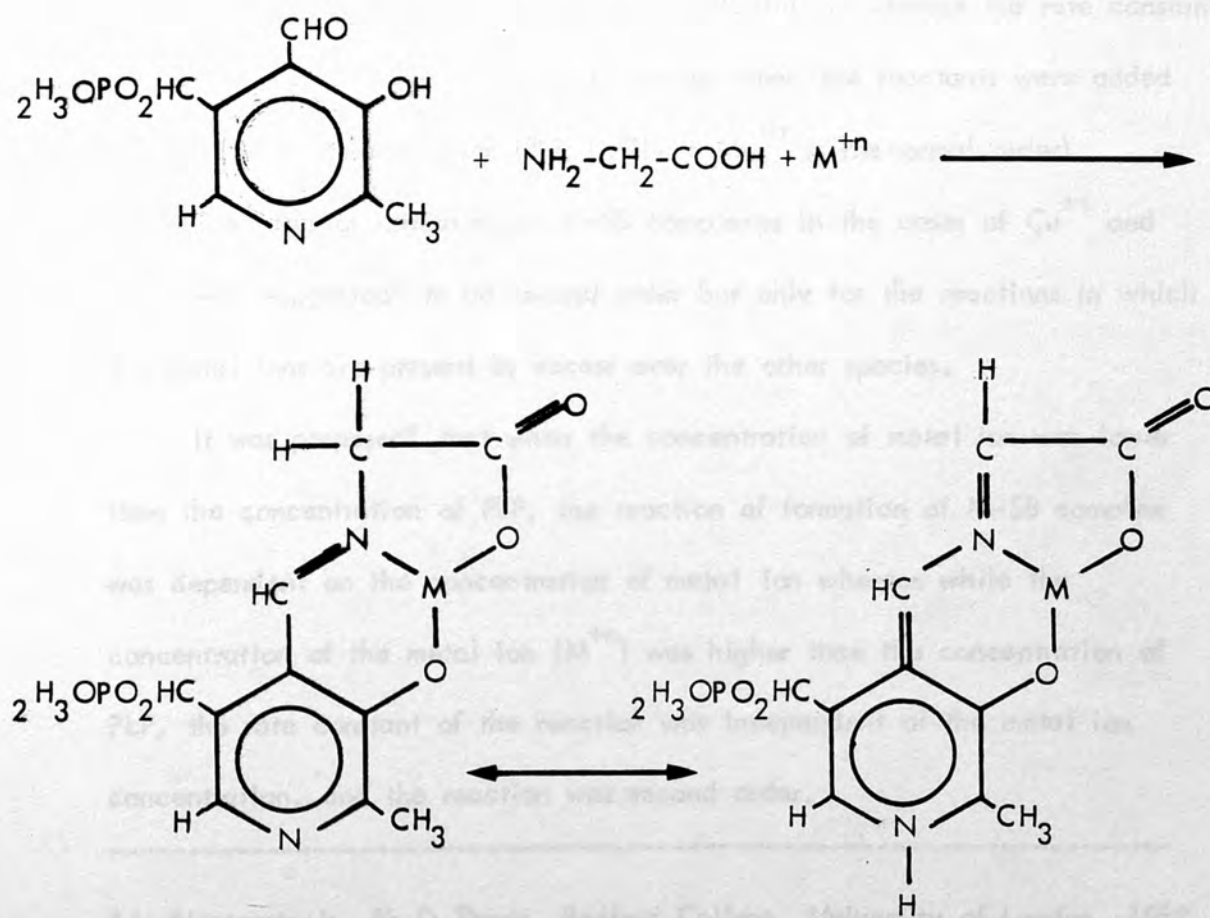


Fig. 1: Phosphopyridylidene-glycine Chelation to Metal Ion

Complex formation in the case of Cd^{++} is not possible due to the absence of suitable vacant d-orbitals to accommodate the electrons on complexing with the amine.

The same result is obtained for Mn^{++} . This is due to the fact that the d^5 configuration has little or no ligand field stabilization energy, except in the case of low spin complexes. High spin complexes of Mn^{++} have the $t_{2g}^3 e_g^2$ electron distribution. The energies of the orbitals will therefore be equivalent and degenerate, and the Jahn-Teller effect will not operate.

The K values for the Cu^{++} , Co^{++} and Al^{+++} compounds were increased by increasing pH (Table 1, 2, 3).

Varying the concentrations of reactants did not change the rate constant significantly, but there was a small change when the reactants were added to the cell in reverse order (PLP + Gly + Mn^{+n} is the normal order).

The rates of formation of M-SB complexes in the cases of Cu^{++} and Al^{+3} were suggested* to be second order but only for the reactions in which the metal ions are present in excess over the other species.

It was proposed* that when the concentration of metal ion was lower than the concentration of PLP, the reaction of formation of M-SB complex was dependent on the concentration of metal ion whereas while the concentration of the metal ion (M^{+n}) was higher than the concentration of PLP, the rate constant of the reaction was independent of the metal ion concentration, and the reaction was second order.

*J. Mastrantonis, Ph.D Thesis, Bedford College, University of London, 1982.

Appendix 2

Buffers used in the Present Work:

Acetate was found to be the only type of buffer suitable for systems containing strongly co-ordinating ligands. Sodium hydroxide was used in one instance (Page 274) for pH values above 7.

The acetate buffer solutions were normally made up as follows:

In 50 ml of 1M sodium acetate solution, X ml of 1M hydrochloric acid were added and the solution was made up to 250 ml. The pH of each solution was measured at 20°C with a Pye Dynacap pH meter.

50 ml 1M Sodium acetate + X ml 1M HCl made up to 250 ml					
pH	X(ml) HCl	pH	X(ml) HCl	pH	X(ml) HCl
0.65	100	1.99	52.5	3.79	42.5
0.75	90	2.32	51.0	3.95	40.0
0.91	80	2.64	50.0	4.19	35.0
1.09	70	2.72	49.75	4.39	30.0
1.24	65	3.09	48.5	4.58	25.0
1.42	60	3.29	47.5	4.76	20.0
1.71	55	3.49	46.25	4.92	15.0
1.85	53.5	3.61	45	5.20	10.0

Appendix 3

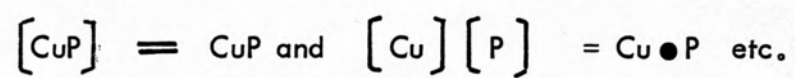
The following abbreviations and symbols have been used throughout this thesis:

PN	Pyridoxine
PL	Pyridoxal
PLP	Pyridoxal-5'-Phosphate
PM	Pyridoxamine
PMP	Pyridoxamine-5'-Phosphate
en	Ethylenediamine
Gly	Glycine
acac	Acetylacetone
α -KG	α -Ketoglutaric Acid
Glu	Glutamate
SB	Schiff Base
SB'	The Schiff's base derived from Pyridoxal Phosphate and Glutamate
SB''	The Schiff's base derived from Pyridoxamine Phosphate and α -Ketoglutaric Acid
P	PLP or PMP
G	α -KG or Glu
D	Optical density
D_o	Initial optical density
E	Extinction coefficient
C_p	Total concentration of PLP or PMP
C_m	Total concentration of metal ion

[]

Concentration of species in brackets. These brackets have been omitted in certain parts for convenience.

Where this is so the character '●' distinguishes between



A

The ratio (Total free PMP/Anionic PMP)